

*Artificial, ground-based, multifunctional, long-term  
thermal storage facilities in models, in the laboratory,  
and in practice*

Dissertation

zur Erlangung des Grades  
Doktor der Naturwissenschaften (Dr. rer. nat.)

der

Naturwissenschaftlichen Fakultät III  
Agrar- und Ernährungswissenschaften,  
Geowissenschaften und Informatik

der Martin-Luther-Universität Halle-Wittenberg

vorgelegt von

Herrn Bott, Christoph  
Geb. am 02.07.1992 in Solingen

*Gutachter:*

*Prof. Dr. rer. nat. Peter Bayer*

*Prof. Dr. rer. nat. Philipp Blum*

*Tag der Verteidigung: 25. Januar 2024*



# Abstract

Energy storage is considered the backbone of the energy transition and one of the key elements on the path to a climate-neutral economy. To store thermal energy (i.e., heat and cold) on extended, predominantly seasonal time scales, several closed-loop, large-scale, ground-based, seasonal thermal energy storage facilities were built and scientifically monitored in the past decades. These serve to enable a high share of strongly fluctuating renewable energies in innovative heating/cooling systems. However, this technology has so far been established mainly in Germany and Central Europe. Despite constant advancements in various areas, critical challenges remain that hinder global market availability.

These challenges consist of technical weaknesses, especially insufficiently optimized building components, and uncertain, often overestimated storage efficiencies. This leads to economic weaknesses, e.g., if the surrounding energy system is not balanced and energy losses have to be compensated by increased primary energy consumption. Ultimately, interactions between seasonal storages and their environment are not sufficiently explored, causing shortcomings concerning the environment and ecology. Especially in the case of hydrogeological influences, the transition of lost thermal energy into the subsurface is important, and may even exceed regulatory limits.

To overcome these weaknesses, the objective of this project is to develop different solutions strategies, and tools. Before that, the state of technology of seasonal thermal energy storage is evaluated, related to the technological types of Tank-, Pit-, and Water-Gravel Thermal Energy Storage. Within this study, an analysis of 31 sites reveals best practices and new research perspectives. Based on this analysis of research and development over the past decades, research questions are identified in detail and weaknesses of existing systems and components as well as potentials for further technical development are identified.

To mitigate the identified weaknesses of the storage membrane, a series of laboratory tests is presented. They involve small-scale tests to investigate the usability of an innovative combined insulation and sealing using paraffin wax. Using this latent storage material in an extended storage envelope proves to offer large potential. On the one hand, the phase change effect can effectively be used to reduce energy losses and buffer peak loads. On the other hand, a second effect is demonstrated: A self-healing feature through liquefied paraffin wax closing local defects in the sealing.

Within another technical focus of the project, a new, component-based, numerical model for the simulation of crucial storage processes is presented. Due to its flexible parameterization, the model can be used to optimize the planning of seasonal thermal energy storage under variable site conditions. As an example, the new model is used to analyze trends of storage efficiency caused by different design changes (e.g., insulation thickness, and material selection). The results provide the basis for deriving general design advices. The model allows fast analyses of a range of scenarios to investigate sensitivities, thereby enabling optimization of storage designs.

In addition, an enhanced simulation framework is presented to improve the accuracy of operational predictions. By coupling the previously developed model for the internal storage structure to a high-resolution, numerical, multi-physical model,

---

the operational behavior of a seasonal storage facility as well as hydrogeological and other environmental boundary conditions are captured. The results of a parameter study reveal how different environmental conditions (especially hydrogeological conditions) can affect seasonal thermal energy storage systems — and that common process simplifications can otherwise yield significant deviations for achievable performance parameters.

Ultimately, the results of the different innovation steps are synthesized and contrasted to the identified weaknesses, and perspective approaches for further optimization are presented. Altogether, this thesis represents a multidimensional contribution to the further development of artificial, ground-based, multifunctional, long-term thermal storage facilities.

## Kurzfassung

Energiespeicher gelten als Rückgrat der Energiewende und eines der Schlüsselemente auf dem Weg zu einer klimaneutralen Wirtschaft. Zur Speicherung thermischer Energie (d.h. Wärme und Kälte) auf längeren, vorwiegend saisonalen Zeitskalen, wurden in den vergangenen Jahrzehnten zahlreiche geschlossene großskalige, erdgebundene, saisonale thermische Energiespeicher gebaut und wissenschaftlich begleitet. Diese dienen dazu, einen hohen Anteil stark fluktuierender, erneuerbarer Energien in innovativen Wärme-/Kältenetzen zu ermöglichen. Dennoch ist diese Technologie bisher vor allem in Deutschland und Zentraleuropa etabliert. Trotz konstanten Weiterentwicklungen in diversen Bereichen verbleiben kritische Herausforderungen, die eine globale Marktverfügbarkeit behindern.

Diese Herausforderungen bestehen aus technischen Schwächen, vor allem aus nicht hinreichend optimierten Baukomponenten und unsicheren, oft überschätzten Speichereffizienzen. Dies führt zu ökonomischen Schwächen, z.B. wenn die Lasten des umgebenden Energiesystems nicht ausgeglichen werden können und Energieverluste durch höhere Primärenergieverbräuche kompensiert werden müssen. Zudem sind Wechselwirkungen zwischen Saisonspeichern und ihrer Umwelt nicht hinreichend erforscht, was Schwächen hinsichtlich der Umwelt und Ökologie verursacht. Gerade im Fall hydrogeologischer Einflüsse spielt der Übergang von Wärme in den Untergrund eine Rolle, wobei letztlich auch regulatorische Grenzen überschritten werden können.

Um diese Schwächen zu überwinden, ist das Ziel dieses Projekts, verschiedene Lösungsstrategien und Werkzeuge zu erarbeiten. Zuvor wird der Stand der Technik saisonaler Wärmespeicher, bezogen auf die Technologietypen der Tank-, Pit-, und Kies-Wasser-Speicher evaluiert. Die Literaturstudie spiegelt dabei bewährte Verfahren sowie Forschungsperspektiven auf Basis von 31 Standorten wider. Diese Analyse der Forschung und Entwicklung der letzten Jahrzehnte bildet die Grundlage, um die aufgeworfenen Forschungsfragen im Detail zu identifizieren sowie Schwächen bestehender Systeme / Komponenten und Potenziale technischer Weiterentwicklung herauszuarbeiten.

Darauf aufbauend stellen technische Forschungsarbeiten den Fokus des Projekts dar. Zur Minderung offener Schwächen der Speichermembran wird eine Serie von Laborversuchen präsentiert. Sie beinhalten kleinskalige Tests, um eine innovative, kombinierte Isolation und Abdichtung mit Paraffin hinsichtlich ihrer Nutzbarkeit zu untersuchen. Der Einsatz dieses latenten Speichermaterials in einer erweiterten Speicherhülle zeigt dabei, dass dieses Konzept grundsätzlich großes Potenzial bietet. Einerseits kann der Phasenwechsel-Effekt effektiv genutzt werden, um Verluste thermischer Energie zu reduzieren und Lastspitzen zu puffern. Andererseits wird ein zweiter gewünschter Effekt demonstriert: Eine selbstheilende Eigenschaft entsteht, indem verflüssigtes Paraffin lokale Fehlstellen in Abdichtungen verschließt.

In einem weiteren technischen Projektschwerpunkt wird ein neues, komponentenbasiertes, numerisches Modell zur Simulation verschiedener Fragestellungen des Forschungsfeldes präsentiert. Mit seiner flexiblen Parametrierbarkeit dient dieses neue Modell zur Optimierung des Planungsprozesses thermischer Saisonspeicher unter variablen Standortbedingungen. In einer Studie wird das neue Modell genutzt, um Trends der Speichereffizienz zu analysieren, die durch unterschiedliche Design-

Änderungen (z.B. Isolationsmächtigkeit, Materialauswahl) verursacht werden. Die Ergebnisse ermöglichen weiterhin die Ableitung allgemeiner Planungsempfehlungen. Dabei beweist das Modell seine Stärke, indem es schnelle Analysen einer Vielzahl von Szenarien zur Untersuchung von Parameter-Sensitivitäten ermöglicht und somit für die Optimierung von Speicherkonstruktionen geeignet ist.

Darüber hinaus wird ein neues Modellierungs- und Simulationskonzept auf dieser Basis präsentiert, um die Genauigkeit von Betriebsvorhersagen zu verbessern. Durch die Kopplung des zuvor entwickelten Modells des internen Speicherbauwerks mit einem hochaufgelösten, numerischen, multiphysikalischem Modell werden sowohl das Betriebsverhalten eines Saisonspeichers wie auch hydrogeologische und weitere Randbedingungen der Umwelt erfasst. Die Ergebnisse einer Parameterstudie zeigen dabei, wie verschiedene Umweltbedingungen (v.a. hinsichtlich Grundwasserbedingungen) auf saisonale thermische Energiespeicher einwirken können und dass die zuvor oftmalige Vernachlässigung dieser Prozesse zu signifikanten Abweichungen hinsichtlich erreichbarer Leistungsparameter führt.

Schließlich werden die Ergebnisse der verschiedenen Studien des Projekts zusammengeführt und den identifizierten Schwächen gegenübergestellt und perspektivisch Ansätze für weitere Optimierungen vorgestellt. Insgesamt ermöglicht das Projekt so einen mehrdimensionalen Beitrag zur Weiterentwicklung geschlossener, erdgebundener saisonaler thermischer Energiespeicher.

# Publications

This thesis synthesizes the following four contributions (cumulative thesis):

- ▷ Chapter 2 has been published as:  
**Bott, C., Dressel, I., & Bayer, P. (2019).** State-of-technology review of water-based closed seasonal thermal energy storage systems. *Renewable and Sustainable Energy Reviews*, 113, 109241, DOI: [10.1016/j.rser.2019.06.048](https://doi.org/10.1016/j.rser.2019.06.048).  
*Author contributions.* Methodology: C.B.; Formal analysis: C.B.; Writing – original draft: C.B.; Writing – review & editing: C.B., I.D., P.B.; Funding acquisition: P.B., I.D.; Project administration & supervision: P.B.
  
- ▷ Chapter 3 has been published as:  
**Bott, C., Dressel, I., & Bayer, P. (2020).** Paraffin wax as self-sealing insulation material of seasonal sensible heat storage systems—A laboratory study. *Plos one*, 15(7), e0236056, DOI: [10.1371/journal.pone.0236056](https://doi.org/10.1371/journal.pone.0236056).  
*Author contributions.* Conceptualization: C.B., P.B.; Investigation: C.B., I.D.; Methodology: C.B.; Visualization: C.B.; Writing – original draft: C.B.; Writing – review & editing: C.B., I.D., P.B.; Validation: I.D., P.B.; Supervision: I.D.; Project administration: I.D., P.B.
  
- ▷ Chapter 4 has been published as:  
**Bott, C., Ehrenwirth, M., Trinkl, C., & Bayer, P. (2022).** Component-based modeling of ground-coupled seasonal thermal energy storages. *Applied Thermal Engineering*, 118810, DOI: [10.1016/j.applthermaleng.2022.118810](https://doi.org/10.1016/j.applthermaleng.2022.118810).  
*Author contributions.* Conceptualization: C.B., M.E., C.T., P.B.; Methodology: C.B.; Investigation: C.B.; Writing – original draft: C.B.; Writing – review & editing: C.B., M.E., T.C., P.B.; Validation: M.E., C.T., P.B.; Supervision: P.B.
  
- ▷ Chapter 5 represents a submitted manuscript to the *Journal of Energy Storage*:  
**Bott, C., Dahash, A., Noethen, M., & Bayer, P. (2022).** Influence of thermal energy storage basins on the subsurface and shallow groundwater. Manuscript ID: EST-D-23-07631. Date of submission: 30.10.2023.  
*Author contributions.* Conceptualization: C.B., D.A., P.B.; Methodology: C.B.; Investigation: C.B.; Writing – original draft: C.B., D.A., M.N.; Writing – review & editing: C.B., A.D, M.N.; Validation: D.A., M.N., P.B.; Supervision: D.A., P.B.





## Acknowledgments

Completing this Ph.D. project has been a transformative journey, and I am deeply thankful for the support and contributions of many individuals who have made this achievement possible.

First and foremost, I want to express my appreciation to my supervisor, Peter Bayer. He has been an exemplary mentor, providing not only expert guidance but also a continuous source of creativity and motivation. His patience, dedication, and insightful advice have been key in shaping the direction and quality of this research. Apart from the scientific work of this thesis, through him, I had the opportunity to benefit from many unique experiences in applied geology and beyond.

Besides, the collaborative environment within the working group Applied Geology at the Martin Luther University Halle-Wittenberg, fostered by all colleagues, has been an invaluable resource throughout this academic journey. Since starting together in Ingolstadt, with Hannes, Lisa, and Ingo, and then moving to Halle and expanding the group with so many great colleagues, work rarely seems like an occupation – and offices have become quite a home from home. All the collaborative discussions, informal chats, and lively exchanges have been the most valuable energy storage for this project. As part of this productive environment, I would like to acknowledge the support of dedicated student assistants, Mayank Paranjape, and Ryan Pearson, who supported this project in the laboratory and at the writing desk.

Likewise, the many colleagues, outside the working group in Halle and Ingolstadt, were an infinite source of inspiration. In particular, I acknowledge Kathrin Menberg, Mathias Ehrenwirth, and Abdulrahman Dahash for sharing their expert knowledge and the thorough exchanges and discussions that have improved my research.

Finally, I have to extend my gratitude to my family, Irene, Uwe, Anja, and Chris, for their solid support and encouragement throughout my life. Their belief in my potential was a constant energy source and made me the person I am today. It has been a path of ups and downs, yet without the patience, support, and love of my wife Julia, this work would not have been possible.



# Contents

Abstract.....	iii
Kurzfassung.....	v
Publications.....	vii
Acknowledgments.....	ix
Contents.....	xi
List of figures.....	xiv
List of tables.....	xvii
Nomenclature.....	xviii
Abbreviations.....	xviii
Mathematical symbols & units.....	xx
<b>1 Introduction.....</b>	<b>1</b>
1.1 Motivation: Thermal energy storage in the era of energy transition.....	1
1.2 Scope: Ground-based, closed-loop, large-scale seasonal thermal energy storage systems.....	2
1.3 Key barriers of seasonal thermal energy storage application in practice.....	3
1.4 Objectives of this study.....	4
1.5 Overall methodology and implementation of research.....	5
1.5.1 Applied research at the IN-Campus site in Ingolstadt (Germany).....	5
1.5.2 Laboratory experiments for testing paraffin wax as an innovative concept for combined sealing and insulation.....	7
1.6 Structure of the thesis.....	8
<b>2 State-of-technology review of water-based closed seasonal thermal energy storage systems.....</b>	<b>9</b>
Highlights.....	9
Graphical abstract.....	9
2.1 Introduction.....	10
2.2 Evolution and statistics of seasonal thermal energy storage in Europe.....	12
2.2.1 Historical development.....	12
2.2.2 Numbers, volumes and spatial distribution.....	13
2.3 State of technology.....	17
2.3.1 Buried vs. elevated.....	17
2.3.2 Geometry and filling.....	17
2.3.3 Structural elements.....	20
2.3.4 Thermal insulation.....	21
2.3.5 Waterproofing.....	25
2.3.6 Loading systems.....	27
2.3.7 System integration.....	27
2.4 Conclusions and Outlook.....	30
<b>3 Paraffin wax as self-sealing insulation material of seasonal sensible heat storage systems – A laboratory study.....</b>	<b>33</b>
3.1 Introduction.....	33
3.2 Materials and methods.....	35
3.2.1 Enhancement of thermal performance.....	35
3.2.2 Leakage tests.....	38
3.3 Results and discussion.....	41

3.3.1	Enhancement of thermal performance.....	41
3.3.2	Leakage mitigation.....	44
3.4	Conclusions.....	47
<b>4</b>	<b>Component-based modeling of ground-coupled seasonal thermal energy storages.....</b>	<b>49</b>
	Highlights.....	49
	Graphical abstract.....	49
4.1	Introduction.....	50
4.2	Materials and methods.....	53
4.2.1	STORE model.....	53
4.2.2	Plausibility test.....	60
4.2.3	Test study scenarios.....	61
4.3	Results and discussion.....	65
4.3.1	Results of plausibility test.....	65
4.3.2	Evaluation of the test study.....	66
4.4	Conclusions.....	72
<b>5</b>	<b>Influence of thermal energy storage basins on the subsurface and shallow groundwater.....</b>	<b>75</b>
	Highlights.....	75
5.1	Introduction.....	76
5.2	Materials and methods.....	78
5.2.1	Modeling approach.....	78
5.2.2	STORE model.....	79
5.2.3	COMSOL model.....	80
5.2.4	Implementation.....	83
5.2.5	Parameter study: Impact of groundwater flow on seasonal thermal energy storage.....	84
5.3	Results and discussion.....	87
5.3.1	Base case.....	87
5.3.2	Technical perspective.....	89
5.3.3	Environmental perspective.....	91
5.4	Conclusions and outlook.....	94
<b>6</b>	<b>Synthesis.....</b>	<b>95</b>
6.1	Conclusions: Findings in the field of seasonal thermal energy storage.....	95
6.2	Outlook.....	98
6.2.1	Perspectives for further technical, economic, and ecological improvements as part of future research activities.....	98
6.2.2	Perspectives for the IN-Campus as an application site for innovative seasonal thermal storage concepts.....	103
	<b>Appendices.....</b>	<b>105</b>
	Appendix A.....	105
	Appendix A-1: Details on fillings & geometries.....	105
	Appendix A-2: Details on thermal insulation.....	106
	Appendix A-2: Details on waterproofings.....	107
	Appendix A-2: Details on structural elements.....	108
	Appendix B.....	109
	Appendix B-1: Records of experiments on thermal performance enhancement.....	109

Appendix B-2: Records of experiments on leakage mitigation.....	109
Appendix C.....	110
Appendix C-1: STORE model inputs – Design Scenario Database.....	110
Appendix C-2: STORE model setup.....	111
Appendix C-2: STORE model – Default probe configuration.....	112
Appendix D.....	113
Appendix D-1: Model validation .....	113
Appendix D-2: Mesh refinement.....	117
Appendix D-2: Design scenario datasets .....	118
<b>References.....</b>	<b>I</b>
<b>Curriculum vitae.....</b>	<b>XX</b>
<b>Declaration / Erklärung .....</b>	<b>XXII</b>

# List of figures

Fig. 1.1: Key perspectives on seasonal thermal energy storage. ....	3
Fig. 1.2: Specific cost of seasonal thermal energy storage projects compared to their storage capacity (after [14] and [26]).....	4
Fig. 1.3: a) Schematic construction schedule of the IN-Campus; b) illustration of the envisioned, innovative, dynamic energy system (left) compared to a conventional energy system approach (right; after [35])......	5
Fig. 1.4: a) Overview of current construction phase at IN-Campus; b) zoomed, re-oriented view of in-ground, basin infrastructure for transformation into seasonal thermal energy storage units.....	6
Fig. 1.5: (a) State-of-the-art engineering methodology for the construction of a Pit Thermal Energy Storage with welded plastic liners as sealing component shown by the example of Dronninglund, Denmark [42]; (b) observed temperature increases induced by leakage at probe points [43] adjacent to the sidewalls of the Tank Thermal Energy Storage facility in Friedrichshafen, Germany (after [37]). ....	7
Fig. 2.1: Heat demand and solar heat yield of a hypothetical example household in Munich, GER (heated area: 150 m <sup>2</sup> , energy demand: 70 kWh/(m <sup>2</sup> ·a), solar thermal area: 10 m <sup>2</sup> , long-term efficiency: 0.5).....	11
Fig. 2.2: Schematic layouts of the systems selected for further analysis.....	11
Fig. 2.3: Timeline showing some of the important steps in the history of the development of seasonal Thermal Energy Storage (orange: inventions; green: climate actions; blue: milestone systems; red: research activities). ....	12
Fig. 2.4: a) Evolution of the number of different seasonal storage systems and large storage buffers. b) Development of the total number and annual newly built systems (TTES, PTES, WGTES and large storage) and cumulative number of storages (black line). c) Development of the installed volume in Europe for seasonal thermal energy storage (TTES, PTES, WGTES, incl. large buffer storage) with annual newly-installed volumes. d) Development of the average size of newly installed seasonal storage systems (TTES, PTES, WGTES) and large buffer storages. ....	14
Fig. 2.5: a) Installed number of different TES types compared to b) the total available installed storage volume and c) the average individual storage volumes.....	15
Fig. 2.6: a) Map showing the locations of the different seasonal storage types, including large buffer storages in Europe, b) country-wise installed volumes (m <sup>3</sup> ) and c) numbers. ....	15
Fig. 2.7: Development of number of applications a) and today's application distribution b) for the different materials for structural elements. Concrete and reinforced concrete clearly predominate, while pile walls or GRP were only used in single pilot projects. (GRP: glass fiber reinforced plastic). ....	20
Fig. 2.8: Absolute a) and relative b) numbers of the insulated storage domains, differentiated according to the different storage types. While TTES always represent top and laterally insulated storages, particularly PTES lack sidewall insulations. The bottom is rarely insulated for all system types. ....	21
Fig. 2.9: Number of materials used for a) bottom, b) sidewall, and c) top insulation. Foam glass is primarily applied at the bottom, whereas the sidewalls are insulated mainly with conventional mineral wool and expanded glass. The largest variability is found in the top insulations, where natural, conventional, and recycling materials are used. ....	22
Fig. 2.10: Evolution of applied insulation materials used at the sidewalls for all storage types (TTES, PTES, WGTES). Mineral fiber has been used intensively since the mid-1990s, but solely for TTES. Until 1999, EPS, XPS and PUR foams gained attention. Meanwhile, expanded glass has become the preferred choice. ....	23
Fig. 2.11: a) Development of a number of applications and b) current application distribution of waterproofing materials for all storage types (TTES, PTES, WGTES).....	25
Fig. 2.12: Generations of seasonal storage systems with the most important inventions in the different domains. ....	32

Fig. 3.1: Schematic top view of the thermal performance experimental setup showing the positions of temperature sensors and materials used. PVC: polyvinyl chloride foil, PS: polystyrene glass plates. ....	35
Fig. 3.2: Experimental variants with (a) black PVC foil and (b-d) PS as sealing layer. 1: surrounding material, 2: paraffin wax insulation layer, 3: PVC sealing foil, 4: filling/water, 5: PS sealing plates, 6, 7: temperature sensors in paraffin wax/filling, 8: heating device, 9: camera. ....	36
Fig. 3.3: a) Workflow of thermal performance experiments; b) experimental phases with definition of delay and stored heat content (schematic illustration). Pink box: delay in heating/cooling due to phase change effects. Line colors in Fig. 3.3 b: blue: water, green: paraffin wax, yellow: surrounding material. ....	37
Fig. 3.4: a) Sketch and b) top view of leakage experiments. Green: paraffin wax, blue: water, red: PVC layer, yellow: surrounding material. Sensor positions marked with dots. PVC: polyvinylchloride, PS: polystyrene glass plates. ....	38
Fig. 3.5: a) Laboratory set up, b) fissure in polyvinyl chloride foil with outflowing paraffin wax, c) solid body of sand with paraffin wax, d) impermeable compound of surrounding material with pore spaces filled by paraffin wax. ....	39
Fig. 3.6: Workflow for leakage experiments, b) top view of measurements of formed bodies after induced leakage. PVC: polyvinylchloride. ....	40
Fig. 3.7: a) Delay in heating of laboratory heat storage due to paraffin wax melting; b) additional stored heat in paraffin wax during heating phase. PVC: polyvinylchloride, PS: polystyrene glass plates. ....	42
Fig. 3.8: a) Delay in cooling of laboratory heat storage due to paraffin wax solidification; b) additional released heat by paraffin wax measured in the cooling phase. PVC: polyvinylchloride, PS: polystyrene glass plates. ....	43
Fig. 3.9: Measurements of formed bodies after paraffin wax loss. The lengths and widths were defined as depicted in FIG. 3-7 b, while the height of the solids was measured vertically. A: total surface area of passageways as size of the leakage, d: grainsize of the surrounding material. ....	44
Fig. 3.10: Masses (a) and volumes (b) of formed bodies consisting of paraffin wax and surrounding material, after induced leakage. vert: vertical fissure, horiz: horizontal fissure, A: total surface area of passageways as size of the leakage, d: grainsize of the surrounding material. ....	46
Fig. 4.1: Conceptual design of the model with components in cross-sectional view (a) and top view (b). ....	55
Fig. 4.2: Simplified flow chart for sTES control: Hystereses or subordinated strategies, e.g., with transition periods, are not considered. $t$ : simulation time, $t_{end}$ : last simulation time step, $T_{Storage}$ : temperature reference of the storage, $T_{Target}$ : temperature of the target system. ....	59
Fig. 4.3: Top and side views of the sTES structure of the test study, with an illustration of filling, thermal insulation, walls and foundation, as well as external top covering and surrounding soil (suppressed in the top view). ....	62
Fig. 4.4: Illustration of the annual load profiles for charging and discharging with a) volumetric flow rates and b) inlet/supply temperatures of the heat exchanger (HX). ....	64
Fig. 4.5: Annual temperature profile of potential energy gain through hourly global irradiation from the sun as well as the b) hourly resolved annual temperature profile of ground and air temperature. ....	64
Fig. 4.6: a) Cooling curves of the STORE model and the comparative model of the CARNOT toolbox (Storage Type 3, modified best-fit); b) differences between mean temperatures of CARNOT and STORE. ....	65
Fig. 4.7: Operational diagram of the base case (a-d) and the high-tech scenario (e-h). For temperatures in the heat exchanger (HX), setbacks (i.e., temperature differences to the supply) are displayed. ....	67
Fig. 4.8: Changes in evaluation parameters over the upgrade stages (increasing thicknesses) of the respective components (top covering, thermal insulations). The diagram shows a) the maximum storage level, as well as b) the maximum, and c) average filling temperatures	

over the entire simulation period. Furthermore, the diagram shows d e) trends in endpoint parameters of storage and subsystem efficiency for storage upgrades, and f) annual rates of increase in the subsystem efficiency.....71

Fig. 5.1: Key modeling domains of sTES: a) seasonal thermal energy storage, b) surrounding environment, and c) energy system. BIO-CHP: Combined heat and power plant based on bioenergy.....76

Fig. 5.2: Key issues reported for sTES basins: a) heat losses of different sTES installations (after [318]), b) observed ground temperatures in Hamburg, Germany (after [37,135]), c) temperature regulations/recommendations for shallow geothermal energy applications in different countries as of 2010 (after [30]).....77

Fig. 5.3: Sketch of the STORE model for simulating WGTES, modified for the co-simulation framework in cross-sectional view (a) and top view on one layer (b). ....79

Fig. 5.4: a) side, and b) cut plane view of the COMSOL model with top cover, unsaturated (vadose) zone, groundwater domain (phreatic zone), and bedrock layer, tailored for co-simulation. ....80

Fig. 5.5: Operation data for the parameter study, consisting of available temperatures (a and b, in °C) and volumetric flow rates (c and d, in  $m^3 h^{-1}$ ) for charging (a and c) and discharging (b and d).....85

Fig. 5.6: Environmental data used in the case study, consisting of a) temperatures for soil and air, b) solar irradiation, c) precipitation, and d) wind speed. ....86

Fig. 5.7: Result of the sTES operation for the base case scenario over 10 years. From top to bottom: mode of operation (C: charging, S: standby, D: discharging), charging and discharging temperature, heat exchanger (HX) heat flow, sTES filling temperatures (layer-resolved), sTES wall temperatures (layer-resolved), thermal losses.....88

Fig. 5.8: Key performance indicators for comparison of the different scenarios (cf. TAB. 5.3) of the parameter study: a) efficiency and simulated maximum capacity, b) filling temperatures (min., mean, max.), c) values of the sTES energy balance (charged, discharged, and lost energy quantities at the top, sidewalls, and bottom). ....90

Fig. 5.9: Impacts of sTES on subsurface: environment temperatures in 2 m / 5 m distance. The pink dotted lines indicate the legal threshold value of 20 °C for Germany and Austria.....91

Fig. 5.10: Impacts of sTES on its surrounding environment: 20 °C (black) and +6 K (magenta) thermocline around sTES at a height of  $0.5 \cdot h_{sTES}$  after 10 years of operation for each scenario (cf. TAB 5.3). ....93

Fig. 6.1: Example of a sophisticated monitoring setup for the sTES of the basin compound ABC at the IN-Campus (cf. FIG. 1.4) and the surrounding environment based on point probes as well as DTS. ....98

Fig. 6.2: Advanced concept of the STORE model for modeling combined sTES compound systems. ....101

Fig. 6.3: Exemplary concept of a Life Cycle Assessment model for Water-Gravel Thermal Energy Storage including the construction and operation phase.....102

Fig. 6.4: Basins (a: sub-basin A of the basin compound ABC, b: basin D of the basin compound DEF, c: Basin H), which may serve for re-use as seasonal thermal energy storage at the IN-Campus (cf. FIG. 1.4). ....103

Fig. 6.5: Planned upcoming research activities and challenges at the multi-sTES "ABC" of the IN-Campus. ....103



## List of tables

Tab. 2.1: Overview of all seasonal thermal energy storage and large buffer storage locations recorded in this survey. ....	16
Tab. 4.1: Variables and parameters used for the test scenarios. XPS: Extruded polystyrene. HX: heat exchanger. ....	62
Tab. 5.1: Material properties of the example storage facility. Values used for filling material according to the WGTES installation in Chemnitz, Germany [37,63], and for foam glass gravel according to a manufacturer's data sheet ([295], ideal conditions assumed). ....	84
Tab. 5.2: Material properties of the surrounding subsurface around the storage facility. ....	86
Tab. 5.3: Scenarios for parameter study with variations of different groundwater (angle of inflow / 0° short side, 90° wide side, groundwater table depth, groundwater flow gradient) and insulation scenarios. (BGL: below ground level, $h_{sTES}$ : sTES height). ....	87

# Nomenclature

## Abbreviations

2D	Two dimensional
2.5D	2.5 dimensional
3D	Three dimensional
AI	Artificial intelligence
AT	Austria
ATES	Aquifer thermal energy storage
BC	Boundary condition
BGL	Below ground level (m)
BTES	Borehole thermal energy storage
CFD	Computational fluid dynamics
CHP	Combined heat and power
CTES	Cavern thermal energy storage
CSHPSS	Central solar heating plant with seasonal storage
DEN	Denmark
DHC	District heating and cooling
DHS	District heating system
DIN	German industrial standard
DTS	Distributed temperature sensing
EPDM	Ethylene propylene diene monomer rubber
EPS	Expanded polystyrene
FDM	Finite difference method
FEM	Finite element method
FMU	Functional mockup unit
GER	Germany
GRP	Glass fiber reinforced plastic
HDPE	High-density polyethylene
HX	Heat exchanger
IEA	International energy agency
IEA SHC	International energy agency solar heating & cooling programme
ITA	Italy
LCA	Life cycle assessment
MUMPS	Multifrontal massively parallel sparse direct solver
PCM	Phase change materials
PE	Polyethylene
PE-X	Cross-lined polyethylene
PP	Polypropylene
PS	Polystyrene glass
PTES	Pit thermal energy storage
PUR/PIR	Polyurethane/polyisocyanurate
PVC	Polyvinyl chloride
RMSE	Root mean square error
SWE	Sweden
SWI	Switzerland

---

TES	Thermal energy storage
sTES	Seasonal thermal energy storage
TTES	Tank thermal energy storage
UA	Storage thermal envelope value
WGTES	Water gravel thermal energy storage
XPS	Extruded polystyrene

## Mathematical symbols & units

$\alpha$	Convective heat transfer coefficient ( $\text{W m}^{-2} \text{K}^{-1}$ )
$A$	Interface or surface area ( $\text{m}^2$ )
$\beta$	Groundwater inflow angle ( $^\circ$ )
$c$	Heat capacity ( $\text{J kg}^{-1} \text{K}^{-1}$ )
$d$	diameter (m)
$D$	Hydraulic diameter (m)
$\delta_{\text{ITC}}$	Inversed thermocline coefficient ( $\text{W m}^3 \text{kg}^{-1}$ )
$\varepsilon_p$	Effective porosity
$\epsilon$	Surface roughness (mm)
$g$	Gravitational acceleration ( $9.81 \text{ m s}^{-2}$ )
$G_m$	Mass source ( $\text{kg m}^{-3} \text{s}^{-1}$ )
$h$	Height (m)
$H$	Hydraulic head (m)
$i$	Hydraulic gradient ( $\%$ )
$\kappa$	Permeability ( $\text{m}^2$ )
$k_{\text{disp}}$	Dispersive thermal conductivity tensor ( $\text{W m}^{-1} \text{K}^{-1}$ )
$K$	Hydraulic conductivity ( $\text{m s}^{-1}$ )
$\lambda$	Thermal conductivity ( $\text{W m}^{-1} \text{K}^{-1}$ )
$l$	Distance (m)
$l_{\text{env},x/y}$	Characteristic side length in x and y direction (m)
$L$	(Characteristic) plate length (m)
$\mu$	Dynamic viscosity (Pa s)
$\dot{m}$	Mass flow rate ( $\text{kg h}^{-1}$ )
$M$	(Layer) thickness
$\eta$	Efficiency ( $\%$ )
$n$	Number of storage layers
$N$	Normal vector on a boundary
$Nu$	Nusselt number
$o$	Output vector
$p$	Parameter vector
$\rho$	Density ( $\text{kg m}^{-3}$ )
$R^2$	Coefficient of determination
$Re$	Reynolds number
$p$	Pressure (Pa)
$P$	Precipitation rate ( $\text{mm h}^{-1}$ )
$Pr$	Prandtl number
$\ddot{q}$	Heat transport rate ( $\text{W m}^{-3}$ )
$\dot{q}$	Heat flow rate ( $\text{W m}^{-2}$ )
$\dot{q}$	Heat flux ( $\text{W m}^{-1}$ )
$\dot{Q}$	Heat flow rate (W)

$Q$	Energy quantity (MWh)
$\sigma_b$	Stefan-Boltzmann constant ( $5.67 \cdot 10^{-8} \text{ W m}^{-2} \text{ K}^{-4}$ )
$s$	State vector
$\theta$	Volume fraction
$t$	time (s or h)
$T$	Absolute temperature ( $^{\circ}\text{C}$ or K)
$\Delta T$	Temperature difference (K)
$u$	Darcy velocity ( $\text{m s}^{-1}$ )
$v$	Velocity ( $\text{m s}^{-1}$ )
$\dot{V}$	Volumetric flow rate ( $\text{m}^3 \text{ h}^{-1}$ )
$V$	Volume ( $\text{m}^3$ )
$\chi$	Block input vector
$\omega$	Surface emissivity
$z$	Elevation (m)



# 1 Introduction

## 1.1 Motivation: Thermal energy storage in the era of energy transition

Secure provision of thermal energy plays a key role in everyday life. In particular, the industrial and residential sectors of Central Europe represent substantial consumers [1,2], and for instance in Germany, more than half of the energy is used for heating [3]. Thereby, conventional primary resources for energy production are becoming scarce, energy prices are rising, environmental standards are being tightened, and the demand for alternative energy sources is growing.

The EUROPEAN UNION (EU) is committed to a fast decarbonization of the energy sector. This is not least defined by the *Fit for 55 package* [4] — as part of the *RePowerEU* plan [5] — and by the *Green Deal* [6]. In Germany, early efforts focused on the decarbonization of electricity, while the similarly important but more complex supply of thermal energy remained nearly overlooked [7]. Meanwhile, to reduce cost and the carbon footprint, the application of smart thermal energy systems that integrate multiple renewable energy sources is considered part of future heat supply standards. Due to the diversity of these sources, their integration for secure supply, however, is not trivial. The functioning and performance of a supply system need to be adjusted to the requirements of all sources and sinks. Meeting simultaneous heating/cooling demands of various sectors, such as residential and industrial, is only one challenge. To maximize benefits and minimize losses in such systems, production variations in the short and long term need to be compensated, and this may be achieved by thermal energy storage (TES) [8–10]. Therefore, innovative and cost-efficient technological solutions for TES are key for achieving the ambitious international climate targets, such as underlined by the *EC Recommendation on Energy Storage* [11], identifying TES elementary for promoting stable, reliable, and low-carbon heat supply.

TES enables peak shaving and minimization of total energy consumption. On the one hand, TES technologies are connected to sources for collecting energy when demand is low. On the other hand, they provide energy when there is high demand, but production cannot efficiently provide the desired loads. For minimizing relative heat loss in the long-term, especially large-scale TES is considered an essential component of future systems. A recent analysis [12] revealed a global TES market size of \$ 22.6 billion in 2022. Further, this market is expected to have an annual growth rate of 8.9% from 2022 to 2032.

The EU garnered the highest share of about 40% due to its described initiative on energy efficiency and renewable energy, the presence of key technology providers and a large number of users. Globally, the need for affordable low-carbon energy will even enhance the TES demand in the future. For example, as a consequence of increased energy use and employment of modern energy systems, especially the regions of North America and Asia Pacific are demanding suitable TES solutions.

## 1.2 Scope: Ground-based, closed-loop, large-scale seasonal thermal energy storage systems

Thermal energy storage can be employed for different time scales (diurnal vs. seasonal), and short-term TES are nowadays common for individual buildings in residential and industrial applications. In contrast, large-scale, seasonal thermal energy storage (sTES, one or two cycles per year) technologies enhance the usability of decentralized, locally generated thermal energy to be supplied to local district heating and cooling (DHC) networks. By collecting excess energy from industry, data centers, solar thermal, or geothermal systems, options for enhanced sTES use arise. Therefore, ideal sTES solutions are economically attractive based on a high capacity, efficient heat transfer and low costs for environmentally favorable materials, and if they retain their efficiency even after decades of operation.

The currently most common approach is sensible sTES, with water used both as heat carrier and storage medium [13]. One family of the technologies applied are geothermal solutions that utilize the natural subsurface (aquifer or borehole heat exchangers, ATES, BTES) or water-filled caverns (CTES) [14]. They are economically attractive but strongly dependent on the specific site conditions, e.g., shallow groundwater with minimum flow velocity for ATES, or ideally groundwater absence for BTES. As an alternative, to bypass these limiting factors, three concepts of artificial, ground-based, large-scale technology concepts for sTES have emerged: Pit Thermal Energy Storages (PTES), Tank Thermal Energy Storages (TTES) and Water-Gravel Thermal Energy Storages (WGTES) [15]. These different types are distinguished by their construction, the components used, as well as the applied materials: While PTES are large sloped pits, which are usually only sealed with a plastic liner, filled with water, and insulated at the top surface, TTES are more complex facilities with various geometries. Such geometries are enabled by the installation of static components, such as concrete walls. WGTES, in contrast, are distinguished by their two-component filling and thus more sophisticated loading systems.

Such technically enclosed variants have been in the scope of extensive research programs for more than 25 years, including several pilot and demonstration facilities in Germany [16–18], Denmark [19], and Sweden [20]. These installations were designed mostly for the storage of solar energy from summer to winter, and many of them are still in operation. The gained experience with earlier variants of TTES, PTES, and WGTES has been the basis to further develop “4<sup>th</sup>-generation multifunctional systems”. These advanced concepts apply to a broader variety of use cases, not only for heating in residential areas, and they can respond better to variability in source availability and demand such as in industrial districts [13]. The evolution and further development of ground-based, closed-loop, large-scale sTES is fundamental for reliable low-carbon heat supply and thus also at the fore of this presented thesis.



### 1.3 Key barriers of seasonal thermal energy storage application in practice

The rising demand for thermal energy, enhanced infrastructures, and deployment of decentralized renewable energy is encouraging a disrupting shift in the energy sector. Thereby, the role of sTES must be strengthened through optimized installations, which can be integrated as robust elements into the diversity of DHC systems. Still, seasonal storage, in contrast to diurnal storage, is not common practice. This thesis offers new pathways for further sTES development that address technical, economic, as well as regulatory, and environmental aspects (FIG. 1.1). In the following, the barriers hampering full market availability of the sTES technology are exposed. These serve as the basis for motivating the objectives of the thesis.

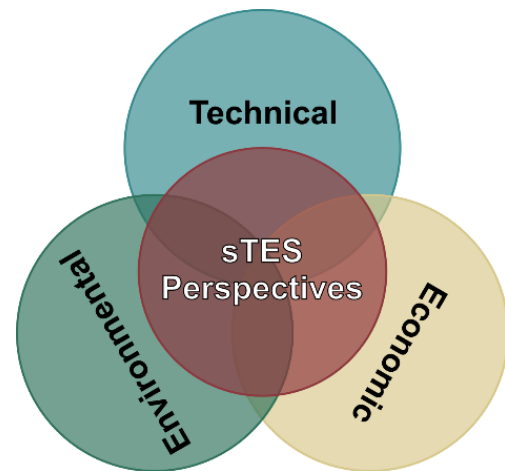


Fig. 1.1: Key perspectives on seasonal thermal energy storage.

The first critical technical issue is the weakness of sTES building components. To minimize energy losses, different materials for sealing and thermal insulation are used [21]. Recently, there has been continuous progress in the refinement of these components, but still, most of the available concepts for efficient sealing and insulation are not satisfying. The major remaining challenges include defective sealings or long-term material fatigue. This was observed, for example, at the 3,000 m<sup>3</sup> large PTES in Herlev (Tubberupvaenge, Denmark, [22]), and the TTES in Hoerby (500 m<sup>3</sup>, Denmark, [23]). The second technical issue is the short- and long-term understanding and optimal control of internal hydraulic and thermal conditions. For the robust integration of sTES into energy systems, one challenge is to maximize the overall technical efficiency, i.e., to minimize thermal losses during operation. Even though energy losses are reported to be reducible to 10%, the previously realized sTES revealed values of no less than 30% [24]. To reach optimum storage efficiency and minimize primary energy demands, several scientific innovations are required. Among these, improved models and benchmarks are needed as adaptive tools to define optimum designs. Thereby, the accuracy of model prediction has to be balanced against computational demand, and the improved or new tools have to be applicable for rigorous sensitivity analysis, to cover, e.g., effects of geometry (i.e., size, shape), landscape integration, or materials (e.g., insulation) and their required cubature.

The first economic issue relates to the risk of malfunctioning sTES sealings described above. Even if this occurs only after decades, it may result in dramatically increased thermal losses over several years or even in total failures, turning an entire project uneconomical. Secondly, a considerable need for large-scale sTES is faced with enormous construction and operational costs (FIG. 1.2). Aside from this, growing numbers of sTES mean growing space requirements, which may be technically and economically prohibitive, especially in urbanized areas [25]. Consequently, the economic attractiveness of future sTES installations needs to be strengthened by achieving specific costs, while maintaining the storage capacity (FIG. 1.2). The third

economic key issue relates to the previously described uncertainties and deviating efficiencies in sTES operation, which lead to a lower level of investor commitment. Especially during operation, in the case of incorrectly anticipated and insufficient storage efficiencies, and hence a reduced self-consumption of energy in the system, cost-intensive use of primary energy sources must be increased.

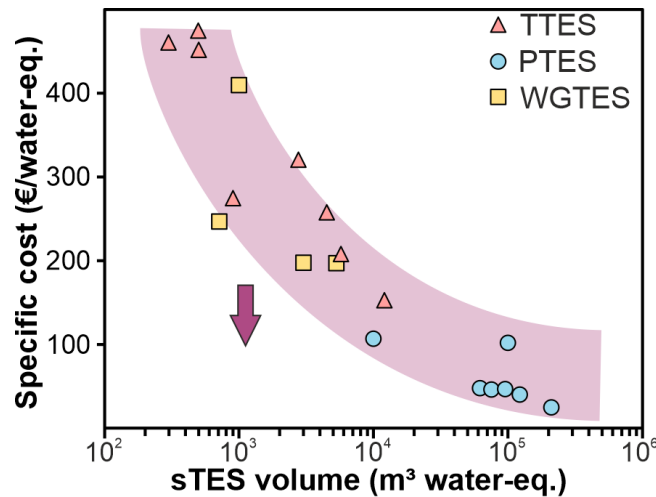


Fig. 1.2: Specific cost of seasonal thermal energy storage projects compared to their storage capacity (after [14] and [26]).

Referring to the environmental perspective, conditions in the subsoil are usually largely uncertain [27,28]. Ground-based, basin-sTES may continuously release heat into soil and groundwater, and this is assumed to be one main reason why predicted efficiencies and amortization periods are often not achieved. Especially in the case of adverse environmental conditions (e.g., due to a suboptimal geometry of a basin and/or high groundwater flow velocity), comprehensive knowledge about the operational characteristics of sTES embedded in the subsurface is required. In contrast, thermal and hydraulic properties of the environment, and site-specific thermal energy losses towards the underground are commonly neglected. Another barrier related to the environmental dimension is associated with legal requirements. These especially refer to allowed temperature conditions in the surrounding subsoil and groundwater [29,30]. So far, little attention has been given to local environmental and ecological effects, although sTES may create unnatural thermal conditions with potentially adverse implications [31].

## 1.4 Objectives of this study

The overall goal of this thesis is to achieve technical, economic, and environmental improvements for ground-based, large-scale sTES. For this, three specific objectives are formulated:

The first objective is to improve the technical components of sTES and enhance the robustness of the technology, as one key factor for reaching a higher market maturity. By developing improved insulation and sealing components, the project aims at a reduced risk of failure, while simultaneously achieving improved efficiency. Further, the purpose is to reduce thermal losses to mitigate environmental impacts associated with ambient temperature increase.

The second objective is further development of modeling and planning tools for sTES. Enhanced models for the analysis of internal and external sTES behavior aim at improving storage performance and operation prediction capabilities. Moreover, more favorable economic conditions can be achieved since integrated planning tools are crucial to demonstrate market competitiveness. Besides, improved modeling tools for the subsurface domain are key to understand long-term environmental and ecological impacts. Finally, they are needed to ensure safe operation and compliance with legal threshold values over the entire lifetime of sTES.

To finally tackle the different key barriers simultaneously, a third objective is to examine a fundamentally new concept. Investment costs of previous sTES are dominated by expenses for excavation, static components, and sealing layers [32,33]. In contrast, this research focuses on the re-use of existing structures to enable significant cost reductions: If existing basins can be re-used as sTES, cost-intensive steps associated with new construction are omitted.

## 1.5 Overall methodology and implementation of research

### 1.5.1 Applied research at the IN-Campus site in Ingolstadt (Germany)

The main reference case for the research of this thesis is located in Ingolstadt, Germany. There, IN-CAMPUS GMBH, a joint venture of AUDI AG and the city of Ingolstadt, is constructing a new research and development (R&D) campus (“IN-Campus”) on a former refinery site. The total area (FIG. 1.3 a) of the brownfield is more than 750,000 m<sup>2</sup>. In four construction phases, up to 70 buildings will be used for innovative R&D topics based on different use types (office, workshop, test benches, virtual development, etc.) [34]. During the initial construction phase (2021 to 2023) the first buildings are being completed, which offer space for 1,400 workers. The three further phases are planned for the next decade [34]. Synchronous with this development, the energy demand will grow dynamically, and accordingly, a dynamically adaptive planning strategy for optimal energy supply is needed.

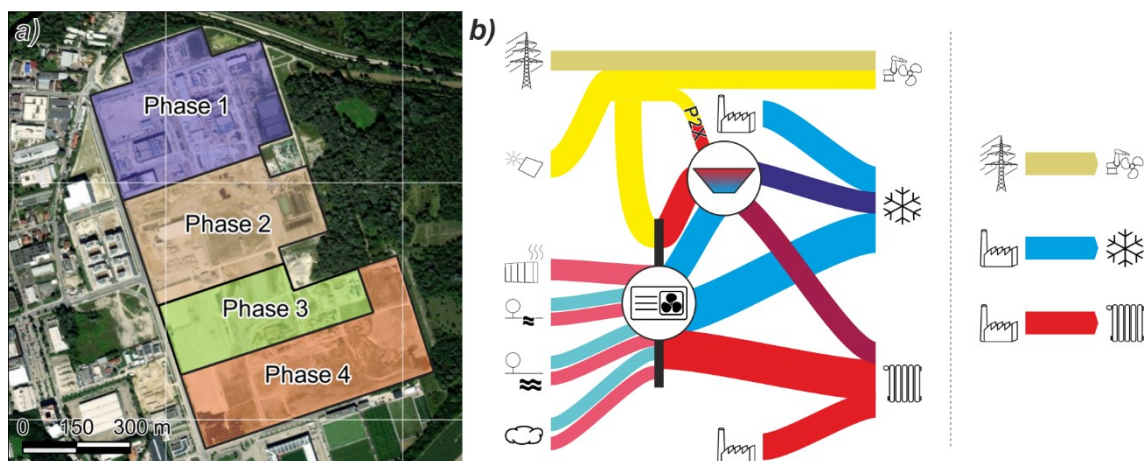


Fig. 1.3: a) Schematic construction schedule of the IN-Campus; b) illustration of the envisioned, innovative, dynamic energy system (left) compared to a conventional energy system approach (right; after [35]).

The energy supply at the site is planned to be autarkic, low-carbon, and highly efficient, and the conventional approach of energy supply has thus been replaced by a smart concept that interconnects all thermal energy sources and sinks (FIG. 1.3 b)

[35]. An uninsulated low-temperature (max. 35 °C) grid is being established for controlled management of decentralized facilities (e.g., reversible heat pumps, different renewable sources, waste heat). The aim is to supply at least 85% of thermal energy via renewable sources and to actively employ peak shaving and load-shifting mechanisms [34]. Thereby, costs and primary energy demands (e.g., for active cooling) are to be minimized. During the initial planning phase, the thermal energy demands were prospected as 26 MW for cooling and 20 MW for heating at the end of the last construction phase [35]. Given the climatic conditions and high construction standards, the demand for cooling will exceed the heating demand by 20 to 30%.

The IN-Campus represents a unique opportunity for the further development of the sTES technology. There, the described advantages are complemented by high expected economic and ecological benefits resulting from innovative sTES solutions. The required adaptive planning of energy supply is ideally realized by the support of applied research activities that validate and demonstrate innovative concepts.

At the IN-Campus, basins exist that (FIG. 1.4) were formerly used for storage of water for firefighting, as well as for water treatment (activation, clarification, post-aeration). These artificial basins may be re-used for storage of (excess) thermal energy. Given a total volume of almost 29,000 m<sup>3</sup> (excluding retrofitted sTES components) [36], a complete re-use would constitute the largest multi-sTES closed-basin facility in Europe. Ideally, a multifunctional solution for heat and cold storage, operating both seasonally and as a short-term buffer, is developed. In contrast to conventional sTES strategies, this system would not only store heat generated by solar energy but also excess thermal energy at different temperatures from a variety of sources.

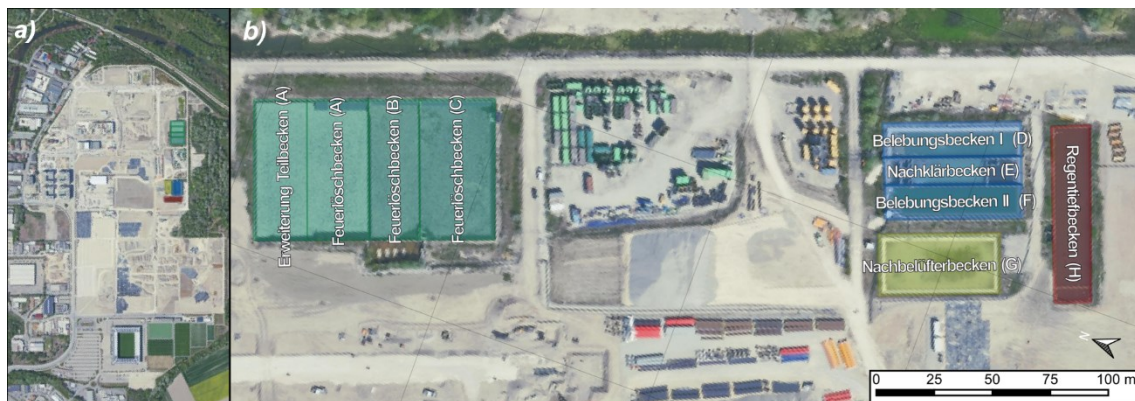


Fig. 1.4: a) Overview of current construction phase at IN-Campus; b) zoomed, re-oriented view of in-ground, basin infrastructure for transformation into seasonal thermal energy storage units.

The re-use strategy avoids costs for demolition and construction of new basin structures. Also, by implementation as WGTES, the basin surfaces can be used e.g., as green spaces or for parking. However, re-using existing structures restrains the flexibility of the sTES design (e.g., surface/volume ratio). In this case, efficiency predictions are complex and need to be tailored to the given site conditions. Besides innovative approaches to increase the efficiency of individual components, new strategies are required, since conventional planning practices are not suitable for the activities planned at the site. Challenges relate to the degree of freedom in sTES type selection, planning, installation, and operation strategy, altogether with the necessary integration into a highly optimized local district energy system.

### 1.5.2 Laboratory experiments for testing paraffin wax as an innovative concept for combined sealing and insulation

Lateral heat losses in the case of existing large-scale, ground-based sensible sTES substantially increase associated technological costs [37]. Conventional sealing solutions based on plastic are often subject to leakage, while a repair is estimated impossible, especially for gravel-based systems sTES [38,39]. To overcome these issues, the development of a novel, thermally insulating, self-sealing sTES component utilizing paraffin wax, is proposed and examined in laboratory experiments.

Based on the physical properties of paraffin wax as a common storage material of latent TES [40,41], the proposed new strategy suggests this material as a thermal insulator of sensible sTES. The underlying hypothesis is that the low thermal conductivity of solid paraffin prevents lateral heat loss, while phase change effects intentionally absorb energy, and this lowers the temperature gradient inside this component. In addition, the application is expected to exploit this induced phase change for automatic sealing: liquefied paraffin can actively flow through defects, cool again, and impede loss of further thermal energy and storage filling material (i.e., water for sensible sTES) due to its hydrophobic behavior.

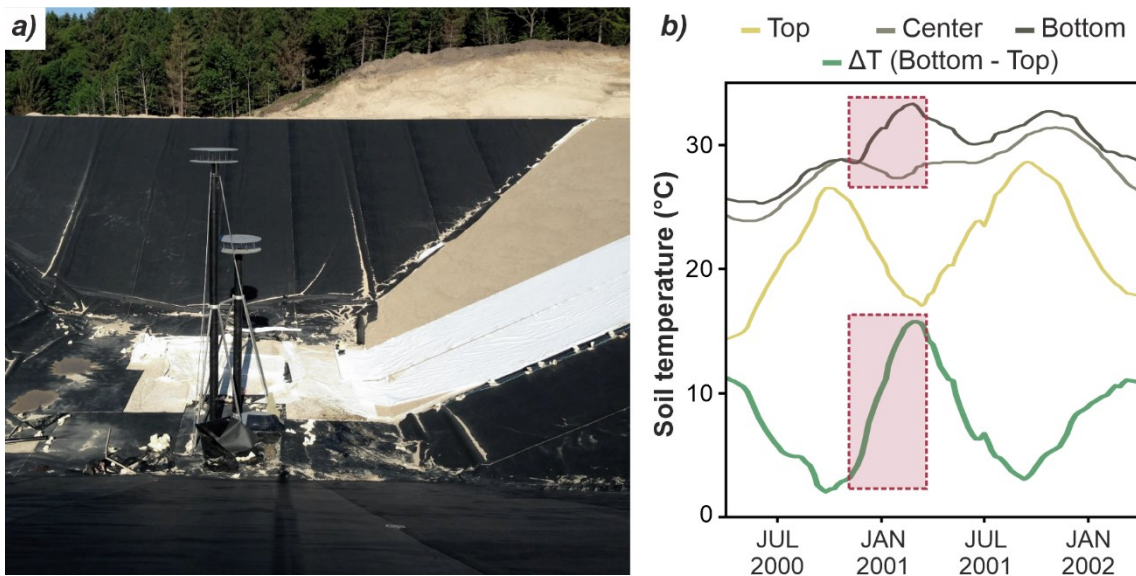


Fig. 1.5: (a) State-of-the-art engineering methodology for the construction of a Pit Thermal Energy Storage with welded plastic liners as sealing component shown by the example of Dronninglund, Denmark [42]; (b) observed temperature increases induced by leakage at probe points [43] adjacent to the sidewalls of the Tank Thermal Energy Storage facility in Friedrichshafen, Germany (after [37]).

Due to the unknown practical behavior of the material and the complex coupled thermal-hydraulic-mechanical processes involved, this entails a substantial risk of failure [44,45]. In comprehensive laboratory experiments, sTES operation conditions with temperatures beyond the melting point of paraffin are resembled. Detailed visual and temperature monitoring are employed to reveal thermal and hydraulic insulation performances for different design variants. The tests reveal the general feasibility and potential of this concept. Furthermore, detailed and scaled effects of phase change and flow on the efficiency of the new, combined sealing-insulation component are addressed.

## 1.6 Structure of the thesis

This dissertation is prepared as a cumulative thesis and is therefore constituted by three individual, peer-reviewed, published scientific papers, as reflected in Chapters 2 to 4. Further, Chapter 5 represents a fourth manuscript submitted to a peer-reviewed journal.

Chapter 2 provides an in-depth analysis of the state of the technology of water-based, closed, seasonal thermal energy storage systems. This chapter therefore sets the scope for the specific research presented in the following chapters.

To tackle the technological and technical weaknesses of sTES construction components via a novel approach, laboratory experiments with paraffin wax are detailed in Chapter 3. After the description of the methodology, its implementation in the laboratory, and evaluation of the experimental data, interpretations are derived on the feasibility, practicability, and potential of combined thermal insulation and sealing with paraffin wax.

The study in Chapter 4 provides a different dimension for the multifaceted improvement of the reliability and performance of sTES. Here, a novel, dynamic, component-resolved model “STORE” is developed, which particularly focuses on the design and planning stage of WGTES in re-used infrastructures. Following a description of the underlying model approach and based on an in-depth analysis of the state of the art for modeling sTES, the structure of the new model, its underpinning thermal mechanisms, and its implementation in the MATLAB/SIMULINK software environment is given. Subsequently, the validation of the model and a comprehensive synthetic parameter study are presented. General conclusions and construction recommendations are derived, and the remaining weaknesses are discussed, which relate, in particular, to the reproduction of environmental processes (especially concerning hydrogeological influences).

To eliminate these identified shortcomings and to further address the perspective of environmental barriers in the field of sTES, Chapter 5 presents a refinement of the STORE model. An innovative, previously rarely used approach of co-simulation between two ideally customized modeling tools is employed. By coupling the STORE model, used for accurate internal storage modeling, with a 3D multiphysics model in COMSOL, the study enables the capture of heterogeneities as well as asymmetric boundary conditions in the surrounding subsurface. The chapter presents the applied modeling approach for a synthetic parameter study in which the influences of different subsurface conditions on a WGTES are explored. Based on this, enhanced sTES performance prediction accuracies and estimates of local environmental impacts are interpreted and summarized.

Ultimately, based on the scientific studies in Chapters 2 to 5, Chapter 6 summarizes key conclusions and confronts the research questions addressed in the introduction to the advances achieved by the different studies. Finally, the chapter outlines and discusses further research efforts required in the area of sTES.

## 2 State-of-technology review of water-based closed seasonal thermal energy storage systems

This chapter is reproduced from:

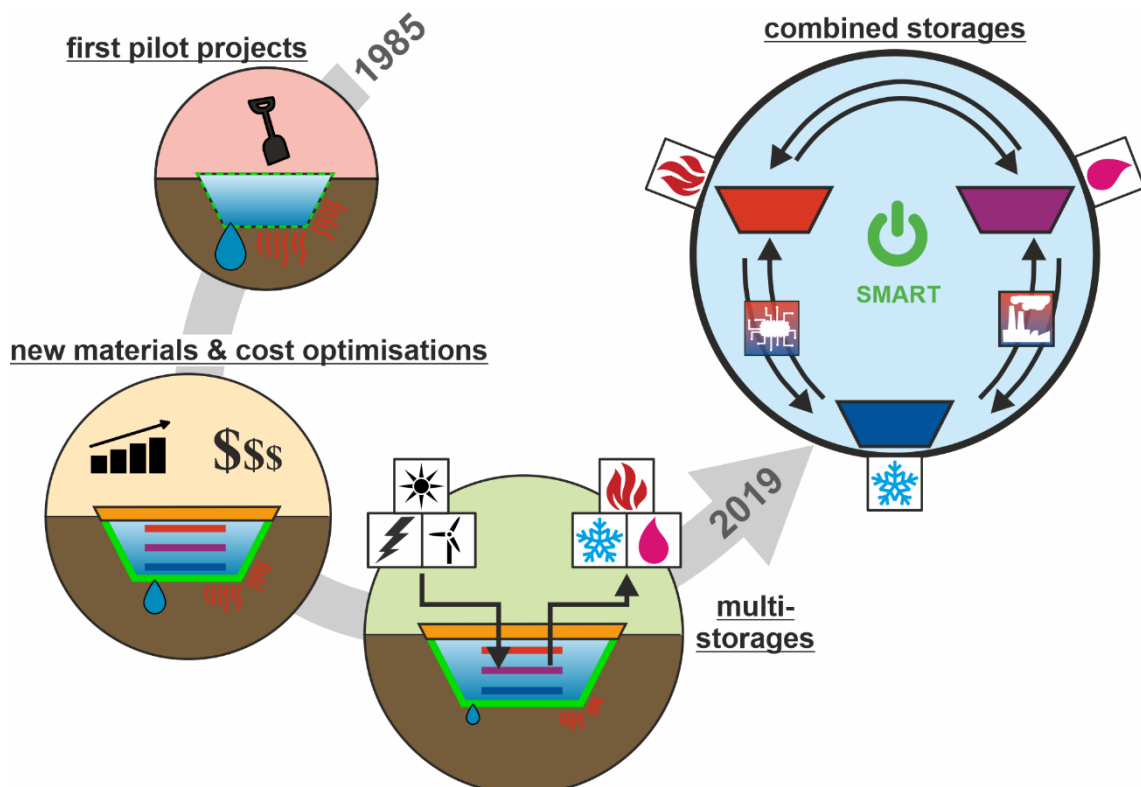
**Bott, C., Dressel, I., & Bayer, P. (2019).** State-of-technology review of water-based closed seasonal thermal energy storage systems. *Renewable and Sustainable Energy Reviews*, 113, 109241, DOI: 10.1016/j.rser.2019.06.048.

The study was financially supported by the Volkswagen Foundation and the Bavarian State Ministry of Education and Culture, Science and the Arts within the framework of the "Programm zur Förderung der angewandten Forschung und Entwicklung an Hochschulen für angewandte Wissenschaften – Programmsäule Strukturimpuls – Forschungseinstieg".

### Highlights

- ▷ Review of variants for water-based closed seasonal thermal energy storage (TES).
- ▷ Analysis of all construction elements of seasonal TES based on 31 systems in Europe.
- ▷ Definition of barriers to overcome for market maturity of the selected technologies.
- ▷ Revelation of innovative attempts to utilize overlooked potentials of presented TES.

### Graphical abstract



## 2.1 Introduction

Sustainable energy management aims to reduce the carbon footprint by utilizing higher shares of renewables through smart coordination of centralized and decentralized supply, and by integrated storage concepts. Future energy supply, ideally, relies on a combination of mostly fluctuating renewable sources such as wind, biomass, solar, and geothermal energy [46,47]. These sources are especially needed for decarbonization of the heating, cooling, and hot water supply sector which is responsible for a large fraction of energy consumption. Today, however, worldwide space heating and hot water production is dominated by burning fossil fuels. Since 2010, despite auspicious green energy plans on all political levels, global direct emissions from heating in buildings have not declined, representing the fastest growing end-use in buildings [48].

The slow pace of sustainable energy transformation has many causes, one being the high dependency of renewable sources on environmental conditions. These are difficult to describe, predict, and quantify for guaranteeing a reliable supply. Thermal energy storage systems (TES) offer the opportunity to collect the thermal energy from different fluctuating renewable and non-renewable sources independent of the demand and to transfer temporarily available energy into permanently accessible energy. Thermal energy storage allows peak shaving of cost-intensive energy productions [15,49]. In combination with renewable energies, it ultimately facilitates savings in heat consumption on the one hand and substitution of heat provided by fossil fuels on the other [50–53].

All types of energy storage systems are equipped with a storage medium and a loading and unloading system. At times of low demand and high supply, the storage is charged to enable low-loss provision at times of shortage and high demand. TES are differentiated from other types of storage by their low price, longevity, and sufficiency of resources [54]. According to SOCACIU [55], there exist various methods of classification. For instance, they differ with respect to storage material (sensitive, latent, thermochemical), and in their technological concepts (underground, hot water, and above ground, use of phase change materials (PCM), thermochemical storage [49]). In practice, sensible heat storage is still most common [55–58]. During recent years, attention has been growing towards seasonal sensitive heat storage. This is especially of interest for storing the huge surplus of solar heat collected during summer, thus compensating for the limited availability of solar heat during the primary heating period in winter (FIG. 2.1). Seasonal applications differ fundamentally in their requirements and designs from diurnal storage systems and are more difficult to apply. Long-term or seasonal TES have only one to two cycles per year [59]. Clearly, such long-term storage of sensitive heat requires a substantial volume of storage space. Only large-scale applications can meet the heat demand for months while minimizing the continuous conductive heat loss during storage.

The best-known types of seasonal TES variants are aquifer storages (ATES), borehole storages (BTES), cavern storages (CTES), pit storages (PTES), and seasonal tank storages (TTES). ATES, BTES, and CTES are geothermal applications utilizing natural ground that is mechanically not contained [60]. In the present study, the focus is exclusively on a family of closed artificial storage systems, which are less dependent



on (hydro-) geological boundary conditions and therefore conceivable at almost any location [61,62]. This work reviews the current technological status of closed seasonal TES based on the information which is widely dispersed in heterogeneous scientific literature sources and languages. This is complemented by the experience reported from the growing number of applications in practice, in order to arrive at a condensed overview of the state-of-the-art storage systems.

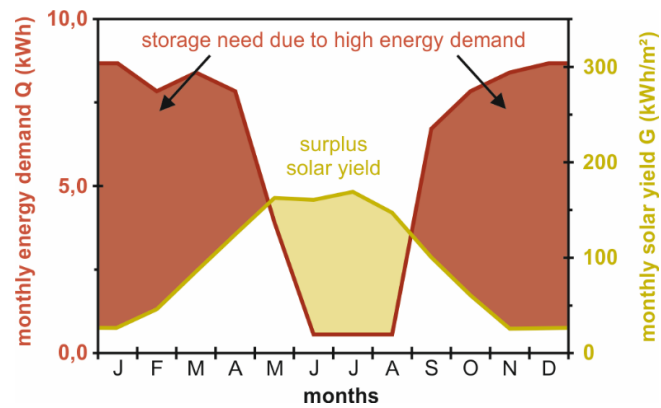


Fig. 2.1: Heat demand and solar heat yield of a hypothetical example household in Munich, GER (heated area:  $150 \text{ m}^2$ , energy demand:  $70 \text{ kWh}/(\text{m}^2 \cdot \text{a})$ , solar thermal area:  $10 \text{ m}^2$ , long-term efficiency: 0.5).

Since water is the most common seasonal heat storage medium by far, the scope of this study is only on water-based TES. As major categories, solely water-based technologies and those with multi-component filling materials are distinguished (FIG. 2.2). Exclusively water-based technologies are either TTES systems, which represent constructed basins that stick partially or completely out of the ground surface, or water-filled sealed pits (PTES) without any structural element for stabilization. All applications with a multi-component filling material are classified as Water-Gravel Thermal Energy Storage systems (WGTES). Strictly speaking, gravel is not always used for WGTES in practice, and thus multi-component-based variants can be further subdivided into earth-water and gravel-water storages according to their filling [63]. For convenience, however, these variants are not separately discussed here.

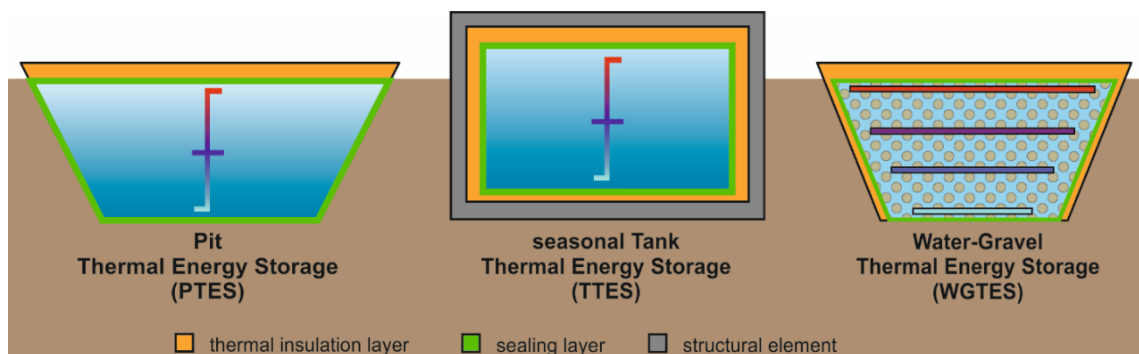


Fig. 2.2: Schematic layouts of the systems selected for further analysis.

In the following paragraphs, first, a statistical view is presented, also including the historical evolution of large-scale closed TES. Furthermore, the developments of closely related large-scale non-seasonal heat storage buffers are shown. Although their type of usage varies from those of PTES, WGTES, and TTES, there exist common technological features, and therefore buffers are added here for comparison.

Then, the technological characteristics such as fillings, structural components, thermal insulations, waterproofing methods, and construction techniques are examined. The regional focus is set on Europe, where the major developments in seasonal TES have been installed.

## 2.2 Evolution and statistics of seasonal thermal energy storage in Europe

### 2.2.1 Historical development

Well-known early, pre-industrial applications of long-term thermal energy storage were subsurface depots of ice used to conserve food. The recent history of closed seasonal TES (FIG. 2.3) can be traced back to 1959 when MARGEN [64] presented a first technically sophisticated attempt for seasonal storage of thermal energy in subsurface rock chambers. A few years later, BRUN [65] published ideas for storing solar energy in the subsurface. However, both studies represented mainly theoretical thoughts without any practical applications. According to FLEUCHAUS et al. [60], SOCACIU [66], COLCLOUTH [67], and PAVLOV & OLSEN [68], pioneering works can be found especially in the early 1970s when the oil crisis raised public awareness of the importance of energy supply (FIG. 2.3).

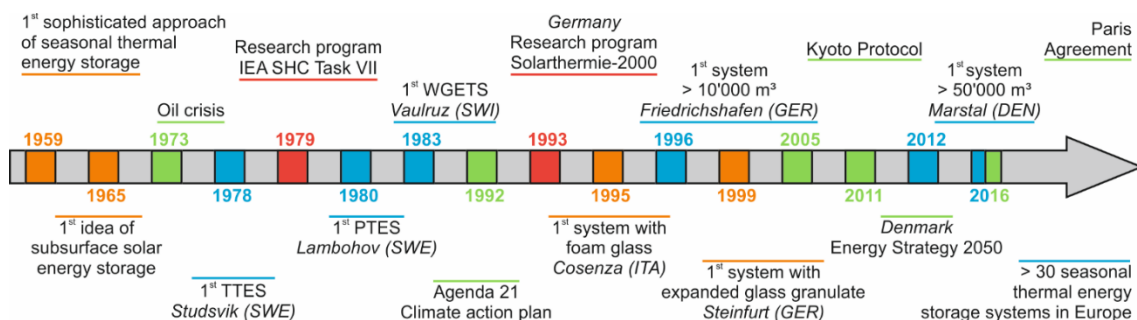


Fig. 2.3: Timeline showing some of the important steps in the history of the development of seasonal Thermal Energy Storage (orange: inventions; green: climate actions; blue: milestone systems; red: research activities).

The first buried closed seasonal heat storage system was built in 1978 as a PTES in Studsvik (Sweden) and had a volume of just 800 m<sup>3</sup> [69]. WGTES projects were first realized in 1983 in Stuttgart [70] and Vaulruz (Switzerland, [63]). A few years later, the appearance of central solar heating plants with seasonal storage (CSHPSS) was an additional factor to push the research from 1980 onwards [71]. During this time, Sweden was leading the technology with many projects (e.g., Studsvik [69], Ingelstad [20,72], Lambohov [20,23], Malung [73]) focusing on solar power generation and the development of a strategy with seasonal solar thermal energy storage systems [62]. In these years, the technology of seasonal storage also got attention from the International Energy Agency Solar Heating & Cooling Programme (IEA SHC), mostly under Task VII “Central Solar Heating Plants with Seasonal Storage” carried out from 1979 to 1988 [69]. According to this program, knowledge and commitment of 18 IEA member states were brought together, resulting in the definition of basic concepts and designs [74,75], methods for cost analysis [76], and a significant number of project sites, e.g., Herlev (Denmark), Stuttgart, Ingelstad, and Vaulruz.

Apart from research on how to store energy for longer times, international climate treaties (e.g., Agenda 21 climate action plan in 1992 or Kyoto Protocol in 2005) represented important motivations for the development of new technologies. With the Paris Agreement in 2016, new applications and further developments in combination with renewable energy sources will also be needed in the future.

Most of the existing seasonal TES are located in Germany and Denmark. This is the result of several dedicated research programs in these countries. In Germany, these were, among others, the programs Solarthermie-2000 (1993-2002, [53,77,78]) and Solarthermie2000-plus (2004-2008, [16,53,79,80]). In Denmark, the main driver for developing new energy technologies was the government's "Energy Strategy 2025" (published in 2005) and the "Energy Strategy 2050" (published in 2011) with an ambitious goal to achieve an energy market independent of fossil fuels (FIG. 2.3, [81]).

Apart from storing only heat in storage systems, combined systems for heating and cooling in the context of district heating and cooling networks were already proposed in 1997 for WGTES [82]. A corresponding test was conducted at the storage facility in Stuttgart, which had been built in 1985 [70], proposing a heating and cooling concept to develop the technology further. More recently, LÓPEZ-VILLADA et al. [9] discussed various locations in Spain with special focus on the respective climatic conditions. Annual energy demands for cooling and heating were estimated and numerical simulations showed that solar district heating and cooling systems with long-term storage can be an economically viable alternative to conventional systems.

### 2.2.2 Numbers, volumes and spatial distribution

Since the first construction of a seasonal TES in 1978, there has been a small but continuously growing number of systems installed (FIG. 2.4 b). Around 1995, an increase in the total number of seasonal TES was stimulated by the research programs in the early 1990s. Among the technological variants (FIG. 2.4 a), TTES were most popular with a significant rise in installed systems around 1995. The PTES were less popular than TTES from 1978 to 1995, but their number increased at almost same rate. There was a pause from 1995 to 2012, then after new systems were built again in Denmark (e.g., Marstal [83,84], Dronninglund [42,85,86], FIG. 2.4 a). The past development of WGTES was similar to that of PTES; however, constant growth in numbers was found without interruptions. In contrast to the seasonal storage systems, sizeable heat buffer storage applications were listed first in 1999 with an installation in Aeroeskoebing (Denmark [19,87,88]). Subsequently, the number of these systems stepped up rapidly. This was caused particularly by the growing popularity of district heating in countries such as Denmark (Samsø [89]), Austria (Linz [90], and Salzburg [54,91]), and Germany (Nuremberg [92]).

The evolution of the installed storage volume shows a moderate development until 2010 (FIG. 2.4 c). This is due to the initial construction of only smaller systems within pilot projects. From 2010 onwards, a nearly exponential trend is found in the total installed volume, being coincident with the recently rising number of PTES (FIG. 2.4 a). FIG. 2.4 c shows the total installed storage volume for each year, whereas FIG. 2.4 d depicts the average size of the single installed storages. On this basis, it is evident that the exponential volume increase is not the result of an exponential increase in the number of built systems (FIG. 2.4 b), but that the volumes of individual systems (FIG.

2.4 d) have followed an exponential growth trend since 2010. To date, the largest seasonal storage facility is located in Vojens (Denmark) as a PTES with a volume of around 200,000 m<sup>3</sup> of water at a former gravel pit [42,84,93,94]. In contrast, until 2010, the largest seasonal storage system only had a volume of 12,000 m<sup>3</sup> (TTES Friedrichshafen, Germany [24,82,87,95,96]). Due to their more challenging design, the typical WGTES is smaller in size, with the largest plant situated in Eggenstein (Germany), having a volume of 4500 m<sup>3</sup> [97–99]. In summary, the exponential growth of total storage volume and average individual storage volume is in contrast to the almost linear development of the number of systems. This clearly points towards a trend of larger facilities during the last decade, stimulated by ongoing technological advancements, experience, and economies of scale.

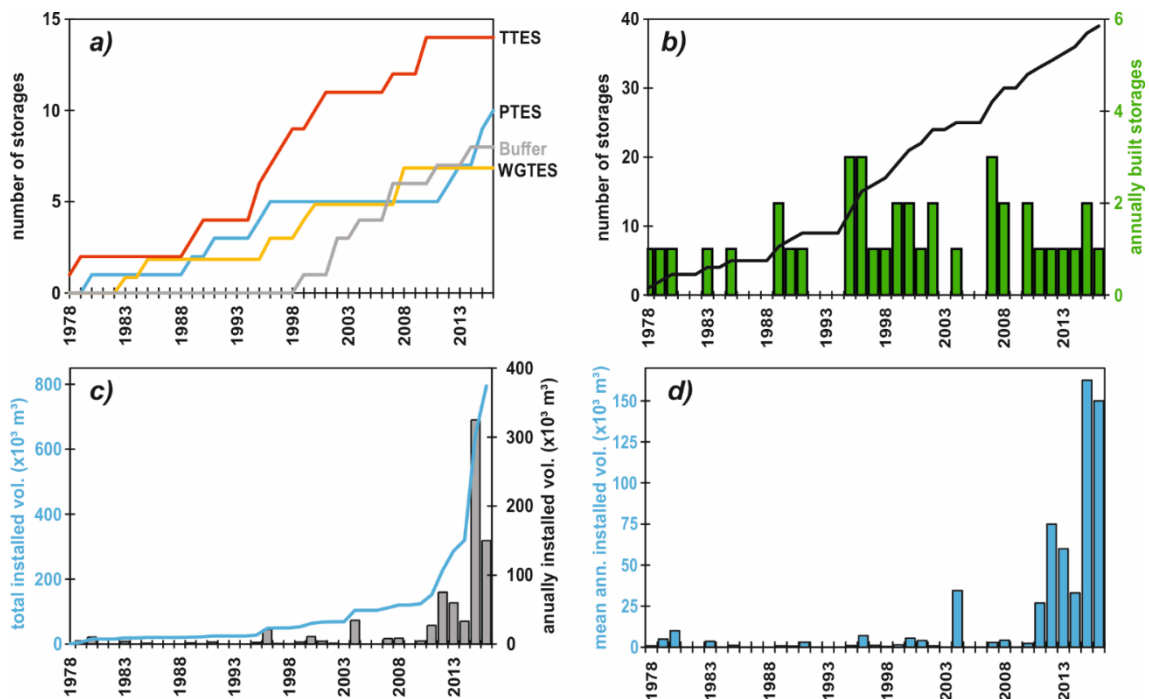


Fig. 2.4: a) Evolution of the number of different seasonal storage systems and large storage buffers. b) Development of the total number and annual newly built systems (TTES, PTES, WGTES and large storage) and cumulative number of storages (black line). c) Development of the installed volume in Europe for seasonal thermal energy storage (TTES, PTES, WGTES, incl. large buffer storage) with annual newly-installed volumes. d) Development of the average size of newly installed seasonal storage systems (TTES, PTES, WGTES) and large buffer storages.

Considering the present-day state statistics, it is also useful to differentiate between the various types of thermal energy storage (TAB. 2.1). Apart from seasonal systems (PTES, WGTES, TTES), there is also a relevant number of sizeable short-term buffer storage systems. Regarding these four types of storage systems, TTES are predominant, followed by PTES and WGTES. Although the number of PTES is lower than the number of TTES, the volume of PTES is larger than that of any other storage system, both in terms of individual storage volumes and the total sum of all storage volumes in Europe (FIG. 2.5). It is also noticeable that WGTES are on average larger than TTES, but at lower total volume. This is because WGTES balance their reduced heat storage capacity due to the use of gravel by a larger volume.

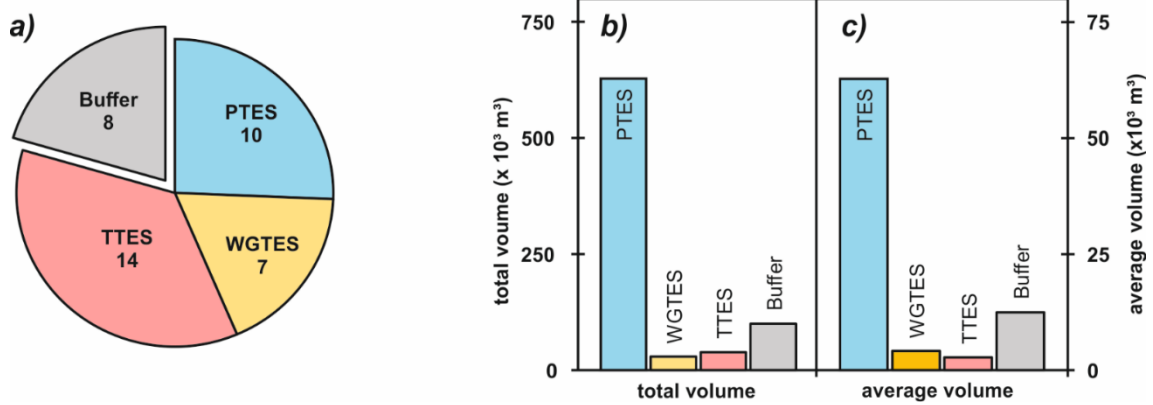


Fig. 2.5: a) Installed number of different TES types compared to b) the total available installed storage volume and c) the average individual storage volumes.

The distribution of seasonal thermal energy storage locations varies geographically in Europe (FIG. 2.6 a). In total, our survey identified 39 storage facilities. Most systems are installed in Germany, followed by Sweden, Austria, Switzerland, and Italy (FIG. 2.6 a, FIG. 2.6 b, TAB. 2.1). Because of the recent developments with several large-scale applications, the greatest storage volume is installed in Denmark, followed by Germany, Austria, Sweden, Switzerland, and Italy (FIG. 2.6 c). This is a result of the continuous research activities and public interest that stand out in these countries.

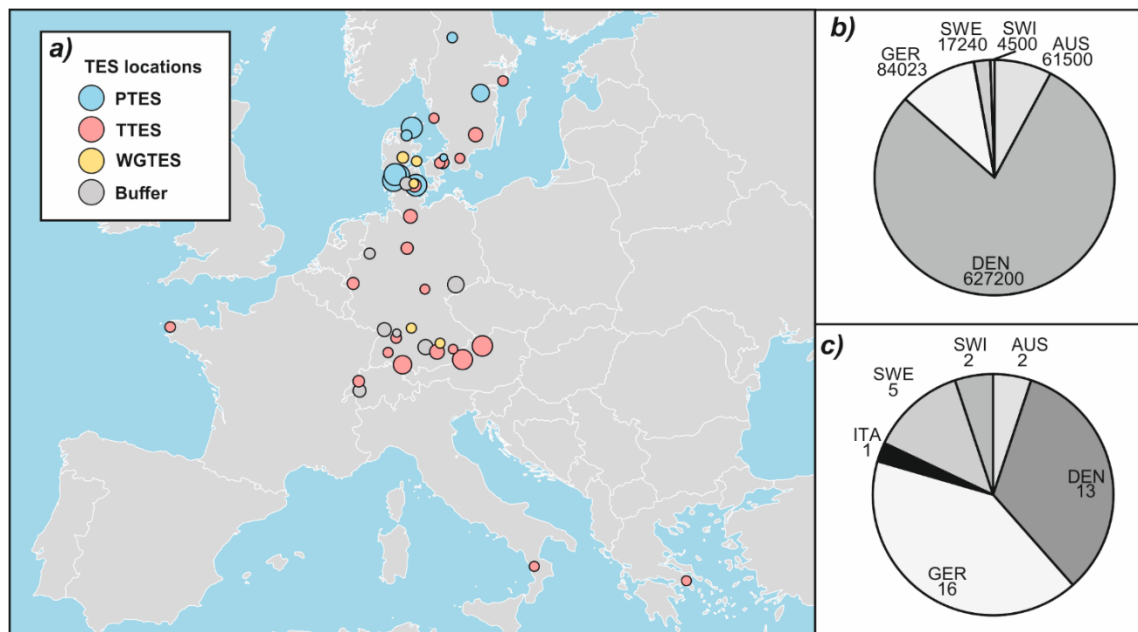


Fig. 2.6: a) Map showing the locations of the different seasonal storage types, including large buffer storages in Europe, b) country-wise installed volumes (m<sup>3</sup>) and c) numbers.

Tab. 2.1: Overview of all seasonal thermal energy storage and large buffer storage locations recorded in this survey.

#	Name	Year	Country	Storage type	Volume (m <sup>3</sup> )	Water equivalents (m <sup>3</sup> )	References
1	Lambohov	1980	SWE	PTES	10,000	10,000	[15,58,69,100–102]
2	Malung	1989	SWE	PTES	800	800	[101,103]
3	Herlev (Tubberupvaenge)	1991	DEN	PTES	3,000	3,000	[19,22,58,68,69,86,101,104–106]
4	Ottrupgaard	1995	DEN	PTES	1,500	1,500	[20,22,62,70,73,86,87,101,105,107–109]
5	Jülich	1996	GER	PTES	2,500	2,500	[15,101,107,110]
6	Marstal (SUN STORE 4)	2012	DEN	PTES	75,000	75,000	[83,91,107,109,111–113]
7	Dronninglund	2013	DEN	PTES	62,000	62,000	[42,85,101,102,109,111,114]
8	Gram	2015	DEN	PTES	122,000	122,000	[84] [42] [114] [115] [116]
9	Vojens (1+2)	2015	DEN	PTES	203,000	203,000	[91,93,94,117,118]
10	Logumkloster	2016	DEN	PTES	150,000	150,000	[118,119]
11	Studsvik	1978	SWE	TTES	800	800	[100,101,105,107]
12	Ingelstad	1979	SWE	TTES	5,000	5,000	[15,20,50,68,69,72]
13	Särö	1989	SWE	TTES	640	640	[69,70,73,101,105–107]
14	Hoerby	1990	DEN	TTES	500	500	[15,22,57,72,101,120–122]
15	Rottweil	1995	GER	TTES	597	597	[15,70,82,123–125]
16	Cosenza (Calabria)	1995	ITA	TTES	500	500	[15,126,127]
17	Friedrichshafen (Wiggenhausen)	1996	GER	TTES	12,000	12,000	[16,51,70,77,82,87,95,96,101,124,128–130]
18	Neuchatel	1997	SWI	TTES	1,000	1,000	[20,49,57,87,131]
19	Ilmenau	1998	GER	TTES	300	300	[73,78,124,125,132–134]
20	Hannover (Kronsberg)	2000	GER	TTES	2,750	2,750	[16,51,79,95,124,128,135,136]
21	Rise	2001	DEN	TTES	4,000	4,000	[86,114,119,137,138]
22	Munich (Ackermannbogen)	2007	GER	TTES	5,700	5,700	[17,24,51,79,87,95,128,139–141]
23	Hamburg (Bramfeld)	2010	GER	TTES	4,500	4,500	[24,51,59,62,70,79,87,107,129,134,135]
24	Mühdorf	2010	GER	TTES	16.4	16.4	[142]
25	Vaulruz	1983	SWI	WGTES	3,500	<i>n.a.</i>	[63,69,143–145]
26	Stuttgart	1985	GER	WGTES	1,050	725	[15,18,61,63,69,70]
27	Augsburg	1996	GER	WGTES	6,500	3,250	[63,87,101,105,121,124,143]
28	Steinfurt (Borghorst)	1999	GER	WGTES	1,500	1,000	[16,18,51,59,77,87,95,101,135,144,146]
29	Chemnitz	2000	GER	WGTES	8,000	5,300	[15,16,51,57,61–63,68–70,87,124,144,147–151]
30	Eggenstein (Leopoldshafen)	2008	GER	WGTES	4,530	3,000	[16,17,24,62,79,87,95,98,152–155]
31	Sonderborg Vollerup	2008	DEN	WGTES	4,000	<i>n.a.</i>	[87]
32	Aeroeskoebing	1999	DEN	Buffer	1,400	1,400	[19,88,122]
33	Attenkirchen	2002	GER	Buffer	500	500	[16,24,51,128]
34	Samsø	2002	DEN	Buffer	800	800	[89]
35	Linz	2004	AUS	Buffer	34,500	34,500	[90,101,121]
36	Braedstrup	2007	DEN	Buffer	2,000	2,000	[111,156,157]
37	Crailsheim (Hirtenwiesen)	2007	GER	Buffer	580	580	[16,51,62,78,79,95,101,129,154,155]
38	Salzburg (North)	2011	AUS	Buffer	27,000	27,000	[54,91]
39	Nuremberg	2014	GER	Buffer	33,000	33,000	[92]

## 2.3 State of technology

### 2.3.1 Buried vs. elevated

Closed TES that are partially or fully buried in the ground (PTES, WGTES) rely on certain (hydro-)geological conditions such as ground stability and absence of groundwater. Applications above the ground are less site-dependent, and so most TES are constructed above ground. This is also a favorable option due to excavation cost savings, and because constructive elements and tank casings handle the stress caused by the filling [15,143]. Sometimes, a useful hydraulic pressure gradient from the storage device to the heating network can be achieved by construction of elevated applications.

DINÇER & ROSEN [56] describe a fully buried concrete storage system and emphasize that the surrounding soil is advantageous as it offers additional storage capacities, which is also supported by simulations [158]. According to the numerical modeling results by N-ERGIE AG [92], buried facilities exhibit higher storage temperatures at greater depth. For reasons of better storage performances and aesthetics, it is often recommended to bury and integrate the storages into the visible environment [159]. The TTES in Hannover (Germany) was integrated into an urban playground. In Munich (Germany), soil was piled up around the storage in order to integrate it into the landscape [62]. Also in Sweden, there has been a shift to buried storage facilities, and the last above-ground storage facility in Ingelstad was built in 1979 [69]. In many cases, excavation costs could be minimized by reclamation of former gravel pits.

### 2.3.2 Geometry and filling

#### Size and volume

The size and volume of a TTES facility might be restricted by regulations on maximum height above the surrounding terrain, depending on the location and the respective building laws (e.g., Hamburg (Germany) [135], APPENDIX A, TAB. A- 1) or due to requirements on structural properties. PTES can be scaled to enormous volumes [24], especially because these are built beneath the ground surface and thus contained by the surrounding soil.

To minimize conductive energy losses through the shell, the geometry of the TES should always aim at the lowest possible surface-to-volume ( $A/V$ ) ratio ( $\text{m}^{-1}$ ) [59,99,144]. By referring to typical geometries such as cubes or spheres, DUFFIE & BECKMAN [160] illustrate this with the third power increase in the volume compared to the second power increase in the surface area. Simultaneously, the  $A/V$  ratio behaves reciprocally to the height or diameter of the system. This also means that larger storage volumes have a positive effect [24] on storage efficiency. MANGOLD [62] states that energy-efficient seasonal storage only works with a volume of 1,000  $\text{m}^3$  or more. The values listed in APPENDIX A, TAB. A- 1 confirm that generally  $A/V$  ratios decrease with the volume of the installed TES, even so a closer look reveals that a strong variability exists. This indicates that other site-specific aspects play a crucial role in the layout of each system. In addition to the  $A/V$  ratio, often the height to diameter ( $h/d$ ) ratio is given and also listed in TAB. A- 1 (APPENDIX A). With values close to one, the outer surface tends to be smallest, but generally, the  $h/d$  ratio decreases with the filling volume of the reported case studies. This is especially the case for the Danish large-scale PTES,

where  $h/d$  ratios of around 1/10 are found. These values reflect that the TES forms are strongly defined by size and geometry of the original pit, where the TES was constructed. As the PTES and WGTES are preferably built in existing subsurface basins, their form is much more predefined than that of TTES. PTES and WGTES are commonly constructed as inverted truncated cones or pyramids (e.g., two German facilities: Steinfurt [146,161], and Stuttgart [70]). The TTES in Hamburg is built as a combination of an inverted truncated cone (bottom) and a cylinder and therefore has an optimized  $A/V$  ratio [135]. A reverse configuration can be found at the storage in Hannover, where the truncated cone is located at the top and the  $A/V$  ratio is even better due to optimized dimensioning [135].

Modelling of storage performance in energy systems is often done with the commonly used software TRNSYS for large and small facilities (e.g., [162,163]). However, MARX et al. [24] conclude that simulations under ideal conditions usually result in underestimated heat losses, in comparison to measured values of built systems [164,165]. FORKEL & DANIELS [166] conducted numerical simulations to find an optimal storage geometry and the best boundary conditions. Basins that have cubical, cuboidal, and vertical cylindrical geometries, as well as interconnected large pipes, were investigated. A cylindrical basin was found to be the best geometry for large facilities, providing the best approximation to a sphere. Furthermore, FORKEL & DANIELS [166] proposed the implication of internal walls for an even better thermal stratification. This study focused exclusively on geometrical design optimization, but the different costs for the different layouts were not examined. Thus, theoretically, a sphere would always be optimal by minimization of conductive heat loss (and lowest  $A/V$  ratio). Due to the constructional challenges, however, a cylinder may be economically more efficient. Also in practice, cylinders represent a standard form, especially when no critical layout constraints need to be obeyed, such as revealed in APPENDIX A, TAB. A- 1 for many TTES and buffers.

#### Water as filling material

Water is by far the most common filling material. It is a natural media, harmless, and nearly available everywhere, which is a particular advantage compared to custom-designed phase change materials and high-quality gravel fillings [167]. Water is favored because of its thermodynamic properties [24,55]. According to THESS et al. [54], the heat storage capacity of water is around  $1.16 \text{ kWh m}^{-3} \text{ K}^{-1}$  ( $4.18 \text{ MJ m}^{-3} \text{ K}^{-1}$ ) in a temperature range from  $0 \text{ }^\circ\text{C}$  to  $100 \text{ }^\circ\text{C}$ . This value is only around  $0.69 \text{ kWh m}^{-3} \text{ K}^{-1}$  ( $2.50 \text{ MJ m}^{-3} \text{ K}^{-1}$ ) for soil or  $0.33 \text{ kWh m}^{-3} \text{ K}^{-1}$  ( $1.20 \text{ MJ m}^{-3} \text{ K}^{-1}$ ) for a gravel bed with 45% pore space. Within a temperature range from  $35 \text{ }^\circ\text{C}$  to  $60 \text{ }^\circ\text{C}$ , resulting storage capacities are  $15\text{-}30 \text{ kWh m}^{-3}$  for ground material, such as soil or rock, and  $30\text{-}50 \text{ kWh m}^{-3}$  for gravel-water mixtures compared to  $60\text{-}80 \text{ kWh m}^{-3}$  for water only [15]. This means a reduced storage capacity of 60% for soil and of 20% for gravel [87].

To avoid clogging, and because flow paths within the matrix are difficult to control, WGTES require heat exchangers which reduce efficiencies and amplify heat losses. In contrast, water can serve as storage media and heat carrier at the same time. Heat exchangers thus are avoided and the storage can be integrated into the connected heating/cooling system when the water is directly used as fluid [55]. Negative properties of water include the low operating range between melting and boiling points, corrosive effects on other storage elements, and the complication of natural



convection on maintaining thermal stratification [55]. Additionally, the thermal conductivity of water ( $0.6 \text{ W m}^{-1} \text{ K}^{-1}$ ) is below that of water-saturated soil ( $0.6$  to  $4 \text{ W m}^{-1} \text{ K}^{-1}$ ) [131].

For systems with small volumes, the use of a combination of water and custom-designed phase change materials has been suggested [168]. This yields a higher storage capacity by latent heat conversion. Because such special phase change materials are relatively expensive, they are not common in seasonal storage systems; instead, it is often more economical for seasonal storages to design a larger storage volume of water. However, in several applications also the phase change from water to ice (or snow) is used [169]. Here, the working temperatures of the storage device are low, but latent heat is stored and released in addition to the release of sensible heat [49,170,171]. Ice ponds were first introduced in 1984 by TAYLOR [172] as a technical variant for storing thermal energy, and are further discussed by AKBARI & SEZGEN [169]. In the recent work by YAN et al. [173], the combination of ice and cold water storage units for cooling applications revealed to be economically advantageous.

#### Water-gravel fillings

For WGTES, the filling consists of a solid phase and a liquid phase [148]. Soil, sand, gravel, or various mixtures of these are mostly used as fillings [24,55]. Compared to unsorted soil grains, well-sorted gravels offer a higher permeability when using direct loading systems, higher homogeneity, and higher water content, which results in increased storage capacities.

Backfilling of excavated material can be economically advantageous since costs for disposal and purchase of gravel or soil are avoided [63]. For example, during the construction of the storage in Eggenstein it was found that the building ground consisted of well-permeable sand. Accordingly, costs were reduced by using the ground material as filling [98].

Detailed descriptions of gravel and soil fillings are given by HAHNE [70] and OCHS et al. [63] for the two German WGTES in Stuttgart, and by URBANECK et al. [148] and BENNER et al. [37] for Chemnitz. The water-gravel mixture in Chemnitz consists of coarse gravel with an average diameter of 22.3 mm (range of 16 - 32 mm). With a porosity of 0.43, the mean density of the two-phase system is  $1928 \text{ kg m}^{-3}$ , and the heat capacity is  $0.83 \text{ kWh m}^{-3} \text{ K}^{-1}$  ( $2.98 \text{ MJ m}^{-3} \text{ K}^{-1}$ ). A value of  $2.4 \text{ W m}^{-1} \text{ K}^{-1}$  was determined as thermal conductivity [37,148], which is four times larger than the thermal conductivity of water ( $0.6 \text{ W m}^{-1} \text{ K}^{-1}$ ). WGTES have a lower heat capacity, caused by the gravel or soil components [24,155]. A comparison between WGTES and the water-filled systems (TTES, PTES) can be done by water equivalents. For example, the  $1050 \text{ m}^3$  WGTES storage facility in Stuttgart contains  $355 \text{ m}^3$  of water and  $960 \text{ m}^3$  of gravel. This is equivalent to a TTES or PTES with a water volume of  $725 \text{ m}^3$  [70]. For the other WGTES, the additional gravel material reduces the water volume by 30 to 50% (for example in Chemnitz from  $8,000 \text{ m}^3$  to  $5,300 \text{ m}^3$  [37,62,70], TAB. 2.1).

WGTES provide static advantages as they can be integrated into the subsurface as self-supporting, loadable bodies, obviating the need for structural elements like load-bearing sidewalls and complex roof constructions [18]. As a result, WGTES allow the use of their top surface and are preferred for areas with denser populations [24]. At the WGTES in Steinfurt, the highly stress-resistance cover facilitates to use it as gardens

[18,146]. In contrast, TTES need a technically more complex construction with pilings to carry the top construction (e.g., Hamburg [121,135,165]). The necessary complex thermal structure of the storage diminishes operation and maintenance performance of WGTES. It is almost impossible to carry out maintenance inside the storage or repair leaks in the waterproofing elements [24,121]). Also, it is important to note that modeling of WGTES using a multi-component system with liquid and solid phases is more complex than considering systems with water only [148].

### 2.3.3 Structural elements

As TTES are commonly built above ground, they need a structural element to carry stresses. Mostly, these are fabricated of concrete reinforced by steel to improve mechanical properties (FIG. 2.7 a). The high-performance concrete that was used for the TTES in Hannover represents both the static and waterproofing component (due to an abated permeability) but at disproportionally high costs [62,135,174]. Simultaneously, optimized shapes and construction methods can help to increase the concrete's stability. For example, a high stress resistance was required for the top of the storage in Friedrichshafen, and it was achieved by constructing a pre-stressed shelled roof [123,136].

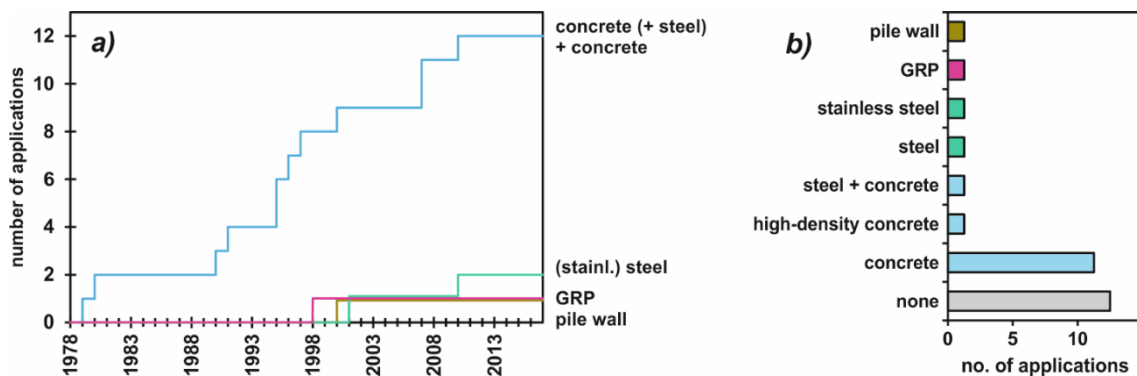


Fig. 2.7: Development of number of applications a) and today's application distribution b) for the different materials for structural elements. Concrete and reinforced concrete clearly predominate, while pile walls or GRP were only used in single pilot projects. (GRP: glass fiber reinforced plastic).

A comprehensive list of the characteristics of researched seasonal storage locations with respect to structural elements is provided in APPENDIX A-2.

According to FIG. 2.7 b, there are a few systems that only use stainless steel. This is common for large buffer storages, but also for smaller seasonal TES. Stainless steel may be advantageous because no further sealings are needed. However, at the same time, the storage volume is limited due to its lower stress resistance. As an alternative, glass fiber-reinforced plastic (GRP) profiles with a thickness of 10 mm were tested at a pilot site in Ilmenau (Germany, [53,133,175], FIG. 2.7 b). The aim was to reduce costs and to benefit from a low thermal conductivity of this material. However, limited static properties of this material restrict the maximum volume of a storage tank.

For the storages built underground (PTES and WGTES), the stability requirements for structural elements are reduced by the enclosing ground. Nevertheless, the geometry of some facilities entails the need for specific structural elements: the WGTES in Chemnitz (Germany) was built with a pile wall to stabilize the excavation hole [16,130,150]. The steeper the slope angles of a given excavation hole, the larger

the storage volume. This is particularly important in areas with limited space. Further examples of non-TTES with structural elements are the PTES in Herlev (steel profiles [22]) and in Lambohov (concrete [15]). The performance of seasonal TES depends not only on their construction elements but also the surrounding (hydro-)geological conditions. YUMRUTAŞ & ÜNSAL [176] provide a theoretical investigation of effects of various surrounding materials, comparing density, thermal conductivity, diffusivity, and heat capacity. It is found that coarse gravel is the preferred surrounding material compared to granite and limestone.

### 2.3.4 Thermal insulation

#### Thermal insulations of top, bottom, and sidewalls

A summary of the materials used, the thicknesses, the configurations, and the engineering practices of thermal insulations for locations in this study are presented in APPENDIX A-2.

Thermal insulation at the top, bottom and sidewalls is fundamental to mitigate conductive heat loss (FIG. 2.8 a, FIG. 2.8 b). For instance, measurements taken at the facility in Stuttgart showed ground heat losses of 40%, because the sidewalls and bottom were not insulated [70]. URBANECK et al. [148] demonstrate that heat losses in uninsulated PTES mainly occur at the cover and the upper edges. By simulating the operation of an exemplary system, a stationary heat loss was observed at the bottom of the storage, while the remaining storage surface had not yet reached a steady state. In the modeled case, a warming of the ground at a distance of 1 m by 43 °C was revealed.

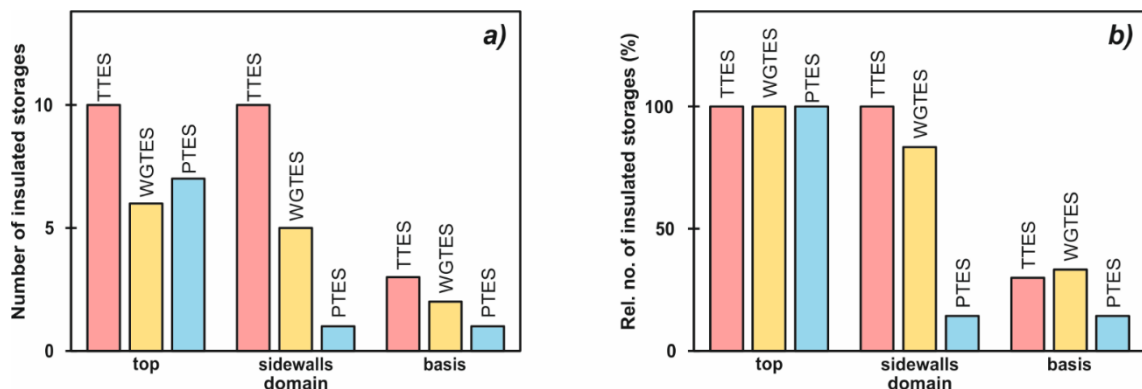


Fig. 2.8: Absolute a) and relative b) numbers of the insulated storage domains, differentiated according to the different storage types. While TTES always represent top and laterally insulated storages, particularly PTES lack sidewall insulations. The bottom is rarely insulated for all system types.

The top of all three storage types (TTES, PTES, WGTES) have already been insulated in the very first projects, as here the largest heat losses are expected [177]. The early facilities in Hamburg (1996) and Rottweil (Germany, 1995) used thermal insulation at the top and at the sidewalls, but due to the high expected costs no insulation was implemented at the bottom [96,123,135,147]. By using materials that are resistant to mechanical stress, like foam glass, the insulation of the bottom was realized for example at the TTES in Cosenza (Italy, [126,127,146]). According to this improvement, subsequent TTES and WGTES were preferably insulated on all sides (e.g., Munich, [99,147]). In contrast, PTES avoid the costs of lateral and bottom insulations, but try to compensate the elevated thermal losses by their larger storage volumes.

Insulation of the storage top is nevertheless recommended for all system types [128]. As a result, currently existing PTES and some WGTES often do not have lateral thermal insulations, while these are always present in TTES (FIG. 2.8 b). This is also because insulation is easily applicable during construction of the sidewalls of TTES.

### Requirements for insulation materials

The different sides of a storage device are ideally equipped with different insulation materials [24,147]. A high mechanical resistance is especially required for the bottom and sidewalls. As a consequence of the higher density of gravel, requirements on resistance to the mechanical stress caused by the weight of the storage material are highest for WGTES. Among other requirements for material properties are uniform and continuous application of insulation, durability, insensitivity to thermal stress or external natural influences, and good drying abilities. For example, Ochs et al. [73] recommend a high temperature resistance of up to 100 °C in the short term and 90 °C in the long term, ageing and pressure resistance, as well as resistance to hydrolysis. In addition, Ochs et al. [73] tested various materials and demonstrated that even with new materials (e.g., foam glass) the thermal conductivity increases by 30% on average when the temperature is raised by 20 °C. This emphasizes the need for uniform material behavior. Not only are moisture problems reported in the old storage systems from Denmark (Herlev, Ottrupgaard, [20,22,73,86]), but from newer systems as well. In Steinfurt, moisture permeation in the insulation (expanded glass granulate) occurred when the drainage system failed [51]. To solve this problem, the expanded glass granulate had to be dried [147]. Measurements revealed that it took more than one year before the insulation material regained its initial value [51].

### Materials for thermal insulation

Conventional insulation materials include mineral fiber, extruded polystyrene foam (XPS), expanded polystyrene foam (EPS), polyethylene foam (PE), and polyurethane/polyisocyanurate (PUR/PIR) foam. FIG. 2.9 demonstrates that these represent over 50% of the materials used for the sidewalls and top. According to Ochs [121], PUR/PIR foams are useful for both sidewalls and top insulations, whereas mineral fibers are only utilized at the top of the storage. Further, mineral fibers were consistently used with TTES. Due to insufficient stress resistance, such conventional materials however are not considered for bottom insulation.

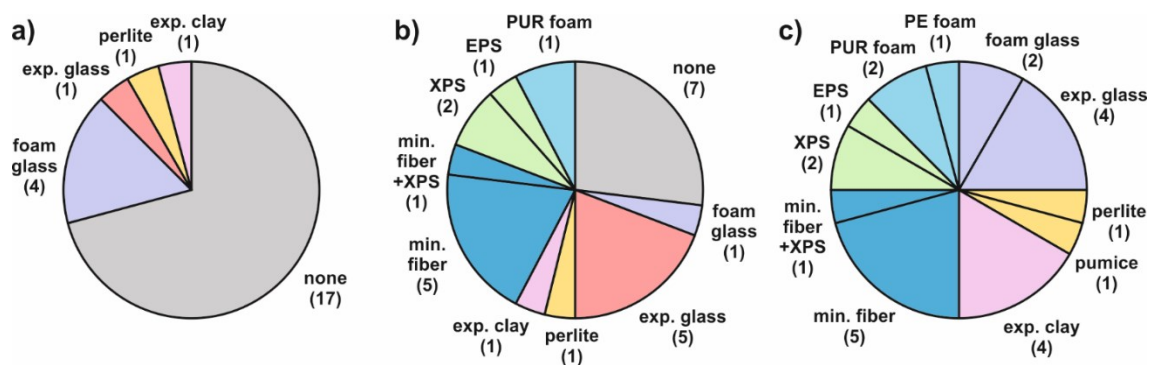


Fig. 2.9: Number of materials used for a) bottom, b) sidewall, and c) top insulation. Foam glass is primarily applied at the bottom, whereas the sidewalls are insulated mainly with conventional mineral wool and expanded glass. The largest variability is found in the top insulations, where natural, conventional, and recycling materials are used.

A main disadvantage of conventional insulating materials is their non-uniform thermal behavior [144]. For mineral fiber, thermal conductivity significantly declines at 40 °C to 90 °C [147]. However, if water infiltrates the insulating layer in the case of leakage, the thermal conductivity strongly increases [73,147]. BODMANN & FISCH [135] measured growing heat losses caused by moisture permeation into the insulation from the outside, which was accelerated by a high groundwater level at the storages in Hamburg and Steinfurt. To avoid this, MANGOLD [147] recommends costly wrapping of XPS or PUR sheets into waterproofing membranes. As an example, in Ottrupgaard, PUR foam was applied in sandwich elements to avoid ingress of moisture [86,178].

Natural materials used as thermal insulators include pumice (e.g., Stuttgart, [70]), expanded perlite (e.g., Mühldorf, Germany, [142]), and expanded clay (e.g., Cosenza, [23,126]). The first two are fine-pored volcanic materials. According to OCHS et al. [73], expanded perlite has the best thermal properties, but is unsuitable due to its low pressure resistance. However, at Mühldorf, a special vacuum insulation technique allowed the use of expanding perlite as thermal insulator not only at the sidewalls and top but also at the bottom [142] (FIG. 2.9, FIG. 2.10). Expanded clay has already been used in early TES, for example in Lambohov, built in 1980 [73]. Floating covers of large PTES rely on expanded clay because of its low density (e.g., Marstal, [62,83,112]). Further advantages of natural materials are the favorable environmental compatibility and often low costs. Despite that, most of these natural materials were not used in storage systems other than those where they have been tested (FIG. 2.10).

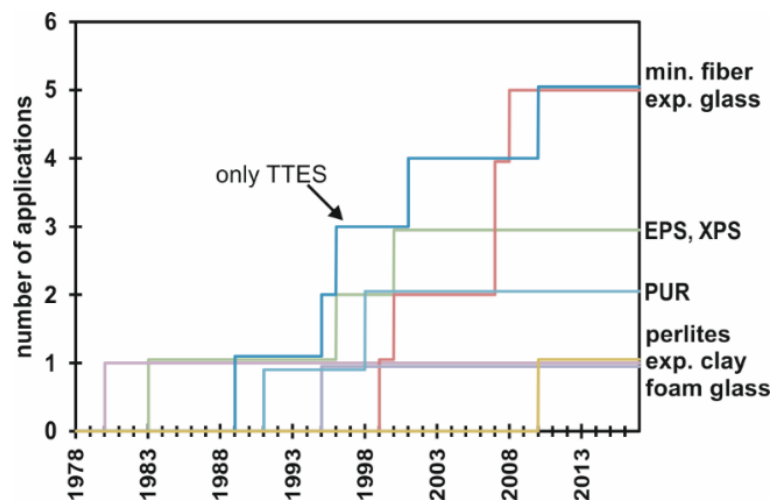


Fig. 2.10: Evolution of applied insulation materials used at the sidewalls for all storage types (TTES, PTES, WGTES). Mineral fiber has been used intensively since the mid-1990s, but solely for TTES. Until 1999, EPS, XPS and PUR foams gained attention. Meanwhile, expanded glass has become the preferred choice.

A newer trend is the use of recycling materials. These include foam glass (as sheets or granulates) and expanded glass granulates, both recovered from waste glass. As shown in FIG. 2.10, this development starts relatively late, beginning from years 1995 (foam glass) and 1999 (expanded glass). Recycling materials have not been available for as long as conventional thermal insulators. Foam glass meanwhile represents a commonly used material for bottom insulation, while expanded glass granulate is often applied for sidewall and top insulations (FIG. 2.9, FIG. 2.10). Aside from attractive thermal insulation properties, they show a good mechanical resistance as well [101].

Among the recycling materials, expanded glass granulate has the lowest thermal conductivity [73]. Furthermore, all recycling materials are water-resistant and can be dried easily. Accordingly, expanded glass granulate was used as a humidity-compatible material on the outside of the storage sidewalls in Hannover, which is made of concrete of critical permeability [135]. The storage in Cosenza is one of the first facilities being equipped with foam glass gravel [23,126]. At the WGTES in Steinfurt, both foam glass and expanded granulate are used [18,146]. Foam glass is installed in 0.15 m thick plates at the bottom while expanded glass granulate is installed in geotextile bags of 0.5 m thickness [130].

OCHS [121] provides a detailed overview of various insulating materials. Based on a definition and prioritization of thermal, mechanical, and other requirements, various data sheets are evaluated. As a conclusion, foam glass gravel, expanded glass granulate, and expanded clays are considered particularly suitable for insulation.

#### Installation techniques of thermal insulations

According to OCHS et al. [73], appropriate configurations and constructions of thermal insulation layers are challenging in terms of building physics and thermodynamics. This is because both heat conduction and vapor diffusion from the inside to the outside and water ingress from the outside to the inside must be avoided at the same time. Materials for thermal insulation are available as plates or as bulk material [121]. Plates do not require the installation of complex frames or textile bags in order to keep the insulating material fixed [121,144]. One disadvantage, however, is that plates always need additional waterproofing. Consequently, for simple installations, bulk materials are preferred as they can be directly filled into prefabricated geotextile bags [146], achieving water tightness and thermal insulation in a single work step. A 25 m<sup>3</sup> body of thermal insulation can thus be built in 30 min [18]. Vacuum evacuation improves stability through compaction and by negative pressure. At the same time, the material is protected against humidity. Aside from this, long-term monitoring via vacuum control is feasible [98] and floating top insulations can be constructed (e.g., at the PTES in Jülich (Germany [110], and Ottrupgaard [86,108]). In all cases, thermal bridges have to be avoided through the proper installation of connecting pipes.

Since the temperature distribution within the storage (and consequently also the heat loss) is not uniform, but it increases from the base to the top, it is recommended to raise the thickness of lateral insulation accordingly. In Hannover, the insulation thickness of the sidewalls rises from 0.3 m at the bottom to a maximum of 0.7 m at the top [135]. Due to the reduced insulation thickness at the storage bottom, a further advantage of this method is that costs can be reduced without efficiency losses, as reported for the TTES in Munich [147]. Both internal and external insulation of the mantle are possible for TTES. External insulations cause higher thermal stresses in concrete and reduce long-term stability [73]. Nevertheless, this technique is used in Hamburg by employing pressure-resistant mineral wool [135,179] and in Munich, where expanded glass granulate is inserted in a membrane formwork between the structural element and the drainage layer [79].

### 2.3.5 Waterproofing

#### Materials for waterproofing

Leakages are a major issue of water-based storage systems. They can be caused by damage during construction, or they can occur later due to material fatigue. Accordingly, there are many methods and materials available to avoid both the loss and infiltration of water and moisture. Materials for TES waterproofing can be adapted from a variety of other application fields. Investigations by OCHS [121] cover conventional materials for landfill, dam, canal, pond, roof, and tunnel construction. Plastic liners, such as ethylene propylene diene monomer (EPDM), high-density polyethylene (HDPE), polypropylene (PP), and polyvinyl chloride (PVC), are common in those areas and have also been used in seasonal TES ([113], FIG. 2.11 a, FIG. 2.11 b). APPENDIX A-2 gives a detailed insight into designs of waterproofings for some selected seasonal TES of this study.

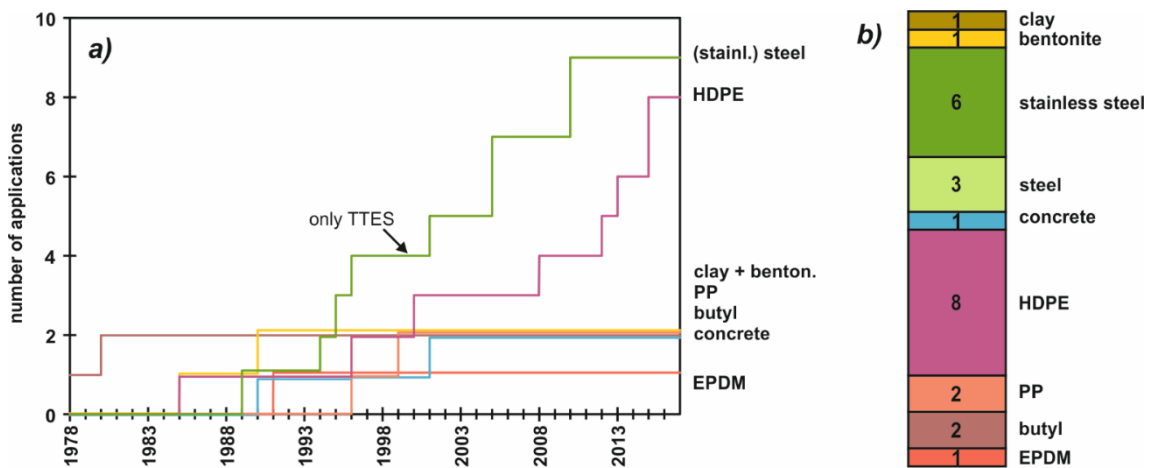


Fig. 2.11: a) Development of a number of applications and b) current application distribution of waterproofing materials for all storage types (TTES, PTES, WGTES).

Linings of steel or stainless steel are used very often, but these are restricted to TTES (FIG. 2.11 a, FIG. 2.11 b). Advantages of stainless steel offer high ageing and diffusion resistances, while disadvantages include potential corrosion, more complex installation procedures, and higher costs [121]. However, by using stainless steel, the maximum storage temperature ( $>> 95\text{ }^{\circ}\text{C}$ ) is much higher than that of plastic liners ( $< 90\text{ }^{\circ}\text{C}$ ) [59,113]. Plastic liners are advantageous because their specific costs, their packaging form as lanes, and the speed of application. HDPE clearly dominates (FIG. 2.11 b), as it is meanwhile well proved as suitable for PTES and WGTES. HDPE is used at two of the three German WGTES storages (Stuttgart, Chemnitz) and at the WGTES in Lyngby (Denmark, [22,150]). In contrast, other geomembranes (PP, butyl, EPDM) have not survived their experimental stage (FIG. 2.11 a).

WGTES often use plastic liners to separate the storage material from the surrounding soil [55]. In addition, these liners allow for leakage control. In Steinfurt, a double-layer polypropylene (PP) liner, which can be tested by vacuum for tightness even after installation, was applied for the first time in 1999. The plastic PP was modified to ensure a better long-term temperature resistance of up to  $90\text{ }^{\circ}\text{C}$  [18]. MANGOLD [147] notes that costs for more temperature resistant materials such as stainless steel are significantly higher.

Still, foils are generally vulnerable to leaks, as documented at the storage in Herlev for example, which was equipped with a single-layer EPDM liner at the inner side of steel sheet pilings [22]. To prevent leakage through thermally caused deformation, the PTES in Marstal was equipped with a steel grid [180].

The storage in Ottrupgaard was sealed with a 0.85 m thick clay layer at the bottom and sidewalls [86,87]. Unfortunately, no satisfactory resistance was achieved, and significant water losses occurred shortly after commissioning [22]. OCHS et al. [105] point out that leakage is frequent for related projects with clay or bentonite sealing due to its high susceptibility, such as also observed at the storage in Hoerby (Denmark, [23]). Therefore, use of this natural material also in the future is uncertain. A high-performance waterproofed concrete with an optimized diffusion rate (quality level B85,  $4 \text{ L m}^{-2} \text{ a}^{-1}$ ) was tested in Hannover. The quality was achieved by adding micro silica, superseding stainless steel liners [135,174]. Cost reductions of 15% were expected but could not be accomplished due to elevated costs for reinforcement that was needed to limit fracture widths [62,130].

### Vapor diffusion

Water losses are not only caused by water in liquid phase. Vapor, which penetrates through the storage shell to the outside significantly reduces the efficiency of the insulation material and, as a result, also reduces the system's overall efficiency. Since the moisture transfer occurs mainly in areas with higher temperatures (at the top and the sidewalls), this is primarily where vapor diffusion barriers are used. For economic reasons, these are often neglected at the relatively cold storage bottom [146].

TTES do not need vapor diffusion barriers as they already contain an inner stainless steel lining [24,59]. For example, in Hamburg, a welded 1.25 mm thick stainless steel sheet serves as a completely impermeable layer [135]. In contrast, plastic liners exhibit a notable permeability [144]. Since the first German WGTES in Stuttgart and Chemnitz did not have vapor diffusion barriers, water losses through the HDPE liner were detected. In Stuttgart, 10 to 15 m<sup>3</sup> of water had to be refilled every year, corresponding to a fraction of 3% of the total water volume [70]. Due to these experiences, additional materials, predominantly metal foils, had to be applied to prevent moisture transfer between the storage and the surroundings [24,121,144]. In Steinfurt, a PP-Al-PE liner was installed [100,146]. The concept of composite foils is also common in other application areas (e.g., in the building sector). In Eggenstein, the aluminum barrier is placed within the plastic liner that was welded to chambers [98,130].

### Drainage layers

Energy losses are often increased in buried systems if groundwater is present, as it promotes convective heat transfer in the storage surrounding and reduces the insulation material performance when penetrating the respective layer [135,165]. To avoid this, drainage layers should be installed to deflect rainwater from the surface of the storage. These are usually installed as gravel layers (e.g., Hannover, [135]) or geotextile mats (e.g., Steinfurt [135]). Mats with an additional protection fleece are mainly used and recommended for PTES [73], for example in Marstal [113]. To minimize infiltration of groundwater, PFEIL & KOCH [18] recommend a bentonite layer on the outer side of the storage shell, but these also represent another cost factor, and leakage problems with clay layers are common.



### 2.3.6 Loading systems

Effective storage systems for heat and cold require reliable loading and unloading systems to establish and maintain an effective thermal stratification inside the facility [181]. In contrast, insufficient temperature stratification reduces storage efficiency enormously - often expressed as internal energy loss or exergy loss [24,182]. THESS et al. [54] state that turbulent flows mix the storage fluid, destroying a stable stratification, while URBANECK et al. [183] point out that free convection due to density differences takes place at a temperature difference as low as 0.01 K.

Direct and indirect loading systems are distinguishable. Direct loading means that the loading system is in direct contact to the filling material, while indirect loading systems use heat exchanger and hydraulically separate the inner parts of the storage from the loading- and unloading circuit. WGTES usually only contain indirect loading systems [181]. One example is Steinfurt with a 7,500 m long PE coil system on six levels [59]. To test different strategies, the WGTES in Stuttgart offers three different possibilities to insert or extract heat [70]. The indirect system consists of an eight-level plastic tube heat exchange with a length of 4,853 m. A ring and a star distribution device facilitate water flowing in at upper levels and out at lower levels during charging (and vice versa during discharging).

TTES and PTES solely use direct systems. BODMANN et al. [146] explain that for larger storages direct loading systems are to be preferred due to economic reasons. OCHS [121] and MARX et al. [24] state that the direct loading of storage facilities is more energy efficient, due to lower rigidity. At the same time, SCHIRMER et al. [53] and MARX et al. [24] note that layer loading devices of small plants, which were, for example, studied by ABDELHAK et al. [184], are not easily scalable. LOHSE et al. [185] also investigate various direct loading devices and conclude that stationary systems working by fluid mechanics are of particular benefit. They have a longer lifetime and a simpler functional principle, only utilizing density differences of the storage. However, over-simplified designs lead to insufficient thermal stratification. Part of such direct loading systems are radial diffusers, positioned close to the top and the bottom of the storages [185]. Their flow behavior was investigated in detail by FINDEISEN [186], FINDEISEN et al. [187], and LOHSE et al. [181]. A third device in the middle of the storage height was used for the first time in Hannover in 2000 [51].

### 2.3.7 System integration

#### Networks

Proper integration of the TES facility into heating/cooling grids is essential [155]. For example, an in-depth review of modelling methods for district energy systems is presented by ALLEGRINI et al. [188]. In many cases, the installation of new network systems connecting existing TES is expected to improve the cost-efficiency [24,53,62,188,189]. Well-known networks are large district heating networks, e.g., in Marstal where 1,500 households are linked to the PTES [83]. Generally, it is recommended that in urban applications at least 100 households are connected to a seasonal storage [132], but PFEIL & KOCH [18] estimate that at least 50 households enable economical operation. In Hamburg, only 124 households are supplied and in Friedrichshafen 570 households are supplied [51,53,190]. The required size of a new storage can also be defined based on the total area for residential space heating. This

was the case for Hamburg, with a total area of 14,800 m<sup>2</sup> and Friedrichshafen with 39,500 m<sup>2</sup> [51].

The integration of a TES can be realized particularly well in new building projects. As an example, Steinfurt is a location in Germany with a seasonal storage as part of a “solar settlement” [146,161] and the TTES in Hannover is part of a “Solar City” [191]. TES can also be integrated in energy refurbishment projects. The WGTES in Eggenstein was incorporated into an existing district heating network in 2009 as part of a major modernization project [17,154].

Centralized systems with central heating sources, and decentralized systems with independent additional heating systems in individual houses, can be distinguished from each other, but are often used in parallel (Hamburg [135], [179]). Different combinations of these systems are investigated by HSIEH et al. [192] with the result showing that combinations of short and long term storages are optimal. LANAHAN & TABARES-VELASCO [145] also recommend such combined heat generation strategies. To minimize energy losses, directly integrated systems are more suitable than heat exchangers [135]. If this is not possible, e.g., for hygienic reasons in the case of closed systems such as drinking water, efficient heat exchangers must be used [146].

Independent networks for source and target systems allow for either separation of different temperature levels or for creating a mixture of supply and return flows to keep stable temperatures [146]. Further, different operating strategies (direct energy use vs. storage) can be realized [135]. This technical variability yields opportunities, but it also incites a challenge. The risk of technical failure rises with system complexity, and optimal integration of seasonal TES into heating or cooling networks is often underestimated. For example, energy losses of networks can represent an unexpectedly important role [146]. Hydraulic problems in loading and unloading circuits in Eggenstein led to inefficient operation of the storage system [154].

#### Source and target systems

Generally, all heat or cold generating devices can be used as thermal energy sources. Since seasonal TES are often built within renewable energy projects with fluctuating sources, storage facilities try to maximize the proportion of renewable energy by using different systems. OCHS et al. [73] and PFEIL & KOCH [18] propose waste heat from Combined Heat and Power (CHP) and biogas plants, which have a higher productivity in summer due to additional green waste. The concept in Marstal uses 100% renewable energy for heat supply and employs the PTES to help bridge supply gaps through utilization of stored surplus. The system includes a wood chip boiler and a solar thermal system in combination with heat pumps [83,112]. Operation of the cogeneration plant in Hamburg was terminated due to economic reasons [135]. For feeding other TES, conventional source systems such as gas boilers (Steinfurt [146], Hamburg [135], Munich [24]), oil-fired boilers, condensing boilers, or electric flow heaters (Steinfurt [146]) are used. Post heating via an attached district heating system is employed in Hannover [135].

Seasonal TES aim at different target applications. These include space heating and cooling as well as the preparation of domestic hot water. Furthermore, stored thermal energy can be applied to support industrial processes or agricultural applications, such as the energy-efficient heating of greenhouses [193,194].

The volume or thermal capacity of the storage system must match both the demands of the targets and the supplied energy by the source systems. Storage systems that are designed too large require disproportionately high construction costs and often cannot be used in an optimal manner [71]. In Friedrichshafen, one reason for inefficient dimensioning of the storage system was a result of a difference between the projected and constructed area of solar thermal collectors. Consequently, a discrepancy between calculated and actual supply energy was found [17,24]. In contrast, a small storage which is too small is not able to cover the energy demand, which causes additional costs when complementary systems must be installed, e.g. for post-heating. Ultimately, all components must be harmonized so that supply and return temperatures are matched and storage potential is realized most efficiently.

### Temperatures

Different temperature levels are required for different target systems, such as domestic hot water preparation, radiator heating, and underfloor heating. Clearly, low-temperature underfloor systems are most suitable for achieving best storage performances [51]. This is because a lowered temperature within the storage results in lower heat losses [152]. Problems arise with low-temperature storages if targets are connected that require a higher temperature (e.g., domestic hot water preparation or radiator heating) and post-heating is needed. SCHMIDT & MANGOLD [132] propose flow heaters as an effective alternative, while some decentralized systems (e.g., Marstal) use diurnal buffers to modulate feed-in temperatures [83]. In Marstal, resulting temperature differences between supply and return circuits reach 32 K during summer and 43 K during winter. Another solution is the admixture of cooler return flows to ensure a constant supply temperature level (e.g., in Hamburg [135]).

Heat pumps are, for example, installed in Stuttgart [70], in Marstal [83], in Munich [24,79], and in Eggenstein [24,154]. Heat pumps offer two positive features: besides providing higher supply temperatures, they also can be applied to reduce the return temperatures, cooling down the storage to obtain a larger temperature spread between storage inlet and outlet [24,153]. On the one hand, this maximizes the available storage capacity. On the other hand, it promotes stratification and avoids excessively high temperature at the beginning of the next loading period. The latter was observed in the first storages in Friedrichshafen and Hamburg [136,147,165]. A suitable temperature range for optimal storage operation is considered to be 10 °C to 80 °C, designed for the storage in Eggenstein [24,155]. Here, also a heat pump is installed to achieve the low return temperature, and detailed information on methods of TES-coupled heat pump dimensioning can be found in RIEGGER & MANGOLD [98].

Fluid temperatures originating from the supplying systems can show a high variability, especially with solar thermal collectors [135]. Buffers in front of the loading devices are therefore recommended in order to ensure constant temperatures, avoid turbulent flows, and prevent excessive material stress [146]. This is particularly necessary for WGTES, as these have a higher rigidity (e.g., Eggenstein [24]).

### Storage operation

The operating procedure of a seasonal storage begins with an initial heating phase [146], while the desired quasi-stationary state is reached only after some years [51]. During this stabilization phase, the steep lateral temperature gradients promote high energy losses to the surrounding soil [135]. For example, the storage in Hannover was put into operation in 2000 and had a planned start-up phase until 2005 [51].

For the evaluation of storage efficiency, the degree of utilization is expressed as the quotient of stored and withdrawn energy (due to internal and external energy losses). For well insulated storages, values above 90% are considered feasible [24], but currently thermal loss still accounts for up to 50% of the storage capacity.

Due to the different energy source and target systems, appropriate measurement and control systems are necessary to promptly detect malfunctions early [135]. The suitable position for control and automation in centralized networks are the heating stations [135,147]. For instance, pilot storage plants are often equipped with a sophisticated measuring grid. In Stuttgart, for example, 415 thermal sensors and nine heat flow meters were installed [70]. In Chemnitz, 20 internal and 10 external temperatures are monitored [148,151]. On the one hand, sampling of the water inside the storage system has to be carried out in order to detect corrosion at an early stage. In Stuttgart, sampling is possible at two locations within the storage [70]. On the other hand, monitoring groundwater quality around the storage is most important for storages with (potentially) greater water losses. The storage in Hannover is thus accompanied by an extensive hydrochemical measurement program [135].

## **2.4 Conclusions and Outlook**

Seasonal storage of thermal energy is still in its early stage. This is surprising, considering its elementary role in modern heating networks that rely on multiple, often fluctuating heat sources, and that are based on smart modulation of temperatures. In fact, the historical evolution of the closed seasonal storage of thermal energy has its roots in the early 1960s. After only a short time, theoretical ideas were transformed into applied pilot projects within the framework of extensive research projects. The main focus of research activities was mainly concentrated in Europe, backed up by international cooperation and activities in other countries. Recently, since the beginning of the 2010s, the installed closed thermal energy storage (TES) volumes show an exponential increase, which displays the recent transition from pilot-plants to well-functioning large-scale applications. The three most attractive concepts in the field of water-based closed seasonal TES are Pit Thermal Energy Storages (PTES), Tank Thermal Energy Storages (TTES) and Water-Gravel Thermal Energy Storages (WGTES). PTES are water-filled sealed pits while TTES are enclosed basin structures. In contrast, WGTES are commonly filled with a mixture of gravel and water, allowing static loads to be placed on their top surfaces. In addition to their application as seasonal storage tanks, large-volume short-term buffer storage tanks also gained importance by growing integration into district heating networks.

Intensive research activities in the different European countries are reflected in the present geographical distribution of seasonal storage systems. Germany, Denmark, and Sweden clearly dominate both in terms of installed volume and the number of TES built. At present, this article identified 39 systems in Europe, comprising 31 seasonal TES and eight large buffer storages. The total storage volume is about 797,000 m<sup>3</sup>, with about 87% (697,220 m<sup>3</sup>) total TES volume. Assuming an optimal but still realistic temperature spread of 70 K for all facilities, the present TES would result in an available storage capacity of 56,600 MWh. Adding the potential capacity of the listed large buffer storages, a total of 64,700 MWh is achieved. Interestingly, TTES is the most common variant, while PTES represent the largest volume. This is due to the relatively simple design of PTES without structural elements, allowing cost savings and the possibility to expand the volume. WGTES are more complex, and are therefore more dependent on-site conditions. They also entail higher technological risks.

Ongoing developments in the sector of seasonal storage systems show a steady progress in the various system components. This is demonstrated by the developments of the storage filling (especially important for WGTES), the thermal insulation and waterproofing, as well as the structural element (mainly for TTES). Progress is primarily related to new materials and construction methods. Regarding the geometry and size of new systems, special attention is given to finding optimized surface/volume ratios. In contrast, the latest PTES systems in Denmark use very large volumes to compensate for energy losses through simpler construction concepts.

The most important innovations are shown in FIG. 2.12. Here, a multi-generational development can be derived in all domains [16,18,19,122]. While pilot projects first proved the principle feasibility of seasonal TES, new waterproofing and thermal insulation materials have already been applied in the second generation. Efficiencies were thus increased (e.g., through optimized loading and unloading systems) and the first problems (especially leakages) were solved at the same time. In the third generation, priority shifted to introducing cost reductions, for instance by using prefabricated elements for thermal insulations or structural elements of TTES. The new insulation techniques and especially bottom thermal insulation improved efficiencies, while composite foils with vapor diffusion layers and testable waterproofing techniques further reduced water losses. Today, at the fourth-generation level, special attention is set on effective storage integration and operation in larger networks. This is complemented by tuning of temperature levels and combining different energy sources.

Nevertheless, a number of unresolved critical issues remain which require further attention. In FIG. 2.12 they can be attributed to the next, fifth generation. Concerning technical aspects, improvements and new developments of suitable materials are needed. Achieving long-term robustness is a widespread challenge of existing sites, e.g., due to structural fatigue of waterproofing materials. TES need to minimize heat loss during a lifetime lasting decades, not only for the sake of storage efficiency, but also to minimize environmental risks. For instance, BODMANN & FISCH [135] measured a warming from 8 °C to 30 °C in 4 m below surface next to the storage in Hannover. Generally, such significant ground heating is rarely detected, and this is supported by simulations [177]. However, in practice, suitable monitoring and control systems are required to save the ambient ground and groundwater environment [195].

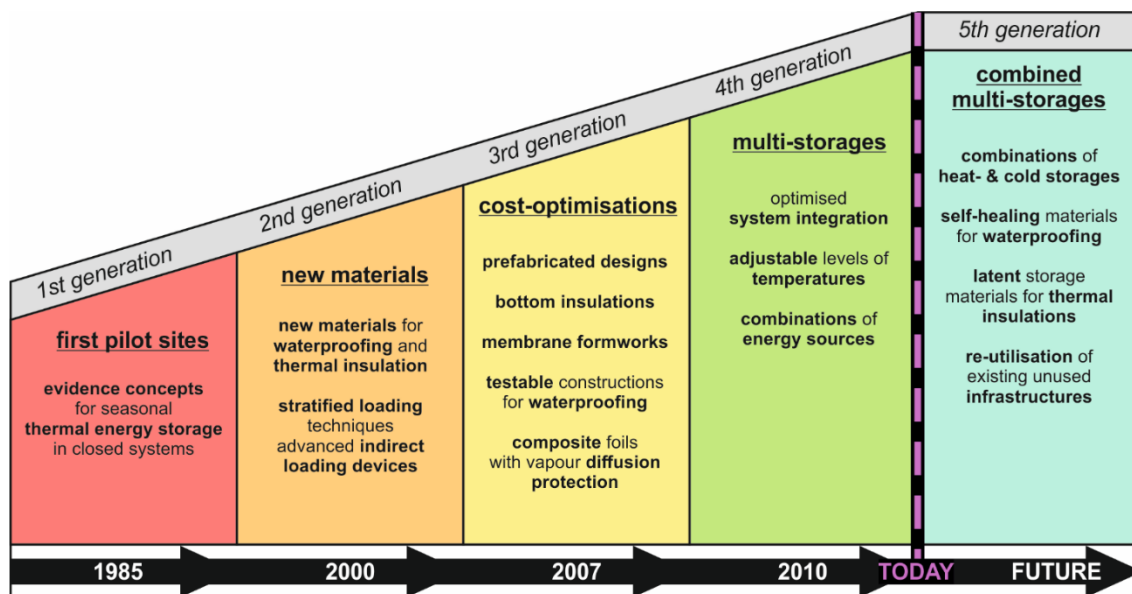


Fig. 2.12: Generations of seasonal storage systems with the most important inventions in the different domains.

Regarding TES operation, the vast opportunities to integrate new and diverse energy sources are still not exploited. Most TES rely on solar energy storage, but smart integration in heating and cooling networks facilitates storage of industrial excess energy, geothermal energy, and waste heat from office buildings and data centers. Aside from this, the optimal use of storages requires attuned control engineering. In many cases, for example, the return temperatures are too high, and in others the achieved thermal stratification was suboptimal. For solar-based systems, the solar fraction can be increased by one percent if the return temperature is reduced by only one degree [51]. A future direction for more flexible control and diverse source use is the consideration of combined storage facilities that represent multi-storage solutions of different sizes and different temperature ranges. Such solutions offer not only more flexibility, but also can be extended and upgraded more easily in case of network expansion or innovative materials in the future. Such modular development of TES can also reduce the high initial costs of construction, which are often decisive for realization of a project.

### 3 Paraffin wax as self-sealing insulation material of seasonal sensible heat storage systems – A laboratory study

This chapter is reproduced from:

Bott, C., Dressel, I., & Bayer, P. (2020). Paraffin wax as self-sealing insulation material of seasonal sensible heat storage systems—A laboratory study. *Plos one*, 15(7), e0236056, DOI: [10.1371/journal.pone.0236056](https://doi.org/10.1371/journal.pone.0236056).

The paraffin wax used in the experiments was donated by Hansen & Rosenthal KG, Hamburg, Germany for research purposes. The authors acknowledge this support for the study. Furthermore, the authors acknowledge the research associate Hannes Hemmerle and the student assistant Mayank Paranjape, who contributed essentially to the set-up and the execution of the experiments and Ryan Pearson for language edits. The study was financially supported by the Volkswagen Foundation within the framework of the “Initiative Experiment!” under grant agreement number 93847. The funder provided support in the form of salaries for author Ingo Dressel, but did not have any additional role in the study design, data collection and analysis, decision to publish, or preparation of the manuscript.

#### 3.1 Introduction

Seasonal heat storage has evolved as a promising strategy for storing thermal energy from fluctuating sources over long periods. Solar energy collected in the summer or any momentarily available excess heat can be stored for feeding a district heating network during the winter season [49,196,197]. The wide variety of available concepts covers latent, chemical and sensible variants [40,56,198]. While latent heat storages utilize phase change effects (e.g., of water/ice or hydrocarbons) [199–201], thermochemical storages are based on reversible endo- and exothermic reactions, such as salt hydrations [202,203]. However, both of these concepts are often not applicable to large-scale applications due to high material costs. Sensible heat storage, in contrast, features the utilization of temperature changes [57,58,204,205]. In this context, large seasonal storage systems are generated via borehole fields (Borehole Thermal Energy Storage [145,206]) or wells in aquifers (Aquifer Thermal Energy Storage, e.g., [60,207,208]). Another common technological variant, which is also the focus of this study, is the storage of thermal energy in large, artificial, ground-based basin structures. In these, water or water-filled gravel with volumes of several thousand cubic meters are used as storage media [55,58,113,167]. Especially for Pit Thermal Energy Storages (PTES) and Water-Gravel Thermal Energy Storages (WGTES), standard solutions for thermal insulation are non-existent. However, long-term thermal storage efficiency strongly depends on a competent and reliable technique that minimizes lateral heat loss from the basin [49,209]. This means, the storage media needs to be embedded in a stable waterproof shell of low thermal conductivity. This shell thus commonly consists of an internal impermeable sealing layer, that is, plastic foils encapsulating the water in the basin [55,59,105,121]. For thermal insulation,

highly porous and relatively cheap materials such as layers of foam glass or expanded glass gravels are used. As these are not resistant against the high structural loads of the overlying storage media, most of the previously constructed storage systems are insulated only at the top and side walls [70,177,196].

A main barrier for seasonal thermal storage basins to reach market maturity relates to technical vulnerabilities of the sealing and insulation components. The assessment of numerous existing sites reveals that there are two most important categories of deficiencies:

- 1) Efficiencies/heat losses: In many cases, higher energy losses and lower system efficiencies were measured than previously predicted (e.g., [70,135,165]). The reasons for heavily reduced performances were, among others, water ingress into the thermal insulation and interaction with groundwater, promoting the dissipation of heat [22,51,73,86]. Ultimately, these high energy losses reduce the efficiency of the storage facilities, raising questions about their general economic viability [37,147,210].
- 2) Leakages: A significant number of systems suffered from leaks, leading to irreparable damages and sometimes even total failures (e.g., [22]). Insufficient long-term resistance of the materials used for basin sealings could not withstand the highly variable thermal conditions and the static load of the filling material. Material fatigue is further intensified by the contrasting cold environment and hot storage filling during intense charging and discharging processes [59,86]. As large-scale storage basins thus dispense with the cost-intensive use of insulation, sealing layers are positioned directly on the surrounding soil and are exposed to a higher risk of injury. It is striking that most problems occur in the transition area from the storage media to the surrounding environment.

Based on these key issues, this study examines the suitability of a novel membrane concept based on paraffin wax, which may be suited for simultaneous insulation and sealing of seasonal heat storage basins. Paraffin wax is a mixture of hydrocarbon molecules with varying numbers of carbon atoms. The lengths of the C-chains range between 20 and 60 for soft and hard paraffin waxes and this controls both melting and solidification points of the bulk material used. For example, for a solidification point of 42 °C and a melting point of 40 °C, the molecules have a chain length of around 21 C-atoms. With an enthalpy of fusion between 150 kJ kg<sup>-1</sup> and 220 kJ kg<sup>-1</sup>, paraffin wax is one of the most popular storage materials [40,41,44,45,211–213].

Its thermal conductivity is relatively low, with values of 0.15 W m<sup>-1</sup> K<sup>-1</sup> to 0.30 W m<sup>-1</sup> K<sup>-1</sup> around one order of magnitude below that of a water-saturated gravel (2.4 W m<sup>-1</sup> K<sup>-1</sup> in the case of an implemented Water-Gravel Thermal Energy Storage described in [37]) [148,214]. Aside from this, it is hydrophobic and non-toxic [215]. These favorable properties support the use of paraffin wax for lateral thermal insulation and energy absorption, while melting of paraffin wax consumes energy and thus keeps it in the system [45,212,213,216]. A recuperation effect may be utilized when the storage cools down and paraffin wax solidification enables recovery of the heat stored in the phase change. The conventional use of paraffin wax as a thermal storage medium already makes use of these effects in various respects [217–220].



In encapsulated form or as a composite material with polymers, it has been employed, for example, for thermal component activation within buildings and for small-scale thermal storage applications [200,221–223]. However, if the paraffin wax is integrated directly and made available as a mobile medium in its liquid, molten state, it may be able to clog leakages in the sealing layers of storage systems via its hydrophobic property. In direct contact with cold surroundings next to the insulation membrane, it would cool down and prevent water loss from the basin. The objective of this work is to investigate these expected self-sealing properties of paraffin wax considering the conditions of seasonal storage applications in downscaled laboratory experiments.

By integrating a latent heat storage material in the marginal section, the critical vulnerabilities of existing storage membrane concepts are attacked while, at the same time, new benefits are added. Thereby, the presented approach is both technically simple and somewhat paradoxical, as paraffin wax is already a well-established material for thermal energy storage. Thus, this study provides a substantially new application strategy for thermal insulation.

With the objective of providing an initial proof of feasibility and to demonstrate the applicability of the intended mechanisms, this study is divided into two separate sections. The first part inspects the thermal performance of paraffin wax in a multi-stage laboratory experiment. Here, variants of implementing paraffin wax as insulation material are tested at variable temperature ranges. The second part is dedicated to the imperviousness of the storage membrane. For this purpose, various types of artificially induced leakages and selected surrounding materials are analyzed and the paraffin wax’s migration behavior is scrutinized.

## 3.2 Materials and methods

### 3.2.1 Enhancement of thermal performance

#### Experimental setup

The first laboratory test was designed to investigate energy losses when using paraffin wax inside two sections of sealing layers of a PTES structure. A schematic illustration of the experimental setup is given in FIG. 3.1, while FIG. 3.2 shows images of the erected set up in the laboratory.

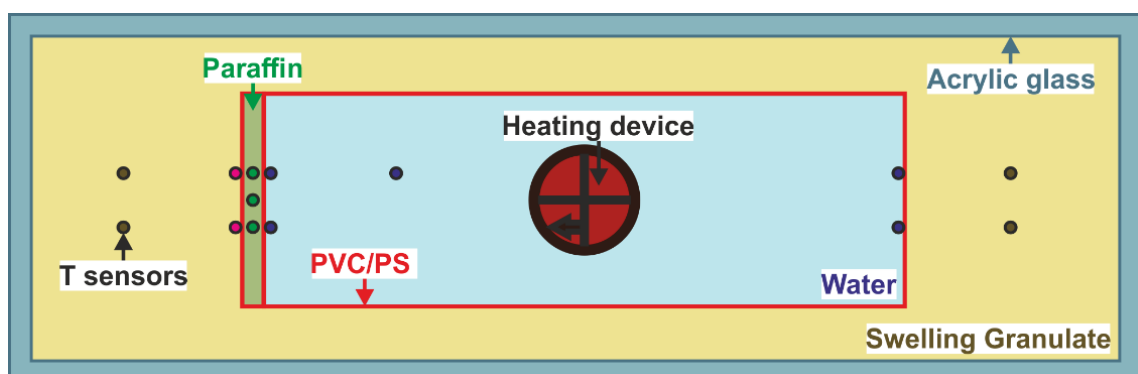


Fig. 3.1: Schematic top view of the thermal performance experimental setup showing the positions of temperature sensors and materials used. PVC: polyvinyl chloride foil, PS: polystyrene glass plates.

As outer enclosure, a container made of acrylic glass with internal dimensions of 1,000 mm x 300 mm x 600 mm (length, width, height) was used. A small-scale heat storage with deionized water as filling material was implemented inside, with its inner dimensions (600 mm x 200 mm x 400 mm) encapsulated by the inner sealing component. In the first series of experiments, sealing was conducted via rigid 5 mm thick plates of polystyrene glass (PS). In the second series, the PS plates were replaced by a 0.5 mm thick polyvinyl chloride (PVC) foil, which is commonly used for sealing in existing storage basins [105,131,196]. Comparing the use of non-formable PS plates with flexible, standard PVC foils facilitates to focus on potential mechanical deformation when including the paraffin wax. The latter was cast between another layer of the sealing membrane on one short side of the container (FIG. 3.2 a and b). The form of unadulterated paraffin wax was chosen to exploit the direct availability as a molten liquid to reseal leakages in the second part of the experiments.

Within the sealing membrane, the paraffin wax was distributed over the entire surface without pore spaces, which would not be the case with the paraffin composite materials frequently used in the construction sector, such as encapsulated paraffin wax. Here, this simultaneously provides a larger volume for additional storage of energy. In the case of the PS plates, a cavity distance of 20 mm was implemented (FIG. 3.2 b), and hence a paraffin wax volume of 1,600 ml was employed. In the experiment series with PVC, the same volume of paraffin wax was cast as a 20 mm thick plate, coated in PVC foil (FIG. 3.2 a). The paraffin wax chosen (Tudamelt 40/42, HANSEN & ROSENTHAL KG, Hamburg, Germany) has a relatively low solidification point at 42 °C and a melting point at approximately 40 °C. This is expected to resemble realistic conditions in favored low-temperature systems [51,152,167]. Gas chromatographic analyses by the manufacturer on the paraffin wax quality showed a dense distribution of the chain lengths of around 20 to 23 C-atoms (approx. 80%) within a total range between 17 and 32 C-atoms.

A top cover of the container made of transparent plastic foil (for better visibility not present in FIG. 3.2) minimized evaporation effects. To further shield the experiment from environmental influences and to emulate granular properties of soil surrounding a storage basin in the field, expanded glass granulate (Ecoglas, STEINBACH SCHAUMGLAS GMBH & Co. KG, Salz, Germany) was used (FIG. 3.2). As a recycling material with a grainsize of 5-8 mm, it is also installed as outer insulation material (thermal conductivity of  $\lambda_{\text{eff}} = 0.084 \text{ W m}^{-1} \text{ K}^{-1}$ , [224]) at some existing facilities [73,121,126].

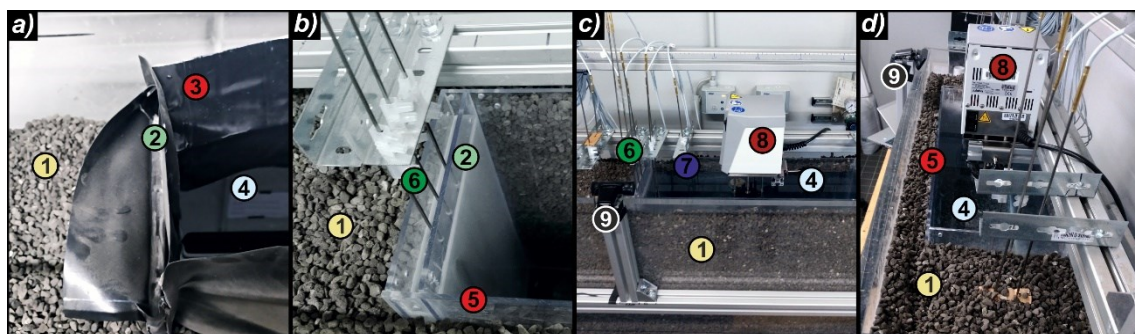


Fig. 3.2: Experimental variants with (a) black PVC foil and (b-d) PS as sealing layer. 1: surrounding material, 2: paraffin wax insulation layer, 3: PVC sealing foil, 4: filling/water, 5: PS sealing plates, 6, 7: temperature sensors in paraffin wax/filling, 8: heating device, 9: camera.

For heating the storage media, a laboratory thermostat (JULABO ED immersion thermostat) with an electrical power input of 2 kW was applied (FIG. 3.2 c and d), whereby the heating coil with a circulation pump was installed in the center of the water column. This simulated a direct loading procedure without thermal stratification in the basin but ensured a homogenous temperature distribution at all interface regions. For temperature measurements and data logging, two 20-channel Keysight 34901A multiplexers and one Keysight 34972A were used. In total, 15 Pt100 temperature probes were connected (stainless steel, waterproof, 4 wires, length 500 mm, measuring tip 20 mm, accuracy 1/10 DIN (German Industry Standard), FIG. 3.2 d). The accuracy of the sensors is temperature-dependent. Within the temperatures of all experiments it ranges between  $\pm 0.04\text{ }^{\circ}\text{C}$  (at  $20\text{ }^{\circ}\text{C}$ ) and  $\pm 0.06\text{ }^{\circ}\text{C}$  (at  $60\text{ }^{\circ}\text{C}$ ). Three probes were directly cast into the paraffin wax body at different heights. The distribution of the temperature sensors is shown in FIG. 3.1. A high-definition camera for time-lapse recordings facilitated visual observation.

### Testing procedure and data processing

The overall workflow of the thermal performance experiments is depicted in FIG. 3.3 a. After casting the paraffin wax directly into the PS or PVC cavity (FIG. 3.2), all temperature sensors were installed at the respective positions (FIG. 3.1). The experiment was operated in three phases for six different target temperatures between  $34\text{ }^{\circ}\text{C}$  and  $40\text{ }^{\circ}\text{C}$ . In the first phase, the system initiated at ambient temperature was heated up to the predefined target temperature (heating phase). Although the heating rate could not be directly measured, it was constant for all experiments, because the heating device always operated at full power. The equilibrium state, implying a constant gradient to the environment, was maintained for at least 12 hours (maintaining phase). This second phase was stopped by switching off the heating thermostat and the whole structure cooled down until the ambient temperature was reached again (cooling phase, FIG. 3.3 b, left). During all phases, temperatures at all sensor positions were recorded at intervals of 30 s and time-lapse videos (frame rate 100 frames per second from 30 s image intervals) were recorded with the camera.

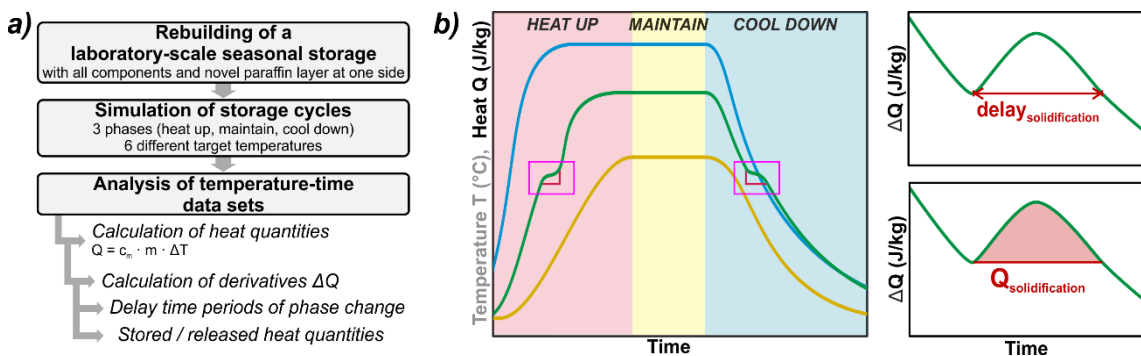


Fig. 3.3: a) Workflow of thermal performance experiments; b) experimental phases with definition of delay and stored heat content (schematic illustration). Pink box: delay in heating/cooling due to phase change effects. Line colors in Fig. 3.3 b: blue: water, green: paraffin wax, yellow: surrounding material.

For data evaluation, focus was set on two parameters to judge the suitability of paraffin wax for enhancing heat capacity and thermal insulation performance of the membrane: (i) a retardation factor that represents the delay of lateral heat transfer during melting or solidification of the paraffin wax; (ii) the amount of stored heat while melting during the heating phase or, vice versa, recovered from the solidifying paraffin wax in the cooling phase. In the following, all temperature data sets were firstly converted into heat quantities via the deployed masses ( $m$ ) and the specific heat capacities ( $c_m$ ) of paraffin wax, water, and surrounding material, respectively (using the caloric equation for heat  $Q = c_m \cdot m \cdot \Delta T$ ). In this context, the rather heterogeneous quality of the technical paraffin wax was considered by assigning an uncertainty of 5% to the specific heat capacity of the respective material. Combined with the measuring accuracy of the temperature sensors, the prolonged uncertainties of heat values resulted in max.  $\pm 8.5 \text{ kJ kg}^{-1}$ .

Although phase change effects are already detectable in these datasets (pink box in FIG. 3.3 b, left), the derivatives of these curves reveal the changes in the heat content of the paraffin wax more precisely and provide information on the accurate retardation timeframes (FIG. 3.3 b, right top). Ultimately, the amount of stored and retrieved heat was quantified using the integral of energy changes over the retardation period (FIG. 3.3 b, right bottom).

### 3.2.2 Leakage tests

#### Experimental setup

The leakage tests served to prove the desired self-healing mechanism when using paraffin wax in the waterproofing storage membranes. Since it is used in neat form, the material has a direct thermal junction with the interfaces of the inner and outer layers and therefore should first melt in the heating phase. Subsequently, it should be available as a hydrophobic, mobile liquid to clog pathways into the colder surrounding material in case of leakages.

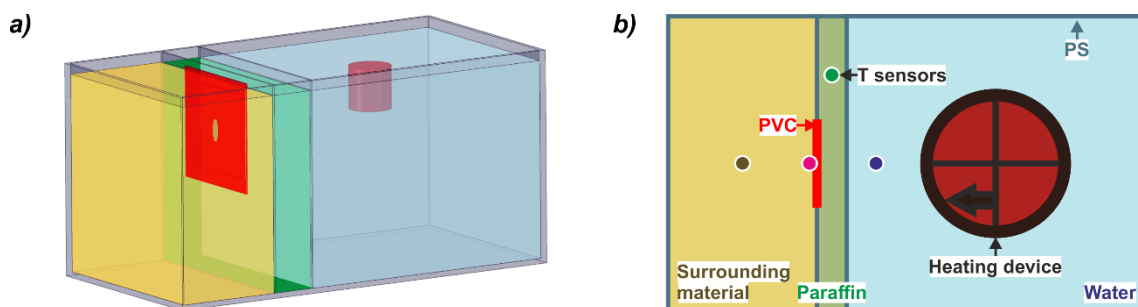


Fig. 3.4: a) Sketch and b) top view of leakage experiments. Green: paraffin wax, blue: water, red: PVC layer, yellow: surrounding material. Sensor positions marked with dots. PVC: polyvinylchloride, PS: polystyrene glass plates.

The set-up is shown in Fig. 3.4 and Fig. 3.5 and, for consistency and comparability, consists of many components of the previous tests. The operation and measurement equipment, such as sensors and the heating thermostat, were the same as in the experiments of thermal enhancements described above (Fig. 3.5). However, a much smaller external PS casing of 400 x 200 x 200 mm (length, width, height) was used to simulate a cross-section through the storage membrane and the surrounding material was only installed on one side (Fig. 3.5 a).

A 20 mm thick paraffin wax layer (volume: 800 cm<sup>3</sup>) was implemented in direct contact to the interior filling of deionized water (280 mm x 200 mm x 200 mm). In the outer PS plate, a 50 mm x 50 mm wide window was covered with a PVC film to simulate various leakage types in the sealing foil, such as fissures, larger holes and perforated zones (FIG. 3.5 b).

The area of the surrounding material finally resulted in a volume of 100 x 200 x 200 mm and allowed to observe and measure the outflow and dispersion behavior of the paraffin wax (FIG. 3.5 c and b). Two surrounding materials were deployed in separate test series: (i) a fine sand (grain size: 0.063 to 2 mm) was used to reproduce realistic field conditions, while (ii) glass balls with a diameter of 3 mm were chosen to imitate an ideal grain structure and to test the behavior of molten paraffin wax in mediums with a larger pore space (FIG. 3.5 a).

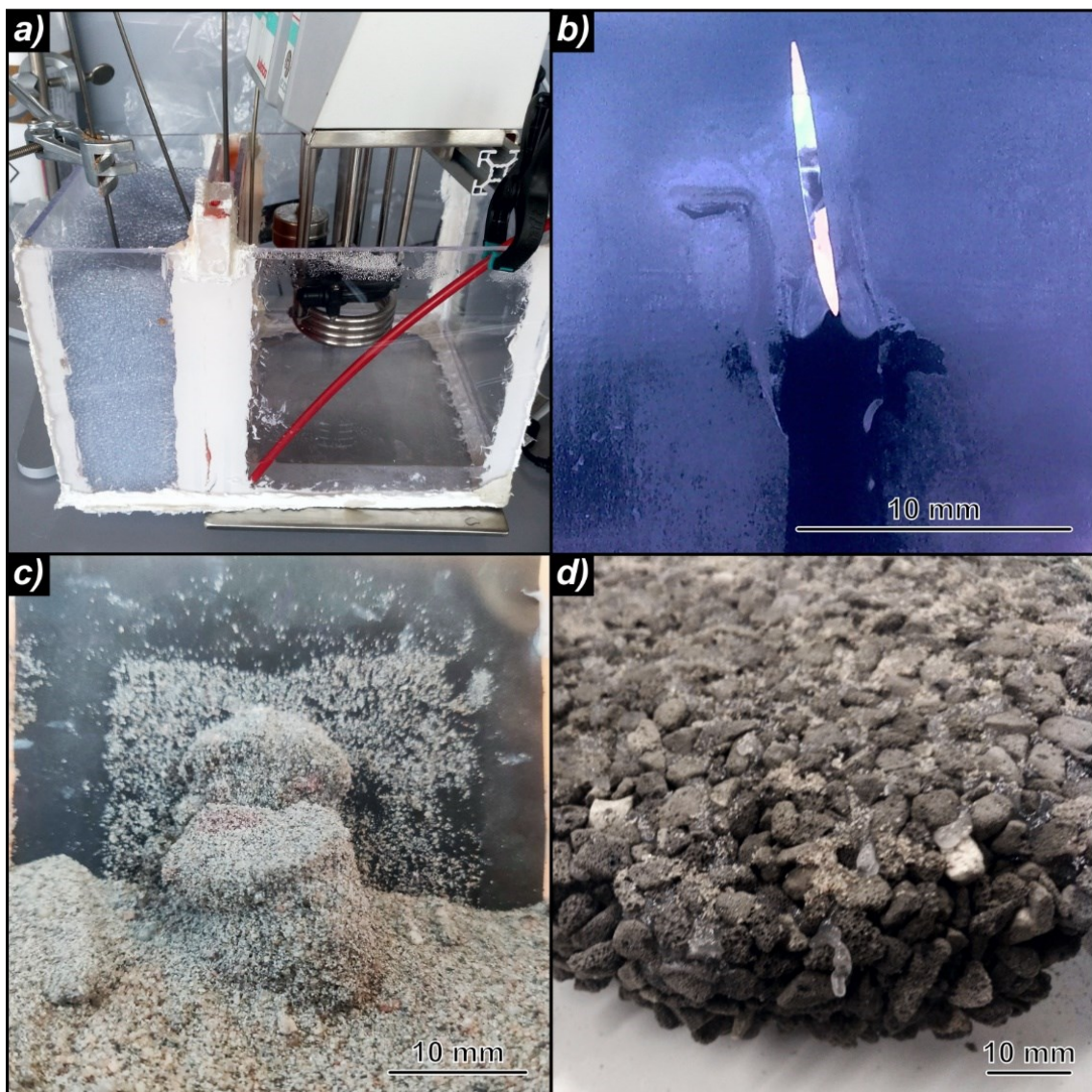


Fig. 3.5: a) Laboratory set up, b) fissure in polyvinyl chloride foil with outflowing paraffin wax, c) solid body of sand with paraffin wax, d) impermeable compound of surrounding material with pore spaces filled by paraffin wax.

### Testing procedure and data evaluation

The workflow of the leakage experiments is shown in FIG. 3.6 a. In the different scenarios, a certain type of artificial leakage was incised into the PVC foil and temporarily sealed with adhesive tape. Both vertical and horizontal fissures with an area of 20 mm<sup>2</sup>, a vertical fissure with an area of 40 mm<sup>2</sup>, as well as a large hole with an area of 380 mm<sup>2</sup>, and a foil containing a perforated region (total leakage area of 23.6 mm<sup>2</sup>) were tested. The storage tank was then filled with water and paraffin wax was cast in the cavity of the simulated storage membrane. After the paraffin wax solidified, the adhesive tape was removed, uncovering the defective zone, and the surrounding material (sand or glass balls) was inserted. For a rapid heating, the thermostat was set to 60 °C and the data logging was started. Just as all of the paraffin wax was in liquid state, the thermostat was turned off and the system cooled down to ambient temperature. For evaluation, the compound body of paraffin wax and sand or glass beads embedded in the surrounding material was exposed and sampled. Ultimately, the complete set-up was returned to its initial state for a new iteration.

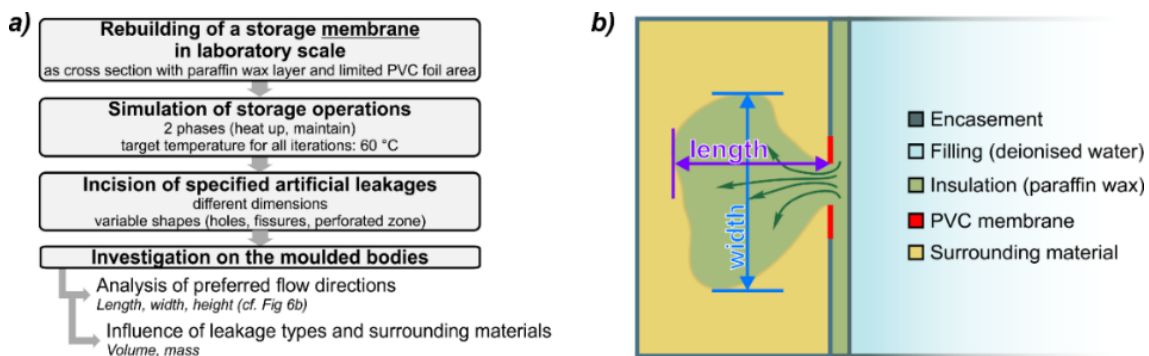


Fig. 3.6: Workflow for leakage experiments, b) top view of measurements of formed bodies after induced leakage. PVC: polyvinylchloride.

After each of these tests, the molded compound bodies of solidified paraffin wax and surrounding material were exposed, and their dimensions (length, width, height) and masses were recorded by caliper rule. The volume was calculated via the density and the mass of the compound material. Assuming a measuring precision of 0.5 mm for expansions and 1 g for the weight of the composite bodies, the resulting overall accuracy of the volume data resulted in max.  $\pm 2.7 \text{ cm}^3$  for bodies of compound material and  $\pm 1.4 \text{ cm}^3$  for data on volumetric paraffin loss. Special attention was further paid to the observed directions of paraffin wax dispersion. Accordingly, length and width of the bodies were defined as shown in FIG. 3.6 b, while the height was measured vertically.

## 3.3 Results and discussion

### 3.3.1 Enhancement of thermal performance

#### Visual observations

FIG. 3.7 and FIG. 3.8 summarize the results of the thermal performance experiments in both the heating and the cooling phases for six selected experimental settings. FIG. 3.7 a and FIG. 3.8 a show the retardation by melting or solidification of paraffin wax. In contrast, the absorbed/stored heat in the paraffin wax, which represents the extension of the storage capacity, is depicted in FIG. 3.7 b and FIG. 3.8 b. The results cover only experiments with PVC as sealing material, except for one iteration with PS for comparison.

First results and striking features of the presented concept are already apparent in the evaluation of the time-lapse recordings, as liquid components could be observed even at low temperatures. Therefore, even experiments with target temperatures below the melting point of the used paraffin wax show significant retardation effects and a storing/recycling of thermal energy. This can be attributed to the paraffin wax composition, as the technical quality employed in the experiments here is not a highly purified material. As it contains different chain lengths of hydrocarbon molecules, fractionalization occurs while heating or cooling and different partial sections melt and solidify in different temperature ranges.

It should be noted that this applies to all induced phase changes, resulting in no clear and sharp but soft and slow transitions. While this can be expected also in applications in practice, this adds uncertainties to the interpretation of the measurements. However, these effects are also considered within an uncertainty assessment, since all values of measurements and physical properties were assigned with error coefficients during the data evaluation (see section 3.1.2).

The second result already shown by visual monitoring were deformations of the paraffin wax layer during the melting process when using PVC foils. Displacement of the paraffin wax due to the pressure of the filling in direction of the surrounding material resulted in a wedge-shaped bulge. As a result, the thickness of the paraffin wax layer was substantially reduced at the bottom and enlarged at the top, raising technical questions on robust implementation techniques at the field scale. Even if these deformations could be avoided in the laboratory by using the stable PS plates, for large-scale storage systems it would be problematic to use a configuration between PVC foils without stabilizing structures.

#### Retardation and energy storage effects in the heating phases

Following the evaluation of visual documentation, the analysis of the temperature data records starts with the heating phase (FIG. 3.7). Thereby the results show significant delays due to the paraffin wax melting in all six test variants. This is remarkable, since this phase is comparatively short with a linear temperature increase of 0.49 to 0.71 K min<sup>-1</sup>.

The range of retardation period values (FIG. 3.7 a) among the different experiment settings is high, spanning from 360 s to 1600 s, with an average melting delay of about 1,000 s, but a correlation with the applied target temperatures is not apparent. Similarly, due to the given uncertainties, it cannot be deduced from the increased

individual value of the test with PS instead of PVC that the use of this alternative material solely generates a higher retardation. Nevertheless, the retardation value of 1590 s for the PS-variant is 80% higher than the average value of about 880 s for the tests with the PVC film. However, the results of all of the test executions prove the desired mechanism to be effective: Based on the retardation times, it can be expected that quick charging of an application storage can be effectively delayed by the melting processes of the paraffin wax. Simultaneously, the results also indicate a reduction of lateral heat losses.

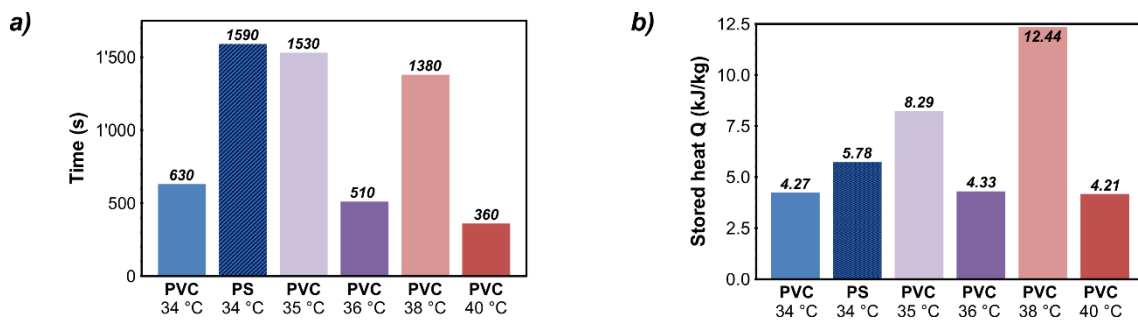


Fig. 3.7: a) Delay in heating of laboratory heat storage due to paraffin wax melting; b) additional stored heat in paraffin wax during heating phase. PVC: polyvinylchloride, PS: polystyrene glass plates.

As described in section 3.1.2 and visible in FIG. 3.3 b, there is a close correlation between the retardation times and the thermal energy stored in the heating phase (FIG. 3.7 b). Therefore, the results of the latter also show large fluctuations, ranging from 4.21 kJ kg<sup>-1</sup> to 12.44 kJ kg<sup>-1</sup> paraffin wax at an average value of 6.55 kJ kg<sup>-1</sup>. While these values are low, it is likely that slower melting processes could not be detected due to the rapid heating. No clear influence of the sealing material could be observed. The difference between PVC and PS at the same temperature is low, and the value for PS of 5.78 kJ kg<sup>-1</sup> is not significantly above the average of 6.71 kJ kg<sup>-1</sup> for all PVC experiments.

In conjunction with the given mass of paraffin wax used (1,200 g for a volume of 0.0016 m<sup>3</sup> or 1.6 l and a density of 750 kg m<sup>-3</sup>), the results of stored energy quantities are used for a linear upscaling to field conditions. Based on the frustum geometry of common Pit Thermal Energy Storage systems (PTES) [70,113,135], a storage volume of 50,000 m<sup>3</sup> and a thickness of the paraffin wax layer of 0.1 m, a paraffin wax volume of 1,000 m<sup>3</sup> can be assumed.

The results ultimately reveal an enhancement of storage capacity for this test case of about 3.16 · 10<sup>6</sup> MJ or 0.88 MWh to 9.33 · 10<sup>6</sup> MJ or 2.59 MWh. This additional energy reservoir would thus be available during a quick and intense charging process by applying the paraffin wax. However, compared to the storage capacity of the PTES water filling of 1.16 GWh (for a temperature spread of 20 K and a storage capacity of water of 4.19 kJ kg<sup>-1</sup> K<sup>-1</sup>), this is a small benefit and thus the additional heat storage capacity only is not sufficient for justifying the use of paraffin wax.



### Retardation and energy storage effects in the cooling phases

For comparison, the same measurement series was considered for evaluation of the cooling phases (FIG. 3.8). As expected from FOURIER'S LAW [225], the cooling phase is not reflected by a linear gradient of temperature and energy content, but by an exponential decrease converging to the ambient temperature. As a result, this phase covers much longer time frames until the ambient temperatures are reached again (FIG. 3.8 a, average 95 h, max. 144 h). The first results of the cooling phase already show substantial differences as the retardation periods caused by the solidification of the paraffin wax are several orders of magnitude higher (FIG. 3.8 a). They range between 8,500 s (~ 2.5 h) to about 17,000 s (~ 4.7 h), with an average value of 14,000 s (~ 3.9 h). Furthermore, a remarkable difference between the values for PS and PVC at the same temperature (34 °C) indicates a significant influence of the sealing material, since more paraffin wax can be utilized when deformation processes are prevented. However, there is no distinct trend observable for longer retardation times at higher operating temperatures. Altogether, results of retardations in the cooling phase demonstrate a more efficient applicability of the presented approach. Due to the long-lasting delays, subsequent energy can be provided in the marginal area of the storage in case of a rapid discharge of a storage unit. As a result, the steepness of thermal gradients in towards the surroundings can be reduced and energy losses are minimized.

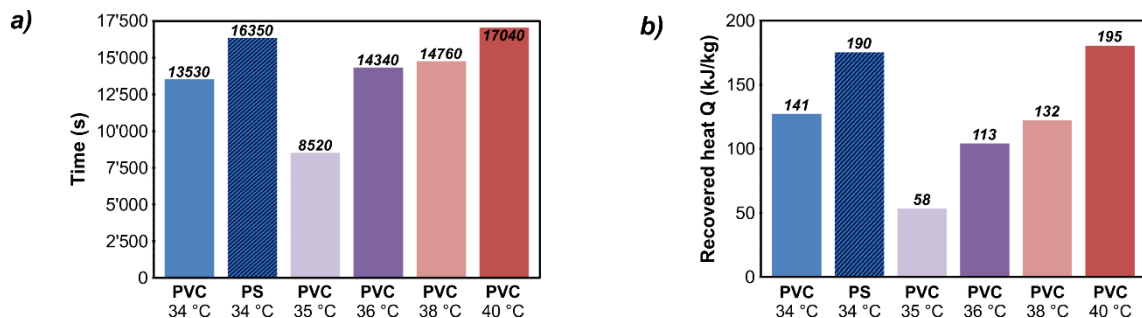


Fig. 3.8: a) Delay in cooling of laboratory heat storage due to paraffin wax solidification; b) additional released heat by paraffin wax measured in the cooling phase. PVC: polyvinylchloride, PS: polystyrene glass plates.

By evaluating the cooling phase, results on energy recovery can also be determined more accurately (FIG. 3.8 b). This is because this experiment phase represents an unaffected cooling process in contrast to the heating phase, where rapid energy inputs to the filling may superimpose phase change effects within the paraffin wax. As a consequence, the cooling phase allows to observe the entire sequence of phase change effects without interferences of external energy flows, also enabling much slower processes to be resolved. Hence, the results of energy recovered from the paraffin wax are several orders of magnitude higher than those determined during heating with an average of  $138 \text{ kJ kg}^{-1}$  at a range from  $57 \text{ kJ kg}^{-1}$  to  $195 \text{ kJ kg}^{-1}$ . Although a natural cooling curve as applied in the experiments does not properly represent the conditions of intermittent storage discharging in an application case, the findings prove that cooling is delayed by the energy recovered from the paraffin wax solidification. Thus, short-term discharge processes could be buffered and compensated over a longer period, resulting in slower temperature decreases in the storage shell and therefore in less impact on the sealing material's durability.

The amount of recovered heat is not affected by the operating temperature, but by the sealing material. The stable PS construction with constant, uniformly interface ensures the utilization of a larger volume of the paraffin wax. The recovered energy of  $190 \text{ kJ kg}^{-1}$  is significantly higher than the corresponding value using PVC ( $141 \text{ kJ kg}^{-1}$ ) and it is even higher than the average of all measurements using PVC ( $138 \text{ kJ kg}^{-1}$ ).

The values of the energy recoveries of the cooling phases are also applicable for scaling to the previously described use case scenario of a  $50,000 \text{ m}^3$  PTES. At this, the results show a striking difference: The volume of  $1,000 \text{ m}^3$  paraffin wax would provide an additional storage capacity of 12.01 MWh to 40.70 MWh (average: 28.77 MWh), being additionally available during a slow cooling or discharging process. Ultimately, these results are by one order of magnitude higher than those of the heating phases. They show an effective utilization of the desired processes and an added value of the new concept in terms of thermal enhancement of seasonal heat storage systems.

### 3.3.2 Leakage mitigation

#### Dispersion directions

The self-healing properties of the newly presented concept are based on the desired mechanism of actively sealing leakage pathways by the hydrophobic paraffin wax. Within this second series of tests, six different scenarios were examined. FIG. 3.9 shows the dimensions of the molded bodies of paraffin wax and surrounding material (according to FIG. 3.6 b) in relation to the respective type of leakage and the surrounding material. In one scenario, glass balls were used as surrounding material instead of sand. As the shapes of the different types of leakage (fissures, circular shaped apertures and perforated zone) are very different, it is not expedient to consider their lengths or diameters. Instead, the total surface area of these passageways is used as an auxiliary parameter for comparing the size (“A” in FIG. 3.9) of the leakage.

For all leakages, the results show a dominating dispersion in vertical direction (height) and horizontal to the surface of the sealing membrane (width). The heights, which show the greatest variance (29 mm to 105 mm), indicate a trend with increasing surface area of the defect. These also comprise the smallest values, between two and nine times lower compared to the vertical extents. In contrast, the values of widths and lengths scatter around their averages of 49.5 mm and 17.8 mm, respectively, within small ranges (min: 37.0 mm and 5.0 mm, max: 59.0 mm and 25.0 mm).

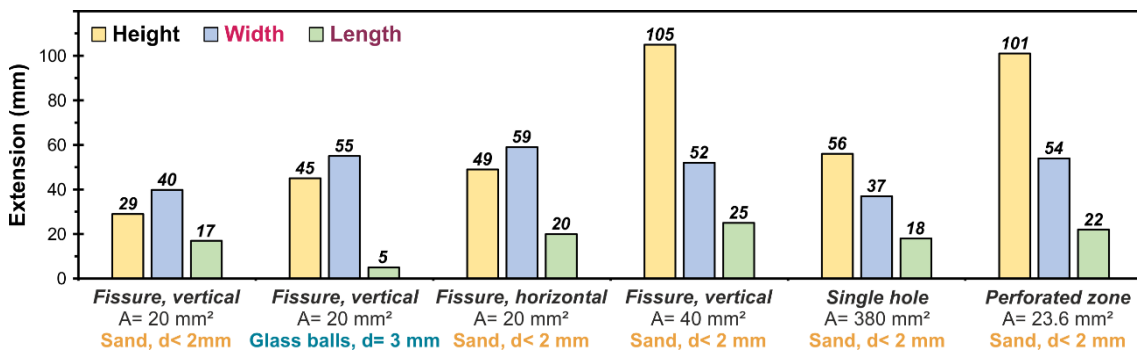


Fig. 3.9: Measurements of formed bodies after paraffin wax loss. The lengths and widths were defined as depicted in FIG. 3-7 b, while the height of the solids was measured vertically. A: total surface area of passageways as size of the leakage, d: grainsize of the surrounding material.

These results can be attributed to the influence of the gravitational force. Thereby the paraffin wax preferentially flows along the outer PVC foil of the storage membrane and spreads mainly vertically. However, the horizontal spread along the sidewall of the storage is also remarkable, which even exceeds the vertical component in case of smaller fissures. The high temperature at the outer membrane interface obviously plays a crucial role, ensuring that the paraffin wax does not immediately solidify after flowing out of the insulation layer. Thus, it can propagate laterally with significant material losses, representing a major weakness of the suggested overall concept.

Nevertheless, the self-healing mechanism of the presented concept already proves to be effective within these results, since dispersal in a horizontal direction straight away from the storage is successfully hindered. In this regard, the cold surrounding material represents an effective barrier, leading to a rapid solidification of the paraffin wax and clogging of the leakage.

#### Influence of leakage types and surrounding materials

The evaluation regarding the influence of the type of leakage (hole, fissure or perforation) does not initially reveal any major disparities. However, there are indications that vertical fissures of the same surface area uniformly lead to smaller spreading of the paraffin wax in all directions. Additionally, in the case of fissures, larger defects enhance propagations in vertical direction.

A more striking difference becomes apparent when comparing the two surrounding materials (glass balls and sand): Even though the pore space in the larger and uniform glass balls provides significantly more volume for dispersal, the length is reduced while the expansion in width and height is increased. Here, the glass bead provides the advantage of a larger reservoir of cold, preventing a flow into the surrounding material and allowing for a faster solidification but causing a deviation along the other two directions.

Further parameters for analysis of leakage types and surrounding materials include the mass of the molded bodies as well as their bulk volumes and finally the volume of the dispensed paraffin wax (FIG. 3.10). For comparison, the same series of experiments as in the previous analysis of dispersion directions are presented. The masses of the formed bodies (FIG. 3.10 a) show a comparatively small range with values from 11 g to 85 g. The maximum mass value resulted from the experiment of the perforated PVC foil, with its value of 85 g being almost three times higher than the average paraffin wax loss of 31.3 g. A difference in the surrounding material is not evident in these results, but there is again a noticeable difference in horizontal instead of vertical fissures. For the horizontal fissure, the value is more than doubled from 12 g to 25 g.

The results of total volumes (FIG. 3.10 b) reveal more distinct differences between the individual configurations. As already indicated in the previous evaluation of the bodies' dimensions, dispersions also vary in their volumetric extent, ranging from 12 cm<sup>3</sup> to 137 cm<sup>3</sup>. The share of paraffin wax in the compound bodies ranges from 36% to 67%, implying an additional variability in the volumes of released paraffin wax. Therefore, these data contain a comparatively larger span of 5 cm<sup>3</sup> to 80 cm<sup>3</sup>. Related to the total volume of 800 cm<sup>3</sup>, paraffin wax losses are small, ranging from 1.5% to 17%. These results prove that the self-healing properties can be applied without major discharges of the material used and that the proposed approach works effectively.

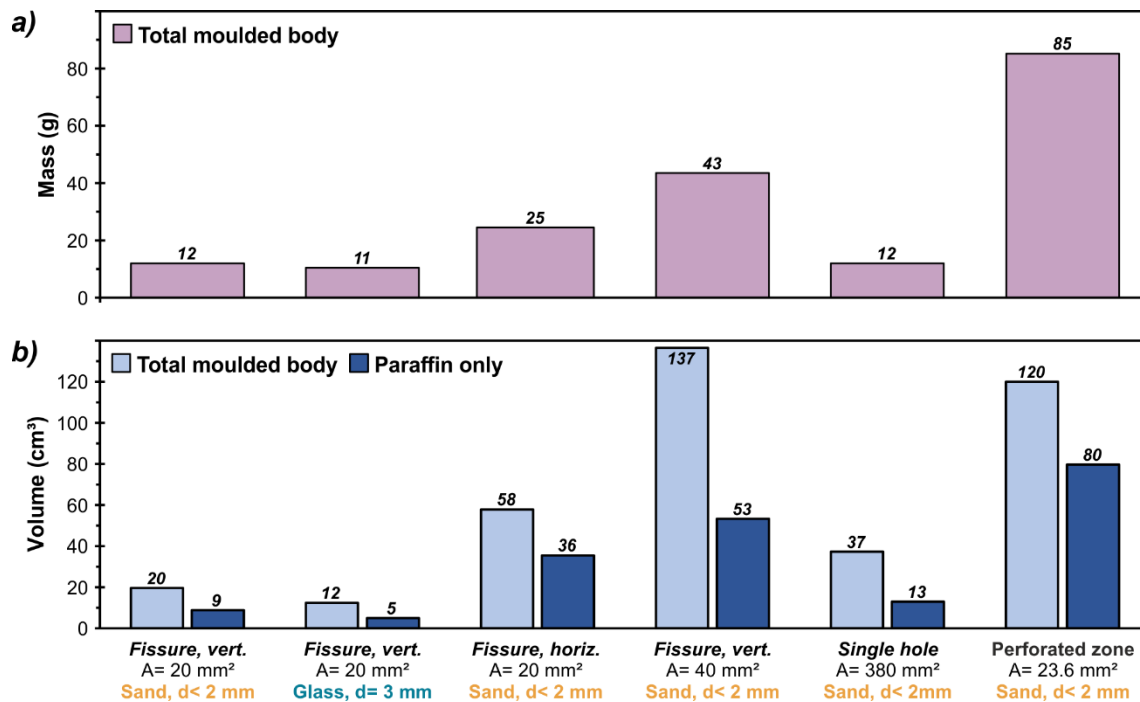


Fig. 3.10: Masses (a) and volumes (b) of formed bodies consisting of paraffin wax and surrounding material, after induced leakage. vert: vertical fissure, horiz: horizontal fissure, A: total surface area of passageways as size of the leakage, d: grainsize of the surrounding material.

The surface area of the defectives revealed as the most significant influence on the amount of paraffin wax lost, whereby elongated fissures represent a more severe problem than a circular, locally limited hole with a 10 times larger surface area. These results discovered by the tests can be explained by the optimal relationship of circumference to surface area of a circle. Conversely, linear leakages, e.g., like fissures, embody a larger heat reservoir, resulting in a wider surrounding warm surface which favors lateral propagation. The same applies to a perforated and porous foil, which, for example due to material fatigue, has a large number of small defectives. Moreover, a comparison of vertical versus horizontal fissures of the same size and surface area indicates a greater loss of paraffin wax for horizontal gaps in the outer sealing foil. Here, in comparison to vertical fractures, the vertical forces affecting the storage shell intensify the divergence of the incision gap.

Regarding the different types of leakage, the results ultimately show that there are distinct influences of both, the shape, size and orientation of the various defects. Nevertheless, although there are many different drivers, it is proven for all test series that the use of paraffin wax not only adds thermal benefits for seasonal heat storage systems, but can also provide longer operating times by eliminating the problems of material fatigue due to the new inserted self-healing feature.

### 3.4 Conclusions

The seasonal storage of thermal energy in large-scale basins already offers high potential to increase the flexibility of district heating networks by balancing out fluctuating regenerative energy sources. However, many of the present systems show deficiencies in regard to their thermal performance (emerging as excessive energy losses, significantly reducing profitability) and in regard to their technical set-up, as leakages in sealing foils can result in total system failures. This study tackles these key aspects by introducing a radically new concept for a combined insulation and sealing membrane. Starting as an unconventional approach, the use of paraffin wax as a hydrophobic and latent heat storage material in the marginal area of the storage was extensively evaluated in the laboratory and tested in two separate experiment series.

The advantages of the concept in regard to thermal optimization of seasonal storages were proven by the following results:

- ▷ A fast availability of these processes during a rapid heating of the storage filling was observed after only a few minutes.
- ▷ Conversely, a uniform energy recovery from the paraffin wax was observed during natural cool-down over periods of 2.5 to 4 hours.
- ▷ The additionally usable amount of heat provided by the paraffin wax revealed values in the laboratory of around  $6.55 \text{ kJ kg}^{-1}$  during the intensive heating phase and around  $138 \text{ kJ kg}^{-1}$  during the slow cooling phase.
- ▷ For full-scale application cases, a theoretical scale-up indicated a storage capacity expansion of up to 40.70 MWh.

On the one hand, these results show that both the buffering of intensive, short-term charges and discharges as well as normal operation can be optimized as desired. In this respect, the advantages of a low-cost storage material with a fast thermal applicability (water) and a latent, more stolid storage material (paraffin wax) are perfectly combined for maximizing long-term performances by increasing total storage capacities and reducing thermal stress on the materials because thermal gradients are flattened.

On the other hand, certain disadvantages of the new concepts in regard to its thermal behavior have to be mentioned:

- ▷ The added storage capacity by the paraffin wax represents only a small fraction of the total storage capacity, raising questions regarding the economic viability.
- ▷ A technical issue was detected, as the previously uniform layer of paraffin wax was deformed into a wedge-shaped structure, leaving no paraffin wax remaining in the lower section.

Although this technical disadvantage could be diminished by the incorporation of thermal stratification, further technical refinements are advisable, involving for example the application of a suitable support structure. However, attention has to be paid to the appropriate relationship between investment and added value in further developments of the concept, which would not be satisfactory considering only the total capacity increase.

With this foresight, the second series of experiments investigated the technical feasibility of self-sealing effects and also revealed significant benefits of the newly presented approach:

- ▷ After emerging from artificially incised leakages, the paraffin wax cooled down already after very short distances from the sealing foil.
- ▷ Furthermore, the proportions of lost paraffin wax are comparatively small between only 1.5% to 17%.
- ▷ Especially with coarser-grained substrates, the molded bodies led to the intended clogging of defects in the sealing membrane.
- ▷ Thereby, the mechanism was effective for all scenarios of different leakage types and sizes of the defects as well as in case of different surrounding materials.

However, by analyzing the several influencing parameters, it was also possible to identify potential shortcomings and technical disadvantages of the presented concept:

- ▷ Especially in the case of widely distributed, diffuse material deficiencies (e.g., perforations), an increased risk of large paraffin losses prevails because heat can be continuously supplied over a large area by the remaining paraffin layer.
- ▷ The warm surface of the storage shell allowed the paraffin wax to spread along this structure in the direction of the gravitational force.
- ▷ With these preferred flow directions, a total closure of the leakage might not be ensured because the desired clogging effect can only be realized in one direction, while dispersion along the outer storage surface can still lead to major losses of paraffin wax.

In conclusion, the general objective of the study as a proof of concept is successful, although unexpected risks are for now hindering a direct implementation to large-scale application cases. Both thermal utilization and an enhancement of the storage capacity could be demonstrated, but the paraffin wax proved to be highly mobile after the melting process, which also poses a problem to the desired self-sealing mechanism.

## 4 Component-based modeling of ground-coupled seasonal thermal energy storages

This chapter is reproduced from:

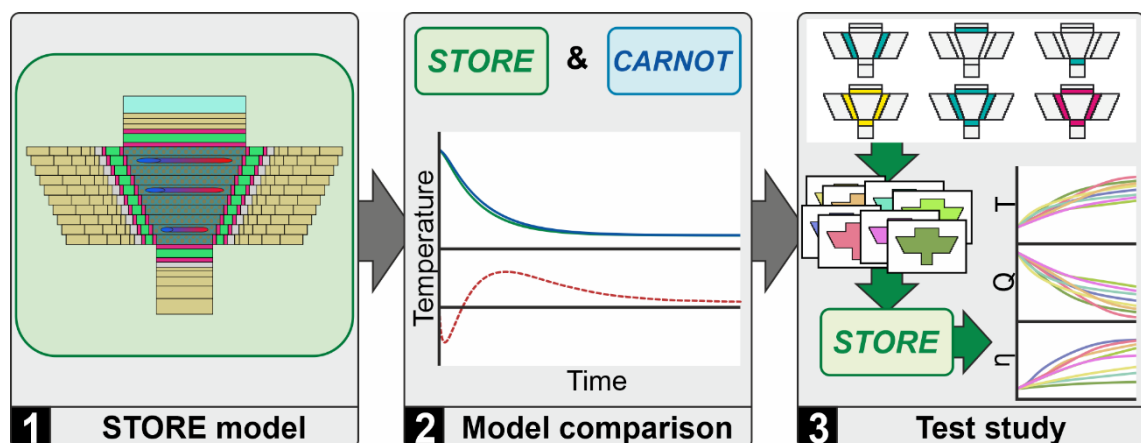
Bott, C., Ehrenwirth, M., Trinkl, C., & Bayer, P. (2022). Component-based modeling of ground-coupled seasonal thermal energy storages. *Applied Thermal Engineering*, 118810, DOI: [10.1016/j.applthermaleng.2022.118810](https://doi.org/10.1016/j.applthermaleng.2022.118810).

The authors acknowledge Olivia Zoch and Ryan Pearson for language edits. The study was financially supported by the Bavarian State Ministry of Education and Culture, Science and the Arts within the framework of the “Programm zur Förderung der angewandten Forschung und Entwicklung an Hochschulen für angewandte Wissenschaften – Programmsäule Strukturimpuls – Forschungseinstieg” (grant agreement no. VIII.2-F1116.IN/19/2).

### Highlights

- ▷ A new component-based model for seasonal thermal energy storage is introduced.
- ▷ It enables fast and versatile analysis of design variants and long-term operation.
- ▷ A comparison against an established tool proves its plausibility and applicability.
- ▷ A test study shows the model’s abilities, investigating several design parameters.
- ▷ The results conclude with generalized design recommendations for future projects.

### Graphical abstract



## 4.1 Introduction

Today, around half of the global final energy consumption is related to the supply of heat used for industrial processes and domestic applications. Worldwide heat production relies heavily on fossil-based fuels and thus is carbon-intensive. In contrast, non-biomass renewables contribute by a share of only 10-12% [226]. Due to their fluctuating nature, secure utilization of renewable sources such as solar thermal energy requires efficient temporal storage solutions, which in most cases are realized as water-based sensible heat storage systems [49,57,196,227]. When applied to the seasonal storage of the solar energy abundant during the warmer months, these installations need to be sizable to minimize the relative heat loss until being used in the colder months.

There exist a variety of concepts ranging from domestic buffer tanks applied in residential buildings [158,163,228–230], via volume tanks or pools integrated into heating networks [71,231–234], to large-scale, earth-bound, open-loop geothermal or closed-basin seasonal thermal energy storages (sTES). Geothermal implementations such as Aquifer Thermal Energy Storage (ATES) [60,235] and Borehole Thermal Energy Storage (BTES) [27,236–239] strongly depend on site-specific (hydro-)geological conditions [240]. In comparison, closed solutions, such as tanks (TTES), pits (PTES) and water-gravel thermal energy storages (WGTES), represent artificial installations with engineered fillings, constructed walls, sealings and insulations [58,196,241,242]. These technologies are classified firstly according to their structural design. For example, PTES installations are naturally sloped excavations (e.g., former gravel pits), which are sealed with waterproofing membranes and usually comprise a floating top with integrated insulation. WGTES and TTES, in contrast, commonly include static elements such as vertical sidewalls, a foundation, and a self-supporting roof. Aside from this, classification can focus on the filling of the storage: WGTES rely on a two-component filling media (matrix and fluid), while PTES and TTES are only filled with water [231,234,243,244]. Consequently, installations may also represent a combination of these storage types. The scope of this study is set on the category of artificial closed basins, which are less site-dependent than geothermal storage systems, but based on more complex engineered structures and devices.

Modern heating concepts do not only realize static seasonal storage but also flexible peak shaving and load shifting. Here, one seasonal cycle of solar supply is superimposed by secondary, short-term loads for integrating waste heat from industry, data centers, power-to-heat, or connected geothermal sources [245]. The design of the sTES may have a significant impact on the performance of the entire (district) heating system (DHS) [246]. Extended usability such as a storage device, buffer, and balancer, comes along with new performance requirements, which are ideally assessed and monitored by efficient computer-based simulations [188,236,247,248].

Available closed-basin sTES simulation techniques are manifold [249,250] and are performed most conveniently by assuming bulk efficiency coefficients or cycle losses [251–253]. However, this cannot resolve the transient thermodynamic behavior of storages, which is better tackled by process-based analytical [254] or numerical models, which often employ a finite element method (FEM) [255–257].



A comprehensive study on the state of the art of numerical modeling and simulation of sTES including a comparison of current tools is provided by OCHS et al. [38]. Accordingly, models for sTES analysis can be classified into five categories, ranging from energy system and building simulations (e.g., in TRNSYS [162,258] and MODELICA [259,260] via computational fluid dynamics (CFD) and multiphysics approaches (e.g., in COMSOL [261] and ANSYS [262]) to subsurface modeling tools (e.g., FEFLOW [263]) [38]. These all differ in the level of detail, the scope of the components considered, and the spatial and temporal discretization methodology [241,264].

High-resolution CFD approaches were presented, e.g., by AMIRI et al. [265]. However, their model implemented in ANSYS-Fluent addressed turbulent airflow in small-scale packed beds of other use cases and is not applicable to large-scale thermal storages. Among others, BAI et al. [243] and FAN et al. [266] found that detailed CFD models based on NAVIER-STOKES equations are only useful for detailed analyses of direct charging/discharging systems, as developed for instance by SUN et al. [267] or POWELL et al. [268]. This is due to the generally high computational requirements of CFD simulation. The complex meshing has been identified as another drawback of CFD models [264,269]. A multiphysics FEM approach for detailed subsurface modeling has recently been demonstrated by DAHASHI et al. [264] using a model developed in COMSOL, where the radially symmetric configuration allowed for a reduction of computational effort.

A strongly simplified CFD setup focusing on thermal stratification was developed in MATLAB by BASTIDA et al. [270] to analyze only the thermal behavior of the filling during direct charging/discharging processes within a cylindrical, 100 m<sup>3</sup> large TTES for various control options. Within the SIMULINK environment, OCHS [271] developed a radially symmetric model, coupling a one-dimensional (1D) finite difference method (FDM) model for the storage filling (water) and a 2D-FEM model for the surrounding ground.

In TRNSYS, 3D approaches were developed as types 1300 (truncated cone, PTES) and 1301 (“Surrounding Earth”) for PTES [272]. The resolution of these models is limited to a 2D radially symmetric model of the subsurface and a 1D vertical setup of PTES. Type 1322, which is the latest but private development, merges these two domains for truncated pyramid geometries and enables a 3D resolution for the surrounding soil [273]. However, these models are also limited in the storage type and have a low resolution of the internal structure. Furthermore, material properties are only specified as constants and not all relevant processes are covered (e.g., solar irradiation). Different types for energy system simulation in TRNSYS model do not consider detailed internal storage processes at the component level, as the focus is on the performance within its connected energy system. A study by LI et al. [245] compared storage types 342, 343 and 534. Type 142/342 was developed to consider cylindrical water storage systems (TTES) as so-called “coarse-structure” [274] and was e.g., used by SWEET et al. [163] to determine optimal systems of individual houses with solar thermal energy. An alternative is type 343 (“ICEPIT”) developed by HOMBERGER [275], which offers modeling of alternative filling materials (e.g., gravel-water), yet it is limited to truncated cones. For geometry analysis, BAI et al. [243] applied coordinate transformation methods to a simplified sTES model (type UGSTS, [210]) in order to improve flexibility regarding slope angles and heights. However, the wall composites remained unresolved.

A non-proprietary alternative is the tool developed and tested in a series of studies by NARULA et al. [253,276,277]. It allows analyzing different configurations of energy systems, while the sTES sub-model is strongly simplified and lacks information about internal storage processes as well as environmental interactions. Before, SORKNÆS [278] developed a modeling tool optimized for an energy system consisting of solar thermal, heat pumps and a PTES and aimed at high computational speed, yet resulting in high errors (ca. 35%) of calculated heat losses. Within the MODELICA/DYMOLA platform, DAHASH et al. [279] and REISENBICHLER et al. [280] developed models for simulating PTES to extend the MODELICA Buildings Library [259,260] with large-scale applications. Again, these models are combinations of radially symmetric, 1D models for water fillings and 2D heat conduction models for PTES. They cannot resolve internal storage components and depict indirect charging/discharging methods, and they have limited flexibilities with respect to storage design and environmental conditions.

The objectives of this study are derived from the identified shortcomings of existing applications. The aim is to provide a versatile model that captures relevant processes of large-scale, ground-based seasonal thermal energy storage basins, which can be adapted to any spatial scale, geometry, and time scale for fast system design, model-based control, and optimization. Furthermore, one goal is to implement processes, components, and system complexities that have not been sufficiently considered yet, with a particular focus on indirect charging/discharging systems. With the developed model, the simulation-based design process of a sTES is intended to be empowered by parallel, rapid, accurate analyses. On this basis, the aim is to enable straightforward parameter studies to rapidly identify the suitable configuration of a sTES system.

The novelties of the developed model relate to several aspects, while the modeling concept builds upon previous work and is intended to lend features from analytical and numerical procedures. For being straightforward to set up and use, as well as computationally efficient to execute, a component-based resolution of the storage device and ambient environment is employed. To ensure high flexibility, no limiting assumptions are made with respect to symmetry or radial configuration. This facilitates applicability to any geometry of the storage and resolves different lateral heat flux conditions in predefined discrete horizontal, and vertical directions. Thus, lateral, top, and bottom heat losses can be accounted for as well as effects of different insulation materials.

By discrete lateral process implementation, the geometric flexibility is maximized. Moreover, the model is able to cover complex designs (variable slope angles, height-dependent insulation thicknesses at different sides) or heterogeneous environmental conditions (e.g., height-dependent thermal conductivities). By achieving component-level detail, for example, unwanted, life-time-reducing temperature fluctuations in building components can be detected, while extensive parameterizations allow in-depth scenario analyses based on different material selections and thicknesses. This is not possible in models with compound  $U$  values or balanced  $UA$  values for larger domains. Additionally, one advantage is the consideration of energy gains and losses due to radiation to the ambient and solar irradiation to the storage's surface, as well as the ability to apply multiple temperature boundary conditions to different

interfaces. Besides, detailed and flexible, indirect charging/discharging mechanisms allow to evaluate temperatures, pressures, and energy fluxes.

Implemented in MATLAB/SIMULINK, the model allows flexible connectivity to other energy system components, while still providing a high resolution. It supports interfaces for further development, e.g., multiphysics co-simulations for implementing hydrogeological processes and/or soil heterogeneities, as proposed by DAHASH et al. [269]. Ultimately, it is provided as a ready-to-use package with this study.

In the following, firstly, the new approach and its implementation (“STORE”) is introduced. Second, a plausibility test is performed, which includes a benchmark against a commonly used and verified tool for simulation of hot water storages. Third, a test study with a total of 41 scenarios is defined. This is used to analyze the impact of variable storage configurations, ranging between a simple, uninsulated base case and a technically sophisticated high-tech case. The presented simulation results from these scenarios reveal storage performances, temperature trends, and long-term environmental effects for different insulation thicknesses and materials. The findings enable the derivation of generalized design recommendations for storage projects of closed sTES facilities.

## 4.2 Materials and methods

### 4.2.1 STORE model

#### General approach

In contrast to highly resolving and computationally intense numerical sTES models, the present approach does not rely on a full, 3D spatial discretization of the simulated system. Instead, STORE distinguishes individual building components, resulting in a component-based approach similar to common “coarse models” [264,281,282]. The components are connected via process-based transfer functions, which control intercomponent exchange of thermal energy and thus determine the thermal regime for the given boundary and initial conditions.

Assuming a stratified storage model, vertical thermal interactions are only considered in the interior, i.e., the filling of the storage, which thus is resolved as 1D configuration. This also serves as a premise for related radially symmetric node models [163,241,254]. However, starting from this core, its shell is resolved to discrete directions (e.g., north, east, south, west, for representing a cuboidal geometry), including all building components as thermal masses. Between these, respective heat transfer processes are simulated, mostly conduction, but also convection and radiation. In addition, charging and discharging of the sTES facility is mapped in greater detail than by the addition or subtraction of energy quantities to/from thermal masses of the storage filling at defined heights. Existing analytical models and standard correlations of heat exchangers are used to include heat flows and processes of common components. Thus, other relevant mechanisms of the charging and discharging processes, such as pipe hydraulics, are considered. The concept offers the advantage of being able to investigate variable geometries (e.g., multi-basin storages) and technically sophisticated configurations with a flexible choice of building materials and methods.

STORE is developed in the MATLAB/SIMULINK environment [283]. The underlying concept in SIMULINK is commonly known as bond graph modeling. The model is based on function blocks containing input ( $\chi$ ), output ( $o$ ), and state ( $s$ ) vectors, together with associated parameters ( $p$ ). During simulation, states can be represented in discrete-time ( $s_c$ ) or continuous-time ( $s_{d_{k+1}}$ ) form, following the mathematical relationships for outputs (EQ. 4-1), derivatives (EQ. 4-2), and time-stepping updates (EQ. 4-3):

$$o = f_o(t, s, \chi, p) \quad (\text{EQ. 4-1})$$

$$\dot{s}_c = f_d(t, s, \chi, p) \quad (\text{EQ. 4-2})$$

$$s_{d_{k+1}} = f_\chi(t, s, \chi, p) \quad (\text{EQ. 4-3})$$

Moreover, SIMSCAPE [284] is used as a supplementary toolbox to build a physical model with preexisting subfunctions. Within its open-source foundation library, underlying equations of all processes are accessible. The distinctive feature of SIMSCAPE is the ability to allow bi-directional flows between function blocks, in order to allow component-based, physical modeling. Thus, all components are configured as a block diagram including the specification of coefficients and variables, for example, material thicknesses, surface areas, and heat transfer coefficients in case of heat conduction. The simulation procedure involves the initialization of the model, where block parameters and the initial conditions are set. Numerical integration is performed in STORE using the ordinary differential equation solver ode23t, which solves initial state equations and runs the simulation using the FDM discretization method. The maximum step size is set 3,600 s, to calculate accurate results on an hourly basis. Consistency tolerances for initial conditions and transient calculation are set  $10^{-9}$  to provide a reasonable trade-off between computational accuracy and simulation time. Using MATLAB/SIMULINK offers further advantages: First, pre- and post-processing procedures can be incorporated in transparent fashion, for example, to read load profiles or to perform any follow-up evaluations, such as the determination of efficiency indicators. Second, a design database can be generated in advance, providing a simple way to perform parametric or sensitivity studies. For this, different scenario specifications can be run in parallel, ensuring optimal utilization of computational resources.

For parametrization, the design scenario database represents a further, novel key aspect. It contains all material properties of all individual domains, information about the basin's geometry, as well as other relevant parameters for design and operation. The structure and contents of the database are illustrated in APPENDIX C-1.

#### Modeled components and processes

FIG. 4.1 shows the structure of a storage system and its implementation in the component-based STORE model. Here, the cross-sectional view of FIG. 4.1 illustrates the individual components of the storage shell, which are resolved as thermal masses. By default, the components involved, from the interior to the exterior are: (i) the filling medium, (ii) an internal sealing, (iii) the insulation material, (iv) an external sealing, (v) the structural component (i.e., sidewall), and (vi) multiple thermal masses to provide a transition to the surrounding soil.

Internal and external sealing layers are required for storage systems, where the bulk insulation material is placed between two waterproofing membranes, as is common practice [146,196,285]. In the technical implementation of the model, thermal masses and transfer functions are grouped into assemblies. This allows flexible adaptation to different concepts or designs, which may also cover composites of multiple, partitioned basins with intermediate walls, which cannot similarly be considered with symmetric sTES models. Likewise, parallel or serially combined setups can be simulated.

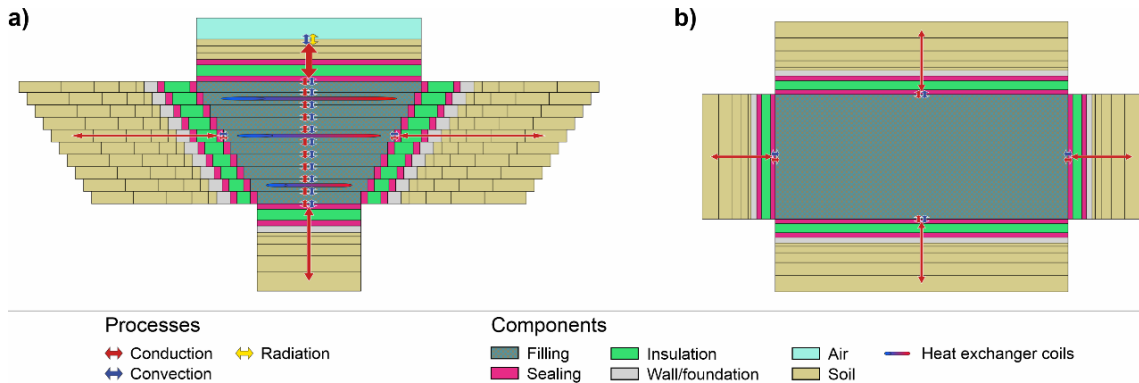


Fig. 4.1: Conceptual design of the model with components in cross-sectional view (a) and top view (b).

As a stratified sTES model, STORE is divided into  $n$  vertical sections using a height fraction ( $h_{\text{layer}}$ ) based on the height of the storage filling ( $h_{\text{sTES}}$ ) according to

$$h_{\text{layer}} = \frac{h_{\text{sTES}}}{n} \leftrightarrow h_{\text{sTES}} = n \cdot h_{\text{layer}} \quad (\text{EQ. 4-4})$$

This ensures that the internal storage height is uniformly divided and that the thermal masses represent the corresponding fractions of the building. The absolute elevation of each layer, i.e., its position within the storage, is used to automatically assign height-dependent parameters (e.g., fill volumes due to lateral slope angles, decreasing insulation thicknesses towards the bottom of the storage, etc.). The geometric flexibility of the model is exemplified in the cross-sectional view in FIG. 4.1 a as a variable insulation thickness at the top and the bottom as well as height-dependent at the sidewalls. This exemplary setup represents a configuration with ten vertically arranged layers, whereby the thermophysical, vertical interconnections between the thermal masses of the filling and the top and bottom assemblies are depicted. The laterally modeled processes are indicated in the central layer. However, this view shows that gaps are left in the model corners, where the discrete, spatial directions diverge. For simplification, influences between the different directions are neglected here. Instead, adiabatic boundary conditions are assumed. The top perspective in FIG. 4.1 b illustrates the lateral arrangement of the components in one horizontal layer, while the structure in this configuration is based on a rectangular base plane. However, the model allows other shapes and even a cylindrical design to be realized by a straightforward reconfiguration approach. Contrary to other models of sTES [188,243,266,270], here, the model's structure is not radially symmetric.

The superordinate, simplified energy balance of the sTES under consideration (EQ. 4-5) consists of the energy stored in the storage's filling  $Q_{sTES}$ , the charging/discharging fluxes ( $\dot{Q}_{ch}$ ,  $\dot{Q}_{dis}$ ), and interactions with the ambient ( $\dot{Q}_{sol,out}$  radiation to the ambient,  $\dot{Q}_{sol,in}$  for solar irradiation,  $\dot{Q}_{soil}$  and  $\dot{Q}_{air}$  for energy exchange with the surrounding soil/air), based on the thermal transfer functions described below:

$$Q_{sTES} = \dot{Q}_{ch} + \dot{Q}_{sol,in} - \dot{Q}_{dis} - \dot{Q}_{sol,out} - \dot{Q}_{soil} - \dot{Q}_{air},$$

where  $Q_{sTES} = c_{fill} \cdot V_{fill} \cdot \rho_{fill} \cdot \Delta T_{sTES}$  (EQ. 4-5)

Besides, the energy balances of the individual components are defined based on all processes at their respective positions. For example, exchanges of energy by radiation ( $\dot{Q}_{sol,in}$ ,  $\dot{Q}_{sol,out}$ ) are associated only with the thermal masses of the uppermost layer. Thus, the energy balance of these thermal masses changes accordingly. Heat transfer between all components is quantified by several thermal transfer functions, as illustrated by the arrows in FIG. 4.1. Here, vertical connections only exist between the thermal masses of the filling, and in the top and bottom sections, where thermal interactions with the ambient air or soil occur.

As a prevailing process, thermal conduction, which depends on the provided material parameters (effective thermal conductivity  $\lambda_{eff}$ , thickness  $M$ , interface area  $A$ ), is simulated laterally on each layer and in the vertical direction between the thermal masses of the filling. The governing equation used is FOURIER'S LAW, described as:

$$\dot{q}_{cond} = \lambda_{eff} \cdot \frac{A}{M} \cdot \Delta T$$
 (EQ. 4-6)

In the storage's filling, however, thermal conduction only dominates for indirectly charged and discharged water-gravel storages, where flow paths are assumed to be strongly limited. Thus, buoyancy effects are neglected in the current version of STORE. In contrast, for pure water fillings (e.g., in the case of TTES systems), and to model subordinated mixing effects due to convection in WGTES during longer standby periods, convection can be included as an essential process using the corresponding parameters (convective heat transfer coefficient  $\alpha$ , interface area  $A$ ). Heat transfer by means of convection is modeled using NEWTON'S LAW of cooling:

$$\dot{q}_{conv} = \alpha \cdot A \cdot \Delta T$$
 (EQ. 4-7)

By default, the top part of the STORE model reflects the sidewall configuration, including internal and external sealings with an interposed insulation. A static component is included, e.g., for water-filled tanks with self-supporting roofs. Furthermore, a key component represents an external top covering of the storage (e.g., soil), which is particularly relevant for low-insulated systems. To take higher thicknesses of the top covering and a steeper temperature gradient to the air into account, this component is resolved by three thermal masses. Radiation is also introduced here as a further thermal process using the equation of STEFAN-BOLTZMANN, based on the radiation coefficient  $\sigma_b$ , the emitting surface area  $A$ , the distance, and the temperatures of two thermal masses  $T_A$  and  $T_B$  [286]:

$$\dot{q}_{rad} = \sigma_b \cdot A \cdot (T_A^4 - T_B^4)$$
 (EQ. 4-8)

As the considered STES technology types are in-ground structures, the same configuration as the lateral storage shell is realized in the bottom part of the model. However, instead of the sidewall, conduction through the storage's foundation and transition to the underlying soil are modeled.

STORE is primarily used to model WGTES systems, which employ indirect heat transfer via an internal coil system as a heat exchanger (HX) for charging and discharging on multiple, predefined levels [37,196,287]. Hence, no operation involving fluid mass transfers at inlets and outlets of the filling is considered and mass conservation is ensured anytime. The number of charging/discharging levels as well as their absolute height in the filling are governed by the model's structure (FIG. 4.1 a). The coils of the HX are mapped using a pipe flow model obtained from the SIMSCAPE library, allowing fluid flow to be described analytically. Based on mass flow rates and temperatures of the charging fluid, as well as geometrical and material specifications, conductive and convective heat transfer (to obtain  $\dot{Q}_{ch}$ ,  $\dot{Q}_{dis}$  of the system's energy conservation equation), and pressure loss by friction at the pipe walls, are simulated. Heat transfer at the pipe wall due to conduction is calculated based on the hydraulic diameter of the pipe ( $D$ ), the thermal conductivity of the charging/discharging fluid ( $\lambda_l$ ), the surface area of the pipe wall ( $A_p$ ), the pipe wall temperature ( $T_p$ ) and the charging/discharging fluid's temperature at each pipe node ( $T_{in}$ ):

$$\dot{q}_{PipeCond} = \left( \frac{\lambda_l \cdot A_p}{D} \right) \cdot (T_p - T_{in}) \quad (\text{EQ. 4-9})$$

EQ. 4-10 is used to calculate heat transfer due to convection, based on the fluid's average specific heat ( $c_{p,avg}$ ), its average mass flow rate through the pipe ( $\dot{m}_{avg}$ ), its temperature at the inlet ( $T_{in}$ ), its average thermal conductivity ( $\lambda_{avg}$ ), the NUSSELT number ( $Nu$ ) and the hydraulic diameter ( $D$ ).

$$\dot{q}_{PipeConv} = c_{p,avg} \cdot |\dot{m}_{avg}| \cdot (T_p - T_{in}) \left[ 1 - \exp\left( \frac{Nu \cdot \lambda_{avg} \cdot S_H}{D \cdot c_{p,avg} \cdot |\dot{m}_{avg}|} \right) \right] \quad (\text{EQ. 4-10})$$

Turbulent flow is modeled analytically via the GNIELINSKI correlation [288–290], using the NUSSELT number ( $Nu$ ) as a function of Reynolds ( $Re$ ) and Prandtl numbers ( $Pr$ ), the hydraulic diameter ( $D$ ) and the internal surface absolute roughness ( $\epsilon_R$ ):

$$Nu = \frac{f/8 \cdot (Re-1000) \cdot Pr}{1+12.7 \cdot (f/8)^{\frac{1}{2}} \cdot (Pr^{\frac{2}{3}}-1)}, \text{ with } f = \left\{ -1.8 \cdot \log_{10} \cdot \left[ \frac{6.9}{Re} + \left( \frac{\epsilon_R}{3.7 \cdot D} \right)^{1.11} \right] \right\}^{-2} \quad (\text{EQ. 4-11})$$

To analyze the behavior of the charging/discharging system and temperature fluctuations which may cause adverse effects on the materials used, conductive heat transfer through the pipe walls is coupled to the pipe model prior to heat transfer to the filling. A graphical representation of the developed model showing boundary conditions, fundamental equations of modeled processes, and initial conditions is also available in APPENDIX C-2.

### Boundary conditions of environment and storage operation

Lateral energy exchange with the ambient ground is simulated in each layer as conduction through the surrounding soil at a resolution of five serially arranged thermal masses. In order to ensure a sufficient distance between the outer wall of the storage and the boundary of the model, their distances (i.e., volumes or thermal masses) can be adjusted and assigned with a linear increment. Preliminary studies during model development showed a required minimum distance of 2 m and a recommended increment of 2 m. However, these values may be modified for specific studies, depending on dimensions and operating conditions of the facility, while probe points may be used to verify sufficient distance. At the end of this sequence, interference with the ambient ground is modeled by a transient, specified temperature boundary condition ( $T = T_t$ ), based on an annual temperature profile  $T_t$ . This temperature can further be specified as a depth-dependent variable, which can be a decisive characteristic for the considered, buried, artificial basin structures. At the top, interactions with the unsaturated zone occur, while at the bottom, interactions with the groundwater may exist. Ambient groundwater flow cannot be simulated in STORE, but increased effective thermal conductivities of the soil due to groundwater flow may be used as a proxy to account for higher energy losses by heat dissipation.

The top part of STORE contains a component of surrounding air, where losses by convection and radiation are simulated. Similarly, an annual air temperature profile is laterally coupled to this component by a transient, specified temperature boundary condition. Energy gains by solar irradiation are modeled by a transient, specified heat flow rate boundary condition, which uses an irradiation profile ( $P_t$ ) directly linked to the external top covering (surface area  $A_{\text{Top}}$ ):

$$\dot{q}_{\text{sol,in}} = \frac{P_t}{A_{\text{Top}}} \quad (\text{Eq. 4-12})$$

Hence, required weather data may be obtained from nearby stations and contain temperature time series for air and soil, while groundwater temperatures replace soil temperatures in the lower sections in case of high groundwater levels, or if soil temperature data is not available.

The connected DHS is represented by a boundary condition based on load profiles, which covers temperatures and volume or mass flows. Time-resolved datasets provide information on supplied charging energy or demands for discharging and are directly linked to the analytical HX model (Eqs. 9-11). However, the presented model aims at longer-term operation over several months and years and prefers hourly resolved datasets. Since the DHS is not modeled explicitly, feedback effects caused by temperature alterations of the storage cannot be quantified.



To simulate the system's operation, a control function is defined, governing charging and discharging operations, as well as idle phases. To illustrate a default operation strategy, FIG. 4.2 shows a flowchart of operation mode decisions.

There, decisions are based on the storage's state (i.e., filling temperature,  $T_{Storage}$ ) and on the availability of charging supplies or discharging demands respectively, while a superordinate check uses maximum or minimum thresholds ( $T_{max}$ ,  $T_{min}$ ) to protect components by not exposing them to excessively high or low temperatures. The return temperature of the heat exchanger ( $T_{Return}$ ) is used to reflect the available energy flow for discharging. Time and temperature hystereses may optionally be included, to allow sufficient time for slow processes of heat propagation within the storage and to prevent rapid changes in operating modes, thus preventing stress on building components and pumps.

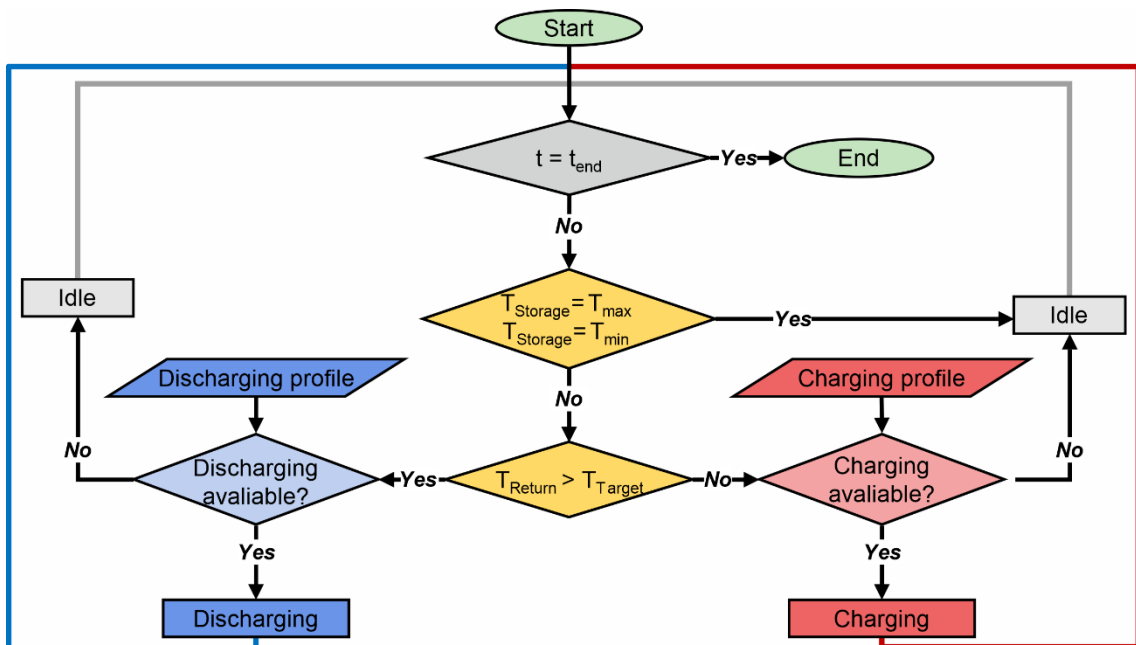


Fig. 4.2: Simplified flow chart for sTES control: Hystereses or subordinated strategies, e.g., with transition periods, are not considered.  $t$ : simulation time,  $t_{end}$ : last simulation time step,  $T_{Storage}$ : temperature reference of the storage,  $T_{Target}$ : temperature of the target system.

### Outputs and efficiency evaluation

STORE is equipped with an extensive configuration of default probes for monitoring (default configuration explained in APPENDIX C-3). These analyze information on operation states, temperatures and energy flows in the storage, the HX, as well as interactions with the ambient, or any other physical measures. Thus, a variety of outputs are generated for evaluating the storage's behavior and performance in different scenarios.

For endpoint evaluation, temperatures and energy flows represent initial rating metric. Furthermore, the efficiency is calculated based on two different approaches. Regarding the connected DHS, the amount of energy supplied by the storage via discharging is determined:

$$\eta_{\text{Subsystem}} = \frac{\sum Q_{\text{Discharged}}}{\sum Q_{\text{Charged}}} \quad (\text{Eq. 4-13})$$

Accordingly, this subsystem efficiency,  $\eta_{\text{Subsystem}}$ , is obtained from the ratio of discharged and charged energy quantities, both given in MWh, specified over a defined period. This indicator is particularly important for evaluating the potential for energy conservation, as the utilization of energy from the sTES may substitute other sources, which could emit greenhouse gases or be costlier. Thus, it is a practice-oriented parameter, which is focused on the benefits of a given storage facility. In contrast, the accumulated surpluses in the sTES are also of particular interest in multi-year storage operation or in case of a temporal or quantitative imbalance between demand and supply of thermal energy. Therefore, the system-related efficiency is compared to an internal storage efficiency,  $\eta_{\text{Storage}}$ , which is used to evaluate the raw efficiency of the sTES building to store thermal energy at low losses.

Accordingly, it is defined as the ratio of total energy losses to the total quantity of energy stored over a specific period and considers remaining excess energy quantities at the end of the observation period:

$$\eta_{\text{Storage}} = 1 - \frac{\sum Q_{\text{Loss}}}{\sum Q_{\text{Charged}} + Q_{\text{Excess}}} \quad (\text{Eq. 4-14})$$

A clear distinction between these two endpoint parameters is evident in the application case, as well as in the scope of balancing. This is critical, as the consideration of excess energy contents at the end of an observation period may significantly affect the storage's performance. Likewise, in the heat-up phase of a sTES, these values are strongly deviating, given the high imbalance between the storage and its environment. In this case, an evaluation regarding the energy quantity dissipated to the environment is of higher interest and should be separated from the direct discharge evaluation.

The operation time is discretized by given time frames and all values are expressed in MWh. For seasonal storage, consecutive cycles (mostly on the annual scale) are most appropriate. Initial heating phases deserve special attention, which often are most dynamic before the facilities converge to a quasi-stationary state. Therefore, the period until this state is reached serves as a further decisive performance criterion.

#### 4.2.2 Plausibility test

To determine the accuracy of the newly developed model, a plausibility test is first performed comparing STORE to a homogeneous body without thermal stratification. Thermal losses across the shell are distinguished from surfaces with contact to the air (top) and the surrounding soil (bottom and sides). The ambient temperatures are linked to these surfaces without interposed components, while the shell is described as a single component with a balanced value for thermal conductivity of the total compound, preventing resolution at the component level. Charging and discharging mechanisms are implemented using a simplified heat exchanger equation with homogeneous heat transfer to the entire body. With this simplified model, a basic energy balance is solved, calculating storage energy contents and temperatures based on charging/discharging energies, as well as interactions with the environment.

In a second step, results of a benchmark scenario are compared to an experimentally verified model. A customizable thermal storage model of the CARNOT toolbox (Storage Type 3) is used in this instance [291,292]. It bases on a similar approach of Type 342 of TRNSYS, using a 1D node model [163,274]. In comparison to the presented component-based model, it supports only one temperature boundary condition and the storage shell is represented as a compound structure. Furthermore, it relies on a radially symmetric setup, and thus only cylindrical geometries with uniform sidewall configurations can be modeled.

Therefore, in contrast to the configuration shown in FIG. 4.1, the geometry of STORE has to be simplified for comparability to a rectangular 20 m x 20 m x 10 m (length, width, height) basin. A best-fit geometry with equivalent UA values is calculated for the parametrization of the CARNOT model, assuming similar external surface areas at minimal differences in diameter and height. To closely approximate the charging and discharging processes, modifications additionally involve replacing the default heat exchanger in the Storage Type 3 model with a pipe model with similar specifications. The test covers a facility completely surrounded by soil. The influence of the surroundings is minimized using small volumes for the surrounding soil thermal masses in STORE. Further a homogeneous insulation at all sides with a thickness of  $M=0.3$  m and a thermal conductivity of  $\lambda_{\text{eff}}=0.1$  W m<sup>-1</sup> K<sup>-1</sup> is assumed. With these settings, different simulations of storage operation were performed. As an example, the presented results in section 4.1 cover a cooling curve starting from a filling temperature of 75 °C with static ambient conditions (20 °C).

#### 4.2.3 Test study scenarios

To further evaluate the capabilities of STORE, a test study with a variety of scenarios is conducted. A typical application is used where a robust feasibility assessment of an existing installation is needed in the design process. Here, STORE perfectly meets challenging demands of flexible parameterization to evaluate a large number of scenarios in order to provide design recommendations for an optimal solution.

Assuming generic load profiles and environmental characteristics, five years of operation are simulated. Different material parameters, conceptual and geometric settings of sTES are varied to identify crucial aspects for system optimization. An overview of the simulated scenarios is provided in TAB. 4.1. An uninsulated storage serves as the base case, which is modified in subsequent steps, assuming different external top covers, insulation thicknesses, and materials at the different sTES interfaces. By separately considering these aspects, efficacies of the various optimizations are to be determined. The results are evaluated with respect to the measures of efficiency (eqs. 13 and 14) and storage temperature characteristics, both covering the entire operation period and the last simulated year.

Tab. 4.1: Variables and parameters used for the test scenarios. XPS: Extruded polystyrene. HX: heat exchanger.

Domain	Parameter	Top covering (m), increment	Insulation thickness (m), increment: 0.05			No. of scenarios
			Top	Sidewalls	Bottom	
Base case	Uninsulated storage system - HX spacing: 1.00 m - HX diameter 0.05 m	0	0			1
Top covering	◆ Thickness (m)	0.25...1.00, 0.25	0			4
Insulation thickness	▲ Top (Foam glass)	0	0.05...0.3	0	0	6
	▲ Sidewalls (Foam glass)	0	0	0.05...0.3	0	6
	▲ Bottom (Foam glass)	0	0	0	0.05...0.3	6
Insulation material	● All sides: Foam glass	0	0.05...0.3			6
	● Top, sidewalls: XPS Bottom: Foam glass	0	0.05...0.3			6
	● Top: Mineral wool Sidewalls, bottom: Foam glass	0	0.05...0.3			6
<b>Total number of scenarios</b>					<b>41</b>	

### Setup of the seasonal thermal energy storage facility

FIG. 4.3 shows the conceptual outline and geometry of the basin structure for all scenarios of the test study. It has a cuboid shape with internal dimensions of 25 x 12.5 x 3.0 m, which is completely embedded in surrounding subsoil. These are chosen based on the approach of the re-use of existing infrastructure (here: swimming pool) for seasonal thermal energy storage. Previous studies [231] already discussed such a scenario, for example, to optimize heat pump operations by using an outdoor pool as a seasonal source of heat and cold [293,294]. With a surface/volume ratio of  $0.90 \text{ m}^{-1}$  this case is suboptimal in comparison to other storage basin geometries and considering the optimum ratio of  $0.49 \text{ m}^{-1}$  for a sphere with the same volume. However, for such unfavorable conditions, understanding and managing lateral heat loss is particularly of high importance.

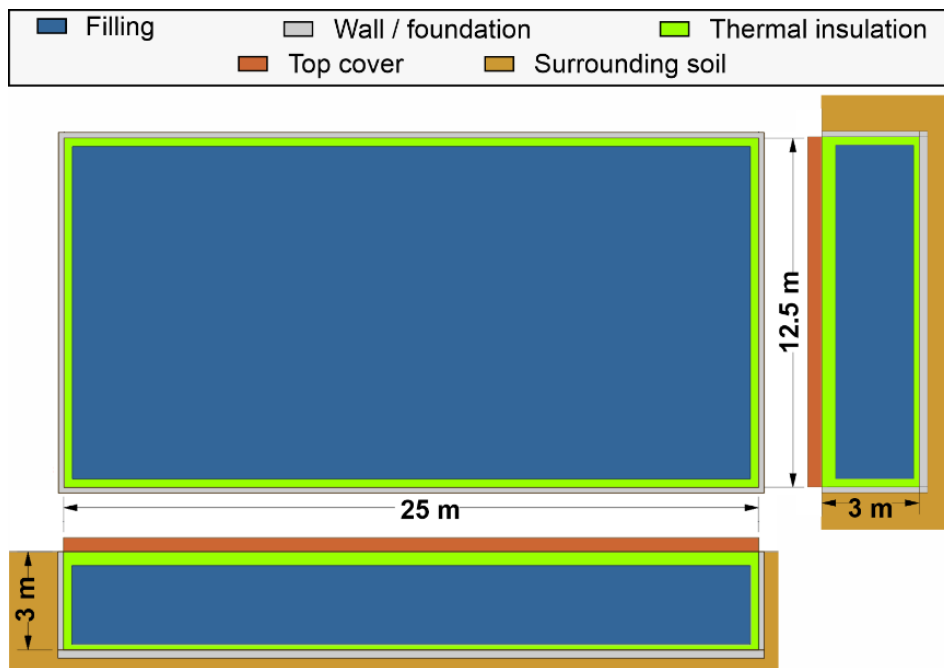


Fig. 4.3: Top and side views of the sTES structure of the test study, with an illustration of filling, thermal insulation, walls and foundation, as well as external top covering and surrounding soil (suppressed in the top view).

The storage media is a water-filled gravel matrix with a grain size between 16 and 32 mm. Based on existing field cases [37,287], a porosity of 0.4 is assumed, resulting in a total specific heat capacity  $c_p = 1,545 \text{ J kg}^{-1} \text{ K}^{-1}$  for the composite filling material. Effective thermal conductivity is set  $\lambda_{\text{eff}} = 2.4 \text{ W m}^{-1} \text{ K}^{-1}$  according to measured values of the WGTES facilities in Chemnitz (Germany) and Steinfurt-Borghorst (Germany) [143,151,285]. Convective heat processes are assumed to be minimal, quantified by a convective heat transfer coefficient in the filling of  $\alpha = 0.1 \text{ W m}^{-2} \text{ K}^{-1}$ . In the sTES, rigid cross-lined polyethylene (PE-X) pipe coils are installed as a heat exchanger. The internal spacings of the installation grid as well as the distances to the sidewalls of the basin are kept constant at 0.1 m. The pipe wall thickness is assumed to be 5 mm. The heat exchanger is installed at three levels within the storage filling, at 25%, 50%, and 80% of the total filling height.

A supporting shell structure of concrete is built up by vertical sidewalls with a constant thickness of 0.2 m and a foundation of 0.3 m. The sealing layer consists of two 2 mm thick high-density polyethylene (HDPE) foils. In the scenarios focusing on variable thermal insulation of the system, the insulation layer is embedded between these foils. It is important to note that, for similar temperatures, increasing insulation thickness reduces the filling's volume and thus the capacity of the storage. Foam glass gravel is among the most commonly used materials [49,196,241] and thus selected as the default insulation material. It is characterized by a low thermal conductivity of  $\lambda_{\text{eff}} = 0.05 \text{ W m}^{-1} \text{ K}^{-1}$  and a low density of  $\rho = 160 \text{ kg m}^{-3}$  [126,295]. Moreover, it is anti-capillary as well as pressure-resistant, which is particularly relevant because of higher loads at the bottom in the case of gravel-water fillings [295]. In comparison, XPS and mineral wool represent more cost-effective materials with better thermal properties ( $\lambda_{\text{eff}} = 0.04 \text{ W m}^{-1} \text{ K}^{-1}$  for XPS and  $0.03 \text{ W m}^{-1} \text{ K}^{-1}$  for mineral wool, [296]). However, they are not pressure-resistant, and used only at the top and sidewalls. These alternatives are investigated in twelve different "insulation material scenarios" (TAB. 4.1).

To compare the base case of a simple setup (without internal thermal insulation and external top covering) to a technically sophisticated variant, a high-tech case is defined. In this scenario, the basin is equipped with the most thermally effective insulation components, and at the same time, it represents the potentially most expensive design option. Each of the three interfaces of the storage filling is equipped separately: while the top is equipped with a 0.3 m thick layer of mineral wool, the sidewalls are insulated using 0.3 m XPS layers. At the bottom, foam glass gravel with a thickness of 0.3 m is applied. Due to the substantial use of insulation material, the storage volume is reduced in this high-tech scenario from  $937.5 \text{ m}^3$  to  $696.9 \text{ m}^3$ , while higher temperatures may counterbalance this reduction of the static capacity.

#### Boundary and initial conditions

For simulation of the storage operation, synthetic load profiles of a connected energy system are applied. As realized in practice [37,87,256], it is assumed that the facility is integrated into a decentralized solar thermal system with a small-scale DHS, while the modeled sTES is assumed to be hydraulically decoupled from the connected DHS. With one operating cycle per year, the scenarios represent seasonal charging/discharging. Thus, energy losses of infrastructures beyond the simulated storage as well as efficiencies of heat exchangers are neglected.

The annual charging load profile is shown in FIG. 4.4 (red), comprising a constant volume flow rate of  $10 \text{ m}^3 \text{ h}^{-1}$  and a constant HX inlet/supply temperature level of  $50 \text{ }^\circ\text{C}$  in summer. Since the storage is only used for heating of residential buildings in winter, the opposite period used for discharging is shown in FIG. 4.4 in blue, with a constant HX inlet/supply temperature of  $15 \text{ }^\circ\text{C}$  and a volumetric flow rate of  $20 \text{ m}^3 \text{ h}^{-1}$ . Temperature and temporal hystereses are set to  $5 \text{ K}$  and  $12 \text{ h}$ .

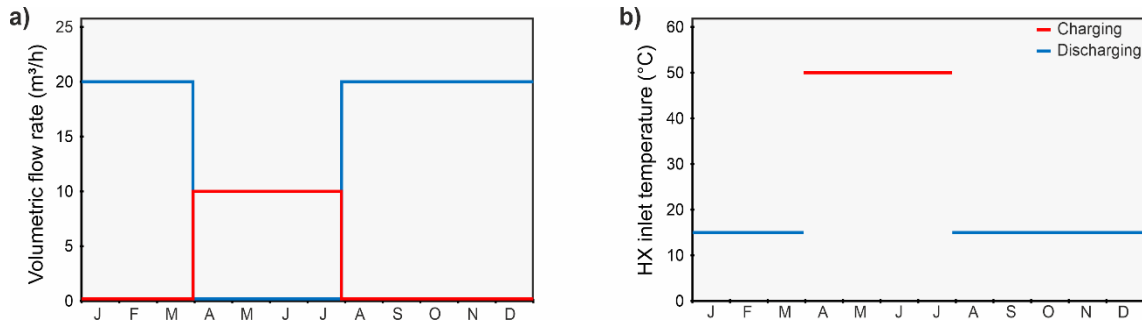


Fig. 4.4: Illustration of the annual load profiles for charging and discharging with a) volumetric flow rates and b) inlet/supply temperatures of the heat exchanger (HX).

In this test study, environmental conditions during storage operation depict the city of Ingolstadt, Germany. To specify the boundary conditions, the German Weather Service (DEUTSCHER WETTERDIENST, DWD) provides datasets on test reference years [297]. These are commonly used for the simulation of energy systems in construction projects. Hourly resolved air temperatures and solar irradiation datasets were obtained for moderate weather conditions throughout a reference period from the year 1995 to 2012 (FIG. 4.5). For specifying the thermal conditions in the embedding soil, local, long-term measurement series of soil temperatures at a depth of  $1 \text{ m}$  from a nearby weather station result in an average annual temperature profile, shown in green in FIG. 4.5 b. Any influence of ambient groundwater flow is neglected.

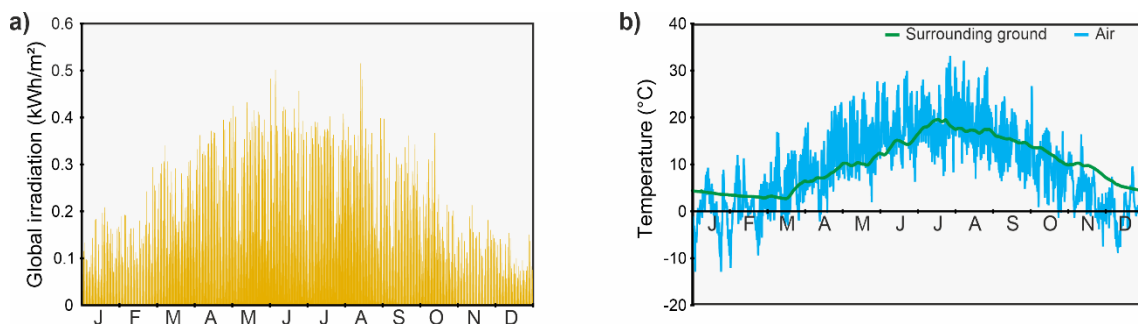


Fig. 4.5: Annual temperature profile of potential energy gain through hourly global irradiation from the sun as well as the b) hourly resolved annual temperature profile of ground and air temperature.

The material properties of the surrounding soil and the external top covering are oriented at standard values for dry soil ( $\lambda_{\text{eff}} = 2.2 \text{ W m}^{-1} \text{ K}^{-1}$ ,  $c_p = 800 \text{ J kg}^{-1} \text{ K}^{-1}$ ,  $\rho = 1,500 \text{ kg m}^{-3}$  [296];  $\omega = 0.95$  [298]). In contrast to internal insulation components, the top covering is applied externally and does not reduce the volume of the storage's filling. The thickness of the five surrounding soil blocks starts at  $2 \text{ m}$  and further increases linearly at increments of  $2 \text{ m}$ , in order to facilitate sufficient distance from the storage's external walls and to prevent interfering influences of boundaries.

It is assumed that between completed construction and commissioning of the facility, the basin is at thermal equilibrium with its environment. Therefore, all thermal masses, both inside the investigated sTES (i.e., fillings, insulation, seals, static elements) and outside (top covering, surrounding ground) are initialized with the soil temperature at the moment of commissioning (assumption: beginning of a fiscal year, 1<sup>st</sup> of January, 4.43 °C). The charging/discharging system is initialized unpressurized (not operating) without initial mass flow in the heat exchanger coils.

## 4.3 Results and discussion

### 4.3.1 Results of plausibility test

The results of the plausibility test are shown in FIG. 4.6 and include the individual temperature profiles of the cooldown curves (average, minimum and maximum temperatures of the sTES layers) simulated with the model of the CARNOT toolbox and the newly developed STORE model (FIG. 4.6 a). Furthermore, FIG. 4.6 b depicts the differences between CARNOT and STORE, which reach 0.93 K and -1.21 K (RMSE max. 0.396 K), while both models correlate by at least  $R^2 = 0.947$ .

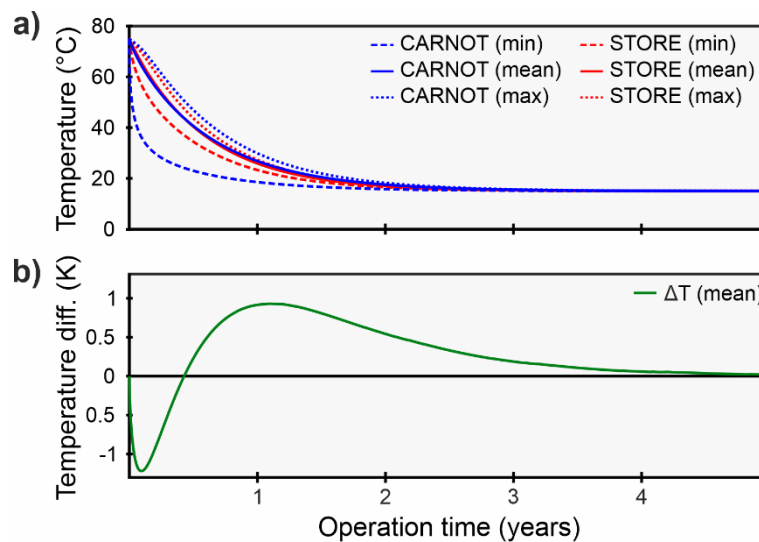


Fig. 4.6: a) Cooling curves of the STORE model and the comparative model of the CARNOT toolbox (Storage Type 3, modified best-fit); b) differences between mean temperatures of CARNOT and STORE.

The remaining discrepancies are explained by the conceptual differences of the two models, which also evolve because no additional adjustment procedures (e.g., further refinements of UA values) were considered. While the CARNOT toolbox applies a radially symmetric 1D-node model [292], the presented component-based approach of STORE is optimized for rectangular configurations. Additionally, more flexible temperature boundary conditions for modeling environmental conditions are used, including different temperatures at exterior interfaces and multiple thermal masses of soil embedding the storage basin. In this way, the outwardly decreasing temperature gradient is simulated and the additionally activated thermal capacity of the surrounding soil is considered. In the results of the simulation, these design disparities are reflected as trailing effects: initially, the temperature differences between the two models show a negative tendency (i.e., adverse effects), but then develop slightly higher values (i.e., positive effects).

Having these conceptual differences in mind, the comparison is considered successful, indicating robust applicability of the model. Furthermore, this comparison method, including an automatic parameterization script for the CARNOT model, may be included as a subcomponent within the model, in case further analyses are desired. This option allows for parallel benchmark comparisons for subsequent studies.

### 4.3.2 Evaluation of the test study

#### Base case vs. high tech case

The results of the test study start with the most simple and non-insulated base case (FIG. 4.7 a-d) in contrast to the technically most complex high-tech case (FIG. 4.7 e-h) and the results for the described seasonal 5-year operation of the storage are presented. The recorded energy quantities of charging, discharging and losses, temperature key parameters, capacity levels of the storage facility, as well as efficiency endpoint parameters are examined.

The base case system performs quite poorly, as the subsystem efficiency only reaches 11.6% in the last simulated year. Peak capacity levels of the uninsulated basin reach 26.5 MWh (FIG. 4.8 a), with a fraction of 59.8 MWh recovered (i.e., discharged) of the 444.8 MWh charged energy over the five simulated years. The heat losses and interactions with the environment are highest in this scenario, with an average of 91.6 MWh per year. This leads to a derived storage efficiency of 12.4%. The maximum and average storage temperatures over the entire simulation period are 42.8 °C and 39.1 °C, respectively (FIG. 4.8 b-c).

Evaluations of the high-tech scenario reveal a much higher storage efficiency of 57.1% and a subsystem efficiency of 69.5%. However, due to the reduced volume by internal insulation components, the peak capacity level is reduced by about 11% to 23.5 MWh (FIG. 4.8 a). The fraction of discharged thermal energy sums up to 68.8 MWh, compared to 99.1 MWh of heat charged to the basin. Due to the high insulation and reduced heat losses, the maximum storage temperature shows a 3.0 K higher value of 45.8 °C, while the mean temperature of 45.2 °C is raised by about 6.1 K in comparison to the base case (FIG. 4.8 b-c). The latter can be considered an advantage since thermal energy can be supplied at a higher exergetic level during discharge [299,300]. The significance of such exergy-based evaluations is underpinned by the results of previous studies [230] which discovered similar relationships with temperature levels and temperature stratification in the sTES facilities. However, in this case, it cannot counterbalance the reduction of capacity due to the reduced filling volume.

The operation shows effective control, especially after the charging phases. While this study does not consider a heat pump, the configured time and temperature hystereses effectively reduce periods of pump operation to promote the charging flow. Thus, as illustrated similarly in [234,245], the coefficient of performance and/or solar fraction, or renewable energy fraction of an integrated system, may be optimized. In FIG. 4.7 a and FIG. 4.7 e, this becomes evident by alternating operations of idle and charging. In fact, most of the idle phases in the last simulated year occur in the high-tech scenario (2,516 h), hence minimizing auxiliary energy consumption by circulating pumps, heat pumps, and other installations. In contrast, the base case scenario shows only 1,536 h of idle time periods in the last simulated year.



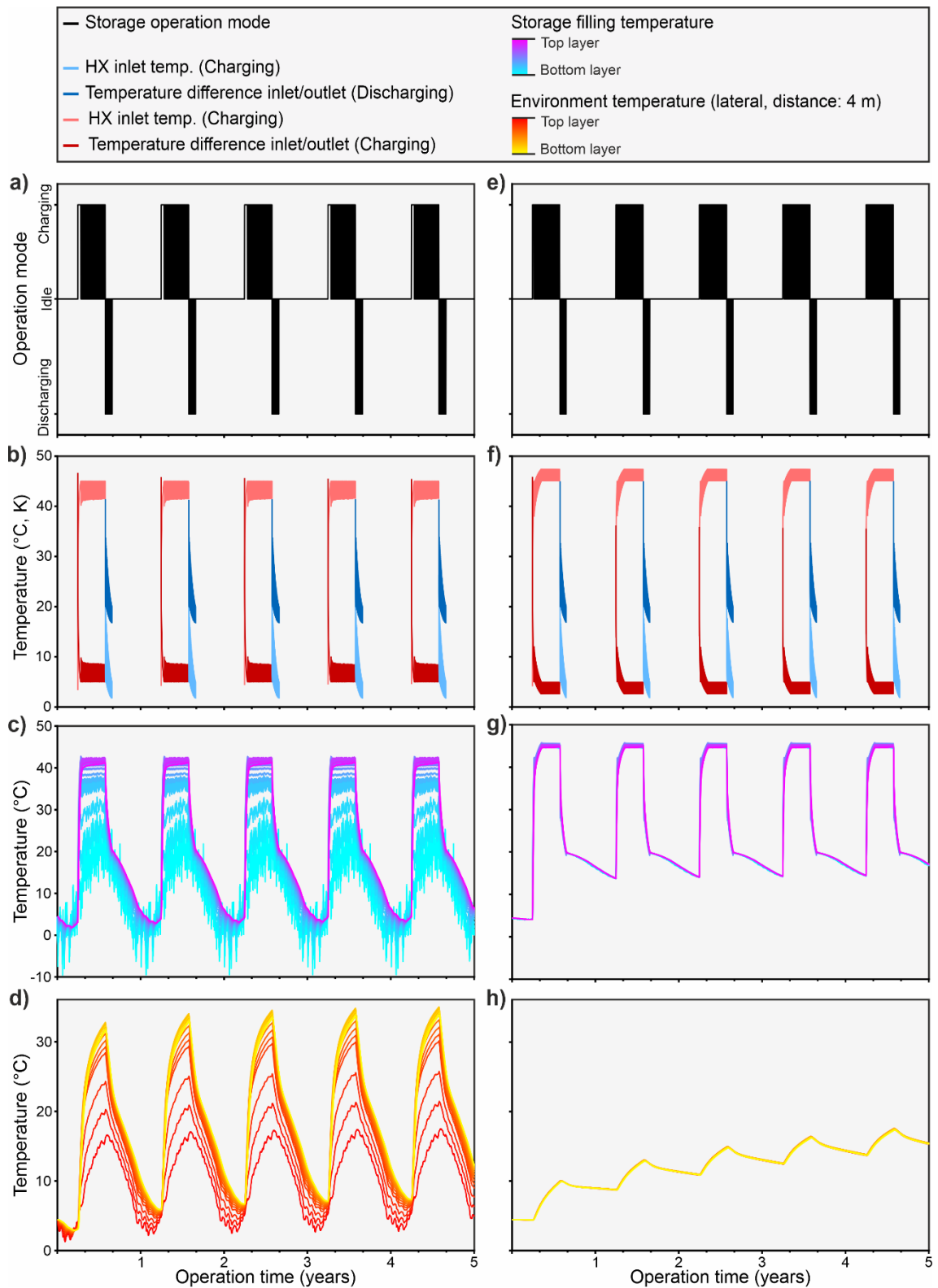


Fig. 4.7: Operational diagram of the base case (a-d) and the high-tech scenario (e-h). For temperatures in the heat exchanger (HX), setbacks (i.e., temperature differences to the supply) are displayed.

In the two extreme cases, as well as among all scenarios, the maximum temperature of the filling never fully reaches the temperature of the charging flow (FIG. 4.7 b/c, FIG. 4.7 f/g). Average temperatures range between 42.0 °C and 45.2 °C, with an offset of 2 K compared to the maximum temperature. This is due to the heterogeneous temperature distribution in the filling. Here, the storage medium of a gravel-water mixture prevents pronounced convective thermal energy flow in comparison to the conditions in pure water TTES.

Charging and discharging are carried out indirectly from top to bottom via a pipe coil heat exchanger. As illustrated in FIG. 4.7 c, this intensifies the characteristic internal temperature spreading and stratification within the storage in the base case scenario. However, this is mitigated by insulation as shown in FIG. 4.7 f. Here, the more substantially homogeneous profile originates from reduced internal and external losses, which is of primary importance in exergy analyses, as similarly demonstrated in related studies [210,299]. In contrast, FIG. 4.7 c reveals much more pronounced temperature fluctuations, predominantly in the upper storage section, which is strongly controlled by the ambient air thermal conditions.

The temperatures of the heat exchanger return flow provide information about the appropriate dimensioning of the coil system. In both scenarios, the charging/discharging flows are consistently well exploited, as the temperatures are effectively lowered to the filling temperature during charging. As depicted in FIG. 4.7 b and FIG. 4.7 f, the spread between supply and return flows is at its highest at the beginnings of charging and discharging periods in each year of the simulation. For charging, it is at least 45.9 K, while it reaches up to 30.1 K during discharging.

#### Effects of top covering and thermal insulation at different external interfaces

Considering minimum temperature values of the sTES filling, it becomes evident that an external top covering or insulation at the top of the basin is essential. Particularly during winter months, a risk of freezing can exist in this section of the storage, which would result in massive material degradation or even damage caused to interior components. This risk is particularly high at the beginning of storage operation, as the storage is initialized with ambient temperature. In contrast, insulation of the sidewalls and the bottom of the storage is ineffective or even adversarial, as it would prevent compensation of thermal losses by heat flux from the thermal mass of surrounding soil, which was also reported in practice [70]. The results show that at least a top covering of 1.0 m of soil is needed for ensuring a minimum temperature above 0 °C. Artificial insulation is more favorable, where a thickness of only 0.1 m already provides sufficient protection. Besides, during long-term operation, freezing may also be prevented by not fully discharging, resulting in a higher temperature at the end of the discharging period. This, however, reduces the exploitable capacity and thus the cost-effectiveness of the facility.

Thermal insulation at the bottom of the storage may hinder basal heat loss, but it can also be disadvantageous. Since insulation layers were modeled as internal components, their application reduces both the volume and the capacity of the storage. While DAHASH et al. [241] mention this as a theoretical issue, it is particularly striking for the results of the case study: while energy losses of lateral insulation are improved by about max. 19.2% in comparison to the base case scenario, they change

negligibly if the storage is only insulated at the bottom. This is also due to the low temperatures in the lower part of the filling. Such effects are even more evident for efficiency endpoint parameters: both the storage and subsystem efficiency decrease for bottom insulations, while for wall insulations only the subsystem efficiency increases slightly (max. 15.1% for highest insulation thickness; FIG. 4.8 d). Hence, consistent with the findings from previous studies [37,177], insulation is shown to be most efficient at the top while it is much less favorable at the bottom.

For all scenarios, subsystem efficiencies range from 12.2% to 69.5% (FIG. 4.8 d) and storage efficiencies from 1.4% to 57.1% (FIG. 4.8 e). The lowest storage efficiency is found in the scenario of a 0.3 m sidewall insulation. In fact, an evaluation of storage quality based on this indicator alone does not appear to be suitable: in this scenario, an amount of 52.6 MWh of energy is available, while internal thermal conditions are strongly controlled by interactions with the ambient environment. Therefore, ratings should consider both efficiency parameters: in that case, the high-tech scenario with 0.3 m thick, all-sided, differentiated insulation shows the best performance. With values of 57.1% and 69.5%, both storage and subsystem efficiencies are in the 90th percentile of the values of all simulated scenarios (FIG. 4.8 d-e).

In FIG. 4.8 a, it is furthermore demonstrated for all scenarios with internal insulation, that the maximum capacity levels of the storage unit decrease consistently with increasing insulation thickness (for sidewall and bottom insulations) or after a peak (for top and all-sided insulations). Similar results are obtained for discharge quantities, which are positively influenced by lower energy losses as the insulation increases, but negatively influenced by reduced volumes. This again supports the application of an external top cover. It achieves an efficiency increase of max. 9.2% (FIG. 4.8 d) and does not reduce the volume capacity of the storage. It also ensures a higher maximum capacity level of 27.1 MWh (FIG. 4.8 a).

#### Impacts of different insulation materials for all-sided insulation

The previous scenarios and analyses involved insulations on individual interfaces with only one insulation material – foam glass gravel. In further scenarios, all-sided insulations, as well as alternative insulation materials, are inspected. Thereby, this component is replaced with XPS and/or mineral wool at the top, as well as at the sidewalls. As suggested by MARX et al. [24] and MANGOLD [147], this can further optimize the performance of the system by minimizing thermal losses, yet increasing the complexity and investment costs.

The results show that all-sided insulation is superior to insulation exclusively at the top from at least a thickness of 0.1 m, as insulation translates to the reduction of storage volume. Starting from the base case scenario, the improvement of the storage efficiencies is almost concurrent and not diverging with increasing insulation thickness (FIG. 4.8 e). Based on homogeneous 0.3 m thick insulation of foam glass gravel at all sides, the storage achieves efficiency and reaches values of 48.9% (storage efficiency) and 64.2% (subsystem efficiency). In comparison to the 0.05 m thick insulation, losses are reduced significantly from 178.0 MWh to 57.7 MWh.

Enhanced material characteristics lead to a further increase in the storage efficiency by about 5% to 8%. The highest value is achieved in the high-tech scenario with 0.3 m thick insulation of mineral wool at the top, XPS at the sides, and foam glass gravel at

the bottom (57.1%, FIG. 4.8 e). Regarding average storage temperatures, no major variations are apparent above an insulation thickness of 0.15 m; in the comparison of the maximum storage level, all three materials show similar values (FIG. 4.8 c). This is particularly important for techno-economic design optimization. However, further factors, such as pressure stability, long-term effectiveness, and performance under the influence of groundwater or seepage penetration, must be considered [196]. Nevertheless, the installation of different materials may be associated with higher material expenses and more complicated installation methods, and should therefore be subject to a comparative cost-benefit analysis [241].

#### Long-term performance and thermal conditions in ambient subsurface

The important measures observed during the storage operation are positive and negative losses. While negative losses are directed outwards of the storage, positive losses are considered to be energy quantities absorbed from the surrounding soil. Especially for non- or low-insulated sTES systems, these may be significant or even desired. In addition, gains from solar irradiation can contribute significantly via the storage's top surface, especially in the case of black waterproofing foils and no soil cover. The results of the test study clearly show these effects, in the sense that temperatures in the topmost storage layers replicate ambient conditions in particular – both the air temperature and global irradiation profiles (FIG. 4.7 c). This is also reflected in the temperatures of the near surrounding soil in this scenario (FIG. 4.7 d). In comparison, temperatures of the surrounding ground in FIG. 4.7 h no longer show strong interference of the natural ambient conditions; in contrast, they are clearly superimposed by the annual storage operation cycle, exhibiting significantly larger and phase-shifted temperature amplitudes. Multi-year simulations demonstrate this effect distinctly, as periodically heating (both laterally and below the storage) occurs even at further distances. These conclusions are supported by results gained in practice, for example from the WGTES in Stuttgart, Germany [70].

The degree to which the temperatures in the near field correlate with the average temperature of the storage depends again on the degree of insulation. Thus, heating at a distance of 2 m next to the basin is increased by a maximum of 14.1 K after five years for the high-tech scenario, but only to a maximum of 7.9 K in the case of the uninsulated base case scenario. This also compares closely to results obtained from operating installations. For example, BODMANN et al. [135] measured temperatures between 8 °C and 30 °C up to 4 m away from the TES in Hanover, Germany, while BENNER et al. [37] report a temperature increase of 9 K after one year, 2 m next to the storage in Friedrichshafen, Germany.

During long-term operation, environmental effects also lead to changes in energy flows, which ultimately result in an overall improvement of performance. As theoretically discussed by DINÇER & ROSEN [56], this mechanism is proven by the test study in all scenarios, but to different extents (FIG. 4.8 f). While the base case shows an annual increase in the subsystem efficiency of only 0.2% over five years, this effect is most pronounced for the highest insulation at the top (0.3 m) with an increase of 5.1% per year. Although the latter scenario does not show the highest subsystem efficiency in the last simulated year, its increase from 44.3% to 67.1% reflects the initial phase of a storage's operation until peak efficiency is reached.

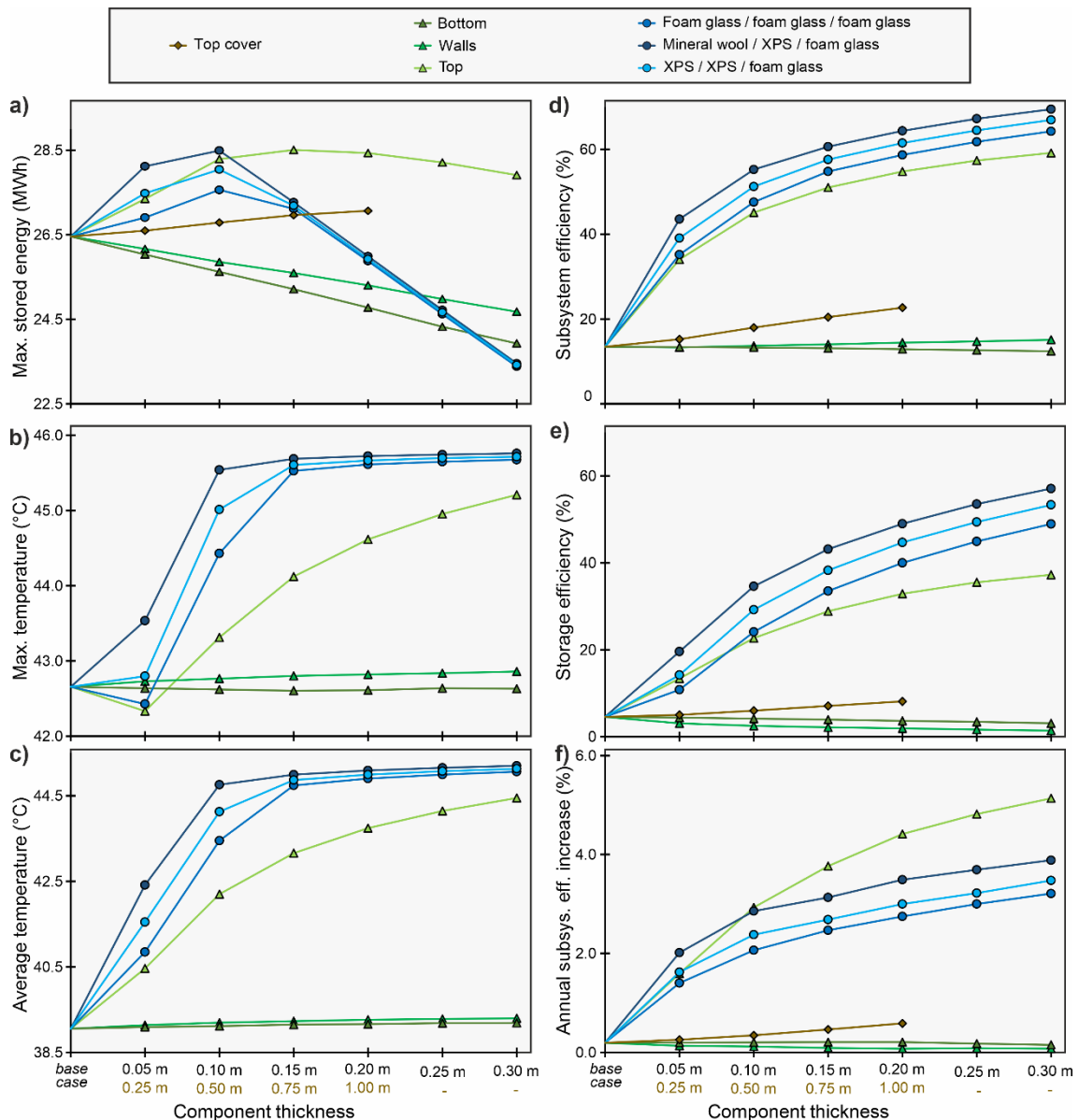


Fig. 4.8: Changes in evaluation parameters over the upgrade stages (increasing thicknesses) of the respective components (top covering, thermal insulations). The diagram shows a) the maximum storage level, as well as b) the maximum, and c) average filling temperatures over the entire simulation period. Furthermore, the diagram shows d) trends in endpoint parameters of storage and subsystem efficiency for storage upgrades, and f) annual rates of increase in the subsystem efficiency.

Similar trends of heating and stabilization phases were measured for sTES systems in Steinfurt, Germany [135,146], and Hanover, Germany [135]. The efficiency increase follows a converging trend to an upper threshold for the scenarios with top and all-sided isolations. This indicates that the optimum configuration as a ratio between storage usability (by maximum discharge quantity) and capacity of the seasonal storage may already be achieved.

Excess energy quantities after the evaluation periods represent an important factor of long-term performance. In general, the highest surplus appears in the last simulated year, since increased temperatures of the surrounding soil prevent rapid and full cooling of the storage. This is most significant in the scenario of insulation exclusively with foam glass gravel at the top, where the surplus is up to 8.34 MWh.

This underlines the beneficial thermal effect of surrounding soil for ground-based systems, since energy is not lost due to effective insulation in the upper storage section, but can be recovered at the same time from the ambient ground heated up by the storage system. This effect is most potent at the beginning of the operation. With continued operation and higher temperatures of the surrounding soil, the effect changes to that of thermal activation, as losses are reduced by flattened thermal gradients.

## 4.4 Conclusions

Reliable planning of water-based seasonal thermal energy storages requires accurate and effective simulation. Several analytical and numerical solutions are at hand to model the behavior of such large-scale devices. For optimal integration, robust predictions about the operation behavior of these facilities are needed. Particularly ground-based systems with diverse geometries prove to be complex in technical respects, with regard to governing thermal processes and interference with the environment. Thus, common axially symmetric models may not be suitable for flexible geometries. Similarly, computational requirements of high-resolution computational fluid dynamics and 3D-finite element method-models are often impractical for extensive parameter studies.

To overcome these issues, the newly developed model “STORE” represents a component-based approach to combine benefits of resolving all building components and relevant processes of seasonal storages with those of comprehensive parametrization, multidimensional geometry, and versatile evaluation capabilities. Based on the *SIMSCAPE* library available in *MATLAB/SIMULINK*, the structure and approach of STORE is first described, including processes, input and output data, and its design database for parametric studies. Accuracy and applicability are confirmed with conventional methods in a plausibility test.

The capabilities of STORE are further demonstrated in a parametric test study with 41 scenarios to identify trends of varying configurations and materials of thermal insulation. The re-use of a swimming pool (raw volume: 940 m<sup>3</sup>) with a soil top covering or different insulation thicknesses is investigated. The results reveal design recommendations for future projects:

- ▷ Thermal insulation at the top or alternatively an external top covering with soil of at least 1 m thickness is essential to guarantee fail-safe operation.
- ▷ The insulating effect is greatest when an external cover is applied, which does not reduce the storage volume and thus its capacity under similar temperature conditions. Accordingly, top insulations are most effective (since the highest temperature gradients also exist here). In contrast, bottom insulations may be adversarial by reducing the capacity, while low losses do not cause efficiency improvements.
- ▷ The use of different insulation materials at individual storage interfaces can be profitable only under certain conditions (e.g., thicknesses), underlining the benefit of simulation-based design for ascertaining optimized component configurations.

- ▷ Heating of the ambient soil results in successive performance improvements via reduced energy losses, as well as increased usability of the system with prolonged service life.
- ▷ Evaluations of different design scenarios must consider multiple criteria (e.g., maximum capacity, storage efficiency, and average temperature) to identify optimal solutions.
- ▷ These criteria may yield opposite effects (e.g., lower energy yield through reduced capacity vs. higher efficiency by increased insulation thickness). Thus, cost-benefit analyses related to improved (but costlier) insulation materials are suggested.

The results of the test study prove the flexibility and diverse evaluation capabilities of STORE. Hence, the model may be utilized in further generic studies or for case-specific planning. The opportunity for computationally efficient, model-based technical optimization will finally enable the minimization of both capital and operational costs of seasonal thermal energy storage systems.





## 5 Influence of thermal energy storage basins on the subsurface and shallow groundwater

This chapter is reproduced from:

**Bott, C., Dahash, A., Noethen, M., & Bayer, P. (2023).** Influence of thermal energy storage basins on the subsurface and shallow groundwater. Manuscript submitted to: *Journal of Energy Storage*, EST-D-23-07631.

The authors acknowledge Ryan Pearson for language edits. The present study is financially supported by the EU Horizon Europe project INTERSTORES (project no. 101136100).

### Highlights

- ▷ A model for co-simulation of seasonal thermal energy storage is introduced.
- ▷ The model facilitates the simulation of sTES and subsurface thermal conditions.
- ▷ A parameter study reveals the model's capabilities and provides planning insights.
- ▷ The study reveals the impacts of groundwater flow on storage key characteristics.
- ▷ Insulation for sTES facilities is inevitable when groundwater is present.

## 5.1 Introduction

Large-scale, seasonal thermal energy storage (sTES) is a key technology for realizing the transformation of the heating and cooling sector [241,301,302]. It is employed to combine different sources and sinks in an energy system, with shifts over days up to several months [303]. While seasonally solar charging is most common, other energy sources cover continuous heat provision, e.g., by data centers, geothermal systems, or variable and unpredictable loads, e.g., from industrial applications (FIG. 5.1). Modern, 4<sup>th</sup> generation sTES also utilize intermittent charging/ discharging processes in a dynamic range of temperatures and volumetric flow rates [26,196]. They are employed on different temporal and spatial scales together with district heating and cooling systems (DHC), ranging from small housing communities [304,305] to large districts with complex management of thermal energy provision [10,82,238,241].

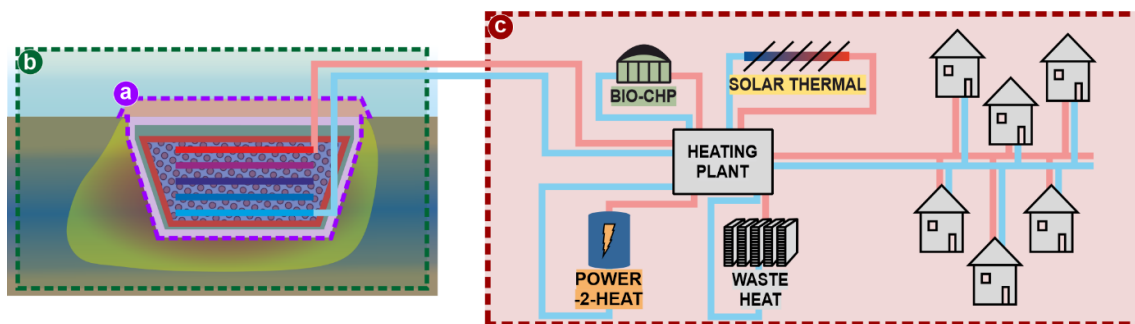


Fig. 5.1: Key modeling domains of sTES: a) seasonal thermal energy storage, b) surrounding environment, and c) energy system. BIO-CHP: Combined heat and power plant based on bioenergy.

The technological variants covered by this study are closed-loop, sensible systems. These utilize artificial reservoirs that can be further classified into Tank- (TTES), Pit- (PTES), and Water-Gravel Thermal Energy Storage (WGTES) [40,58,205,306]. All these types have mostly rectangular or cylindrical shapes and are designed as sloped basins, with a small surface area-to-volume ( $A/V$ ) ratio, to minimize ambient heat loss. Typical volumes of TTES and WGTES are 5,000 m<sup>3</sup> to 15,000 m<sup>3</sup>, while PTES can comprise up to more than 200,000 m<sup>3</sup> [117,196]. The storages are commonly partially or completely buried underground, which is generally advantageous regarding thermal losses since thermal processes in the subsurface proceed more slowly than in the air and it often exhibits a higher average temperature over the year [307]. As a storage medium, TTES and PTES employ water only, while WGTES are filled with a two-component mixture of gravel, sand or soil, and water. Thus, WGTES have a reduced storage capacity by about 20% [15,37,63], but this is contrasted by the advantage that a self-supporting structure is created.

To prevent leakage and heat loss, all different variants are enclosed at all sides by a sealing liner (made of e.g., polyvinyl chloride (PVC), high-density polyethylene (HDPE), or stainless steel [256,272], depending on the planned maximum temperature during operation), and by thermal insulation, which can be added with different thicknesses at the top, sidewall, and bottom. For WGTES, thermal insulation is usually the most cost-intensive part of a storage structure [256,308]. To allow an adequate integration of the installation into the landscape and to minimize heat loss, most of the TTES and WGTES have an external top cover, while the insulation is located inside, or, for PTES, implemented as a floating lid cover [178,309,310].

Especially for TTES and steeply sloped geometries, additional static components are required. They are usually made of (possibly reinforced, prestressed) concrete and comprise a foundation, walls, and a roof. For operation, WGTES require indirect charging/discharging devices consisting of multiple levels of coil racks. In contrast, water-fillings are directly charged and discharged by extracting/re-injecting the storage medium through engineered stratification devices, that are less expensive and have been subject to intense previous research activities [130,184,241,311]. Currently, the worldwide number of sTES is only just above 30 (with a total available storage volume of more than ca. 800,000 m<sup>3</sup>), and they can be found mainly in Europe [196]. Progress toward technology improvements includes, for example, material and method optimization, as well as optimized integration into the DHC system, with combined short-term and long-term storage cycles and connection to multiple sources and sinks [10,188,241,312,313]. At the same time, however, these make the optimal basin structure and thus the planning and operation more complex, which underlines the need for efficient modeling tools [314–316].

This study aims to tackle multiple key challenges in the planning process of sTES (FIG. 5.2). Addressing the technical perspective, past projects revealed that energy losses are often higher than expected and predicted by models (e.g., projects in Germany: Steinfurt-Borghorst [37], Friedrichshafen [24,37,154], Hamburg [154,165], Stuttgart [70]; FIG. 5.2 a). Thus, a major challenge for simulation is the thermal interaction between the artificial storage basin, with the ambient natural subsurface and groundwater domain. Thermal conditions in both domains show at least seasonal patterns but differ greatly concerning short-term variabilities and magnitudes. Planning is hindered by the challenge of coupling these domains in efficient models, that can be used for reliable site-specific design optimization [317]. This underlines a need for more accurate models and improved representation of interfaces that affect the storage performance [38,264].

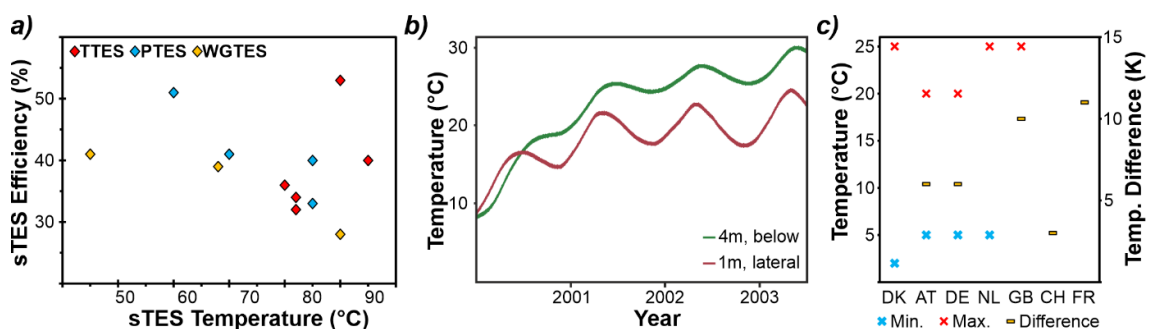


Fig. 5.2: Key issues reported for sTES basins: a) heat losses of different sTES installations (after [318]), b) observed ground temperatures in Hamburg, Germany (after [37,135]), c) temperature regulations/recommendations for shallow geothermal energy applications in different countries as of 2010 (after [30]).

Environmental effects of sTES cover implications that evolve in the long term and may cause ecological concerns. Despite their insulation, sTES embedded in the underground lead to increased temperatures in ambient soil (FIG. 5.2 b) and, if present, groundwater bodies [29,319,320]. Especially for high-temperature applications and non-insulated PTES facilities subsurface temperatures of nearly 30 °C were observed (e.g., in Hamburg, Germany [20,44], FIG. 5.2 b, and Friedrichshafen, Germany [37]). As a consequence, warming by sTES may affect groundwater quality and trigger legal

threshold values ([319,321], FIG. 5.2 c), while legal situations in European countries are diverse, as described by, e.g., [28,30,322]. These aspects must be considered during the planning process, to comply with regulatory frameworks and approval permits.

The aim of this contribution is the development of a simulation framework, which can depict the operational behavior of sTES and their thermal interaction with the environment. The framework comprises an enhanced model for WGTES to be used to simulate interactions with groundwater flow. Hydrogeological and thermal transport processes are implemented in a tailored software configuration. With this, more reliable sTES planning is facilitated, while sensitivities of specific site conditions can be inspected. In the following, first, the developed model with its underlying concept and structure is introduced. Then, after successful validation of the model (cf. APPENDIX D-1) to demonstrate benefits for design and operation, a parameter study to contrast technical (filling temperatures, storage capacity, efficiency, etc.) and environmental characteristics (e.g., heat loss, temperatures in the ambient ground) under different hydrogeological settings is conducted.

## 5.2 Materials and methods

### 5.2.1 Modeling approach

The determination of the optimal sTES layout is a challenging and often evolving process, due to interconnected variables, which are often subject to changes. Prior studies emphasized the sophisticated nature of designing, planning, and constructing sTES. For instance, DAHASH et al. [241] revealed the interplay of variables such as location, size, geometry, and hydrogeological conditions for TTES and PTES. In this context, the choice of size (i.e., volume) and geometry influences thermal losses, due to the  $A/V$  ratio, and the quality of thermal stratification, linked to the height-to-diameter ( $h/d$ ) ratio. As large-scale sTES demand massive space availability, they are often placed in the subsurface. This raises additional planning considerations, particularly regarding the hydrogeological conditions (e.g., soil thermal conductivity, hydraulic conductivity, porosity, permeability, and groundwater flow angle). As a result, simulation-driven planning emerges as a valuable approach for quantifying the impact of various boundary conditions (BCs) on TTES and PTES planning. Calibrated numerical sTES models play a key role in such investigations. In this respect, DAHASH et al. [299] compared sTES geometries, and found that buried tanks outperform other geometries. Subsequently, their work was extended to consider groundwater flow, emphasizing the twofold impact of sTES-groundwater interaction, and the need for measures to prevent elevation in groundwater temperatures beyond legal thresholds [29]. However, both works focused solely on the sTES and did not encompass system simulations with dynamic interactions. Furthermore, these works demanded significant computational efforts. To address this issue, SIFNAIOS et al. [310] developed a simplified sTES model with a focus on short-term operations, using a temperature BC, based on monitored temperature data. This approach, however, neglects dynamic thermo-hydraulic interactions within the sTES' building components. Consequently, this work did not address sTES simulation, potentially leading to misleading outcomes. As a consequence, to the authors' knowledge, no development so far covered a comprehensive simulation framework that dynamically integrates all sTES components with detailed subsurface conditions and groundwater flow.

The new framework is based on a co-simulation approach, where two complementary tools are combined [269]. First, the previously introduced “STORE” model [323] is employed for the sTES domain. Implemented in MATLAB /SIMULINK’S SIMSCAPE library [284,324], it depicts a WGTES in 2.5 dimensions (2.5D) (i.e., vertical layers, and pre-defined, horizontal directions). Second, a three-dimensional (3D) numerical multi-physics model for simulating heat transfer and groundwater flow in the ambiance of the sTES is implemented in COMSOL [325]. Third, the co-simulation is realized using a functional mockup unit (FMU), passing values between both models [326,327]. Advantages of the co-simulation result from flexible parameterization, as part of the design database generation of STORE [323]. Optimal computational performance is achieved by operating the models at different time steps, depending on the complexity of the internal sTES structure, and subsurface conditions.

### 5.2.2 STORE model

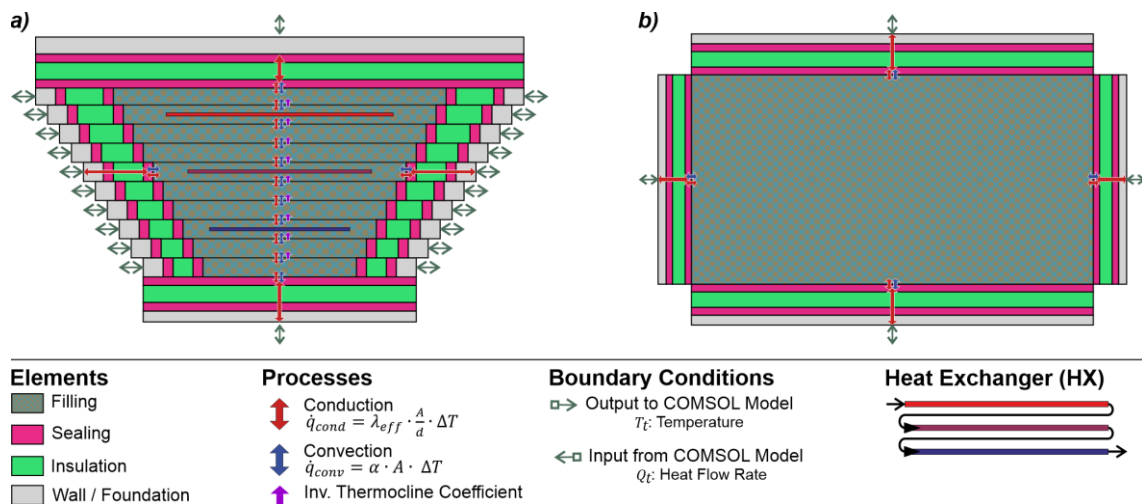


Fig. 5.3: Sketch of the STORE model for simulating WGTES, modified for the co-simulation framework in cross-sectional view (a) and top view on one layer (b).

Building on the first version of STORE [323], further developments are implemented to make the sTES simulation more accurate and flexible. The updated structure of the model is illustrated in FIG. 5.3. While the filling is represented in a vertically layered structure, it features a component-based resolution of all other building components and relevant internal thermal processes. Nevertheless, weaknesses concerning model BCs and the setup are present: STORE is structured in four, pre-defined spatial directions (e.g., north, east, south, west) and does not consider hydrogeological BCs.

For the new framework, the spatial resolution given by the number of storage layers was increased from 15 to 25. This is particularly relevant for facilities with a higher  $h/d$  ratio (i.e., a larger height) since the key feature of thermal stratification is resolved more precisely [24,166]. The temporal resolution is retained at one hour per step, allowing highly dynamic conditions of complex energy systems to be considered. Additionally, the representation of the processes within the filling is refined. During the operation of the facility, layers with higher temperatures below layers with lower temperatures can occur. In this case, mixing is induced by free convection. This density-dependent inversed thermocline phenomenon is implemented according to EQ. 5-1 ( $\delta_{ITC}$ : inversed thermocline coefficient =  $10^5 \text{ W m}^3 \text{ kg}^{-1}$ ,  $\rho_{upper}$ ,  $\rho_{lower}$ : density of the

fluid in the upper/lower storage layer,  $V$ : volume of the layer) based on [274,328] (available, e.g., in the CARNOT TOOLBOX for MATLAB, [329]).

$$\ddot{q}_{ITC} = \delta_{ITC} \cdot (\rho_{upper} - \rho_{lower}) \cdot V \quad (\text{EQ. 5-1})$$

Concerning the included building components, a roof is added to the top layer of the model, which is mainly relevant for water-filled systems. Additionally, to simulate operation utilizing an indirect coil heat exchanger, a new approach with two flow directions is employed. This considers that the flow direction between charging and discharging is commonly reversed to exploit thermal stratification, with high fluid temperatures being injected in and extracted from the top. Pipe hydraulics, e.g., thermal propagation along the pipe as well as pressure losses, are not considered.

For co-simulation, STORE is used exclusively for modeling the sTES structure. For all internal storage components, the necessary thermo-hydraulic processes through all components of the sTES' shell are mapped. In contrast, this means that the top cover and the surrounding soil blocks as originally presented in [323] are now replaced by the COMSOL model. The default configuration of the model features a total of 448 nodes. Charging and discharging processes are represented directly via transient load profiles of temperature  $T$  and volumetric flow rates  $\dot{V}$  or a controller, featuring an operation strategy with hysteresis settings. For simulation, the sTES design (including materials, dimensions, and material properties) and the load profiles are defined based on the specific site. As an initial condition, it is assumed that the structure has a homogeneous temperature directly after construction and before commissioning.

### 5.2.3 COMSOL model

Since the COMSOL model is used to represent the sTES environment, only the top cover is included as a sTES component. Still, this cover is important to avoid heat loss at the top of the surface [37,299,323]. By default, it features a 1 m overlap over the top surface of the sTES shell and a slope of 1:2 to the outside, to create a natural embankment. The underground (FIG. 5.4) is divided into an unsaturated (vadose) zone, which is above the water table, and a saturated (phreatic) zone with groundwater flow governed by transient hydraulic heads. The lateral inflow and outflow sides of the model are defined at the opposite boundaries of the subsurface block, while the angle of inflow  $\beta$  is implemented by rotating the storage structure.

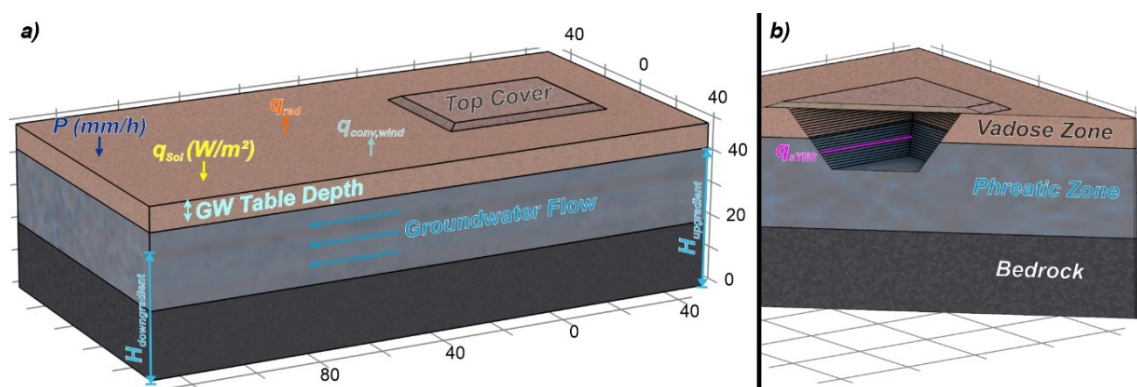


Fig. 5.4: a) side, and b) cut plane view of the COMSOL model with top cover, unsaturated (vadose) zone, groundwater domain (phreatic zone), and bedrock layer, tailored for co-simulation.

Consequently, the hydraulic gradient  $i$  results from the hydraulic heads at the model boundaries  $H_{\text{upgradient}}$ ,  $H_{\text{downgradient}}$  and the boundary distance  $l$ :

$$i = \frac{H_{\text{upgradient}} - H_{\text{downgradient}}}{l} \quad (\text{EQ. 5-2})$$

At the bottom, a bedrock or aquitard is assumed, which delineates the aquifer. The model extensions are three to four times the basin dimensions in width and length, and three times the sTES height  $h_{\text{sTES}}$ . Further, the sTES is positioned at an asymmetrical distance to the model boundaries so that the evolving thermal plume can evolve properly (FIG. 5.4). For model setup, all geometry (layer thickness  $M$ ) and material properties of the surrounding soil are required. These include density  $\rho$ , effective thermal conductivity  $\lambda_{\text{eff}}$ , specific heat capacity  $c_p$ , surface emissivity  $\omega$ , hydraulic conductivity  $K$ , permeability  $\kappa$ , and porosity  $\varepsilon_p$ . To represent the groundwater regime, the angle of inflow, and initial environmental conditions (air and ground temperature) are required.

Based on this parameterization, fundamentally important processes that most existing sTES simulation tools do not depict are modeled. These include Darcian groundwater flow (mass transport through porous domains) with pressure  $p$  as the dependent variable. The mass source term  $G_m$  is calculated based on the fluid's density  $\rho$ , its dynamic viscosity  $\mu$ , and the matrix's permeability  $\kappa$  and porosity  $\varepsilon_p$ :

$$G_m = \frac{\partial}{\partial t} \cdot (\rho \cdot \varepsilon_p) + \nabla \cdot (\rho \cdot u), \text{ with Darcy velocity } u = -\frac{\kappa}{\mu} \cdot \nabla p \quad (\text{EQ. 5-3})$$

Dirichlet conditions are set at the inflow and outflow boundaries of the model to generate the hydraulic head distribution based on EQ. 5-2 and EQ. 5-4. To calculate a pressure  $p$ , the known hydraulic head at the boundary  $H_0$  is specified as a function of the elevation  $z$ , the gravitational acceleration  $g$  ( $9.81 \text{ m s}^{-2}$ ) and the groundwater density  $\rho$ :

$$p = \rho \cdot g \cdot (H_0 - z) \quad (\text{EQ. 5-4})$$

The other model boundaries are specified as no-flow boundaries, which define a zero Darcy's velocity  $u$  of the fluid according to its density  $\rho$  at a no-flow boundary with normal vector  $N$ :

$$-N \cdot \rho \cdot u = 0 \quad (\text{EQ. 5-5})$$

However, this does not apply to the soil surface, where a defined precipitation rate  $P$  with the same density as the groundwater is set as an inflow BC:

$$\rho \cdot P = -n \cdot \rho \cdot u \quad (\text{EQ. 5-6})$$

Thermal transfer processes in the porous subsurface are divided into a fluid and a matrix fraction assuming local thermal equilibrium. Thereby, the dependent variable of temperature  $T$  is used to model the processes of conduction, dispersion, and advection.

Based on the above-described calculation of the coupled Darcy's velocity field  $u$ , the effective specific heat capacity  $(\rho \cdot c_p)_{\text{eff}}$  (EQ. 5-7,  $\varepsilon_p$ : porosity,  $\rho$ : groundwater density,  $c_{p,f}$ : groundwater specific heat capacity,  $\theta_s$ : volume fraction of the matrix,  $\rho_s$ : matrix density,  $c_{p,s}$ : specific heat capacity of the matrix,  $\theta_{\text{imf}}$ : volume fraction of immobile groundwater in porous media,  $\rho_{\text{imf}}$ : density of the immobile fluid in porous media,  $c_{p,\text{imf}}$ : specific heat capacity of the immobile fluid in porous media, the heat flow rate  $q$ , EQ. 5-8), with effective (volume-average approach) thermal conductivity  $\lambda_{\text{eff}}$  (EQ. 5-9,  $\lambda_s$ : thermal conductivity of the matrix,  $\lambda_{\text{imf}}$ : thermal conductivity of the immobile fluid in porous media,  $k_{\text{disp}}$ : dispersive thermal conductivity tensor (assumed isotropic)  $\sigma_b$ : STEFAN-BOLTZMANN constant), the governing equation for the energy balance is shown in EQ. 5-10.

$$(\rho \cdot c_p)_{\text{eff}} = \varepsilon_p \cdot \rho_f \cdot c_{p,f} + \theta_s \cdot \rho_s \cdot c_{p,s} + \theta_{\text{imf}} \cdot \rho_{\text{imf}} \cdot c_{p,\text{imf}} \quad (\text{EQ. 5-7})$$

$$q = -\lambda_{\text{eff}} \cdot \nabla T \quad (\text{EQ. 5-8})$$

$$\lambda_{\text{eff}} = \varepsilon_p \cdot \lambda_f + \theta_s \cdot \lambda_s + \theta_{\text{imf}} \cdot \lambda_{\text{imf}}, \text{ with } \lambda_s = \frac{\lambda_b}{\theta_s} \quad (\text{EQ. 5-9})$$

$$Q = (\rho \cdot c_p)_{\text{eff}} \cdot \frac{\partial T}{\partial t} + \rho_f \cdot c_{p,f} \cdot u \cdot \nabla T + \nabla \cdot q \quad (\text{EQ. 5-10})$$

STORE's environmental processes (solar irradiation as heat flux boundary  $\ddot{q} = -n \cdot \ddot{q}_{\text{sol}}(t)$ ,  $N$ : normal vector on the boundary), and radiation from the storage surface as surface-to-ambient radiation based on EQ. 5-11 with  $\omega$ : surface emissivity,  $\sigma_b$ : STEFAN-BOLTZMANN constant), as well as the interaction with the air (as temperature boundary condition  $T = T_{\text{air}}(t)$ ) are transferred to the COMSOL model.

$$-N \cdot q = \omega \cdot \sigma_b \cdot (T_{\text{air}}^4(t) - T_{\text{ground}}^4) \quad (\text{EQ. 5-11})$$

Further, these thermal BCs are expanded to include forced and natural convection by wind (EQ. 5-12,  $v_{\text{wind}}$ : wind speed,  $\mu_{\text{air}}$ : dynamic viscosity,  $Pr$ : Prandtl number,  $Re$ : Reynolds number), based on a convective heat flux boundary, whereby an averaged heat transfer coefficient is calculated based on the assumption of external forced convection at a plate with a characteristic length  $L$  (EQ. 5-13,  $l_{\text{env},x}$ ,  $l_{\text{env},y}$ : side length in x and y direction).

$$\ddot{q} = h \cdot (T_{\text{air}}(t) - T) \text{ with } h = \begin{cases} 2 \cdot \frac{\lambda_{\text{air}} \cdot 0.3387 \cdot Pr^{1/3} \cdot Re_L^{1/2}}{L \cdot \left(1 + \left(\frac{0.0468}{Pr}\right)^{2/3}\right)^{1/4}} & \text{if } Re_L \leq 5 \cdot 10^5 \\ 2 \cdot \frac{k}{L} \cdot Pr^{1/3} \left(0.037 \cdot Re_L^{4/5} - 871\right) & \text{if } Re_L > 5 \cdot 10^5 \end{cases},$$

$$\text{with } Pr = \frac{\mu_{\text{air}} \cdot c_{p,\text{air}}}{\lambda_{\text{air}}}, \text{ and } Re_L = \frac{\rho_{\text{air}} \cdot v_{\text{wind}} \cdot L}{\mu_{\text{air}}} \quad (\text{Eq. 5-12})$$

$$L = \frac{l_{\text{env},x} \cdot l_{\text{env},y}}{2 \cdot l_{\text{env},x} + 2 \cdot l_{\text{env},y}} \quad (\text{Eq. 5-13})$$



Hence, transient weather data on an hourly resolution is required for specifying the BCs, including air temperature  $T_{\text{air}}$ , wind speed  $v_{\text{wind}}$ , solar irradiance  $\dot{q}_{\text{sol}}$ , and precipitation  $P$ . This data is converted by the co-simulation to mean values according to the step size of the COMSOL model. Similarly, the hydraulic heads are based on a transient dataset of groundwater levels at the inflow and outflow boundaries.

Since flow and transport processes in soil are slower than inside the storage [29,310], an ambient temporal resolution of multiple days can be used, depending on dynamicity and intensity. Besides, spatial mesh refinement in the near field of the storage is needed. The top cover consists of at least four layers, and, by default, 25 boundary layers per direction are advised around the sTES. Further mesh refinement strategies are presented in APPENDIX D-2.

#### 5.2.4 Implementation

For efficient coupling, the chosen interface is the outer shell of the sTES, separating it from its environment. Accordingly, the following input and output data of the models are exchanged during simulation: In STORE, the heat flux  $\dot{q}_{\text{sTES}}$  is recorded in each layer and in each predefined spatial direction, as well as above the roof and below the foundation, and transferred to the COMSOL model. In COMSOL, this heat flux is used as BC (i.e., thermal load) at contact surfaces, which depict the layered surfaces around the sTES. A reflection from COMSOL is obtained as a temperature probe (integrated average of the relevant temperature  $T_{\text{ground}}$ ) at these surfaces, and these values are used as BCs in STORE for the next calculation step. Preliminary testing showed that a communication step size of min. 48–120 h can be considered adequate to prevent numerical fluctuations and generate accurate simulation results. For instance, 48 h is calculated in STORE, followed by simulation of a 48-h time frame in COMSOL. The MATLAB/SIMULINK model operates with an hourly resolution for all datasets while operating with a variable step size solver (ode23t, max. step size 1 h). In COMSOL, a relative tolerance of 0.01 and an absolute tolerance of 0.005 are used. For every individual simulation per communication timestep, an initial step of one hour and a maximum step size of 20 hours are specified. The direct solver MUMPS (multifrontal massively parallel sparse direct solver) is used to achieve a fast simulation.

After simulation, the results are evaluated with both modeling tools, but it is advantageous to include the results of specific COMSOL probes in the STORE results database to enable joint evaluations. The evaluation of the results in COMSOL focuses on the evolving thermal and hydrogeological conditions in 3D representation. Thus, point temperature probes are considered first, which are placed 2 m and 5 m adjacent to the storage wall at a height of  $(0.5 \cdot h_{\text{sTES}})$ . Heat losses  $\dot{q}$  are used as further evaluation indicators and are separated into sidewalls (phreatic and vadose sections), and top and bottom surfaces. In a two-dimensional (2D) perspective, a sectional plane is placed in horizontal orientation at a height of  $(0.5 \cdot h_{\text{sTES}})$ . Here, temperatures and temperature gradients, as well as the groundwater flow velocity distribution can be analyzed. In this context, thermoclines at 20 °C and +6 K compared to ambient soil temperatures are used to check for violations of legal threshold values [30,330]. In STORE, the evaluation is in line with the procedure described by BOTT et al. [323] and includes operation states, the filling temperature, as well as the storage efficiency  $\eta_{\text{storage}}$ , defined as the ratio of discharged vs. charged energy quantities.

For the simulation of a seasonal storage operation, a minimum time frame of at least five to ten years is suggested [38,316], since during a heat-up period of several years the surrounding subsurface is warmed. Consequently, this period is necessarily longer for uninsulated sTES with intensive interaction with the ambient ground. After this period, a quasi-stationary state is expected, in which the heat losses, averaged over longer periods, are nearly constant [38,135,323].

### 5.2.5 Parameter study: Impact of groundwater flow on seasonal thermal energy storage

#### Storage design

Starting from a baseline scenario, the following parameter study includes various assumptions for environmental conditions, to investigate the impacts of groundwater flow parameters. The full design scenario databases with all scenario definitions are provided in APPENDIX D-3, while material properties of all sTES components are summarized in TAB. 5.1 and based on standard literature values. The considered WGTES system is located in Ingolstadt, Germany, where the re-use of an existing basin structure is planned. This strategy has previously been discussed to reduce construction, renovation, and/or demolition costs [231,293,331]. The basin is completely buried in the subsurface, whereas the roof's top surface conforms to ground level. For ideal landscape integration, it features an external top cover of soil (same material properties as unsaturated zone, TAB. 5.1), with 1.5 m thickness and a slope angle of 1:2, overlapping the rim by 1 m. The geometry of the basin represents an inverted truncated pyramid with a slope angle of 1:0.5. The side lengths are arranged in a ratio of 3:2:1 (length/width/height = 45 m / 30 m / 15 m), resulting in a filling volume of 11,814 m<sup>3</sup>.

Tab. 5.1: Material properties of the example storage facility. Values used for filling material according to the WGTES installation in Chemnitz, Germany [37,63], and for foam glass gravel according to a manufacturer's data sheet ([295], ideal conditions assumed).

Component	Material	Density $\rho$ (kg m <sup>-3</sup> )	Effective thermal conductivity $\lambda$ (W m K)	Specific heat capacity $c_p$ (J kg <sup>-1</sup> K <sup>-1</sup> )
<b>Filling</b>	Water saturated gravel	1,928	2.40	1,545
<b>Insulation</b>	Foam glass gravel	160	0.05	900
<b>Sealing</b>	PVC	1,900	0.48	900
<b>Static components</b>	Concrete	2,600	1.00	1,000
<b>Heat exchanger</b>	PE-X	930	0.41	1,900

As filling, a water-saturated matrix of gravel is considered, yielding a self-supporting surface. The material properties used are in line with the investigated construction material of the reported site in Chemnitz [37,63] and the previous study by BOTT et al. [323]. To account for natural convection induced by density differences, an effective heat transfer coefficient  $\delta_{ITC} = 20 \text{ W m}^{-2} \text{ K}^{-1}$  is assumed. To prevent thermal energy loss, apart from the external top cover, the sTES is equipped with an internal, all-sided insulation consisting of the commonly used, pressure-stable, water-resistant material foam glass gravel [26,196,295]. As the thermal stratification is expected to result in the highest temperatures in the upper part, a top thickness of 0.5 m is employed, while the bottom insulation is assumed to be 0.1 m thick. Also, the insulation of the sidewalls is decreased from 0.3 m to 0.1 m from top to bottom.

The sidewalls and bottom insulation are excluded for an uninsulated storage facility scenario. The thermal insulation material is embedded inside compartments of a sealing material, to protect it from moisture penetration [332]. Such insulations have been implemented, for example, in Steinfurt-Borghorst, Germany [37] and Hannover, Germany [101]. The supposed re-use of a given basin structure implies an additional structural component. This component originally served to bear lateral ground stresses due to the steep angle of the basin's slope. Made of cast reinforced concrete, both the walls and the roof measure 0.2 m in thickness, while the foundation is assumed to be 0.3 m thick. An indirect coil heat exchanger on five levels at relative heights of  $h_{\text{STES}}^* = 12\%, 32\%, 52\%, 72\%, \text{ and } 92\%$  with a diameter of 0.05 m and internal distances and a distance to the external wall of 0.5 m, is included. Its total length amounts to 8,729 m and the resulting surface area  $A_s$  is approximately 2,742 m<sup>2</sup>. The pipe material is cross-lined polyethylene (PE-X) and the thickness of the pipe wall measures 0.0025 m.

### Storage operation

The sTES is operated referring to a real dataset for planning a new mixed-used district with energy demands of different commercial, as well as industrial processes. Thereby, the volumetric flow rates and inlet temperatures of the charging/discharging load profiles are scaled to the storage volume, assuming that only specific sources and a partial load of the adjacent DHC are used for optimum integration and operation. The resulting charging and discharging datasets are presented in FIG. 5.5.

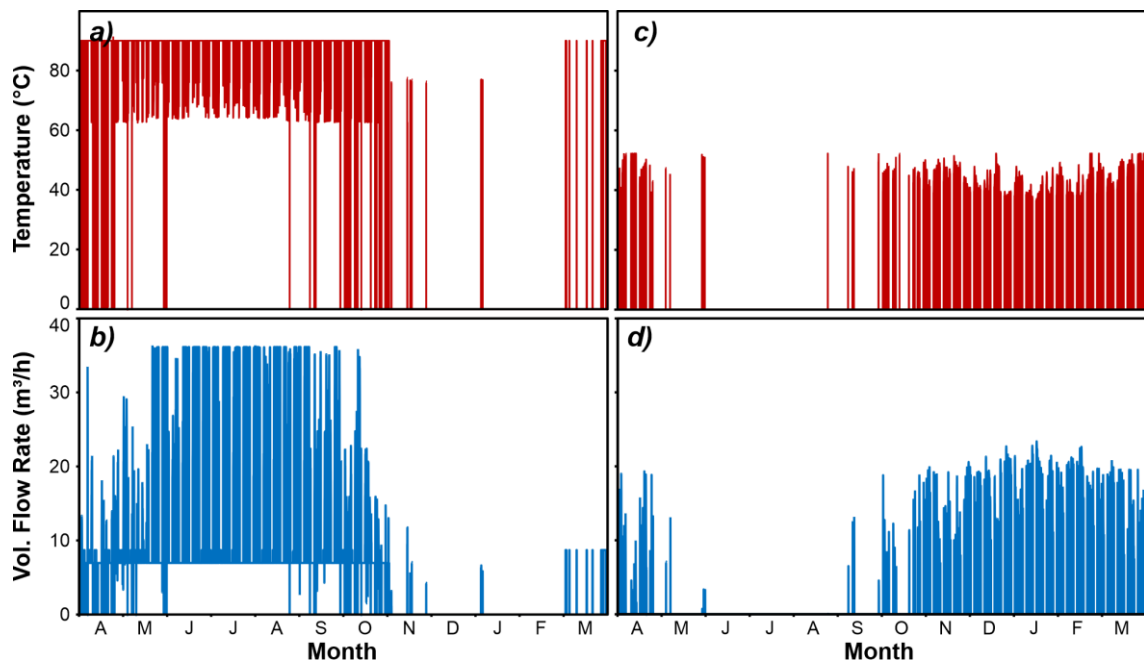


Fig. 5.5: Operation data for the parameter study, consisting of available temperatures (a and b, in °C) and volumetric flow rates (c and d, in m<sup>3</sup> h<sup>-1</sup>) for charging (a and c) and discharging (b and d).

The storage is not operated on a strictly seasonal cycle but rather corresponds to a highly dynamic operation, comprising intermediate charging and discharging phases for buffering peak loads. With 5,053 h in one year of operation, more charging periods are given than for discharging (1,707 h), while in 2,000 h, the sTES is in standby mode. Further, charging is dominating in the summer months and, with approx. 0.08 to 36.15 m<sup>3</sup> h<sup>-1</sup> (mean 12.65 m<sup>3</sup> h<sup>-1</sup>) and temperatures between 62.5 and 90.0 °C (mean

84.14 °C), more intensive than the discharging profile. The latter is operated between temperatures of 36.1 to 52.3 °C (mean 43.3 °C) and volume flow rates of 0.0056 m<sup>3</sup> h<sup>-1</sup> to 23.38 m<sup>3</sup> h<sup>-1</sup>. Time or temperature hysteresis are not considered.

#### Ambient environmental conditions

The site represents an unconfined sedimentary aquifer, and different scenarios are applied for average groundwater table depth and hydraulic gradient, respectively. Besides, the required material properties for the different domains are presented in TAB. 5.2. The 20 m thick bedrock layer is assumed to be a solid rock (e.g., granite) with low effective porosity, hydraulic conductivity, and permeability. Above, the saturated zone with flowing groundwater consists of sandy gravel. The topmost part (vadose zone) consists of the same material as the saturated zone. Assuming a groundwater table depth of 50% of the sTES height, the aquifer thickness is 7.5 m. For the emissivity of thermal energy by radiation, it is assumed that the ground is sparsely vegetated, represented by a surface emissivity coefficient of  $\omega = 0.95$  [333].

Tab. 5.2: Material properties of the surrounding subsurface around the storage facility.

Domain	Density $\rho$ (kg m <sup>-3</sup> )	Effective thermal conductivity $\lambda$ (W m K)	Specific heat capacity $c_p$ (J kg <sup>-1</sup> K <sup>-1</sup> )	Effective porosity $\epsilon_p$	Hydraulic conductivity $K$ (m s <sup>-1</sup> )
Bedrock	2,600	2.9	850	10 <sup>-10</sup>	10 <sup>-10</sup>
Phreatic zone	2,600	3.758	795.4	0.43	10 <sup>-4</sup>
Vadose zone	1,500	2.2	800	0.43	10 <sup>-4</sup>

Datasets for specifying environmental BCs are gained from publicly available databases of the German Weather Service (FIG. 5.6). Meteorological data of the test reference years [297,334] contain wind speed, air temperature, and diffuse solar irradiance. For precipitation and ground temperature data, long-term hourly mean values of a nearby weather station are incorporated. Seasonality is apparent in temperature and solar radiation datasets, justifying need for a sTES at this location.

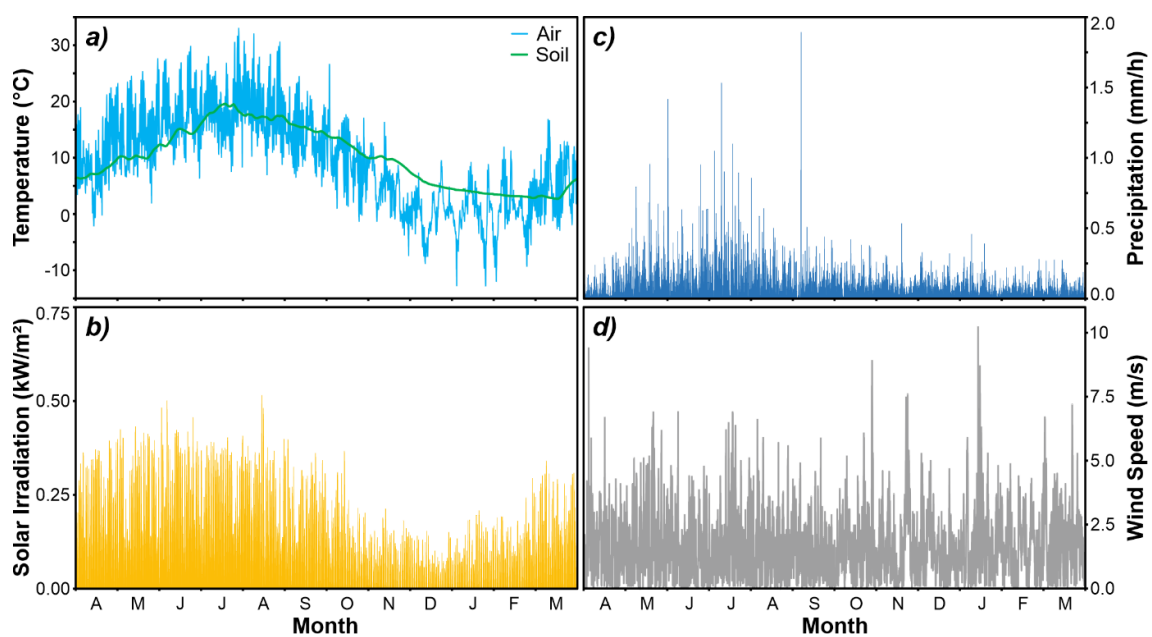


Fig. 5.6: Environmental data used in the case study, consisting of a) temperatures for soil and air, b) solar irradiation, c) precipitation, and d) wind speed.

### Scenario definitions

The scenarios presented in TAB. 5.3 list variable hydrogeological conditions that may affect the sTES. In the base case, the insulated sTES are approached by groundwater from the short side of the basin (i.e.,  $0^\circ$ ), with a mean groundwater table depth of 50% of the height of the basin (i.e., 7.5 m below ground level). The groundwater flow is moderate with a regional hydraulic gradient of 2‰ (= 0.2%). In further scenarios, the parameters varied relate to the groundwater flow direction ( $\beta = 90^\circ$ , i.e., inflow approaching the basin's wide side), the groundwater level (20% vs. 50% of  $h_{sTES}$ ), and the hydraulic gradient (0‰, i.e., stagnant water, and 5‰). One scenario (V5) is used to investigate constant, high groundwater flow velocities of  $10^{-5} \text{ m s}^{-1}$ . In contrast, scenario NoGW inspects when groundwater flow is ignored or cannot be modeled. To emphasize the effects of basin insulation, an uninsulated scenario (top insulation only, I0) is included as an extreme case. For all insulated scenarios, the time communication step size is set to 5 days, while the uninsulated scenario is simulated with a communication step size of 2 days, due to much steeper temperature contrasts between the sTES and the subsurface domain. The simulated total period is set to 10 years for all scenarios.

Tab. 5.3: Scenarios for parameter study with variations of different groundwater (angle of inflow /  $0^\circ$  short side,  $90^\circ$  wide side, groundwater table depth, groundwater flow gradient) and insulation scenarios. (BGL: below ground level,  $h_{sTES}$ : sTES height).

ID	Groundwater inflow angle $\beta$ ( $^\circ$ )	Groundwater table depth (% $h_{sTES}$ )	Groundwater flow gradient $i$ (‰)	Storage insulation
1: Base	0	50 (= 7.5 m BGL)	2	Yes
2: G00	0	50	0	Yes
3: G50	0	50	5	Yes
4: V5	0	50	$u = 10^{-5}$	Yes
5: A90	90	50	2	Yes
6: H20	0	20 (= 12 m BGL)	2	Yes
7: I0	0	50	2	No
8: NoGW	n.a.	n.a.	n.a.	Yes

## 5.3 Results and discussion

### 5.3.1 Base case

In the base case (overview of model results in FIG. 5.7), the sTES shows a storage efficiency of  $\eta_{storage} = 42.5\%$  over the entire simulation period of 10 years. During all charging phases, a total of 5,289 MWh is injected into the storage, whereas the discharged energy amounts up to 2,248 MWh (FIG. 5.8). The heating phase of the sTES can be observed by an increase of the filling and subsurface temperatures (FIG. 5.7), and, likewise, the storage efficiency shows a drastic improvement, from 24.4% in the first year up to 46.9% in the last year of the investigated operation period. Over the entire study period, the average temperature of the filling is 63.1 °C.

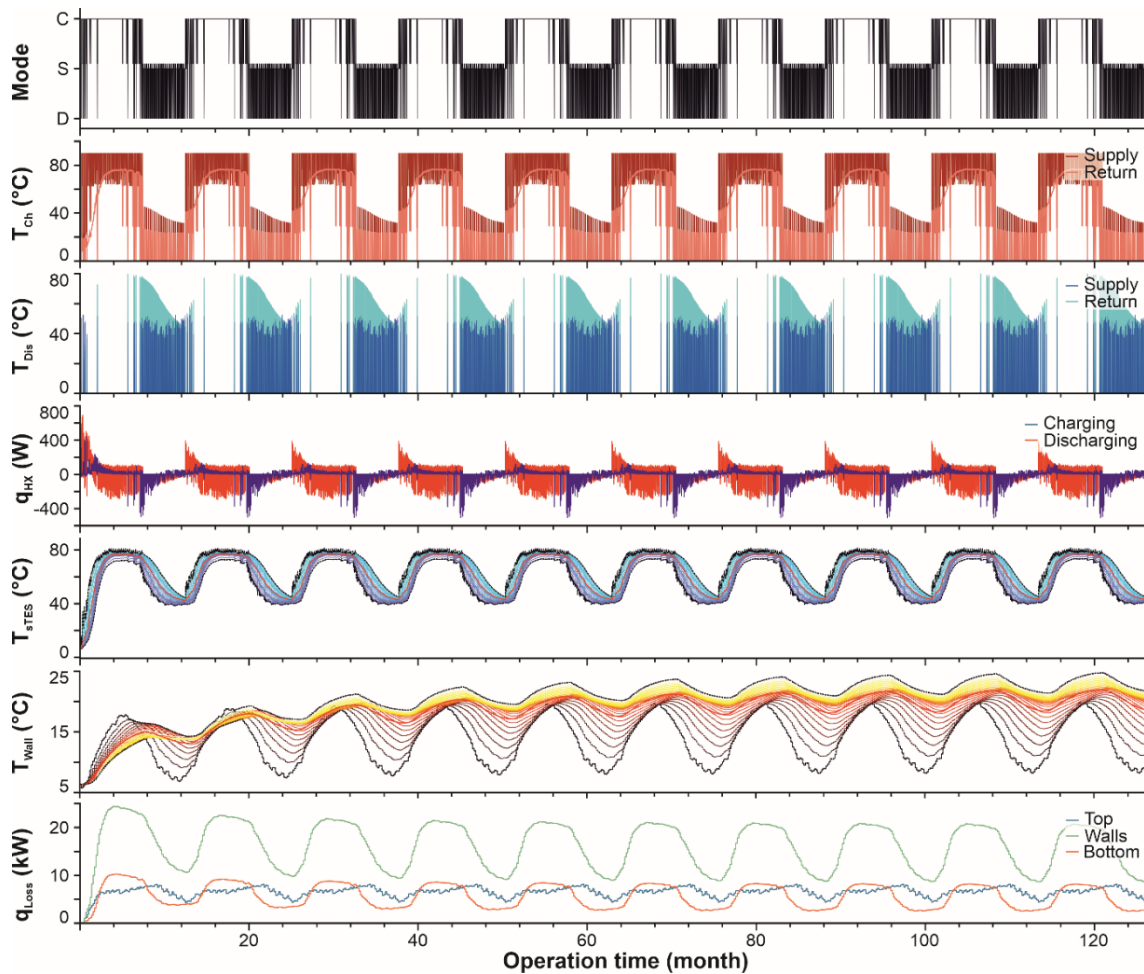


Fig. 5.7: Result of the sTES operation for the base case scenario over 10 years. From top to bottom: mode of operation (C: charging, S: standby, D: discharging), charging and discharging temperature, heat exchanger (HX) heat flow, sTES filling temperatures (layer-resolved), sTES wall temperatures (layer-resolved), thermal losses.

Visually, a stable temperature stratification in the sTES storage medium can be observed. The maximum temperature reached in the last year is 81.1 °C. In contrast, the minimum temperature in the last year is 39.5 °C, resulting in a total capacity of 411 MWh (FIG. 5.8). The specific energy losses that occur in the 10<sup>th</sup> year are highest at the bottom (108.2 kWh m<sup>-2</sup>). In comparison, they are 80.9 kWh m<sup>-2</sup> at the sidewalls and 57.8 kWh m<sup>-2</sup> at the top, proving the significant influence of insulation thicknesses. Also, a more accurate spatial allocation by the co-simulation can be made: In the phreatic zone, heat losses are on average 92.9 kWh m<sup>-2</sup>, which is 17.9% higher than in the vadose zone (76.3 kWh m<sup>-2</sup>). As discussed by previous studies (e.g., [320]) this is linked to the higher thermal conductivity due to water saturation, and enhanced by significant impacts of groundwater flow (e.g., Darcy flow velocity and advection).

Due to the lateral basin insulation, the sTES walls (FIG. 5.7) show a slower temperature increase (ca. 0.8 K a<sup>-1</sup>). At the same time, the duration of the heating phase for ambiance is considerably longer (FIG. 5.9). For temperatures measured at a depth of 7.5 m below ground level (BGL) (0.5 · h<sub>sTES</sub>) and 2 m distance (FIG. 5.9 a), this can be observed very well: Although an exceedance of a 20 °C threshold is observed after 14.6 months at 2 m distance, this occurs only after 19.7 months at a distance of 4 m. Similar values of ca. 21.6 °C in a distance of 1 m after 13.9 months were also observed for the more insulated sTES in Hamburg [37,135], while the simulation study

by SIFNAIOS et al. [310] indicated temperatures of 20 °C at a depth of 8 m at ca. 7 m distance after 11 to 23 months. However, their model uses a less realistic temperature BC at the sTES walls and does not simulate the sTES itself, thus neglecting ambient-sTES interactions. Further, the scenario of their study covered an uninsulated PTES, leading to direct temperature progression into the ambient soil.

### 5.3.2 Technical perspective

Effects of different hydrogeological parameters become evident in the evaluated performance characteristics. Therefore, in FIG. 5.8, values of the energy balance of the sTES, derived storage efficiency levels, temperature ranges, mean temperatures, and the peak capacity levels during the last simulated year are presented. The results reveal that groundwater flow has a significant impact on sTES facilities. Despite moderate insulation in both scenarios, compared with the base case, the NoGW scenario has a 4.1% higher storage efficiency (51.0%) in the last simulated year. While DAHASH et al. [335] reported an efficiency decrease of about 15% for uninsulated PTES, this value is in accordance with a more efficiently insulated TTES in a subsequent study by DAHASH et al. [29]. However, both studies focus on different sTES technology types. For the NoGW case, 7.0 MWh more energy can be discharged, and the mean filling temperature increases up to 64.2 °C. Over the total simulation time frame, the increase in discharged energy equals 62 MWh (2,310 MWh vs. 2,248 MWh in the base case), which is 15.3% of the sTES' capacity. Moreover, inspection of the energy losses shows that due to the heat transport by groundwater (i.e., advection), the sidewalls' contribution to thermal losses increases by ca. 20 MWh (116.9 MWh vs. 136.6 MWh in the base case) and bottom (32.7 MWh vs. 46.8 MWh in the base case), while they are almost constant at the storage's top (58.4 MWh vs. 57.8 MWh in the base case).

In general, the results compiled in FIG. 5.8 show that the individual hydrogeological parameters do not lead to high disparities. Indeed, it can be proven that varying sensitivities of the influencing factors exist, however, for moderate changes of the conditions, no extensive effects are evident. For this study, this is due to the thermal insulation of the TTES system, which efficiently minimizes energy loss and impacts on the environment. However, already a stagnant groundwater body (scenario G00) leads to a decrease in storage efficiency of 2.6% in the 10<sup>th</sup> simulated year compared to the scenario without the presence of groundwater. While such values were not reported for long-term operations of WGTES before, this is in line with the recent findings of the study by SIFNAIOS et al. [310], where it was found that stagnant groundwater leads to increased thermal losses of around 14% for an uninsulated PTES, while groundwater flow can raise thermal losses to around 60%.

Apart from the uninsulated case (see below), the ranges of resulting storage efficiency values for scenarios with groundwater influence in the last simulated year extend from 34.0% (V5) to 48.0% (G00). Therein, for the latter scenario, 68.3 MWh of lost energy is in contrast to a charged energy amount of 475.6 MWh, while in the identified worst case, these values amount to 111.5 MWh and 585.9 MWh, respectively. This also has an impact on the filling mean temperatures, ranging from 61.0 °C to 63.2 °C over the total simulation time frame. In contrast, in the 10<sup>th</sup> year, the largest temperature spread, and capacity of 444.6 MWh is achieved in scenario G00, which is 8.2% more than for the base case.

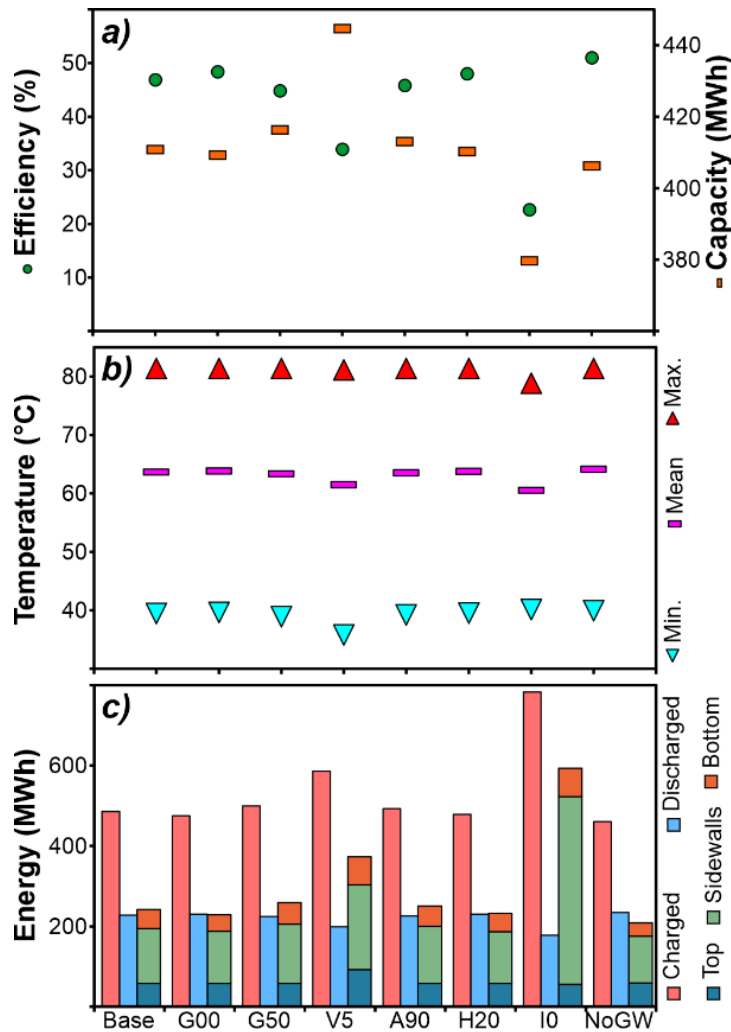


Fig. 5.8: Key performance indicators for comparison of the different scenarios (cf. TAB. 5.3) of the parameter study: a) efficiency and simulated maximum capacity, b) filling temperatures (min., mean, max.), c) values of the sTES energy balance (charged, discharged, and lost energy quantities at the top, sidewalls, and bottom).

Nevertheless, the groundwater flow velocity is identified as the most influencing factor. Compared with the base case, the storage efficiency is reduced by 12.9% in scenario V5. Again, this effect is related to the phreatic zone, where specific heat losses are increased by 55.5% to  $144.4 \text{ kWh m}^{-2}$  if the groundwater flow velocity is significantly increased. Due to a shorter residence time of the groundwater, the thermal plume propagation is extended, however, the temperature gradient between the ambient soil and the sTES wall is increased. Adverse effects in the last simulated year, as the decrease of discharged energy of 12.6% (198.9 MWh vs. 227.6 MWh in the base case), further prove a lower amount of available energy supplied by the sTES. Conversely, the smallest impact is observed for the parameter specifying the groundwater inflow angle, where the reduction in storage efficiency is only 1.0% in the last simulated year, at higher losses of 250.1 MWh. Thus, it can be concluded that the impacts of different hydrogeological BCs lead to distinct implications for the environmental domain, as described in the following section.

In contrast to this stands the effect of sTES insulation, which can be concluded to be inevitable for any facility with groundwater interaction: Comparing the base case with the extreme case of an uninsulated sTES embedded in a groundwater regime, the



10<sup>th</sup>-year storage efficiency is drastically decreased to only 22.7% (24.2% less than the base case). In this case, the average filling mean temperature is only 59.4 °C over 10 years of operation. In the 10<sup>th</sup> year, the maximum filling temperature is only 78.8 °C, while specific losses at the walls and at the bottom amount to 276.7 kWh m<sup>-2</sup> and 163.5 kWh m<sup>-2</sup>, respectively. Consequently, in the case of groundwater impacts, insulation is indispensable for WGTES, and for other sTES types (e.g., for PTES, as in line with findings by DAHASH et al. [29]), to achieve reasonable efficiency.

### 5.3.3 Environmental perspective

Effects of different hydrogeological parameters also become evident in the impact analysis of the sTES on its surrounding soil. The different angles of inflow and hydraulic gradients lead to different groundwater velocity distributions. Thus, they alter heat dissipation in the aquifer zone as well as resulting temperatures in the subsurface and the efficiency of the sTES. In the base case, the velocity of the background flow is  $2.0 \cdot 10^{-7} \text{ m s}^{-1}$  (FIG. 5.10), whereas near the basin, particularly at the corners, they span a range of  $5.2 \cdot 10^{-9} \text{ m s}^{-1}$  to  $1.0 \cdot 10^{-6} \text{ m s}^{-1}$ . For a given steeper hydraulic gradient (scenario G50), the flow velocity range is increased to  $1.3 \cdot 10^{-8} \text{ m s}^{-1}$  to  $2.6 \cdot 10^{-6} \text{ m s}^{-1}$ , resulting in an extensive spreading of the thermal plume.

For a straightforward comparison, soil temperatures are evaluated at the same distance of 2 m (FIG. 5.9 a) and 5 m downstream of the basin (FIG. 5.9 b). Here, for all scenarios, the overprint due to the sTES operation becomes apparent, but to different extents: In the extreme case of an uninsulated sTES, because of the highest energy losses and direct contact heat progression into the surrounding soil, temperatures of 48.1 °C are obtained. Simulations by DAHASH et al. [281] yielded similar values of up to 50 °C near an uninsulated PTES at the same distance.

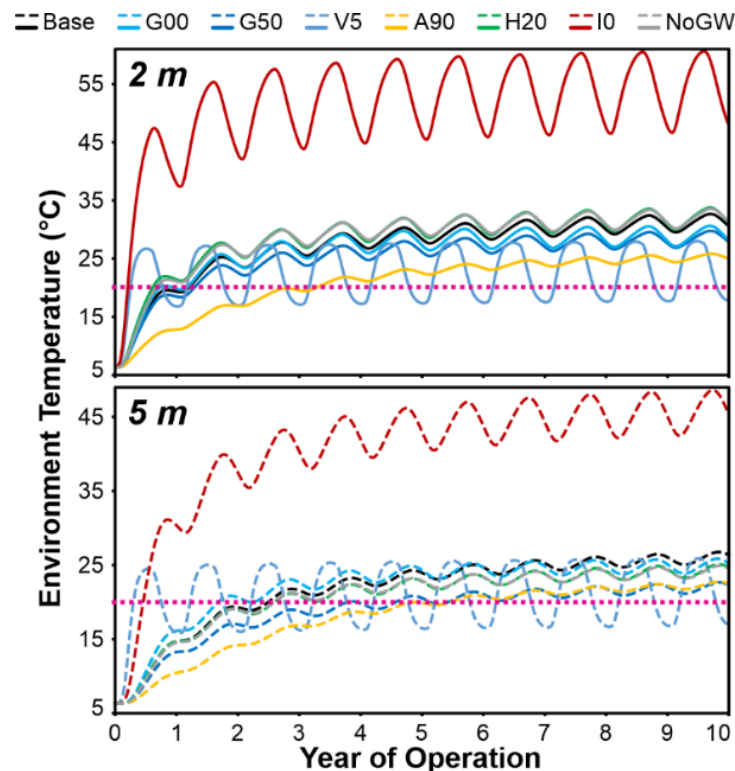


Fig. 5.9: Impacts of sTES on subsurface: environment temperatures in 2 m / 5 m distance. The pink dotted lines indicate the legal threshold value of 20 °C for Germany and Austria.

Among the insulated scenarios with groundwater influences, the temperatures for scenario H20 rise the highest: After 10 years of operation, the surrounding subsurface heats up to 31.3 °C at this probe location, which is 4.5 m above the groundwater table for this scenario. In turn, in scenario V5, with the highest heat dissipation due to groundwater flow, this increase reaches only 17.8 °C. Over all insulated scenarios, the temperature recordings show the highest amplitude (ca. 10.3 K), which is in turn only 1.4 K for scenario A90 with perpendicular groundwater flow. For the scenario without groundwater presence, even higher values of 31.4 °C can be observed. This is not surprising, since solely conductive heat transport (i.e., absence of advection) leads to lower effective thermal conductivity, increased dissipation of thermal energy, and, thus, higher temperature records in the subsurface. Thus, high intensities of groundwater flows lead to lower maximum temperatures in the subsurface, but to a larger impact area. For active geothermal subsurface utilization, similar characteristics have been reported, e.g., by HÄHNLEIN et. al [31] in the case of borehole heat exchangers, but they were so far not reported for any study covering a WGTES.

For a better resolved spatial evaluation, FIG. 5.10 shows the 20 °C and the +6 K thermocline (legally binding in Austria and recommended in Germany [30,330]) in a horizontal cut plane at half the sTES' height after 10 years of operation. Again, the uninsulated scenario represents an extreme case, where the impact of the +6 K thermocline reaches a large maximum distance of 21.7 m. In general, downstream propagations are much greater than in the upstream direction (20 °C / 6 K thermocline distance in the base case: 7.2 m / 12.5 m vs. 3.3 / 5.9 m). Due to the perpendicular angle of inflow  $\beta = 90^\circ$  in scenario A90, a larger and broader heat plume results (downstream/lateral distances of 6 K thermocline: 10.0 m / 7.5 m, vs. 5.9 m / 4.9 m in the base case). In comparison, the scenario without groundwater presence yields extents of 2.4 m and 6.9 m (long side), and 6.1 m and 9.7 m (short side).

Generally, the shape of the resulting thermal plumes (FIG. 5.10) is vastly different: while the NoGW scenario leads to a very homogeneous distribution of heat, the increase in groundwater flow velocity temperatures becomes much more non-uniform, but also less intense. Further, this study also demonstrates the important influence of sTES geometry on resulting potential implications for the environment. For approval processes and further analysis, the observed temperature distributions are significant, because the measurement location for permitted temperature change has a major influence on their result. Consequently, this issue must be highlighted as a critical lack in the heterogeneous regulatory frameworks. An accurate, 3D spatial evaluation of impacts is therefore essential to accurately assess the resulting environmental effects. In contrast, a simple limitation to point measurements would not consider heterogeneous underground conditions.

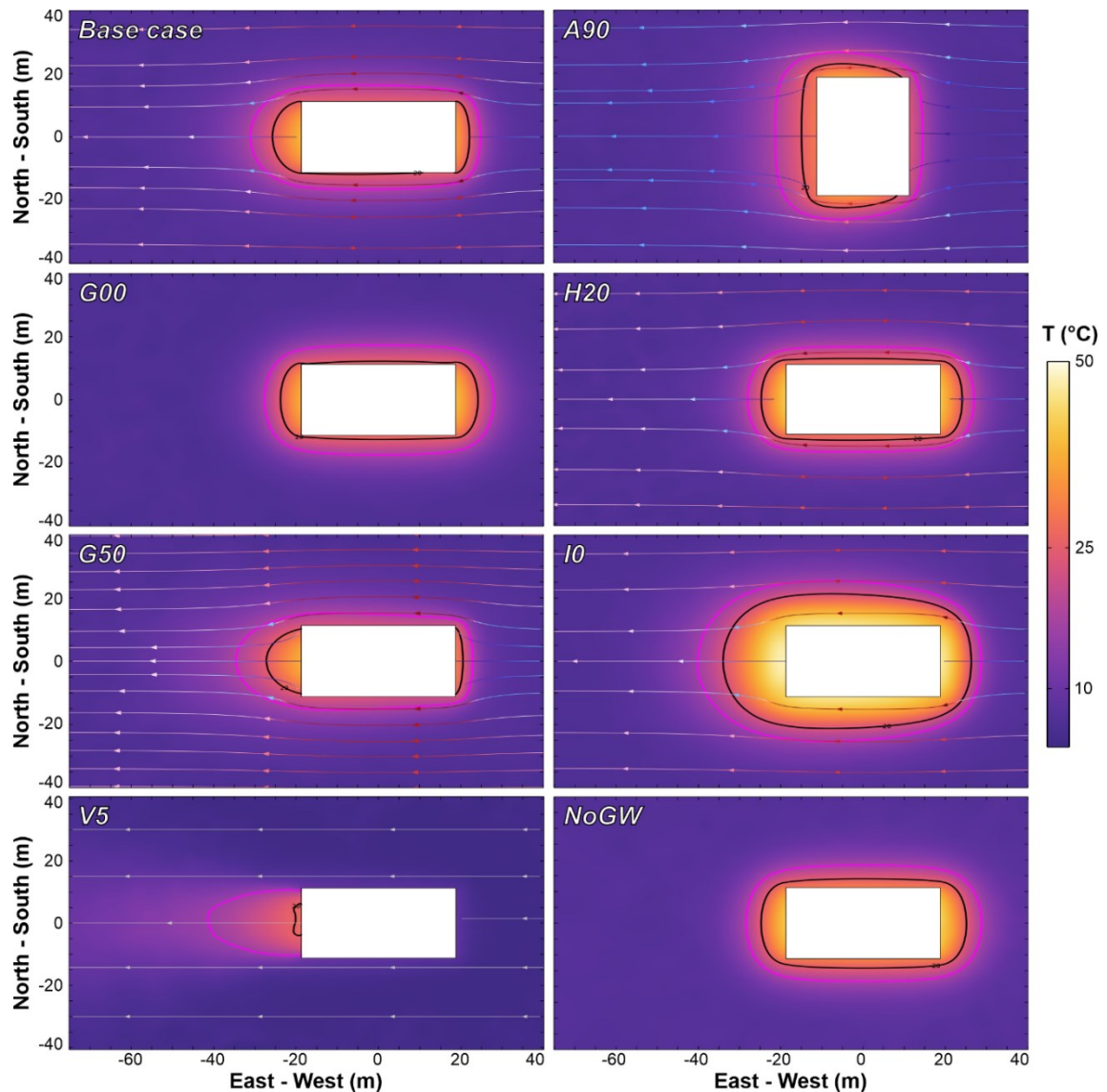


Fig. 5.10: Impacts of sTES on its surrounding environment: 20 °C (black) and +6 K (magenta) thermocline around sTES at a height of  $0.5 \cdot h_{sTES}$  after 10 years of operation for each scenario (cf. TAB 5.3).

Resulting temperature conditions in the close surroundings of the storage facility potentially affect the groundwater ecosystem for all scenarios, as they are above a temperature change of 5–10 K, which is considered to be an acceptable range [195,321]. Even a minor change of 5 K may impact faunal and microbial biodiversity, as these communities are adapted to specific conditions and sensitive to thermal changes [321,336,337]. Moreover, additional heat alters groundwater’s chemical composition and quality [338–341]. Although the aquifer is only affected at a local scale, the storage can still contribute as a heat source to regionally elevated subsurface temperatures when it is embedded into an urban environment. Here, high subsurface temperatures above 20 °C can lead to enhanced bacterial growth, especially in drinking water distribution networks, whose placement should be considered in the planning of sTES [342,343]. Thresholds regarding absolute temperatures or induced changes are still controversial in science [344] and inconsistent in national legislation, resulting in the absence of legally binding regulations in most countries (FIG. 5.2 c, [30]).

## 5.4 Conclusions and outlook

This study provides a new (co-)simulation framework to improve the design and understanding of ambient ground thermal effects of sTES facilities. Using a co-simulation approach between COMSOL and MATLAB/SIMULINK, an expansion of the previously introduced STORE model for ground-based sTES was conducted to include subsurface hydrogeological processes (e.g., groundwater flow) and further environmental impacts. Thereby, the STORE model was further enhanced (e.g., inversed thermocline effect) and extended (e.g., for static roof component). The study described both models with their respective components, modeled processes, interfacing, and required input/output data.

The presented parameter study demonstrated the tool's versatility and applicability. Its results proved that groundwater flow can have a significant impact: Compared to a scenario without groundwater, in the worst case, the storage efficiency of an insulated sTES can decrease from 51% to 34%. A variation of different subsurface parameters (e.g., groundwater inflow angle and velocity, table depth) provided further insights into the impact of these factors. Thereby, a change in flow velocity is most sensitive and leads to increased losses (374 MWh vs. 241 MWh in the base case). As one key conclusion, insulation of in-ground sTES is indispensable for effectively preventing thermal losses (efficiency drops to only 23% for an uninsulated sTES). In contrast, sTES operation can cause negative implications for its surroundings, especially for groundwater ecosystems. This is potentially relevant for approval processes of new projects. Here, it was revealed that, despite sound insulation, a temperature increase of up to 20 °C can occur at a distance of 7.5 m or by up to 31 °C at a 2 m distance after 10 years. However, this increase was limited to 18 °C under favorable conditions (i.e., vast dissipation by groundwater with high flow velocity).

In general, heterogeneous subsurface conditions resulted in increased uncertainties in operation predictions in practice. Thus, the evaluation of 3D propagations of thermal losses using simulation frameworks as presented was to be recommended. For further development, the remaining shortcomings of this framework (surrounding district and the actual topography) need to be addressed, since buildings and subsurface structures can have a significant influence on groundwater flow and thermal regimes. Besides, open questions concern reconciling the accuracy of results and computational efforts by dynamic time stepping.

## 6 Synthesis

### 6.1 Conclusions: Findings in the field of seasonal thermal energy storage

Seasonal thermal energy storage (sTES) can contribute significantly to the energy transition. A transformation in thermal energy supply is inevitable, wherein sTES solutions are considered to be a key element. This thesis concerns the contributions from multiple perspectives to the further development of ground-based, closed sTES in basin systems. Those constitute the variants of Tank (TTES), Pit (PTES), and Water-Gravel Thermal Energy Storages (WGTES), offering the potential to be used as a central element of modern smart energy systems to enable a high share of renewables in the energy mix, higher self-consumption, improved system robustness and resilience, as well as optimized sector coupling (e.g., between heat and electricity supply).

To continuously improve these technological variants, progress has been achieved through technical and scientific initiatives over more than 25 years. As a result, sTES are now considered as largely mature and more than 30 prototypes are in operation in several Central European countries. However, significant barriers hindering global market availability remain, and these relate to technical, economic, environmental, and regulatory issues. To overcome these weaknesses, the overall objective of this work was to develop new methods and concepts to achieve the required improvements in materials and methods.

As a foundation, a comprehensive state-of-technology analysis was conducted. It focused on major operational experiences of past projects in the field of TTES, PTES, and WGTES concepts, to derive the best practices from evolution and to identify previous weaknesses in detail. The focus was laid on the technical characteristics of the different types, such as structural elements, filling, static elements, sealing, thermal insulation, and operation facilities of the sTES. A large variety of engineering parameters were identified that significantly influence both design and implementation performance. While the results covered installations with a total storage volume of almost 800,000 m<sup>3</sup>, representing a theoretically available capacity of 56 GWh, they also demonstrated the potential of innovative solutions. For example, the evidence that new recycled materials effectively replace conventional materials, and how more efficient concepts can improve storage efficiencies and overcome risks of failure. This served as a basis to address specific objectives for the enhancement of the sTES technology currently applied in practice.

The first objective of the work was to provide technical advancements, particularly for the sealing and thermal insulation of sTES. Operational experience indicated that significant heat losses in the periphery range of sTES are key weaknesses. Furthermore, already minor defects in sealing liners involve a high risk of irreparable damage. To achieve an improvement within this domain, the introduction of the latent storage material paraffin wax into the external shell of sTES was suggested. The underlying hypothesis was that liquid and solidifying paraffin wax should actively seal fissures, gaps, or diffuse leaks in sealing membranes based on the hydrophobic properties of the material, while also providing added storage capacity.

Results of a laboratory study show that up to  $138 \text{ kJ kg}^{-1}$  of thermal energy could be accumulated in the paraffin wax component. This is equivalent to an increased storage capacity of 40.7 MWh for a large-scale PTES installation. Moreover, the phase change mechanism is particularly suitable for buffering short-term peak loads, evidenced by the measured retardation times of 2.5 to 4 hours. Consequently, it was shown that the low thermal conductivity of the material provides added value for the overall system. Besides the thermal characteristics, the material losses of the paraffin wax from the new combined sealing and thermal insulation were observed to be only 1.5 to 17% in experiments with different, artificially induced leakages. As a result, it could be proven that the material is capable of effectively sealing defects. This laboratory-based study provided a valuable proof-of-concept for the further technical development of sTES. Even though technical refinements and economic optimizations need to be addressed before practical availability, the proposed new component has the potential to effectively improve the robustness and efficiency of future sTES.

The second objective of the thesis was to develop appropriate analysis tools for a multi-objective enhancement of the sTES technology. It was found that the existing tools for sTES modeling lack sufficient flexibility and robustness. This is due to geometrical weaknesses, as well as drawbacks in defining internal design or modeling important physical processes during operation. To address these, a new model “STORE” for operation simulation of WGTES was developed, providing a component-level resolution and highly flexible parameterization. The setup was documented by describing the storage components considered, the processes modeled, the input data required for the simulation, and the methods used to evaluate results. Furthermore, the model was benchmarked to prove its applicability and accuracy.

In a parameter study, STORE was further used to investigate one example of re-use of an existing basin infrastructure ( $1,000 \text{ m}^3$  large swimming pool), whereby various design scenarios were considered. In the results, simulated storage efficiencies reached up to 69.5% if the basin was equipped with complex, efficient insulation materials. Conversely, a wide range of efficiency was found, with a value of only 12.4% achieved in the case of no insulation. Moreover, important performance parameters, such as attainable storage capacities (23.5 to 26.5 MWh) and long-term trends (e.g., more than five years of an initial heating phase until quasi-steady state with the ambient) were evaluated to derive general design recommendations: It was shown that the top cover as well as thermal insulations in the top section of sTES are most relevant for a technological optimization. As a result, STORE is suitable for simulating technical and systemic optimizations and for generating new knowledge. Employing scenario analyses and sensitivity studies, which can be conducted with high processing speed and accuracy of results, this research step successfully served the objective of finding optimal solutions for sTES designs under variable energy system boundary conditions and specific site characteristics.

For the objective of further refining available frameworks for optimized planning, and accurate operational simulation, a further issue identified was that most existing models do not sufficiently account for processes in the immediate environment around sTES. Consequently, prediction accuracies were typically limited, most notably for locations with significant hydrogeologic drivers (i.e., interactions with groundwater flow). This is in contrast to the fact that even minor environmental alterations can be relevant to groundwater protection.

An assessment of short- and long-term environmental implications is crucial for sustainable storage concepts and reliable approval practices. To achieve this objective, the third scientific step was to further develop and extend the STORE model via a previously rarely used approach. By coupling two individual models, STORE and a 3D COMSOL model were used to enable detailed resolution of the internal storage behavior as well as the processes in the ambient environment. The implementation was documented in detail, including important influencing parameters of the model and simulation (e.g., interfaces, solvers, meshing, and parameterization of the different domains). After successful validation of the novel co-simulation model (cf. APPENDIX D-1), a parameter study was conducted to investigate the influence of different hydrogeological boundary conditions (hydraulic gradient, corridor distance, inflow angle of horizontal groundwater flow) on a synthetic WGTES. The modeling results revealed efficiency ranges of 24% to 57%. Aside from the technical analysis, another focus was to examine the effects of the WGTES on its environment. Based on a spatial simulation analysis, it was shown that after 10 years of operation, temperature increases of +6 K can extend up to 22 m from the sTES. Likewise, in an extreme case, temperatures of up to 45 °C were found at a distance of 5 m. Overall, the successive refinement of STORE and the findings of the parameter study can serve to derive design recommendations and quantify environmental impacts, providing an important basis for planning processes and operating permits in practice. Moreover, they effectively support the achievement of the second objective of enhancing modeling capabilities and achieving more reliable performance predictions within sTES projects.

The last objective of the project was to thoroughly examine the reusability of existing infrastructures for sTES. This is based on the hypothesis that pre-existing installations mitigate high investments for new sTES by avoiding costly construction steps (e.g., excavation, and construction of structural components). However, existing structures often lack optimal prerequisites (e.g., in terms of surface/volume ratio) and design flexibility. The feasibility of this concept could not only be proven by the developments of this project, as the developed modeling tools are particularly suitable for investigating the feasibility of reusing existing infrastructures. At the presented IN-Campus site, this objective can be considered as being achieved: there, the transformation of a compound of former firefighting basins into sTES is foreseen. This ultimately demonstrates the practical significance of the research activities to provide a significant contribution to the energy and thermal transformation and to support structural transformation processes in research and practice.

## 6.2 Outlook

### 6.2.1 Perspectives for further technical, economic, and ecological improvements as part of future research activities

The establishment of new sTES solutions is essential to achieve the energy transition: for example, only in Germany, in the next ten years, demand for about 1,000 new sTES (total storage demand of about 10 TWh) is predicted to be needed for the decarbonization of district heating systems [345].

Accordingly, new research activities to validate the added value of sTES and to target new approaches for optimized sTES solutions will be required also in the future. In the following, emerging scientific potentials are presented and discussed. They include additional methods for digitization, more robust and smarter controls, and conceptual innovations, such as multi-sTES, combined sTES, or coupled geothermal installations for waste heat recovery. These presented technical approaches aim at further reduction of operation and investment costs, especially for the re-use of existing basin infrastructures. Finally, complementary sustainability perspectives, such as those based on the life cycle assessment (LCA) of sTES, can serve to develop internationally applicable technologies with high market potential in the future.

#### Advanced monitoring concepts

To calibrate and validate new models based on high spatially and temporally resolved measurement data, as well as to provide input data for new control strategies and methods described below, a continued effort must focus on scientific monitoring networks within sTES facilities and their surrounding subsurface. As an example, FIG. 6.1 shows one possible implementation of a monitoring system for one of the basin systems at the IN-Campus site. As technical solutions, active, fiber-optical distributed temperature sensing (DTS) devices provide one of the most suitable monitoring methods. DTS is an established technique in geosciences for various applications [346–348] and has already been applied for monitoring large buffer storages [349]. As such, their application in and around sTES offers the possibility to also observe thermal interactions with the saturated and unsaturated zones. Additional monitoring capabilities can be employed by the installation of various sensors within the sTES (e.g., for monitoring heat flow, pressure, temperature, and water level) as well as in the near field of the installation (e.g., groundwater observation wells).

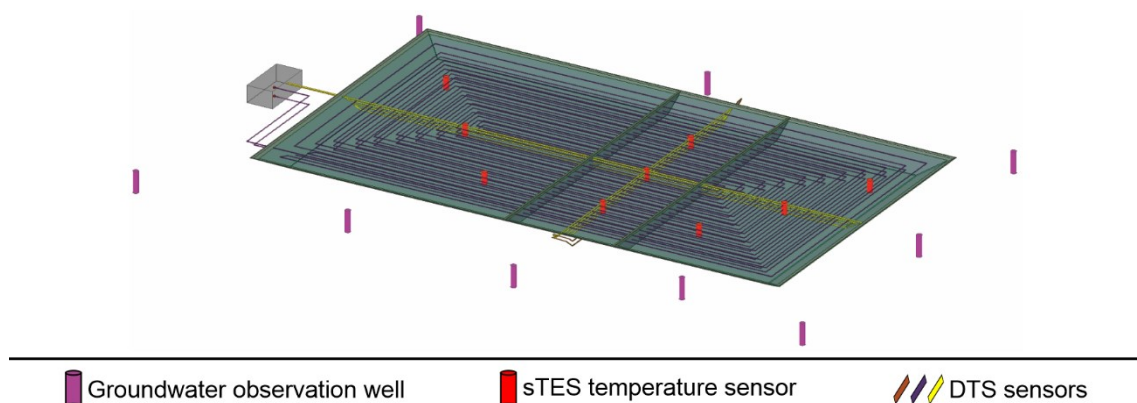


Fig. 6.1: Example of a sophisticated monitoring setup for the sTES of the basin compound ABC at the IN-Campus (cf. FIG. 1.4) and the surrounding environment based on point probes as well as DTS.



These monitoring strategies add scientific value on different time scales: smart monitoring concepts are particularly useful for detecting short-term disturbances during operation. Leakages in sealing materials, local deficiencies in thermal insulation, or incorrect operation of the heat exchanger in gravel-water reservoirs may be detected. On a larger timescale, scientific monitoring systems serve to characterize storage during operation in the long term by tracking the heat-up phase as well as storage cycles and by investigating interactions with the environment in more detail. While such monitoring systems are currently rare, future implementations are of high relevance for the further development of storage technologies based on real data.

#### Development of digital twins

In the future, planned sTES projects and implementations will focus more than ever on computer-based analyses and operation simulations. For this purpose, digital twins for sensitivity and scenario analyses for technological, economic, and ecological optimization could represent highlights of further digitized advancements.

Digital twins [350–352] can reproduce the conditions within a storage facility, in the underground, and in the connected energy system from multiple perspectives, creating room for improvement and a virtual control center for predictive control. One approach to this is the coupling of several component models, which aim at the most realistic possible representation of the site conditions based on important, local influencing factors and processes. Hence, the digital representation of a system can serve not only for monitoring, data collection, and aggregation but also for deriving optimal operating conditions and predictive maintenance [351,352].

The first steps for this progress have already been made within this thesis by coupling a sTES and an environmental model. A full digital twin of an sTES has not been developed so far. However, its potential is indicated by various perspectives: By incorporating real operational data in the storage (e.g., filling temperatures, energy flows), weather data, energy prices and load forecasts, fine-tuned charging and discharging phases can be planned predictively. In the implementation, it will be important to ensure the modularity of the digital twin to ensure high transferability to other sites [353]. Furthermore, the digital twin needs to provide a converged solution for multiple, specialized, validated, and site-calibrated utilities to reflect the key processes of all relevant components of the system. For this, interfacing between different model implementations appears to be one of the major challenges.

#### Innovative, optimized, AI-based control strategies

The optimization of a sTES unit poses challenges to optimum operation: For solar-based systems, for example, it has been shown that the degree of solar energy utilization could be increased by one percent by lowering the return temperature by just one degree [51]. However, smart control solutions for the next generation of sTES will also have to account for additional sources and individual energy system configurations through the intelligent, targeted use of temperature and energy monitoring. In most of these cases, the complexity of a system will be too demanding to use high-resolution (numerical) white-box models for control. In return, demands on the security of supply and system surveillance will be too critical for relying on pure black-box solutions characterized by significant uncertainties in the predictability and reasoning of operating mode selection.

Thus, future research activities need to identify application areas for artificial intelligence (AI) concepts. In addition, a conceptual definition of allowable degrees of freedom of such algorithms is required. AI could initially serve to identify suboptimal operating states and offer suggestions for optimized control. However, scientific support will be essential to specify necessary, accompanying restrictions. In the next step, a future task will be to develop suitable AI algorithms that can learn optimized sTES conditions during real operation and optimize this operation from a multidimensional perspective. For this purpose, the integration of demand and availability forecasts of sources and sinks is particularly useful, e.g., by integrating machine learning solutions [354,355], trained on physical models and based on recorded data in a digital lab. The anticipated, key added value of AI solutions becomes apparent when they can be used to replace complex, computationally expensive physical models. Then, the aforementioned digital twin can be converted into an efficient, optimized, and robust emulator that would manage monitoring and control functions. However, before this, an evaluation of the new AI-based control strategy by comparing real operation under standard conditions with simulated, optimized operation methods is crucial to determine the advantages and drawbacks as well as potentials for a safe, continuous expansion of these control methods.

#### Multi-storage-concepts and combined storage solutions

Especially at sites with the option of re-using existing infrastructures, not only single but multiple structures may be available. This raises further perspective research questions for developing strategies to combine multiple sTES. Similarly, these may not only feature separate elements, but also subdivided infrastructure compounds resulting in new requirements for design, construction, and operation as sTES units.

In cases where multiple, separate basin setups are available for re-use at one location, a variety of storage combinations with different configurations, designs, and operational principles may serve the potential to increase the overall system efficiency. In comparison to single basins, separate systems result in less favorable surface-to-volume ratios. However, additional flexibility in the storage operation (cascaded or parallel systems in terms of temperature levels, and fluid flows) may allow for improved management of diverse, fluctuating energy sources (especially renewables) as well as sinks. This way, varying basin geometries provide options to address different target applications, while subsequent expansion of individual basins may accompany an evolutionary process of a district energy system expansion in a successively transformed energy system.

Despite the apparent advantages of operating combined storages, thus far, their potential for advancing sTES capabilities has been overlooked. Several challenges need to be investigated via comparative studies based on modified modeling tools. In this regard, couplings of several sTES within one model are already practicable with the STORE model developed in this thesis. Subsequent research approaches need to focus on further technical issues, e.g., optimal interconnection, and best control strategy. In addition, added values of combined storages with flexible management, in contrast to static integrations of a single sTES, need to be analyzed, taking several reference units (e.g., energy, storage capacity, power) into consideration.

In the case of composite structures with internal separating walls, such a system offers the possibility of subdividing one basin into multiple sub-sTES systems, allowing different configurations and design optimizations for specific applications. To examine whether such concepts can increase the overall efficiency, further developments of the models are necessary as well. FIG. 6.2 illustrates the extension of the STORE model for a basin network with three sub-basins with different designs.

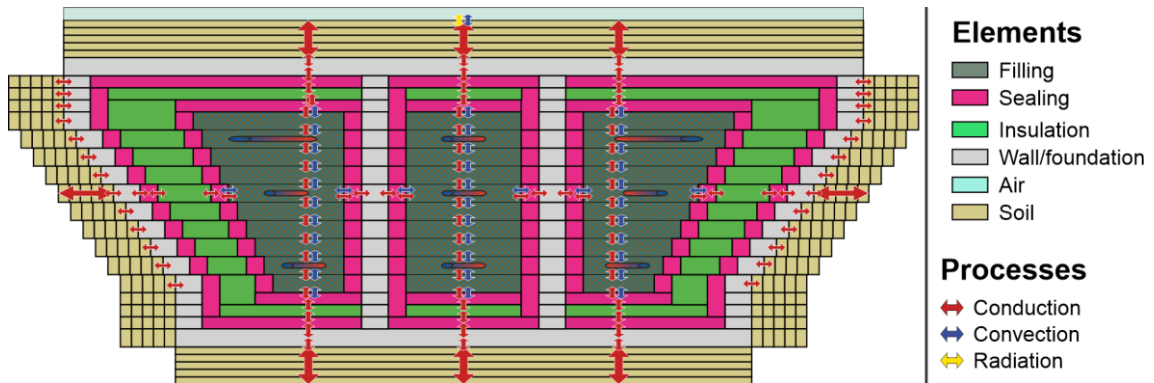


Fig. 6.2: Advanced concept of the STORE model for modeling combined sTES compound systems.

Based on this extended STORE model, sensitivity studies are to be performed to investigate a reasonable matching of temperature gradients by applying a refined design as well as sophisticated modes of operation, e.g., by operating the central basins at the highest temperature level whereas the outer basins are kept at lower temperatures. Then, within the resulting cascaded multi-storage system, the central basin is partly insulated by its surrounding sub-sTES, which can be used to achieve overall techno-economic optimization.

#### Thermal utilization of the subsurface around seasonal thermal energy storage

As shown in this thesis, significant heating of the surrounding soil and in the groundwater is to be expected during sTES operation, depending on its configuration and design. This opens the potential for complementary geothermal use of the “lost” heat to minimize environmental risks, but also to maximize storage efficiencies. The ground can be considered as a complementary storage medium with its own storage characteristics. In this case, it is important to investigate to what extent the heating of the surrounding soil of ground-based storage can be used as an efficient geothermal resource, e.g., by installing groundwater heat pump systems or borehole heat exchangers. On the one hand, geothermal systems for providing a buffer for extreme conditions have already been discussed in the past [344]. However, on the other hand, continuous thermal losses resulting from less insulated (less expensive) sTES may be recovered and adverse thermal impacts on the environment may be avoided. This is supported by the fact that re-used infrastructures are primarily not optimal for storage applications and that insulation can only contribute limited added value in terms of techno-economic optimization in these cases. Also, the waste heat recycling approach may compensate for such weaknesses and add an innovative component to the system, which is based on an existing, commonly used, and well-proven technology.

Research studies for this solution demand an extension of the previous models, for example, the coupled STORE-environment model. By extending this model to include a geothermal device, it is possible to scrutinize changes in the thermal and hydraulic

processes resulting from the active use of the subsurface, i.e., how thermal losses from the storage facility and environmental effects can be minimized. Computer-based analysis enables the innovation to be optimized before field demonstrations can take place. This could involve, for example, installing a geothermal trench [28,356] downstream of an sTES basin and connecting a heat pump as well as specific environmental monitoring. Thus, an underground waste heat recovery system for basin-based sTES would provide further thermal energy. Still, requirements for material selection, construction, and operation of this system have to be addressed.

Application of LCA frameworks for environmental evaluation

sTES not only serves for technical (i.e., energetic) optimization in modern energy systems but also for enhancing integration of fluctuating renewables in the thermal grid and overall environmental performance optimization. The environmental footprint is kept low by re-use of existing structures with minimal consumption of new space and resources. Also, recycled materials can be used for sTES construction. Sustainable concepts need to cover the entire life cycle of the considered technology. To reflect this entire scope of environmental benefits, it is useful to model the entire life cycle within an LCA framework. This follows international standards and norms (DIN EN ISO 14040 – DIN EN ISO 14049 [357]) and provides a detailed quantification in different impact categories (e.g., climate change potential, acidification potential, use of non-renewable resources, etc.). First, all materials and methods associated with energy flow for construction, operation, and decommissioning are summarized in a life cycle inventory. Then, reference data for all processes and materials are applied according to the design of an sTES facility.

In the technology field of sTES, LCA has already been applied to aquifer [358,359] and borehole thermal storage systems [360]. There have not been any studies or initiatives on applying the LCA framework to closed, ground-based sTES. Therefore, a comprehensive analysis is required to fill technology-specific data gaps and to define representative sTES characteristics for a flexible LCA model (a suggested initial scheme for a WGTES LCA model is shown in FIG. 6.3), including site-specific characteristics (e.g., functional units, scope, model boundaries).

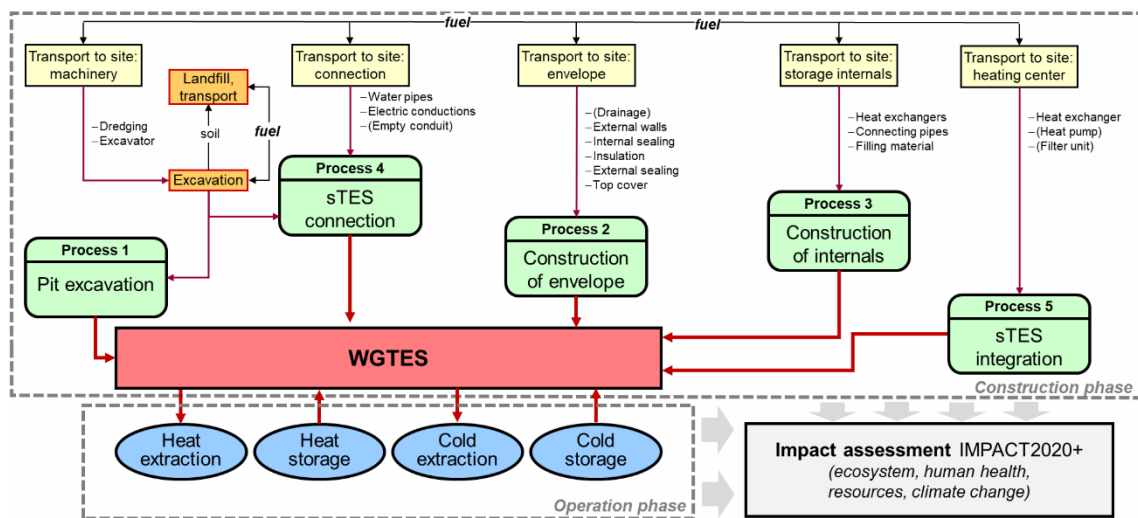


Fig. 6.3: Exemplary concept of a Life Cycle Assessment model for Water-Gravel Thermal Energy Storage including the construction and operation phase.

Results of future research activities with a mainly environmental perspective will identify general and site-specific environmental benefits of innovative storage solutions. Thereby, any new developments, including the presented approaches of combined and multi-sTES, can be addressed, and compared to conventional solutions or systems without sTES. High-quality LCA models can also be used to optimize sTES designs based on environmental criteria and, via sensitivity analyses, to reveal major optimization potentials of individual components and processes. The demonstration of environmental benefits will also improve the acceptance of sTES and support the development of future projects.

### 6.2.2 Perspectives for the IN-Campus as an application site for innovative seasonal thermal storage concepts

Already during this thesis, the IN-Campus revealed itself as an outstandingly suitable yet highly prospective location for investigating the above-described perspective challenges. An important objective of the project was to obtain generic findings and recommendations for the transformation and re-use of existing infrastructures (FIG. 6.4) in areas of transformation based on an analysis of the state of the art in the field of sTES. For this purpose, the IN-Campus offered a unique demonstration target. By building upon the contributions of this thesis, it may become the benchmark of an upcoming sustainability strategy for site development with sTES.



Fig. 6.4: Basins (a: sub-basin A of the basin compound ABC, b: basin D of the basin compound DEF, c: Basin H), which may serve for re-use as seasonal thermal energy storage at the IN-Campus (cf. FIG. 1.4).

Conversely, this pilot location highlights the practical added value of the scientific progress achieved in this thesis. Upcoming activities will support detailed design stages and provide scientific guidance. In this context, the generalized findings, the new conceptual approaches, and the newly developed, flexibly applicable STORE model can be used to enable continued storage construction and operation optimizations. Scheduled future research activities at the IN-Campus are summarized in FIG. 6.5.

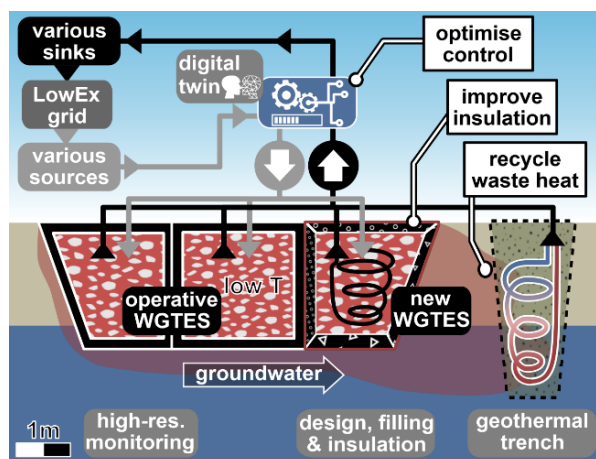


Fig. 6.5: Planned upcoming research activities and challenges at the multi-sTES "ABC" of the IN-Campus.

Altogether, the site will function as a field laboratory and demonstrator for in-depth monitoring activities, model calibrations and validations, and further enhancements (e.g., via dynamic testing of tailored novel materials).

In a first step, in 2024, the existing basin network ABC (FIG. 1.4 and FIG. 6.4) will be transformed into a system with detailed monitoring and it will be connected to the integrated energy system. Aiming to implement an internally differentiated multi-sTES, sub-basins A+B will be upgraded as a fully buried, indirectly charged/discharged WGTES (filling material: re-used gravel from the site) that is sealed on all sides with re-used plastic membranes. In addition, sub-basin C will be developed as a demonstration and transfer object, where further innovations can be tested:

- ▷ Development of innovative concepts for the construction of ground basin storage below the so far valid threshold of 50 €/m<sup>3</sup> water equivalent [18],
- ▷ Establishment of a reference project involving an expanding energy system incl. smart, adaptive, digital control,
- ▷ Deduction of generic procedures for sequential integration of multi-functional, combined multi-sTES,
- ▷ Transfer of generic guidelines for infrastructure re-use for cost-efficient sTES.

In general, innovative efforts can focus on an optimized, flexible transformation of basin structures and optimum sTES integration, while potentials for re-use as thermal storage facilities can be explored for further on-site structures (FIG. 6.4). Here, it is advantageous that the entire IN-Campus is a dynamic project that will successively be expanded in further construction phases. This allows demonstration options for optimized, combined use of multi-sTES in a modern, evolutionary environment.

# Appendices

## Appendix A

### Appendix A-1: Details on fillings & geometries

Tab. A- 1: Fillings and geometric specifications of selected storage systems. (countries: DEN: Denmark, GER: Germany, ITA: Italy, SWE: Sweden, SWI: Switzerland, fillings: W: Water, W-S: Water-Soil, W-G: Water-Gravel).

#	Name	Year	Country	Type	Filling	Buried	Geometry	V <sub>water</sub> (m <sup>3</sup> )	Dimensions (l,w,h) (m)	h / d	Surface (m <sup>2</sup> )	A / V (m <sup>3</sup> )	V <sub>water</sub> / V <sub>total</sub>	References
1	Lambohov	1980	SWE	PTES	W	yes	n.a.	10,000	32.4 x 32.4 x 2	n.a.	1750	0.18	1	[5,14,25,63-65]
2	Herlev (Tubberupvaenge)	1991	DEN	PTES	W	yes	cubeoid	3,000	26.25 x 26.25 x 6	0.23	1630	0.54	1	[5,14,25,63-65]
3	Otrrupgaard	1995	DEN	PTES	W	yes	rev. trunc. pyramid	1,500	26.5 x 26.5 x 5	0.31	1400	0.93	1	[18,26,28,31,47,48,64,68,69,71-73]
4	Jülich	1996	GER	PTES	W	yes	rev. trunc. pyramid	2,500	26 x 26 x 7	n.a.	n.a.	n.a.	1	[5,64,71,74]
5	Marstal (SUN STORE 4)	2012	DEN	PTES	W	yes	rev. trunc. pyramid	75,000	113 x 88 x 16	ca. 0.16	n.a.	n.a.	1	[43,53,71,73,75-77]
6	Dronninglund	2013	DEN	PTES	W	yes	rev. trunc. pyramid	62,000	91 x 91 x 16	0.15	n.a.	n.a.	1	[45,46,64,65,73,75,78]
7	Gram	2015	DEN	PTES	W	partly	rev. trunc. pyramid	122,000	110 x 125 x 15	0.08	n.a.	n.a.	1	[44,46,78-80]
8	Vojens (1+2)	2015	DEN	PTES	W	yes	rev. irreg. 6-sided trunc. pyramid	203,000	n.a.	n.a.	n.a.	n.a.	1	[53,55,56,81,82]
9	Rottweil	1995	GER	TTES	W	partly	cylinder	597	13 x 13 x 5	0.38	470	0.79	1	[5,26,41,87-89]
10	Cosenza (Calabria)	1995	ITA	TTES	W	yes	dome/cylinder	500	10 x 10 x 7.3	0.73	n.a.	n.a.	1	[5,90,91]
11	Friedrichshafen (Wiggenshausen)	1996	GER	TTES	W	partly	trunc. cone/cylinder	12,000	32 x 32 x 20	0.63	2796	0.23	1	[7,26,35,37,41,48,57,59,64,88,92-94]
12	Neuchatel	1997	SWI	TTES	W	n.a.	cylinder	1,000	14.6 x 14.6 x 16.15	1.10	1075	0.45	1	[4,13,28,48,95]
13	Ilmenau	1998	GER	TTES	W	no	cylinder	300	6.9 x 6.9 x 8	1.15	262	0.88	1	[31,36,88,89,96-98]
14	Hannover (Kronsberg)	2000	GER	TTES	W	yes	trunc. cone/cylinder	2,750	19.0 x 11.1 x 13	0.58	1135	0.41	1	[7,37,38,57,88,92,99,100]
15	Rise	2001	DEN	TTES	W	no	cylinder	4,000	20 x 20 x 13	0.65	1445	0.36	1	[47,78,83,101,102]
16	Munich (Ackermannbogen)	2007	GER	TTES	W	partly	trunc. cone/cylinder/ trunc. cone	5,700	? x ? x 15	n.a.	n.a.	n.a.	1	[7,38,48,57,58,92,103-106]
17	Hamburg (Bramfeld)	2010	GER	TTES	W	yes	cylinder/ trunc. cone	4,500	25.7 x 25.7 x 14.7	0.57	1650	0.37	1	[7,15,18,26,38,48,58,71,93,98,99]
18	Mühdorf	2010	GER	TTES	W	no	cylinder	16.4	1.8 x 1.8 x 7	3.80	42.7	2.6	1	[107]
19	Vaulruz	1983	SWI	TTES	W-S	yes	rev. trunc. cone	n.a.	30.5 x 30.5 x 6.2	0.22	6331	1.8	n.a.	[19,25,108-110]
20	Stuttgart	1985	GER	WGTES	W-G	yes	rev. trunc. cone	725	22 x 22 x 4	0.18	835	0.84	0.91	[5,17,19,25,26,111]
21	Augsburg	1996	GER	WGTES	W-G	yes	cubeoid	3,250	n.a.	n.a.	n.a.	0.16	0.5	[19,48,64,68,85,88,108]
22	Steinfurt (Borghorst)	1999	GER	WGTES	W-G	yes	rev. trunc. pyramid	1,000	13.4 x 41.8 x 4.1	0.15	1305	0.80	0.54	[7,15,35,37,48,57,64,99,109,111,112]
23	Chemnitz	2000	GER	WGTES	W-G	yes	cubeoid	5,300	58 x 20 x 7	1.00	3412	0.43	0.66	[5,7,13,17-19,24-26,37,48,88,109,113-117]
24	Eggenstein (Leopoldshafen)	2008	GER	WGTES	W-G	yes	rev. trunc. cone	3,000	27.7 x 27.7 x 8	0.29	1964	0.44	0.67	[18,37,38,48,57,58,61,104,118-121]
25	Craillsheim (Hirtenwiesen)	2007	GER	Buffer	W	no	cylinder	580	14.5 x 14.5 x 6.3	0.43	362	0.75	1	[7,18,36-38,57,64,93,120,121]

## Appendix A-2: Details on thermal insulation

Tab. A- 2: Detailed information on thermal insulations for selected locations.

#	Name	Year	Country	Type	Insulation material basis	Insulation material walls	Insulation material itop	T <sub>max</sub> (°C)	Thermal loss (% / MWh/a)	References
1	Lambohov	1980	SWE	P TES	expanded clay	expanded clay	expanded clay	70	40% / 250 MWh/a	[5, 14, 25, 63–65]
2	Herlev (Tubberupvaenge)	1991	DEN	P TES	PUR foam	PUR foam	PUR foam	85	? / 80 MWh/a	[14, 24, 25, 47, 49, 63, 64, 66–69]
3	Otrrupgaard	1995	DEN	P TES	none	none	PUR foam	60	30% / 85 MWh/a	[18, 26, 28, 31, 47, 48, 64, 67, 68, 70–72]
4	Jülich	1996	GER	P TES	none	none	mineral fiber	n.a.	n.a. / n.a.	[5, 64, 70, 73]
5	Marstal (SUN STORE 4)	2012	DEN	P TES	none	none	PE foam	85	48% / 2908 MWh/a	[43, 53, 70, 72, 74–76]
6	Dronninglund	2013	DEN	P TES	none	none	PE foam	85	41% / 2260 MWh/a	[45, 46, 64, 65, 72, 74, 77]
7	Gram	2015	DEN	P TES	none	none	expanded clay	85	n.a. / n.a.	[44, 46, 77–79]
8	Vojens (1+2)	2015	DEN	P TES	none	none	expanded clay	80	n.a. / n.a.	[53, 55, 56, 80, 81]
9	Rottweil	1995	GER	T TES	none	mineral fiber	mineral fiber	n.a.	n.a. / n.a.	[5, 26, 41, 82–84]
10	Cosenza (Calabria)	1995	ITA	T TES	foam glass gravel	foam glass gravel	foam glass gravel	80	45% / 32 MWh/a	[5, 85, 86]
11	Friedrichshafen (Wiggenhausen)	1996	GER	T TES	none	mineral fiber	mineral fiber	82	47% / 320 MWh/a	[7, 26, 35, 37, 41, 48, 57, 59, 64, 83, 87–89]
12	Neuchatel	1997	SWI	T TES	none	mineral fiber + XPS	mineral fiber + XPS	n.a.	n.a. / n.a.	[4, 13, 28, 48, 90]
13	Ilmenau	1998	GER	T TES	none	PUR foam	PUR foam	78.5	n.a. / n.a.	[31, 36, 83, 84, 91–93]
14	Hannover (Kronsberg)	2000	GER	T TES	none	expanded glass granulate	expanded glass granulate	90	28% / 90 MWh/a	[7, 37, 38, 57, 83, 87, 94, 95]
15	Rise	2001	DEN	T TES	none	mineral fiber	mineral fiber	n.a.	n.a. / n.a.	[47, 77, 96–98]
16	Munich (Ackermannbogen)	2007	GER	T TES	foam glass gravel	expanded glass granulate	expanded glass granulate	95	41% / 195 MWh/a	[7, 38, 48, 57, 58, 87, 99–102]
17	Hamburg (Bramfeld)	2010	GER	T TES	none	mineral fiber	mineral fiber	82	49% / 360 MWh/a	[7, 15, 18, 26, 38, 48, 58, 70, 88, 93, 94]
18	Müldorf	2010	GER	T TES	perlites	perlites	perlites	90	n.a. / n.a.	[103]
19	Vaulruz	1983	SWI	T TES	none	EPS	EPS	53	? / 62 MWh/a	[19, 25, 104–106]
20	Stuttgart	1985	GER	WG TES	none	none	pumice	45	40% / 27 MWh/a	[5, 17, 19, 25, 26, 107]
21	Augsburg	1996	GER	WG TES	none	XPS	XPS	n.a.	n.a. / n.a.	[19, 48, 64, 67, 83, 104, 108]
22	Steinfurt (Borghorst)	1999	GER	WG TES	foam glass plates	expanded glass granulate	expanded glass granulate	68	42% / 70 MWh/a	[7, 15, 35, 37, 48, 57, 64, 94, 105, 107, 109]
23	Chemnitz	2000	GER	WG TES	none	XPS	XPS	85	n.a. / n.a.	[5, 7, 13, 17–19, 24–26, 37, 48, 83, 105, 110–114]
24	Eggenstein (Leopoldshafen)	2008	GER	WG TES	expanded glass granulate	expanded glass granulate	foam glass gravel	90	53% / 105 MWh/a	[18, 37, 38, 48, 57, 58, 61, 100, 115–118]
25	Crailsheim (Hirtenwiesen)	2007	GER	Buffer	foam glass gravel	expanded glass granulate	expanded glass granulate	108	n.a. / 72 MWh/a	[7, 18, 36–38, 57, 64, 88, 117, 118]



## Appendix A-2: Details on waterproofings

Tab. A- 3: Detailed information on waterproofings for selected locations.

#	Name	Year	Country	Type	Waterproofing layer material	Waterproofing layer thickness (mm)	Vapor diffusion barrier material	Drainage layer material	References
1	Lambohov	1980	SWE	PTES	butyl	n.a.	n.a.	n.a.	[5, 14, 25, 63–65]
2	Herlev (Tubberupvaenge)	1991	DEN	PTES	EPDM/steel (Phase II)	0.5 (Phase II)	steel (Phase II)	n.a.	[14, 24, 25, 47, 49, 63, 64, 66–69]
3	Otrrupgaard	1995	DEN	PTES	clay	850	none	tapes	[18, 26, 28, 31, 47, 48, 64, 67, 68, 70–72]
4	Jülich	1996	GER	PTES	PP	n.a.	n.a.	n.a.	[5, 64, 70, 73]
5	Marstal (SUN STORE 4)	2012	DEN	PTES	HDPE	2.5	none	geofabric	[43, 53, 70, 72, 74–76]
6	Dronninglund	2013	DEN	PTES	HDPE	2.5	none	on top only	[45, 46, 64, 65, 72, 74, 77]
7	Gram	2015	DEN	PTES	HDPE	2.5	n.a.	n.a.	[44, 46, 77–79]
8	Vojens (1+2)	2015	DEN	PTES	HDPE	2.5	n.a.	n.a.	[53, 55, 56, 80, 81]
9	Rottweil	1995	GER	TTES	stainless steel	0.5	stainless steel	none	[5, 26, 41, 82–84]
10	Cosenza (Calabria)	1995	ITA	TTES	yes	n.a.	yes	gravel	[5, 85, 86]
11	Friedrichshafen (Wiggenhausen)	1996	GER	TTES	stainless steel	1.2	stainless steel	yes	[7, 26, 35, 37, 41, 48, 57, 59, 64, 83, 87–89]
12	Neuchatel	1997	SWI	TTES	steel	n.a.	steel	none	[4, 13, 28, 48, 90]
13	Ilmenau	1998	GER	TTES	GRP	10	none	none	[31, 36, 83, 84, 91–93]
14	Hannover (Kronsberg)	2000	GER	TTES	concrete	0.3	none	gravel	[7, 37, 38, 57, 83, 87, 94, 95]
15	Rise	2001	DEN	TTES	steel	n.a.	steel	none	[47, 77, 96–98]
16	Munich (Ackermannbogen)	2007	GER	TTES	stainless steel	2.5	stainless steel	gravel	[7, 38, 48, 57, 58, 87, 99–102]
17	Hamburg (Bramfeld)	2010	GER	TTES	stainless steel	1.25	stainless steel	gravel	[7, 15, 18, 26, 38, 48, 58, 70, 88, 93, 94]
18	Mühlendorf	2010	GER	TTES	stainless steel	n.a.	stainless steel	none	[103]
19	Vaulruz	1983	SWI	TTES	n.a.	n.a.	n.a.	n.a.	[19, 25, 104–106]
20	Stuttgart	1985	GER	WGTES	HDPE	2.5	none	gravel	[5, 17, 19, 25, 26, 107]
21	Augsburg	1996	GER	WGTES	HDPE	n.a.	n.a.	n.a.	[19, 48, 64, 67, 83, 104, 108]
22	Steinfurt (Borghorst)	1999	GER	WGTES	PP	2 + 2	Al-PE	gravel	[7, 15, 35, 37, 48, 57, 64, 94, 105, 107, 109]
23	Chernitz	2000	GER	WGTES	HDPE	2.5	none	lattice	[5, 7, 13, 17–19, 24–26, 37, 48, 83, 105, 110–114]
24	Eggenstein (Leopoldshafen)	2008	GER	WGTES	HDPE	2.5	Al-PE	none	[18, 37, 38, 48, 57, 58, 61, 100, 115–118]
25	Crailsheim (Hirtenwiesen)	2007	GER	Buffer	stainless steel	1.5	stainless steel	none	[7, 18, 36–38, 57, 64, 88, 117, 118]

## Appendix A-2: Details on structural elements

Tab. A- 4: Detailed information on structural elements for selected locations.

#	Name	Year	Type	Structural element material	Structural element thickness (m)	Slopes (°)	References
1	Lambohov	1980	PTES	concrete	<i>n.a.</i>	90	[5, 14, 25, 63–65]
2	Herlev (Tubberupvaenge)	1991	PTES	steel profiles + concrete cover	<i>n.a.</i>	90	[14, 24, 25, 47, 49, 63, 64, 66–69]
3	Ottrupgaard	1995	PTES	<i>none</i>	<i>none</i>	27	[18, 26, 28, 31, 47, 48, 64, 67, 68, 70–72]
4	Jülich	1996	PTES	<i>none</i>	<i>none</i>	<i>n.a.</i>	[5, 64, 70, 73]
5	Marstal (SUN STORE 4)	2012	PTES	<i>none</i>	<i>none</i>	34	[43, 53, 70, 72, 74–76]
6	Dronninglund	2013	PTES	<i>none</i>	<i>none</i>	45	[45, 46, 64, 65, 72, 74, 77]
7	Gram	2015	PTES	<i>none</i>	<i>none</i>	<i>n.a.</i>	[44, 46, 77–79]
8	Vojens (1+2)	2015	PTES	<i>none</i>	<i>none</i>	<i>n.a.</i>	[53, 55, 56, 80, 81]
9	Rottweil	1995	TTES	concrete	0.25	90	[5, 26, 41, 82–84]
10	Cosenza (Calabria)	1995	TTES	concrete	0.2-0.5	90	[5, 85, 86]
11	Friedrichshafen (Wiggenhausen)	1996	TTES	concrete	0.3	90	[7, 26, 35, 37, 41, 48, 57, 59, 64, 83, 87–89]
12	Neuchatel	1997	TTES	concrete	<i>n.a.</i>	<i>n.a.</i>	[4, 13, 28, 48, 90]
13	Ilmenau	1998	TTES	GRP	0.02 (0.17)	90	[31, 36, 83, 84, 91–93]
14	Hannover (Kronsberg)	2000	TTES	hq concrete	0.3	90	[7, 37, 38, 57, 83, 87, 94, 95]
15	Rise	2001	TTES	steel	<i>n.a.</i>	<i>n.a.</i>	[47, 77, 96–98]
16	Munich (Ackermannbogen)	2007	TTES	concrete	0.16	90	[7, 38, 48, 57, 58, 87, 99–102]
17	Hamburg (Bramfeld)	2010	TTES	concrete	0.3	90	[7, 15, 18, 26, 38, 48, 58, 70, 88, 93, 94]
18	Mühldorf	2010	TTES	stainless steel	<i>n.a.</i> (0.2)	90	[103]
19	Vaulruz	1983	TTES	<i>n.a.</i>	<i>n.a.</i>	<i>n.a.</i>	[19, 25, 104–106]
20	Stuttgart	1985	WGTES	<i>none</i>	<i>none</i>	45	[5, 17, 19, 25, 26, 107]
21	Augsburg	1996	WGTES	<i>none</i>	<i>none</i>	90	[19, 48, 64, 67, 83, 104, 108]
22	Steinfurt (Borghorst)	1999	WGTES	<i>none</i>	<i>none</i>	50	[7, 15, 35, 37, 48, 57, 64, 94, 105, 107, 109]
23	Chemnitz	2000	WGTES	pile wall	<i>n.a.</i>	90	[5, 7, 13, 17–19, 24–26, 37, 48, 83, 105, 110–114]
24	Eggenstein (Leopoldshafen)	2008	WGTES	<i>none</i>	<i>none</i>	35	[18, 37, 38, 48, 57, 58, 61, 100, 115–118]
25	Crailsheim (Hirtenwiesen)	2007	Buffer	concrete	0.2	90	[7, 18, 36–38, 57, 64, 88, 117, 118]

## Appendix B

### Appendix B-1: Records of experiments on thermal performance enhancement

Tab. B-1: Temperature measurement records of the experiments on the enhancement of thermal performance (Preview). This digital appendix cannot be included in print format due to its large size. Instead, it is available under its own DOI and can be retrieved via the following link:  
<https://doi.org/10.1371/journal.pone.0236056.s001>

	PVC 35	PVC 38	PVC 36	PVC 34	PVC 40	PS 34										
seconds	water bottom left	water top left	ecoglas bottom left	air	water bottom right	paraffin top	paraffin center	paraffin bottom	ecoglas PVC bottom	ecoglas PVC bottom 2	ecoglas top right	ecoglas bottom right	water top right	water center right	water top right 2	
30	21.21551	21.205291	21.438447	21.442343	21.197956	21.254828	21.321083	21.317782	21.331554	21.339817	21.292514	21.21774	21.191285	21.188446	21.196364	
60	21.214509	21.203291	21.439448	21.458348	21.196956	21.253828	21.323079	21.316782	21.332553	21.338816	21.290516	21.219741	21.192286	21.184444	21.197364	
90	21.212508	21.202292	21.439448	21.441343	21.196956	21.254828	21.321083	21.315783	21.330555	21.336815	21.293513	21.21874	21.18328	21.183444	21.196364	
120	21.228514	21.229281	21.439448	21.460349	21.185957	21.254828	21.319086	21.314783	21.331554	21.334815	21.291515	21.21874	21.184281	21.184444	21.194363	
150	21.628661	21.681101	21.438447	21.452346	21.234956	21.252828	21.318088	21.312784	21.327557	21.334815	21.294512	21.221741	21.192286	21.185444	21.186362	
180	21.946778	22.076944	21.44145	21.508363	21.577951	21.254828	21.318088	21.311785	21.326558	21.334815	21.292514	21.219741	21.40943	21.427557	21.440409	
210	22.283902	22.38782	21.439448	21.523368	21.721949	21.251827	21.315094	21.311785	21.327557	21.332814	21.293513	21.219741	21.531511	21.586631	21.598438	
240	22.653037	22.623726	21.442451	21.491358	21.989945	21.252828	21.315094	21.310786	21.325558	21.331813	21.296511	21.221741	21.813698	21.890772	21.856486	
270	22.897127	22.919609	21.44145	21.480355	22.240942	21.253828	21.313097	21.311785	21.324559	21.329812	21.295512	21.219741	22.084878	22.05885	22.575618	
300	23.225247	23.34444	21.44145	21.450346	22.512938	21.254828	21.313097	21.309786	21.324559	21.329812	21.295512	21.219741	22.597218	22.500055	22.53261	
330	23.471338	23.598338	21.440449	21.444344	23.023931	21.255828	21.314095	21.309786	21.324559	21.32581	21.293513	21.219741	22.888412	22.772181	23.022701	
360	23.693419	23.662313	21.442451	21.452346	23.113929	21.258829	21.316092	21.309786	21.321562	21.326811	21.296511	21.221741	22.85639	22.826206	22.967691	
390	23.978524	23.965192	21.442451	21.443344	23.298927	21.26083	21.316092	21.309786	21.32356	21.32381	21.295512	21.221741	23.047517	23.113339	23.120719	
420	24.299642	24.364034	21.442451	21.453347	23.456925	21.266832	21.321083	21.309786	21.32356	21.32381	21.29751	21.22741	23.489811	23.306429	23.569802	
450	24.489711	24.570951	21.444453	21.421337	23.619922	21.275834	21.323079	21.312784	21.321562	21.32381	21.298509	21.219741	23.778002	23.818667	23.93987	
480	24.753808	24.812855	21.443452	21.540373	24.007917	21.284837	21.333061	21.316782	21.324559	21.32481	21.29751	21.221741	24.082204	24.011757	24.182915	
...	...	...	...	...	...	...	...	...	...	...	...	...	...	...	...	

### Appendix B-2: Records of experiments on leakage mitigation

Tab. B-2: Records of the experiments on leakage mitigation (cf. sections 3.2.2 and 3.3.2). This digital is also available under its own DOI and can be retrieved via the following link:  
<https://doi.org/10.1371/journal.pone.0236056.s002>

Type	Area (mm <sup>2</sup> )	Direction	Surrounding material	Surrounding material diameter (mm)	Height (mm)	Width (mm)	Length (mm)	Total Volume (cm <sup>3</sup> )	Paraffin Volume cm <sup>3</sup>
Fissure	20	vertical	Sand	< 2	29	40	12	20	9
Fissure	20	vertical	Glass balls	3.00	45	55	11	12	5
Fissure	20	horizontal	Sand	< 2	49	59	25	58	36
Fissure	40	vertical	Sand	< 2	105	52	43	137	53
Single hole	380	n.a.	Sand	< 2	56	37	12	37	13
Perforated zone	23.6	n.a.	Sand	< 2	101	54	85	120	80

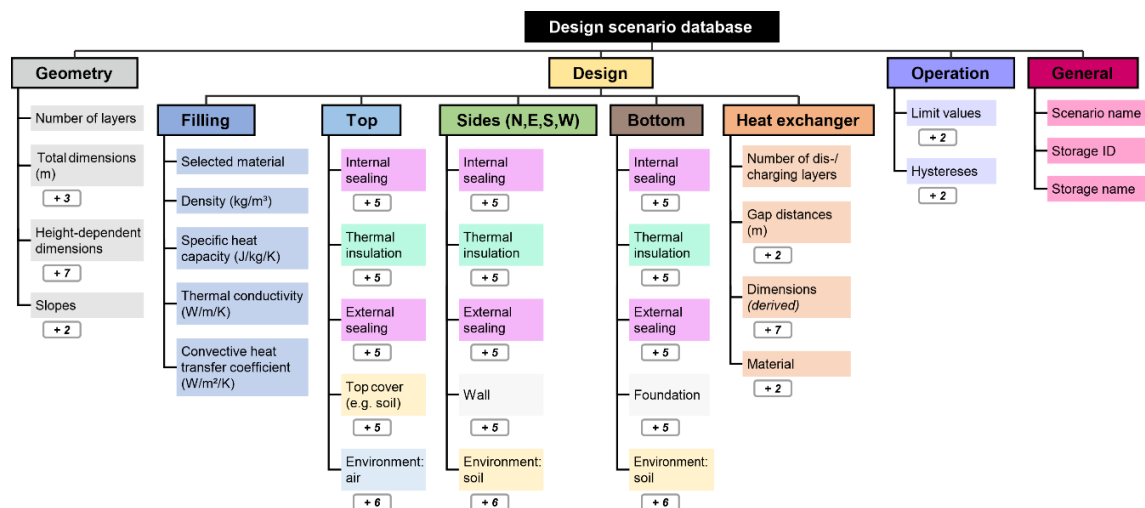
## Appendix C

### Appendix C-1: STORE model inputs – Design Scenario Database

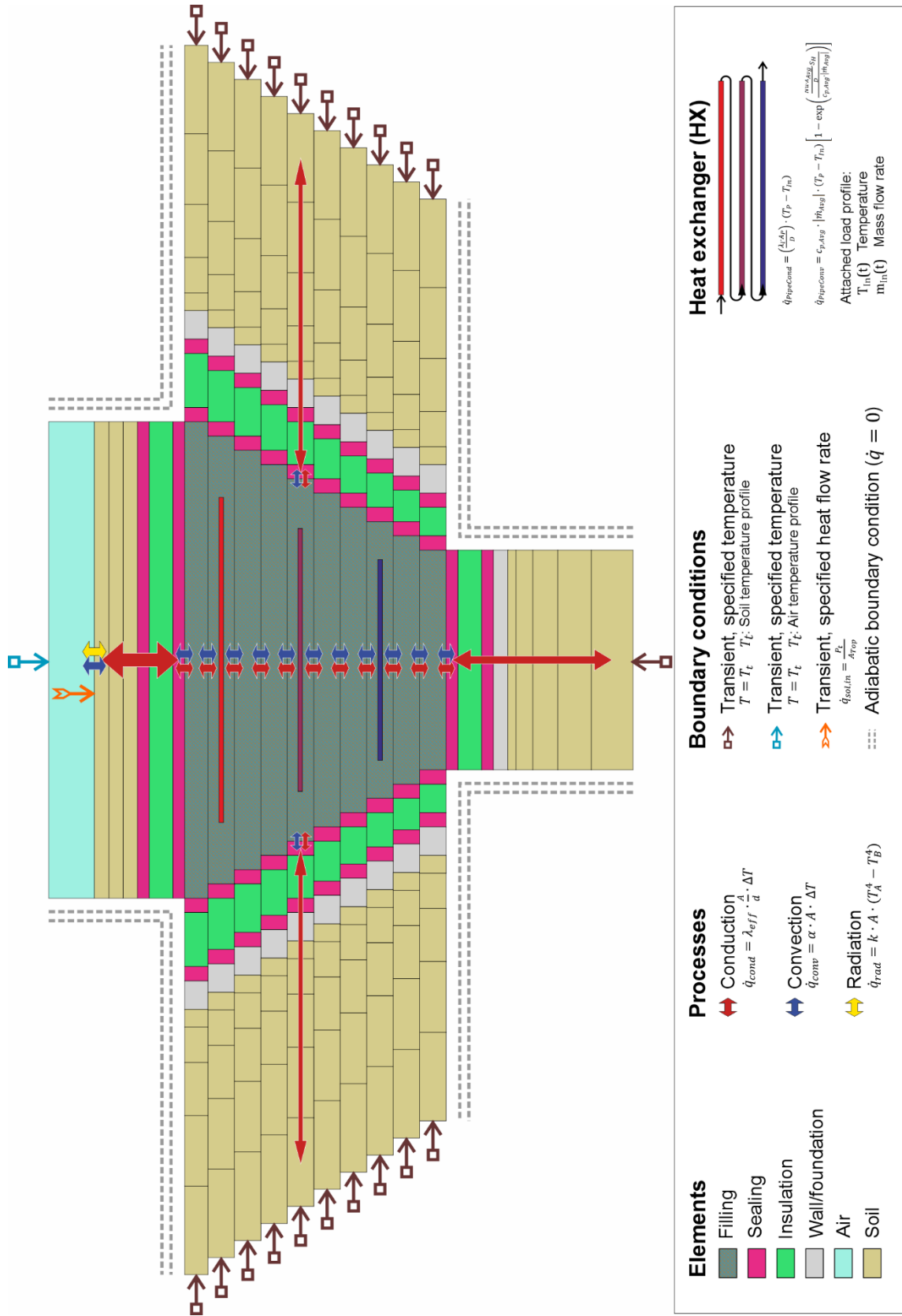
Split into sections (top, bottom, sidewalls in each direction), the design section reflects the layered sequence and indicates chosen materials, their thicknesses, densities, specific heat capacities, and thermal conductivities. In the design scenario database, parameters for convection and global irradiation are additionally included for the filling and air.

In the scenario database, the geometry section is divided into the basin's dimensions, i.e., length, height and width, information on sloped sides and slope ratios, as well as height-dependent data. The latter are important for e.g., different insulation thicknesses and include filling and insulation volumes at all storage sides as well as interface areas of the filling and walls.

Information on storage operation is stored in the design scenario database as primary limits for charging and discharging volume flows, as well as maximum and minimum charging and discharging temperatures. In addition, the hystereses values for optimum storage operations are stored in this section.



## Appendix C-2: STORE model setup



## Appendix C-2: STORE model – Default probe configuration

Information on the operation mode (charging/ discharging/ pause) originates directly in the storage control function and enables evaluations of cycles, pump working hours, or, if applicable, startups of heat pumps. Recorded temperatures of the filling components in all storage layers are used to calculate stored energy quantities by obtaining material specifications from the design scenario (specific heat capacity, volume, density). Thus, evaluations on temperature stratification or temperature distribution homogeneity provide initial insights into performance. Temperature records of other components further enable predictions about material stressors (e.g., longevity due to temperature fluctuations or maximum temperatures).

Heat exchanger processes are investigated based on information on temperature, pressure, mass/ volume flow rate and energy flow in the pipes. These are also valuable for heat exchanger design and optimization (e.g., number and position of heat exchanger levels, diameter, length, or pipe wall thickness). Data on energy quantities enables layer-resolved analyses on the amount of energy supplied to or extracted from the filling. Ultimately, losses are determined using the total energy balance together with information on stored energy.

Information about the volumetric flow rate, the temperature, and the pressure of the return flow at the end of the overall heat exchanger system represent the connecting point to the DHS and show both thermal performance and effectiveness of charging and discharging processes. Sensors for monitoring the storage's surrounding soil are placed in each layer and in the top layer for the top cover.

Domain	Element	Sensor type	Value / Unit	Description
Control	Switch	Operation mode	1 / 0 / -1	Dis-/ Charging or pause
Control	Switch	Hysteresis	1/ 0	Operation pause due to exceedance of control values
Connection	Supply flow	Temperature	°C	Actual load profile at storage grid interface
Connection	Supply flow	Vol. flow rate	m <sup>3</sup>	Actual load profile at storage grid interface
Connection	Return flow	Temperature	°C	Heat exchanger efficiency evaluation
Internal	Filling	Temperature	°C	Each layer
Internal	Heat exchanger pipe	Heat flow inlet/ outlet	W	Charging/ discharging energy flux
Internal	Heat exchanger pipe	Heat flow to filling	W	Effectivity of heat exchanger, in each dis-/ charging layer
Internal	Heat exchanger pipe	Pressure	Pa	For analyses of dimensioning/ durability
External	Soil	Temperature	°C	Each interface (sides, bottom), several distances
External	Top cover	Temperature	°C	Each layer

## Appendix D

### Appendix D-1: Model validation

In a validation, the co-simulation approach was compared with a proven approach. With this, the applicability of the newly developed framework to the later deployments for parameter and sensitivity studies was proven.

#### Model description

For the validation, a COMSOL model is used in which the effects of seasonal storage are implemented as temperature boundary conditions. The geometry of the basin is maintained and the height-resolved temperature differences (due to the temperature stratification present in the filling) are also accounted for. The STORE model previously tested in BOTT et al. (2022) [323] is used to generate a temperature profile corresponding to each layer of the external wall of the storage tank, as well as for the top and the bottom surfaces. Subsequently, the storage operation is simulated on the one hand using the co-simulation approach and on the other hand using the temperature data in a test case described below. In this context, it should be noted that the compared variant cannot represent feedback reactions to the storage facility and that the long-term changed conditions (e.g., less energy required to operate the storage because the surrounding ground is heated up) are deviating.

#### Test case

Despite the above-described differences, to test the new model, a generic test case is generated. From this, general conclusions about the general effects of the newly implemented mechanisms of the model become apparent. The geometry of the storage covers dimensions of 80 x 80 x 15 m and a slope angle of 45°, resulting in a volume of ca. 45,000 m<sup>3</sup>. Material parameters are not varied and are generally representative values for average conditions in the subsoil of construction sites. The storage facility for the validation scenario is assumed to be a low-insulated water-gravel thermal energy storage facility (0.1 m foam glass gravel on all sides), with the static component measuring additionally 0.25 m of concrete on all sides. The storage facility is designed to have a top cover with a thickness of 1 m and a slope angle of 1:2. For the operation of the unit, pipe coil systems made from PE-X on 3 levels with a spacing of 1 m and a hydraulic diameter of 0.05 m are considered. The resulting surface area of the heat exchanger is thus 18,798 m<sup>2</sup> with a length of ca. 5,906 m. The hourly resolved load profiles shown in FIG. D-1.1 are used for the operation simulation, which starts on April 1 (end of the heating period) with a charging of the storage.

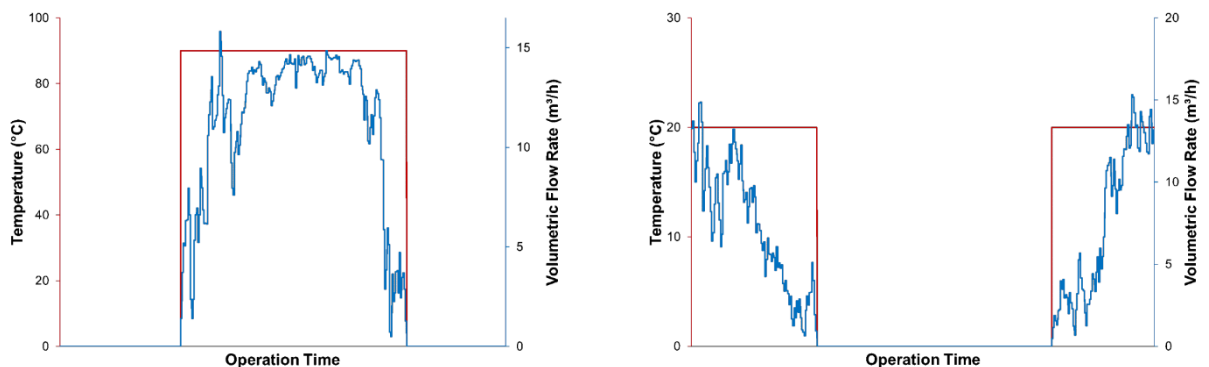


Fig. D-1.1: Charging (left) and discharging (right) operational load profiles used in the validation.

The environmental temperature profile is shown in FIG. D-1.2 and consist of a sinusoidal function according to the equation:

$$T_{\text{air}}(h)[^{\circ}\text{C}] = 10 - 10 \cdot \cos\left(\frac{2 \cdot \pi \cdot t [h]}{8760 [h]}\right).$$

To represent seasonally and daily varying solar irradiation, the following equation is used:

$$\ddot{q}_{\text{sol}}(h) \left[ \frac{\text{W}}{\text{m}^2} \right] = 0.8 - 0.8 \cdot \frac{2 \cdot \pi \cdot t [h]}{24 [h]} + 0.8 - 0.8 \cdot \frac{2 \cdot \pi \cdot t [h]}{8760 [h]}$$

Besides, the environmental boundary conditions of precipitation and convective heat loss based on wind velocities are disabled.

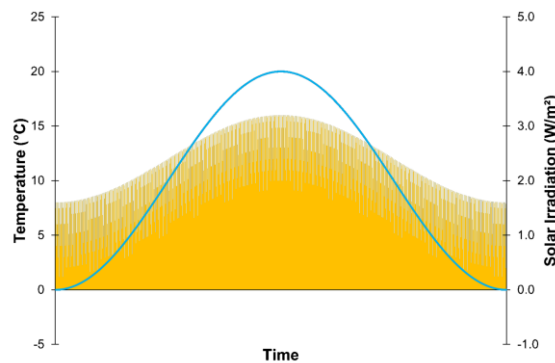


Fig. D-1.2: Environmental boundary condition datasets (ambient temperature: blue, solar irradiation: yellow) used in the validation.

As in the STORE model, a homogeneous subsurface of dry soil is assumed in the COMSOL model for the co-simulation. Appropriately, no groundwater flow conditions are assumed in the validation. The simulation period covered is 5 years, with time steps of 24 h being used in COMSOL. The distances to the model boundaries in COMSOL are 200 m to all sides and 30 m to the ground, the resulting mesh (automatically generated with settings default “fine”) consists of 31,355 elements (average skewness quality: 0.55).

### Validation results

For the evaluation of the results, and comparison of the two methods, focus is first placed on the differences in the thermal losses (FIG. D-1.3). Over the entire simulation period of 5 years, the differences in heat losses are on average  $-0.83$  kW, whereby positive and negative deviations offset each other. The validation generally leads to lower heat losses, with a maximum of 183.28 kW higher heat losses in the co-simulation, yielding a more pessimistic outcome. The range of values in the co-simulation is 238.04 kW ( $-177.50$  kW to  $+60.54$  kW) and in the validation 213.75 kW ( $-178.68$  kW to  $+35.06$  kW). In total, the largest deviations (up to 395.68 kW) occur at the top of the storage facility. This is plausible since the highest storage temperatures and largest temperature differences to the environment occur here. Thus, effects on the newly implemented mechanisms in the subsurface, especially the interaction with hydrogeological boundary conditions, are less influenced at the same time.



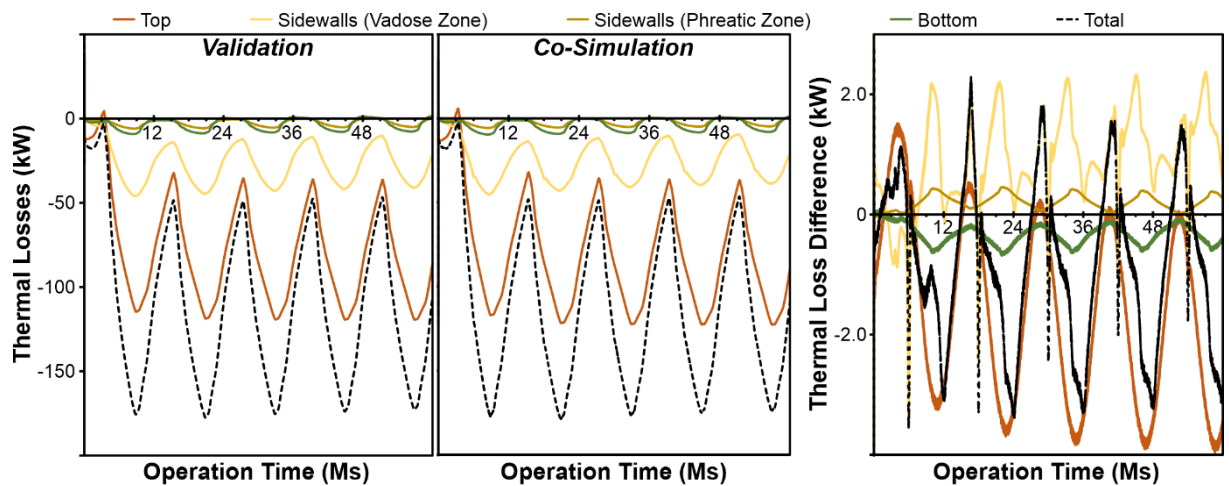


Fig. D-1.3: Results of observed thermal energy losses in the validation. Left, center: Thermal losses for the top, sidewalls, and bottom section of the simulated storage operation. Right: Heat loss difference between the co-simulation and the validation. Ms: months.

Similarly, the resulting temperatures in the subsurface show a quite similar pattern for both variants (FIG. D-1.4). At a distance of 5 m next to the side wall, temperature characteristics are compared at different depths (2 m to 10 m as well as 25% to 75% of the sTES height) as well as 1 m below the center of the foundation. Thereby it can be seen that the deviations for all values next to the storage facility are below 1 K (−0.95 K to +0.93 K). On average, they only differ by 0.30 K. In contrast, the results below the storage foundation show up to three times higher deviations (−0.05 K to 3.12 K).

However, this is because the coupling of a fixed temperature boundary condition at the bottom surface of the storage facility has a different effect than heat loss which better reflects the interference at the boundary (transition to the side walls). This is also clearly visible in the sectional view of FIG. D-1.5.

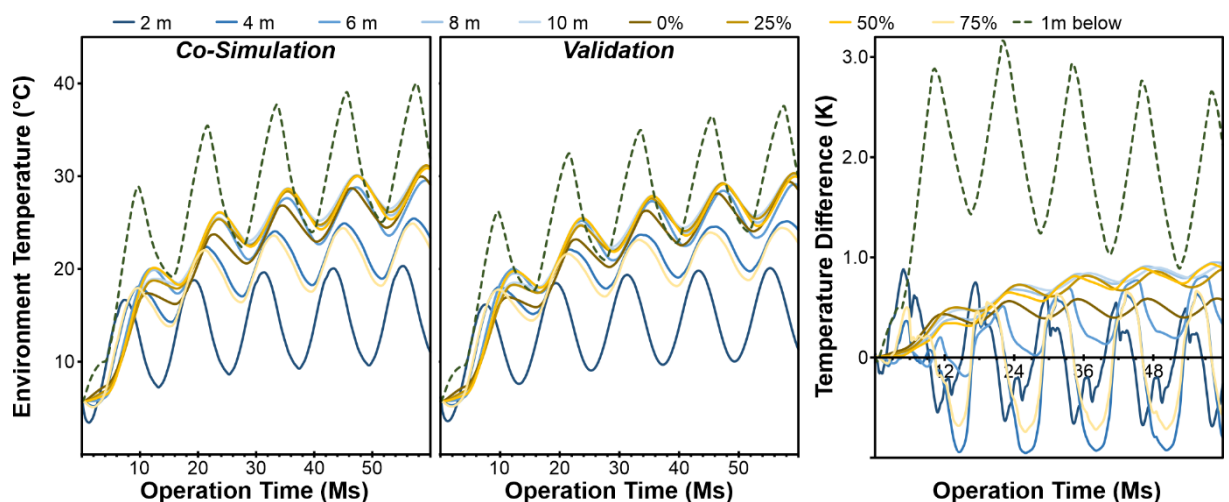


Fig. D1-4: Results of observed temperatures in the validation. Left, center: 5 m next to the seasonal thermal energy storage's sidewalls in different depths, as well as 1 m below the storage's foundation. Right: Temperature difference of the co-simulation and the validation. Ms: months.

By comparing the newly developed tool, which is based on the approach already tested by BOTT et al. (2022) [323], with a well-proven alternative for modeling temperature impacts, it can be summarized that divergences are low. Thus, the applicability of the advanced modeling method is demonstrated, while remaining

uncertainties can be attributed to the weaknesses of the validation variant. The latter is not able to represent the interactions of a storage facility and environment as well as spatially resolved interferences of the heat losses themselves very well.

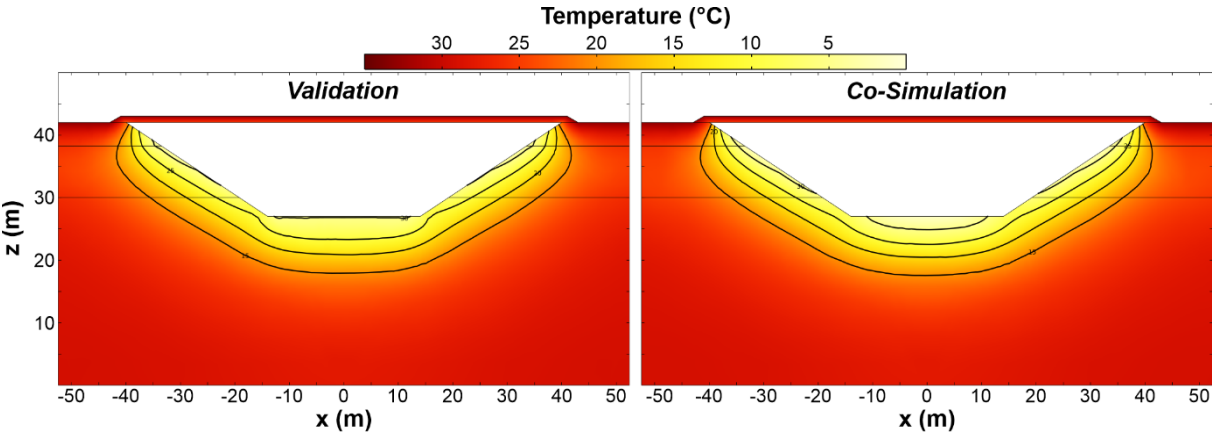


Fig. D-1.5: Results of observed underground temperatures in a cross-sectional view for the validation (left) and the co-simulation (right).

## Appendix D-2: Mesh refinement

To enable a sufficiently accurate simulation of the hydrogeological situation under the highly dynamic conditions of a seasonal thermal energy storage (sTES) operation, the mesh needs to be subject to refinements. Particularly in the near field of the storage, strong temperature gradients are to be expected, so a higher resolution is necessary there.

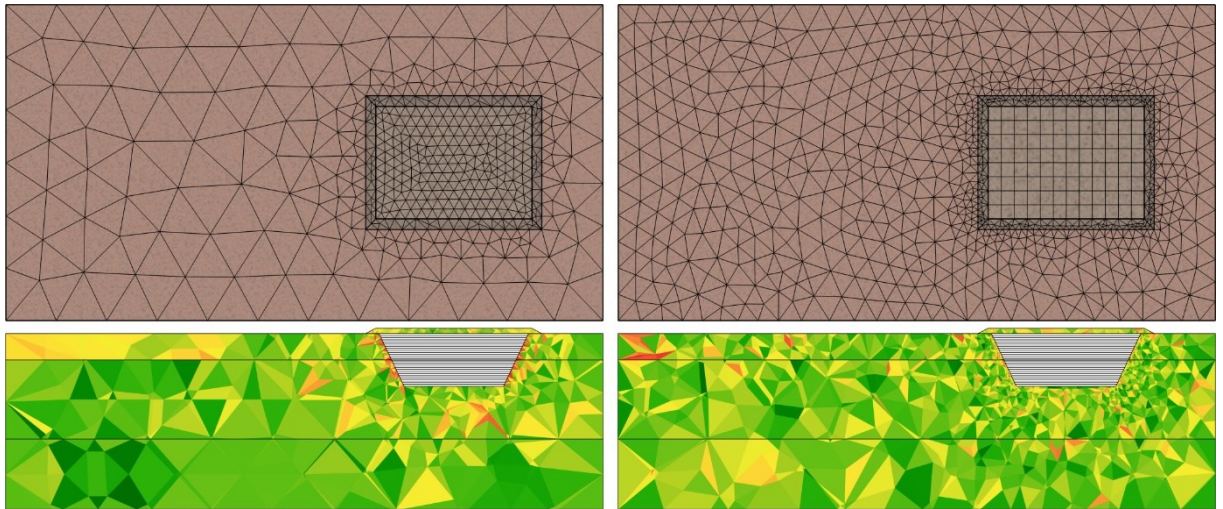


Fig. D-2.1: COMSOL mesh before (left) and after (right) gradient-based refinement in top (upper) and cross-sectional view (lower, color bar indicating skewness quality of elements).

First, four boundary layers with a thickness increase factor of 1.5 are inserted around the storage facility starting from an initial layer thickness of 0.05 m, so that a good transition is achieved at the interface and in the corner area. Based on the physics-based meshing of the model geometry, it is also worth noting that the situation of groundwater flow around the sTES structure results in an asymmetric energy flux and temperature gradient distribution. Therefore, to achieve further refinement of the mesh in the thermal plume generated by groundwater flow, a temperature gradient-based refinement is introduced. For this purpose, a steady-state study is performed in advance. A constant environmental temperature (initial conditions), the average expected heat losses of the basin, and the maximum gradients of the hydraulic heads are assumed. After the simulation of this test, resulting temperature gradients in the model's domains are reported and subsequently used for an error-based refinement. Preliminary investigations revealed that a refinement above a limit of  $dT > 2$  K significantly improves the later, real transient simulation results. Consequently, this refined mesh is designed for extreme situations and adapted to the specific site considered.

---

*Appendix D-2: Design scenario datasets*  
See attached MAT files (digital appendix).

## References

- [1] Eurostat - European statistics, Supply, transformation and consumption of derived heat: Annual data on quantities for crude oil, petroleum products, natural gas and manufactures gases, electricity and derived heat, solid fossil fuels, renewables and wastes covering the full spectrum of the energy sector from supply through transformation to final consumption by sector and fuel type (commodity balance)., online, 2023.
- [2] BP p.l.c., Statistical Review of World Energy 2022: Data compilation by Centre for Energy Economics Research and Policy, Heriot-Watt University, London, UK, 2022.
- [3] E. Sperber, M. Nast, Nahwärmenetze als zentrale Komponente für die zukünftige Energieversorgung, in: Kooperationsforum "Zentrale Wärmeversorgung in Kommunen", Ingolstadt, Germany, 2014.
- [4] European Union, Fit for 55 package: Briefing: Towards climate neutrality, Brussels, 2022.
- [5] T. McPhie, A. Crespo Parrondo, G. Bedini, REPowerEU: A plan to rapidly reduce dependence on Russian fossil fuels and fast forward the green transition, Brussels, 2022.
- [6] European Commission, The European Green Deal: Communication from the Commission to the European Parliament, the European Council, the Council, the European Economic and Social Committee and the Committee Of The Regions, Brussels, 2019.
- [7] A. Sauer, Energieeffizienz in Deutschland - eine Metastudie: Analyse und Empfehlungen, secondnd ed., Springer Berlin Heidelberg, Berlin, Heidelberg, 2016.
- [8] M. Nast, Die Wärmewende gelingt (nur) mit Wärmenetzen, in: 1. Stadtwerke-Forum Nahwärme Schleswig-Holstein, Neumünster, 26.04.2016, 2016.
- [9] J. López-Villada, J.C. Bruno, A. Coronas, Storage Concepts for Solar District Heating and Cooling Systems, in: Vajen (Hg.) – Proceedings of the ISES Solar, 2011, pp. 1–11.
- [10] S. Boesten, W. Ivens, S.C. Dekker, H. Eijndems, 5th generation district heating and cooling systems as a solution for renewable urban thermal energy supply, *Adv. Geosci.* 49 (2019) 129–136. <https://doi.org/10.5194/adgeo-49-129-2019>.
- [11] European Commission, Commission recommendation of 14 March 2023 on Energy Storage: Underpinning a decarbonised and secure EU energy system, *Official Journal of the European Union* C103 (2023).
- [12] Precedence Research, Thermal Energy Storage Market (By Technology: Latent, Thermochemical, Sensible; By Storage Material: Molten salts, Water, Phase change materials, Others; By Application: Process Heating and Cooling, Power Generation, District Heating and Cooling; By End User: Utilities, Residential & Commercial, Industrial): Global Industry Analysis, Size, Share, Growth, Trends, Regional Outlook, and Forecast 2023-2032, Ottawa, Canada, 2023.
- [13] T. Yang, W. Liu, G.J. Kramer, Q. Sun, Seasonal thermal energy storage: A techno-economic literature review, *Renewable and Sustainable Energy Reviews* 139 (2021) 110732. <https://doi.org/10.1016/j.rser.2021.110732>.
- [14] M. Janiszewski, Techno-economic aspects of seasonal underground storage of solar thermal energy in hard crystalline rocks. Thesis for: Doctor of Science in Technology, Aalto, Finland, 2019.
- [15] A.V. Novo, J.R. Bayon, D. Castro-Fresno, J. Rodriguez-Hernandez, Review of seasonal heat storage in large basins: Water tanks and gravel-water pits, *Applied Energy* 87 (2010) 390–397. <https://doi.org/10.1016/j.apenergy.2009.06.033>.
- [16] D. Mangold, T. Schmidt, Saisonale Wärmespeicher - neue Pilotanlagen im Programm Solarthermie2000plus und Forschungsperspektiven, in: Statusseminar Thermische Energiespeicher, Freiburg, 2.-3.11.2006, 2006.
- [17] D. Bauer, W. Heidemann, R. Marx, J. Nußbicker-Lux, F. Ochs, V. Panthalookaran, S. Raab, Solar unterstützte Nahwärme und Langzeit-Wärmespeicher. Forschungsbericht zum BMU-Vorhaben FKZ 0329607 J, Stuttgart, 2009.
- [18] M. Pfeil, H. Koch, Kies/Wasser-Wärmespeicher: Langzeitwärmespeicherung ökologisch und kostengünstig, in: OTTI, 14. Symposium Thermische Solarenergie, Kloster Banz, Bad Staffelstein, 12.-14.05.2004, 2004.

- [19] A. Heller, Advances in Large-Scale Solar Heating and Long Term Storage in Denmark, Proceedings for EuroSun'2000 (2000).
- [20] J.-O. Dalenbäck, European large-scale solar heating network, Department of Building Services Engineering, Chalmers University of Technology, Göteborg, 2002.
- [21] H. Mahon, D. O'Connor, D. Friedrich, B. Hughes, A review of thermal energy storage technologies for seasonal loops, *Energy* 239 (2022) 122207. <https://doi.org/10.1016/j.energy.2021.122207>.
- [22] A. Heller, 15 Years of R&D in central solar heating in Denmark, *Solar Energy* 69 (2000) 437–447. [https://doi.org/10.1016/S0038-092X\(00\)00118-3](https://doi.org/10.1016/S0038-092X(00)00118-3).
- [23] Y. Fan, L. Luo, Energy Storage by Sensible Heat for Buildings, in: R. Wang, X. Zhai (Eds.), *Handbook of Energy Systems in Green Buildings*, Springer Berlin Heidelberg, Berlin, Heidelberg, 2018, pp. 953–993.
- [24] R. Marx, J. Nußbicker-Lux, D. Bauer, W. Heidemann, H. Drück, Saisonale Wärmespeicher - Bauarten, Betriebsweise und Anwendungen, *Chemie Ingenieur Technik* 83 (2011) 1994–2001. <https://doi.org/10.1002/cite.201100064>.
- [25] A.J. Kallesøe, T. Vangkilde-Pedersen, Underground Thermal Energy Storage (UTES) – state-of-the-art, example cases and lessons learned.: HEATSTORE project report, 2019.
- [26] D. Mangold, L. Deschaintre, Seasonal thermal energy storage: Report on state of the art and necessary further R+D. Task 45 Large Systems, 2015.
- [27] P. Bayer, M. de Paly, M. Beck, Strategic optimization of borehole heat exchanger field for seasonal geothermal heating and cooling, *Applied Energy* 136 (2014) 445–453.
- [28] F. Stauffer, P. Bayer, P. Blum, N.M. Giraldo, W. Kinzelbach, Thermal use of shallow groundwater, Online-Ausg, CRC Press, Boca Raton, Florida, 2014.
- [29] A. Dahash, F. Ochs, G. Giuliani, A. Tosatto, Understanding the interaction between groundwater and large-scale underground hot-water tanks and pits, *Sustainable Cities and Society* 71 (2021) 102928. <https://doi.org/10.1016/j.scs.2021.102928>.
- [30] S. Hähnlein, P. Bayer, P. Blum, International legal status of the use of shallow geothermal energy, *Renewable and Sustainable Energy Reviews* 14 (2010) 2611–2625. <https://doi.org/10.1016/j.rser.2010.07.069>.
- [31] S. Hähnlein, N. Molina-Giraldo, P. Blum, P. Bayer, P. Grathwohl, Ausbreitung von Kältefahnen im Grundwasser bei Erdwärmesonden, *Grundwasser* 15 (2010) 123–133. <https://doi.org/10.1007/s00767-009-0125-x>.
- [32] T. Schmidt, Große saisonale Wärmespeicher, Biel-Bienne, 2012.
- [33] D. Mangold, O. Miedaener, E. Primoudi Tziggili, T. Schmidt, M. Unterberger, B. Zeh, Technisch-wirtschaftliche Analyse und Weiterentwicklung der solaren Langzeit-Wärmespeicherung - Forschungsbericht zum BMU-Vorhaben 0329607N: Wissenschaftlich-Technische Programmbegleitung für Solarthermie2000plus. Laufzeit Dezember 2007 bis Februar 2011, 2012.
- [34] M. Faigl, K. Göttl, IN-Campus - Innovative Technologien, *Smarte Energie: Stand: April 2019*, 2019.
- [35] Planungsgruppe M+M AG, IN-Campus - Fortschreibung innovatives Energiekonzept: Ergebnisse Stand Entwurf (PGMM Stand Entwurf 26.03.2018), not published, 2018.
- [36] C. Stettner, G. Ziegenhorn, Untersuchungsbericht zur Zustandsbewertung der Behälter auf dem ehemaligen Bayernoilgelände in Ingolstadt: Projektnummer 154094CS, München, 2016.
- [37] M. Benner, M. Bodmann, D. Mangold, J. Nußbicker, S. Raab, T. Schmidt, H. Seiwald, Solar unterstützte Nahwärmeversorgung mit und ohne Langzeit-Wärmespeicher: Forschungsbericht zum BMBF/BMWA-Vorhaben 329606 (November 1998 bis Januar 2003), Stuttgart, 2003.
- [38] F. Ochs, A. Dahash, A. Tosatto, M. Reisenbichler, K. O'Donovan, G. Gauthier, C.K. Skov, T. Schmidt, Comprehensive Comparison of Different Models for Large-Scale Thermal Energy Storage, in: *Proceedings of the International Renewable Energy Storage Conference 2021 (IRES 2021)*, Global Online Event, Germany, Atlantis PressParis, France, 2022, pp. 36–51.
- [39] D. Mangold, M. Benner, T. Schmidt, E. Hahne, H. Müller-Steinhagen, Solarthermie-2000 TP3: Solar unterstützte Nahwärme: Ergebnisse der wissenschaftlichen Begleitforschung, Neckarsulm, 29. und 2001.

- [40] S. Koohi-Fayegh, M.A. Rosen, A review of energy storage types, applications and recent developments, *Journal of Energy Storage* 27 (2020) 101047. <https://doi.org/10.1016/j.est.2019.101047>.
- [41] F. Setterwall, K. Alexanderson, *Phase Change Materials and Chemical Reactions for Thermal Energy Storage: State of the Art 1996*, Tokyo, Japan, 1996.
- [42] P.K. Åberg, *Construction of a Heat Storage: Photos with courtesy of Dronninglund Fjernvarme amba Denmark, Johan Freylund. Short History, Economy*, Vilnius, 2015.
- [43] M. Benner, *Solar unterstützte Nahwärmeversorgung mit und ohne Langzeit-Wärmespeicher: Forschungsbericht zum BMBF-Vorhaben ; (September 1994 bis Oktober 1998)*, [Electronic ed.], Universitätsbibliothek u. Technische Informationsbibliothek, Hannover, Stuttgart, 1999.
- [44] L. Royon, G. Guiffant, Heat transfer in paraffin oil/water emulsion involving supercooling phenomenon, *Energy Conversion and Management* 42 (2001) 2155–2161.
- [45] M. Akgün, O. Aydın, K. Kaygusuz, Experimental study on melting/solidification characteristics of a paraffin as PCM, *Energy Conversion and Management* 48 (2007) 669–678. <https://doi.org/10.1016/j.enconman.2006.05.014>.
- [46] D.M. Kammen, D.A. Sunter, City-integrated renewable energy for urban sustainability, *Science* 352 (2016) 922–928. <https://doi.org/10.1126/science.aad9302>.
- [47] H. Lund, S. Werner, R. Wiltshire, S. Svendsen, J.E. Thorsen, F. Hvelplund, B.V. Mathiesen, 4th Generation District Heating (4GDH): Integrating smart thermal grids into future sustainable energy systems, *Energy* 68 (2014) 1–11. <https://doi.org/10.1016/j.energy.2014.02.089>.
- [48] International Energy Agency, *Tracking Clean Energy Progress: Buildings*, 2018. <http://www.iea.org/tcep/buildings> (accessed 9 January 2019).
- [49] J. Xu, R.Z. Wang, Y. Li, A review of available technologies for seasonal thermal energy storage, *Solar Energy* 103 (2014) 610–638. <https://doi.org/10.1016/j.solener.2013.06.006>.
- [50] G.K. Pavlov, B.W. Olesen, Seasonal Ground Solar Thermal Energy Storage - Review of Systems and Applications, in: *Proceedings*, P-1.2-07.
- [51] D. Mangold, S. Raab, H. Müller-Steinhagen, Saisonale Wärmespeicherung in solaren Großanlagen - Status und Perspektiven, in: *DGS-Tagung Solares Heizen, Intersolar, Freiburg, 27.06.2003, 2003*, pp. 1–9.
- [52] P. Arce, M. Medrano, A. Gil, E. Oró, L.F. Cabeza, Overview of thermal energy storage (TES) potential energy savings and climate change mitigation in Spain and Europe, *Applied Energy* 88 (2011) 2764–2774. <https://doi.org/10.1016/j.apenergy.2011.01.067>.
- [53] U. Schirmer, T. Urbanek, P. Dionat, Solares Heizen mit Großanlagen: Chancen und Perspektiven, in: *Bautechnik-Forum Chemnitz 2004, VDI, Ingenieurkammer Sachsen, iproplan, VUBIC, TU Chemnitz, 2004*, pp. 80–104.
- [54] A. Thess, F. Trieb, A. Wörner, S. Zunft, Herausforderung Wärmespeicher, *Physik Journal* 14 (2015) 33–39.
- [55] L.G. Socaciu, Seasonal Sensible Thermal Energy Storage Solutions, *Leonardo Electronic Journal of Practices and Technologies* (2011) 49–68.
- [56] İ. Dinçer, M. Rosen, *Thermal energy storage: Systems and applications*, secondnd ed., Wiley, Hoboken N.J., 2011.
- [57] S. Kalaiselvam, *Thermal energy storage technologies for sustainability: Systems design, assessment, and applications*, firstst ed., Academic Press, London, U.K, 2014.
- [58] A. Hesarakı, S. Holmberg, F. Haghghat, Seasonal thermal energy storage with heat pumps and low temperatures in building projects—A comparative review, *Renewable and Sustainable Energy Reviews* 43 (2015) 1199–1213. <https://doi.org/10.1016/j.rser.2014.12.002>.
- [59] M. Bodmann, M.N. Fisch, *Solarthermische Langzeit-Wärmespeicherung*, in: *Eurosolar 2003, Wuppertal, 2003*.
- [60] P. Fleuchaus, B. Godschalk, I. Stober, P. Blum, Worldwide application of aquifer thermal energy storage – A review, *Renewable and Sustainable Energy Reviews* 94 (2018) 861–876. <https://doi.org/10.1016/j.rser.2018.06.057>.

- [61] V. Lottner, M. Schulz, E. Hahne, Solar-Assisted District Heating Plants: Status of the German Programme Solarthermie-2000, *Solar Energy* 69 (2000) 449–459. [https://doi.org/10.1016/S0038-092X\(00\)00125-0](https://doi.org/10.1016/S0038-092X(00)00125-0).
- [62] D. Mangold, Seasonal Storage - a German success story, *Sun & Wind Energy* (2007) 48–58.
- [63] F. Ochs, W. Heidemann, H. Müller-Steinhagen, H. Koch, Erdreich/Wasser-Erdbecken-Wärmespeicher mit direktem Beladesystem, in: OTTI, 16. Symposium thermische Solarenergie, Kloster Banz, Bad Staffelstein, 17.-19.05.2006, 2006.
- [64] P.H. Margen, Thermal energy storage in rock chambers - a complement to nuclear power, *Nuclear Engineering*, June 1959 (1959) 259–262.
- [65] G. Brun, La régularisation de l'énergie solaire par stockage thermique dans le sol, *Revue Générale de Thermique* (1965).
- [66] L.G. Socaciu, Seasonal thermal energy storage concepts, *Applied Mathematics and Mechanics* 55 (2012) 775–784.
- [67] S. Colclouth, Seasonal Thermal Energy Storage, in: Seminar on seasonal thermal energy storage (STES) for District Heating and Smart Cities, San Sebastian, 11.06.2015, 2015.
- [68] G.K. Pavlov, B.W. Olesen, Thermal energy storage - A review of concepts and systems for heating and cooling applications in buildings: Part 1-Seasonal storage in the ground, *HVAC&R Research* 18 (2012) 515–538. <https://doi.org/10.1080/10789669.2012.667039>.
- [69] J.-O. Dalenbäck (Ed.), Central solar heating plants with seasonal storage: Status report, Swedish Council for Building Research, Stockholm, 1990.
- [70] E. Hahne, The ITW solar heating system: an oldtimer fully in action, *Solar Energy* 69 (2000) 469–493. [https://doi.org/10.1016/S0038-092X\(00\)00115-8](https://doi.org/10.1016/S0038-092X(00)00115-8).
- [71] M. Chung, J.-U. Park, H.-K. Yoon, Simulation of a central solar heating system with seasonal storage in Korea, *Solar Energy* 64 (1998) 163–178. [https://doi.org/10.1016/S0038-092X\(98\)00101-7](https://doi.org/10.1016/S0038-092X(98)00101-7).
- [72] B. Akhmetov, A.G. Georgiev, A. Katayev, A.A. Dzhomartov, R. Popov, M.S. Tungatarova, Thermal energy storage systems - review, *Bulgarian Chemical Communications* 48 (2016) 31–40.
- [73] F. Ochs, W. Heidemann, H. Müller-Steinhagen, Langzeit-Wärmespeicher für solare unterstützte Nahwärmesysteme, in: IRES II, Bonn, 2007, 2007.
- [74] P. Chuard, J.-C. Hadorn, Heat storage systems: concepts, engineering data and compilation of projects, Office central fédéral, Berne, Switzerland, 1983.
- [75] A. Boysen, Preliminary designs for ten countries, Swedish Council for Building Research, Stockholm, Sweden, 1984.
- [76] J.-C. Hadorn, P. Chuard, Cost data and cost equations for heat storage concepts, Office central fédéral, Berne, Switzerland, 1983.
- [77] D. Mangold, F.A. Peuser, 10 Jahre Solarthermie-2000, in: OTTI, 13. Symposium Thermische Solarenergie, Kloster Banz, Bad Staffelstein, 14.-16.05.2003, 2003.
- [78] D. Mangold, T. Schmidt, H. Müller-Steinhagen, Saisonale Wärmespeicher in solar unterstützten Nahwärmenetzen: Erfahrungen aus dem Programm Solarthermie-2000, in: VDI-Fachtagung Energiespeicher, Würzburg, 5.-6.11.2002, 2002.
- [79] D. Mangold, T. Schmidt, Die neuen Pilotprojekte mit Langzeit-Wärmespeicher, in: OTTI, 16. Symposium thermische Solarenergie, Kloster Banz, Bad Staffelstein, 17.-19.05.2006, 2006.
- [80] D. Mangold, Gespeicherte Sonnenenergie: Solar unterstützte Nahwärmesiedlungen, Markt - Solares Bauen (2004) 82–85.
- [81] OECD, IEA (Eds.), *Energy Policies of IEA Countries*, OECD Publishing, Paris, 2012.
- [82] R. Kübler, N. Fisch, E. Hahne, High temperature water pit storage projects for the seasonal storage of solar energy, *Solar Energy* 61 (1997) 97–105. [https://doi.org/10.1016/S0038-092X\(97\)00040-6](https://doi.org/10.1016/S0038-092X(97)00040-6).
- [83] K.L. Lasse, Summary of technical description of the SUNSTORE 4 plant in Marstal, 2013. <https://www.solarmarstal.dk/media/6600/summary-technical-description-marstal.pdf> (accessed 9 January 2019).
- [84] A. Dyrelund, 4th generation district energy: The back bone of liveable and resilient campuses and cities, in: *Energy Planning for Resilient Military Installations*, EBC Annex 73 Symposium, Washington D.C., 6.12.2017, 2017.



- [85] ARCON SUNMARK, Large-Scale showcase projects, 2015. [http://arcon-sunmark.com/uploads/ARCON\\_References.pdf](http://arcon-sunmark.com/uploads/ARCON_References.pdf) (accessed 9 January 2019).
- [86] K. Ellehauge, T.E. Pedersen, Solar heat storages in district heating networks: Energinet.dk Project no. 2006-2-6750, 2007.
- [87] M. Guadalfajara, M.A. Lozano, L.M. Serra, Analysis of Large Thermal Energy Storage for Solar District Heating, in: Eurotherm Seminar #99 - Advances in Thermal Energy Storage, 2014.
- [88] SOLARGE, Aeroeskoebing Solar Heating: Project Summary. Aeroeskoebing, Denmark, 2018. [http://www.solarge.org/uploads/media/SOLARGE\\_goodpractice\\_dk\\_aeroeskoebing.pdf](http://www.solarge.org/uploads/media/SOLARGE_goodpractice_dk_aeroeskoebing.pdf) (accessed 9 January 2019).
- [89] SOLARGE, NRGi Samsø: Project Summary. Samsø, Denmark, 2018. <http://www.solarge.org/index.php?id=1645> (accessed 9 January 2019).
- [90] J. Gimmelsberger, Efficient Energy Supply (Electricity and District Heat) for the City of Linz, in: Energy Efficiency in IPPC-Installations, Parallel session: Producing more with less, 2004.
- [91] C. Muser, Machbarkeits-Vorstudie eines saisonalen Groß-Wärmespeichers für Linz: Abschlussbericht der Sondierung, Vienna, 2015.
- [92] N-ERGIE AG, Wahrzeichen der Energiewende: Der Wärmespeicher der N-ERGIE, Nürnberg, 2015.
- [93] F. Ulbjerg, Heat storage pits: Cheap and efficient energy with heat storage pits. Ramboll Group, Copenhagen, 2017.
- [94] B. Stutz, N. Le Pierres, F. Kuznik, K. Johannes, E. Palomo Del Barrio, J.-P. Bédécarrats, S. Gibout, P. Marty, L. Zalewski, J. Soto, N. Mazet, R. Olives, J.-J. Beziau, D.-P. Minh, Storage of thermal solar energy, *Comptes Rendus Physique* 18 (2017) 401–414. <https://doi.org/10.1016/j.crhy.2017.09.008>.
- [95] D. Bauer, R. Marx, J. Nußbicker-Lux, F. Ochs, W. Heidemann, H. Müller-Steinhagen, German central solar heating plants with seasonal heat storage, *Solar Energy* 84 (2010) 612–623. <https://doi.org/10.1016/j.solener.2009.05.013>.
- [96] N. Fisch, R. Kübler, Solar assisted district heating: Status of the projects in Germany, *International Journal of Solar Energy* 18 (1997) 259–270. <https://doi.org/10.1080/01425919708914322>.
- [97] R. Marx, D. Bauer, H. Drück, Next Generation of Seasonal Gravel-Water Thermal Energy Store - Design and Operating Results from Eggenstein-Leopoldshafen, Germany., in: Innostock 2012 – The 12th International Conference on Energy Storage, Lleida, Spain, 15.-18.05.2012, 2012.
- [98] M. Riegger, D. Mangold, Planungsoptimierung und Bau des solaren Nahwärmesystems mit saisonalem Kies-Wasser-Wärmespeicher in Eggenstein-Leopoldshafen, in: 18. Symposium Thermische Solarenergie, Kloster Banz, Bad Staffelstein, 23.-25.05.2008, 2008.
- [99] D. Bauer, Solare Nahwärme und saisonale Wärmespeicherung, in: Clean Energy & Passivehouse 2012, Große solarthermische Anlagen für Mehrfamilienhäuser und Kommunen, Stuttgart, Germany, 29.-31.03.2012, 2012.
- [100] F. Ochs, W. Heidemann, H. Müller-Steinhagen, Saisonale Wärmespeicherung: Eine Herausforderung für Polymere, in: 2. Leobener Symposium Polymeric Solar Materials, 2008.
- [101] F. Ochs, H. Müller-Steinhagen, Abschlussbericht zum Vorhaben Weiterentwicklung der Erdbecken-Wärmespeichertechnologie. FKZ 0329607 E, Stuttgart, 2008.
- [102] A. Lasiera, Energy analysis and simulation of thermal solar plants with seasonal storage. Student thesis, Master degree, Gävle, 2014.
- [103] H. Zinko, T. Hahn, The high temperatures (95°C) water pit storage of Malung, in: Proc Calorstock 1994, 6th International Conference on Thermal Energy Storage, 1994.
- [104] SOLARGE, Tubberupvaenge: Project Summary. Herlev, Denmark, 2018 (accessed 9 January 2019).
- [105] F. Ochs, W. Heidemann, H. Müller-Steinhagen, Seasonal Thermal Energy Storage: A challenging application for geosynthetics, *Eurogeo4* 4 (2008).

- [106] R. Wang, X. Zhai (Eds.), Handbook of Energy Systems in Green Buildings, Springer Berlin Heidelberg, Berlin, Heidelberg, 2018.
- [107] F. Ochs, A. Lichtenfels, H. Koch, W. Heidemann, H. Müller-Steinhagen, Heißwasser-Erdbecken-Wärmespeicher mit freitragender Abdeckung für solare Nahwärmesysteme, in: OTTI, 17. Symposium Thermische Solarenergie, Kloster Banz, Bad Staffelstein, 09.-11.05.2007, 2007.
- [108] A. Heller, Investigation on floating lid construction pit water storage Otterupgaard, Denmark: Pit Water Storage, Ottrupgaard, Denmark. Report R-010, Lyngby, Copenhagen, Denmark, 1997.
- [109] M.V. Jensen, Seasonal pit heat storages - Guidelines for materials & construction: IEA-SHC TECH SHEET 45.B.3.2, in: IEA Solar Heating and Cooling Programme, Task 45 Large Systems, fact sheets, 2014.
- [110] M. Meliß, F. Späte, The solar heating system with seasonal storage at the Solar-Campus Jülich, Solar Energy 69 (2000) 525–533.
- [111] PlanEnergie, Long Term Storage and Solar District Heating: A presentation of the Danish pit and borehole thermal energy storages in Brædstrup, Marstal, Dronninglund and Gram, 2016.
- [112] Marstal Fjernvarme, Innovative, multi-applicable and cost efficient hybrid solar (55 %) and biomass energy (45 %) large scale (district) heating system with long term heat storage – and Organic Rankine Cycle electricity production.: Project final report. 2nd draft, 2014.
- [113] P.A. Sørensen, T. Schmidt, Design and Construction of Large Scale Heat Storages for District Heating in Denmark, 14th International Conference on Energy Storage 25-28 April 2018 (2018).
- [114] R. Radloff, S. Löck, Dronninglund Fjernvarme: Seit 2014 solarthermische Deckungsrate von 41%, Wärmewende-Info (2015).
- [115] R. Radloff, Große Solarthermie in Wärmenetzen: Beispiel Dänemark - In Deutschland Alternative zu Biogas, Wärmewende-Info (2014).
- [116] M. Galindo Fernández, C. Roger-Lacan, U. Gähns, V. Aumaitre, Efficient district heating and cooling systems in the EU: Case studies analysis, replicable key success factors and potential policy implications. EUR 28418 EN, Publications Office of the European Union, Luxembourg, 2016.
- [117] R. Radloff, Weltgrößte Solarthermieanlage in Vojens, Wärmewende-Info (2015).
- [118] R. Radloff, Entwicklung der großen Solarthermie in Dänemark, Wärmewende-Info (2015).
- [119] R. Radloff, S. Löck, Løgumkloster Fjernvarme: 45% solarer Deckungsgrad - "Hick-Hack" um Solarwärmeprojekt, Wärmewende-Info (2015).
- [120] F. Ochs, W. Heidemann, H. Müller-Steinhagen, Geosynthetic clay liner for seasonal thermal energy stores, in: 4th European Geosynthetics Conference, Eurogeo4, Edinburgh, 2008.
- [121] F. Ochs, Stand der Technik erdvergrabener Wärmespeicher: FFG store4grid, 2013.
- [122] A. Heller, S. Svendsen, S. Furbo, Large scale solar district heating: Evaluation, Modelling and Designing, Dept. of Buildings and Energy, Technical University of Denmark, Lyngby, 2001.
- [123] T. Schmidt, M. Benner, W. Heidemann, H. Müller-Steinhagen, Saisonale Wärmespeicher: aktuelle Speichertechnologien und Entwicklungen bei Heißwasser-Wärmespeichern, in: OTTI, Fachseminar Oberflächennahe Geothermie, 18.-19.02.2003, 2003.
- [124] T. Schmidt, D. Mangold, H. Müller-Steinhagen, Seasonal thermal energy storage in Germany, in: ISES Solar World Congress 2003, Göteborg, 14.-19.06.2003, 2003.
- [125] M. Sterner, I. Stadler, Energiespeicher - Bedarf, Technologien, Integration, Springer Vieweg, Berlin, 2014.
- [126] G. Oliveti, N. Arcuri, Prototype Experimental Plant for the Interseasonal Storage of Solar Energy for the Winter Heating of Buildings: Description of Plant and its Functions, Solar Energy 54 (1995) 85–97.

- [127] G. Oliveti, N. Arcuri, S. Ruffolo, First experimental results from a prototype plant for the interseasonal storage of solar energy for the winter heating of buildings, *Solar Energy* 62 (1998) 281–290. [https://doi.org/10.1016/S0038-092X\(98\)00011-5](https://doi.org/10.1016/S0038-092X(98)00011-5).
- [128] M. Bodmann, D. Mangold, J. Nußbicker-Lux, S. Raab, A. Schenke, T. Schmidt, Solar unterstützte Nahwärme und Langzeit-Wärmespeicher: Forschungsbericht zum BMWA / BMU-Vorhaben. Februar 2003 bis Mai 2005, 2005.
- [129] D. Mangold, T. Schmidt, The next Generations of Seasonal Thermal Energy Storage in Germany, in: ESTEC 2007, München, 15.-16.10.2007, 2007.
- [130] S. Göppert, R. Lohse, T. Urbanek, U. Schirmer, B. Platzer, Forschungsbericht - Solarthermie 2000plus - Weiterentwicklung und Optimierung von Be- und Entladesystemen für Tank- und Erdbeckenspeicher: 2004 - 2008. FKZ 0329271A, Technische Informationsbibliothek u. Universitätsbibliothek, Hannover, Chemnitz, 2009.
- [131] J.-C. Hadorn, Storage solutions for solar thermal energy, in: Freiburg Solar Academy, Freiburg, 2004, 2004.
- [132] T. Schmidt, D. Mangold, Status der solaren Nahwärme in Deutschland, in: Status-Tagung Solare Kombianlagen für Mehrfamilienhäuser im europäischen Vergleich, Graz, 14.11.03, 2003.
- [133] B. Milow, G. Stadermann (Eds.), Workshop Wärmespeicherung: FVS Workshop 2001, Köln, 2001.
- [134] D. Mangold, T. Schmidt, H. Müller-Steinhagen, Solaranlagen und Nahwärmenetze: Erfahrungen aus dem Programm Solarthermie-2000, in: AGFW-Seminar "Fernwärme und Solarenergienutzung", München, 10.-11.09.2002, 2002.
- [135] M. Bodmann, M.N. Fisch, Solar unterstützte Nahwärmeversorgung: Pilotprojekte Hamburg, Hannover und Steinfurt, in: 5. FKS-Symposium: FKS-Forschungskreis Solarenergie, TU Braunschweig, Braunschweig, 2004.
- [136] M.N. Fisch, M. Bodmann, Solarcities Friedrichshafen, Neckarsulm und Hannover mit Langzeit-Wärmespeicher, Gleisdorf Solar (2000).
- [137] SOLARGE, Rise Fjernvarme: Project summary. Rise, Aeroe, Denmark, 2018 (accessed 9 January 2019).
- [138] S.Ø. Jensen, F. Ulbjerg, Store solvarmeanlæg med høje dækningsgrader, SolEnergiCentret Teknologisk Institut, Taastrup, Denmark, 2005.
- [139] D. Mangold, T. Schmidt, The New Central Solar Heating Plants with Seasonal Storage in Germany, in: EuroSun 2006, Glasgow, 27.-30.6.2006, 2006.
- [140] M. Reuß, Solar District Heating - an Innovative Approach of an Established Technology, in: Solar District Heating, 24.08.2016, Mikkeli, 2016.
- [141] IEA-ECES, Applications of Thermal Energy Storage in the Energy Transition: Benchmarks and Developments. Public Report of IEA ECES Annex 2018, IEA Technology Collaboration Programme on Energy Conservation through Energy Storage (IEA-ECES), 2018.
- [142] M. Demharter, T. Beikircher, Neue Entwicklungen im Bereich kleiner und mittlerer Speicher mit Superisolation.
- [143] F. Ochs, W. Heidemann, H. Müller-Steinhagen, H. Koch, Soil-Water Pit Heat Store With Direct Charging System, in: Ecostock 2006, Richard Stockton College of New Jersey, 2006, 2006.
- [144] F. Ochs, W. Heidemann, H. Müller-Steinhagen, Weiterentwicklung der Erdbecken-Wärmespeichertechnologie, PtJ Statusseminar Thermische Energiespeicher (2006).
- [145] M. Lanahan, P.C. Tabares-Velasco, Seasonal Thermal-Energy Storage: A Critical Review on BTES Systems, Modeling, and System Design for Higher System Efficiency, *Energies* 10 (2017) 743. <https://doi.org/10.3390/en10060743>.
- [146] M. Bodmann, H. Koch, M.N. Fisch, Solare Nahwärmeversorgung mit Kies/Wasserspeicher in Steinfurt-Borghorst, in: OPET-Seminar Solarunterstützte Nahwärmeversorgung, Neckarsulm, 29.-30.03.2001, 2001.
- [147] D. Mangold, Erfahrungen und Ergebnisse aus der Umsetzung der Bundesforschungsprogramme Solarthermie-2000 und Solarthermie2000plus: Input zum EU-Vorhaben Solarge (Solarthermische Großanlagen), Target GmbH, Hannover, 2006.

- [148] T. Urbaneck, B. Platzer, U. Schirmer, Berechnung von Kies-Wasser-Speichern, in: OTTI, 12. Symposium Thermische Solarenergie, Regensburg, 24.-26.04.2002, 2002.
- [149] F. Pacheco Torgal, M. Mistretta, A. Kaklauskas, C.G. Granqvist, L.F. Cabeza, Nearly Zero Energy Building Refurbishment: A Multidisciplinary Approach, Springer London, London, 2013.
- [150] U. Schirmer, T. Urbaneck, Saisonaler Kies-Wasser-Speicher: Solarthermische Großanlage mit Langzeit-Wärmespeicher im Chemnitzer Gewerbepark SOLARIS, *Sonnenenergie* 98 (1998) 41–43.
- [151] T. Urbaneck, B. Platzer, U. Schirmer, Advanced Monitoring of gravel water storage, in: Futurestock 2003, Warsaw, 2003.
- [152] T. Schmidt, D. Mangold, New steps in seasonal thermal energy storage in Germany, in: Ecostock 2006, Richard Stockton College of New Jersey, 2006, 2006.
- [153] R. Marx, J. Nußbicker-Lux, D. Bauer, W. Heidemann, Integration von Wärmepumpen in solar unterstützte Nahwärmesysteme mit saisonaler Wärmespeicherung, in: OTTI, 21. Symposium thermische Solarenergie, Kloster Banz, Bad Staffelstein, 11.-13.05.2011, 2011.
- [154] J. Nußbicker-Lux, R. Marx, D. Bauer, H. Drück, Lektionen aus Planung und Betrieb von drei Deutschen solaren Nahwärmeversorgungen mit saisonaler Wärmespeicherung, in: Gleisdorf Solar 2012, 10. Internationale Konferenz für thermische Solarenergienutzung, Gleisdorf, 12.-14.09.2012, 2012.
- [155] T. Schmidt, D. Mangold, Neue Anwendungen und Technologien saisonaler Wärmespeicher, in: OTTI, 19. Symposium Thermische Solarenergie, Kloster Banz, Bad Staffelstein, 06.-08.05.2009, 2009.
- [156] SOLARGE, Braedstrup Fjernvarme: Project Summary. Braedstrup, Denmark, 2018 (accessed 9 January 2019).
- [157] Brædstrup Fjernvarme A.M.B.A., Solare Nah- und Fernwärme: Fallbeispiel Brædstrup District Heating. Typ: Solare Fernwärmesysteme mit gekoppelter Strom- und Wärmezeugung "Smart District Heating" (2015).
- [158] A. Ucar, M. Inalli, A thermo-economical optimization of a domestic solar heating plant with seasonal storage, *Applied Thermal Engineering* 27 (2007) 450–456. <https://doi.org/10.1016/j.applthermaleng.2006.06.010>.
- [159] T. Schmidt, H. Müller-Steinhagen, Nutzung des Untergrundes zur Kälteversorgung von Gebäuden: Ergebnisse aus dem EU-Projekt Soil-Cool, in: OTTI Profiforum Oberflächennahe Geothermie, Regenstauf, 14.-15.04.2005, 2005.
- [160] J.A. Duffie, W.A. Beckman, Solar engineering of thermal processes John A. Duffie, William A. Beckman, fourthth ed., John Wiley, Hoboken, 2013.
- [161] A. Gries, Solarsiedlung Steinfurt-Borghorst: 50 Solarsiedlungen in Nordrhein-Westfalen, Ministerium für Wirtschaft, Mittelstand und Energie des Landes Nordrhein-Westfalen, Düsseldorf, 2008.
- [162] L.T. Terziotti, M.L. Sweet, J.T. McLeskey, Modeling seasonal solar thermal energy storage in a large urban residential building using TRNSYS 16, *Energy and Buildings* 45 (2012) 28–31. <https://doi.org/10.1016/j.enbuild.2011.10.023>.
- [163] M.L. Sweet, J.T. McLeskey, Numerical simulation of underground Seasonal Solar Thermal Energy Storage (SSTES) for a single family dwelling using TRNSYS, *Solar Energy* 86 (2012) 289–300. <https://doi.org/10.1016/j.solener.2011.10.002>.
- [164] M.N. Fisch, Solare Großspeicherprojekte in Stadtteilen: Betriebsergebnisse und Erfahrungen, in: 5. Hessischer Energieberaterntag, Frankfurt am Main, 2008.
- [165] M. Schlosser, M. Heuer, M.N. Fisch, Langzeitmonitoring Solar unterstützte Nahwärmeversorgung Hamburg-Bramfeld, in: E.ON Hanse Wärme, 25.07.2007, 2007.
- [166] C. Forkel, H. Daniels, Finite element simulation of circulation in large scale thermal energy storage basins, *Advances in Water Resources* 18 (1995) 147–158. [https://doi.org/10.1016/0309-1708\(95\)00007-6](https://doi.org/10.1016/0309-1708(95)00007-6).
- [167] S.M. Hasnain, Review on sustainable thermal energy storage technologies, Part I: heat storage materials and techniques, *Energy Conversion and Management* 39 (1998) 1127–1138. [https://doi.org/10.1016/S0196-8904\(98\)00025-9](https://doi.org/10.1016/S0196-8904(98)00025-9).

- [168] M. Mazman, L.F. Cabeza, H. Mehling, M. Nogues, H. Evliya, H.Ö. Paksoy, Utilization of phase change materials in solar domestic hot water systems, *Renewable Energy* 34 (2009) 1639–1643. <https://doi.org/10.1016/j.renene.2008.10.016>.
- [169] H. Akbari, O. Sezgen, Case studies of thermal energy storage (TES) systems: Evaluation and verification of system performance: Final report. DE93-001572, LBL-30852, 1992.
- [170] A.J. Gorski, Third international workshop on ice storage for cooling applications: Technical Memo, ANL/CNSV-TM-177; CONF-8311308-Absts. (1986).
- [171] K. Skogsberg, B. Nordell, The Sundsvall hospital snow storage, *Cold Regions Science and Technology* 32 (2001) 63–70. [https://doi.org/10.1016/S0165-232X\(00\)00021-5](https://doi.org/10.1016/S0165-232X(00)00021-5).
- [172] T.B. Taylor, Ice Ponds, *AIP Conference Proceedings* (1985) 565–575.
- [173] C. Yan, W. Shi, X. Li, Y. Zhao, Optimal design and application of a compound cold storage system combining seasonal ice storage and chilled water storage, *Applied Energy* 171 (2016) 1–11. <https://doi.org/10.1016/j.apenergy.2016.03.005>.
- [174] M. Jooß, Dichtigkeit von Heißwasser-Langzeitspeichern aus Hochleistungsbeton: Von der Fakultät Bauingenieur- und Vermessungswesen der Universität Stuttgart zur Erlangung der Würde eines Doktor-Ingenieurs (Dr.-Ing.) genehmigte Abhandlung. Ph.D. Thesis, Stuttgart, 2001.
- [175] J. Bühl, Langzeitwärmespeicherung mit einem neuartigen Speicherkonzept für solar-gestützte Nahwärmesysteme, *FVS Workshop 2001* (2001) 4–13.
- [176] R. Yumrutaş, M. Ünsal, Analysis of solar aided heat pump systems with seasonal thermal energy storage in surface tanks, *Energy* 25 (2000) 1231–1243. [https://doi.org/10.1016/S0360-5442\(00\)00032-3](https://doi.org/10.1016/S0360-5442(00)00032-3).
- [177] A. Matthees, P. Stange, A. Hülser, K. Rühling, GREEN HEAT<sup>3</sup>: Entwicklung innovativer Energieversorgungstechniken und -strukturen mit Kernkomponenten modularer Großwärmespeicher und Maxianlage Solarthermie, in: *Symposium Solarthermie - Technik für die Energiewende, Kloster Banz, Bad Staffelstein, 13.-15.06.2018*, 2018, pp. 389–401.
- [178] A. Heller, Floating lid construction for pit water storage: A survey. Report R-011, Lyngby, Copenhagen, Denmark, 1997.
- [179] T. Schmidt, D. Mangold, The multi-functional heat storage in Hamburg-Bramfeld: innovative extension of the oldest German solar energy housing estate, in: *IRES, 5th International Renewable Energy Storage Conference and Exhibition, Berlin, 22.-24.11.2010*, 2010.
- [180] P.A. Sørensen, Monitoring results from the project and construction of 10,000 m<sup>3</sup> pit heat storage, in: *Sunstorage 2 workshop, Marstal, Aero, 09.2004*, 2004.
- [181] R. Lohse, J. Bühl, T. Urbanek, U. Schirmer, B. Platzer, A. Nilius, Planungsleitfaden zur geschichteten Be- und Entladung thermischer Speicher in solarthermischen Anlagen, Technische Informationsbibliothek u. Universitätsbibliothek/ Techn. Univ. Professur Techn. Thermodynamik/ Techn. Univ. Fachgebiet Thermo- und Magnetofluidynamik, Hannover, Chemnitz, Ilmenau, 2009.
- [182] K. Nielsen, Thermal Energy Storage. A State-of-the-Art report within the research program Smart Energy-Efficient Buildings at NTNU and SINTEF, NTNU, Trondheim, 2003.
- [183] T. Urbanek, B. Platzer, U. Schirmer, Direkte Be- und Entladung von Kies-Wasser-Speichern, in: *OTTI, 14. Symposium Thermische Solarenergie, Kloster Banz, Bad Staffelstein, 12.-14.05.2004*, 2004.
- [184] O. Abdelhak, H. Mhiri, P. Bournot, CFD analysis of thermal stratification in domestic hot water storage tank during dynamic mode, *Build. Simul.* 8 (2015) 421–429. <https://doi.org/10.1007/s12273-015-0216-9>.
- [185] R. Lohse, S. Göppert, C. Kunis, T. Urbanek, U. Schirmer, B. Platzer, Be- und Entladesysteme für thermische Schichtenspeicher: Teil 2 – Untersuchungen des Beladeverhaltens, *Chemie Ingenieur Technik* 80 (2008) 935–943. <https://doi.org/10.1002/cite.200800017>.
- [186] F. Findeisen, Radiale Diffusoren in Warmwasserspeichern: Einfluss des Beladesystems auf Strömungsverhalten und Schichtungsqualität. Ph.D. Thesis, Chemnitz, 2018.

- [187] F. Findeisen, T. Urbaneck, B. Platzer, Radiale Diffusoren - Untersuchung des dreidimensionalen Strömungsverhaltens mittels CFD (Teil 1), *Chemie Ingenieur Technik* 90 (2018) 956–968. <https://doi.org/10.1002/cite.201700023>.
- [188] J. Allegrini, K. Orehounig, G. Mavromatidis, F. Ruesch, V. Dorer, R. Evins, A review of modelling approaches and tools for the simulation of district-scale energy systems, *Renewable and Sustainable Energy Reviews* 52 (2015) 1391–1404. <https://doi.org/10.1016/j.rser.2015.07.123>.
- [189] L. Yang, E. Entchev, A. Rosato, S. Sibilio, Smart thermal grid with integration of distributed and centralized solar energy systems, *Energy* 122 (2017) 471–481. <https://doi.org/10.1016/j.energy.2017.01.114>.
- [190] T. Schmidt, D. Mangold, Solare Nahwärme mit Langzeit-Wärmespeicherung in Deutschland: Aktueller Stand und umgesetzte Projekte, *Solarthermie* (2008) 28–32.
- [191] M.N. Fisch, Integrale Energiekonzepte für den Wohnsiedlungsbau, in: Internationaler Kongress „Nachhaltiger Stadtumbau und erneuerbare Energien“, Dresden, 13.-14.03.2003, 2003.
- [192] S. Hsieh, A. Omu, K. Orehounig, Comparison of solar thermal systems with storage: From building to neighbourhood scale, *Energy and Buildings* 152 (2017) 359–372. <https://doi.org/10.1016/j.enbuild.2017.07.036>.
- [193] L. Zhang, P. Xu, J. Mao, X. Tang, Z. Li, J. Shi, A low cost seasonal solar soil heat storage system for greenhouse heating: Design and pilot study, *Applied Energy* 156 (2015) 213–222. <https://doi.org/10.1016/j.apenergy.2015.07.036>.
- [194] J. Xu, Y. Li, R.Z. Wang, W. Liu, Performance investigation of a solar heating system with underground seasonal energy storage for greenhouse application, *Energy* 67 (2014) 63–73. <https://doi.org/10.1016/j.energy.2014.01.049>.
- [195] H. Brielmann, T. Lueders, K. Schreglmann, F. Ferraro, M. Avramov, V. Hammerl, P. Blum, P. Bayer, C. Griebler, Oberflächennahe Geothermie und ihre potenziellen Auswirkungen auf Grundwasserökosysteme, *Grundwasser* 16 (2011) 77–91. <https://doi.org/10.1007/s00767-011-0166-9>.
- [196] C. Bott, I. Dressel, P. Bayer, State-of-technology review of water-based closed seasonal thermal energy storage systems, *Renewable and Sustainable Energy Reviews* 113 (2019) 109241. <https://doi.org/10.1016/j.rser.2019.06.048>.
- [197] S.K. Shah, L. Aye, B. Rismanchi, Seasonal thermal energy storage system for cold climate zones: A review of recent developments, *Renewable and Sustainable Energy Reviews* 97 (2018) 38–49. <https://doi.org/10.1016/j.rser.2018.08.025>.
- [198] I. Sarbu, C. Sebarchievici, A Comprehensive Review of Thermal Energy Storage, *Sustainability* 10 (2018) 191. <https://doi.org/10.3390/su10010191>.
- [199] M.H. Mahfuz, M.R. Anisur, M.A. Kibria, R. Saidur, I. Metselaar, Performance investigation of thermal energy storage system with Phase Change Material (PCM) for solar water heating application, *International Communications in Heat and Mass Transfer* 57 (2014) 132–139. <https://doi.org/10.1016/j.icheatmasstransfer.2014.07.022>.
- [200] D. Zhou, C.Y. Zhao, Y. Tian, Review on thermal energy storage with phase change materials (PCMs) in building applications, *Applied Energy* 92 (2012) 593–605. <https://doi.org/10.1016/j.apenergy.2011.08.025>.
- [201] Kabir, M. S., Yola, I. A., Beeswax as a low temperature phase change material for thermal storage, *FUDMA Journal of Sciences (FJS)* 4 (2020) 764–769.
- [202] A. Palacios, L. Cong, M.E. Navarro, Y. Ding, C. Barreneche, Thermal conductivity measurement techniques for characterizing thermal energy storage materials – A review, *Renewable and Sustainable Energy Reviews* 108 (2019) 32–52. <https://doi.org/10.1016/j.rser.2019.03.020>.
- [203] G. Airò Farulla, M. Cellura, F. Guarino, M. Ferraro, A Review of Thermochemical Energy Storage Systems for Power Grid Support, *Applied Sciences* 10 (2020) 3142. <https://doi.org/10.3390/app10093142>.
- [204] Yang, T., Liu, W., Kramer, G.J., Sun, Q., State of the Art Review of Seasonal Sensible Heat Storage, in: International Conference on Applied Energy 2019, Vasteras, Sweden, 2019, p. 349.
- [205] S. Bepalko, A.M. Miranda, Overview of the existing heat storage technologies: Sensible heat, *Acta Innovations* 28 (2018) 82–113.

- [206] F.M. Rad, A.S. Fung, Solar community heating and cooling system with borehole thermal energy storage – Review of systems, *Renewable and Sustainable Energy Reviews* 60 (2016) 1550–1561. <https://doi.org/10.1016/j.rser.2016.03.025>.
- [207] N. Hoekstra, M. Pellegrini, M. Bloemendal, G. Spaak, A. Andreu Gallego, J. Rodriguez Comins, T. Grotenhuis, S. Picone, A.J. Murrell, H.J. Steeman, A. Verrone, P. Doornenbal, M. Christophersen, L. Bennedsen, M. Henssen, S. Moinier, C. Saccani, Increasing market opportunities for renewable energy technologies with innovations in aquifer thermal energy storage, *Sci. Total Environ.* 709 (2020) 136142. <https://doi.org/10.1016/j.scitotenv.2019.136142>.
- [208] S. Schüppler, P. Fleuchaus, P. Blum, Techno-economic and environmental analysis of an Aquifer Thermal Energy Storage (ATES) in Germany, *Geotherm Energy* 7 (2019). <https://doi.org/10.1186/s40517-019-0127-6>.
- [209] W. Villasmil, L.J. Fischer, J. Worlitschek, A review and evaluation of thermal insulation materials and methods for thermal energy storage systems, *Renewable and Sustainable Energy Reviews* 103 (2019) 71–84. <https://doi.org/10.1016/j.rser.2018.12.040>.
- [210] Y. Bai, Z. Wang, J. Fan, M. Yang, X. Li, L. Chen, G. Yuan, J. Yang, Numerical and experimental study of an underground water pit for seasonal heat storage, *Renewable Energy* 150 (2020) 487–508. <https://doi.org/10.1016/j.renene.2019.12.080>.
- [211] M. Kenisarin, K. Mahkamov, Solar energy storage using phase change materials, *Renewable and Sustainable Energy Reviews* 11 (2007) 1913–1965. <https://doi.org/10.1016/j.rser.2006.05.005>.
- [212] A. Abhat, Low temperature latent heat thermal energy storage: Heat storage materials, *Solar Energy* 30 (1983) 313–332.
- [213] M.M. Farid, A.M. Khudhair, S.A.K. Razack, S. Al-Hallaj, A review on phase change energy storage: materials and applications, *Energy Conversion and Management* 45 (2004) 1597–1615. <https://doi.org/10.1016/j.enconman.2003.09.015>.
- [214] B. He, F. Setterwall, Technical grade paraffin waxes as phase change materials for cool thermal storage and cool storage systems capital cost estimation, *Energy Conversion and Management* 43 (2002) 1709–1723.
- [215] K. Cho, S.H. Choi, Thermal characteristics of paraffin in a spherical capsule during freezing and melting processes, *International Journal of Heat and Mass Transfer* 43 (2000) 3183–3196.
- [216] S.P. Jesumathy, M. Udayakumar, S. Suresh, Heat transfer characteristics in latent heat storage system using paraffin wax, *Journal of Mechanical Science and Technology* 26 (2012) 959–965. <https://doi.org/10.1007/s12206-011-1017-4>.
- [217] A. Trp, An experimental and numerical investigation of heat transfer during technical grade paraffin melting and solidification in a shell-and-tube latent thermal energy storage unit, *Solar Energy* 79 (2005) 648–660. <https://doi.org/10.1016/j.solener.2005.03.006>.
- [218] H. Ettouney, I. Alatiqi, M. Al-Sahali, K. Al-Hajirie, Heat transfer enhancement in energy storage in spherical capsules filled with paraffin wax and metal beads, *Energy Conversion and Management* 47 (2006) 211–228. <https://doi.org/10.1016/j.enconman.2005.04.003>.
- [219] A. Sari, A. Karaipekli, Thermal conductivity and latent heat thermal energy storage characteristics of paraffin/expanded graphite composite as phase change material, *Applied Thermal Engineering* 27 (2007) 1271–1277. <https://doi.org/10.1016/j.applthermaleng.2006.11.004>.
- [220] J. Zhao, Y. Guo, F. Feng, Q. Tong, W. Qv, H. Wang, Microstructure and thermal properties of a paraffin/expanded graphite phase-change composite for thermal storage, *Renewable Energy* 36 (2011) 1339–1342. <https://doi.org/10.1016/j.renene.2010.11.028>.
- [221] K. Faraj, M. Khaled, J. Faraj, F. Hachem, C. Castelain, Phase change material thermal energy storage systems for cooling applications in buildings: A review, *Renewable and Sustainable Energy Reviews* 119 (2020) 109579. <https://doi.org/10.1016/j.rser.2019.109579>.

- [222] N. Ahmed, K.E. Elfeky, L. Lu, Q.W. Wang, Thermal and economic evaluation of thermocline combined sensible-latent heat thermal energy storage system for medium temperature applications, *Energy Conversion and Management* 189 (2019) 14–23. <https://doi.org/10.1016/j.enconman.2019.03.040>.
- [223] Z. Zhang, N. Zhang, J. Peng, X. Fang, X. Gao, Y. Fang, Preparation and thermal energy storage properties of paraffin/expanded graphite composite phase change material, *Applied Energy* 91 (2012) 426–431. <https://doi.org/10.1016/j.apenergy.2011.10.014>.
- [224] Steinbach Schaumglas GmbH & Co. KG, Technical properties of the product as stated on the producer's website, also available in a prospectus., 2020.
- [225] J.B.J. Fourier, *The analytical theory of heat*, University Press, 1878.
- [226] IEA, *Market Report Series: Renewables 2019 - Analysis and Forecasts to 2024*, 2019.
- [227] P. Gabrielli, M. Gazzani, E. Martelli, M. Mazzotti, Optimal design of multi-energy systems with seasonal storage, *Applied Energy* 219 (2018) 408–424. <https://doi.org/10.1016/j.apenergy.2017.07.142>.
- [228] C.N. Antoniadis, G. Martinopoulos, Simulation of Solar Thermal Systems with Seasonal Storage Operation for Residential Scale Applications, *Procedia Environmental Sciences* 38 (2017) 405–412. <https://doi.org/10.1016/j.proenv.2017.03.124>.
- [229] I. Beausoleil-Morrison, B. Kemery, A.D. Wills, C. Meister, Design and simulated performance of a solar-thermal system employing seasonal storage for providing the majority of space heating and domestic hot water heating needs to a single-family house in a cold climate, *Solar Energy* 191 (2019) 57–69. <https://doi.org/10.1016/j.solener.2019.08.034>.
- [230] M. Jonin, M. Khosravi, A. Eichler, W. Villasmil, P. Schuetz, C.N. Jones, R.S. Smith, Exergy-based model predictive control for design and control of a seasonal thermal energy storage system, *J. Phys.: Conf. Ser.* 1343 (2019) 12066. <https://doi.org/10.1088/1742-6596/1343/1/012066>.
- [231] J.D. Hunt, B. Zakeri, W. Leal Filho, P.S. Schneider, N.d.A.B. Weber, L.W. Vieira, C. Ermel, N.J. de Castro, P.S.F. Barbosa, A. Nascimento, A. Mastrucci, Swimming pool thermal energy storage, an alternative for distributed cooling energy storage, *Energy Conversion and Management* 230 (2021) 113796. <https://doi.org/10.1016/j.enconman.2020.113796>.
- [232] V. Tulus, D. Boer, L.F. Cabeza, L. Jiménez, G. Guillén-Gosálbez, Enhanced thermal energy supply via central solar heating plants with seasonal storage: A multi-objective optimization approach, *Applied Energy* 181 (2016) 549–561. <https://doi.org/10.1016/j.apenergy.2016.08.037>.
- [233] T. Urbanek, J.M. Mücke, F. Findeisen, M. Gensbaur, S. Lang, D. Bestenlehner, H. Drück, R. Beyer, K. Pieper, Demonstration of an Overground Hot Water Store in Segmental Construction for District Heating Systems, *Energy Procedia* 149 (2018) 615–624. <https://doi.org/10.1016/j.egypro.2018.08.226>.
- [234] J. Zhao, L. Lyu, X. Li, Numerical analysis of the operation regulation in a solar heating system with seasonal water pool thermal storage, *Renewable Energy* 150 (2020) 1118–1126. <https://doi.org/10.1016/j.renene.2019.10.077>.
- [235] P. Bayer, G. Attard, P. Blum, K. Menberg, The geothermal potential of cities, *Renewable and Sustainable Energy Reviews* 106 (2019) 17–30.
- [236] D. Rohde, T. Andresen, N. Nord, Analysis of an integrated heating and cooling system for a building complex with focus on long-term thermal storage, *Applied Thermal Engineering* 145 (2018) 791–803. <https://doi.org/10.1016/j.applthermaleng.2018.09.044>.
- [237] E. Saloux, J.A. Candanedo, Optimal rule-based control for the management of thermal energy storage in a Canadian solar district heating system, *Solar Energy* 207 (2020) 1191–1201. <https://doi.org/10.1016/j.solener.2020.07.046>.
- [238] L. Xu, J.I. Torrens, F. Guo, X. Yang, J.L. Hensen, Application of large underground seasonal thermal energy storage in district heating system: A model-based energy performance assessment of a pilot system in Chifeng, China, *Applied Thermal Engineering* 137 (2018) 319–328. <https://doi.org/10.1016/j.applthermaleng.2018.03.047>.
- [239] D. Panno, A. Buscemi, M. Beccali, C. Chiaruzzi, G. Cipriani, G. Ciulla, V. Di Dio, V. Lo Brano, M. Bonomolo, A solar assisted seasonal borehole thermal energy system for a



- non-residential building in the Mediterranean area, *Solar Energy* 192 (2019) 120–132. <https://doi.org/10.1016/j.solener.2018.06.014>.
- [240] C.R. Matos, J.F. Carneiro, P.P. Silva, Overview of Large-Scale Underground Energy Storage Technologies for Integration of Renewable Energies and Criteria for Reservoir Identification, *Journal of Energy Storage* 21 (2019) 241–258. <https://doi.org/10.1016/j.est.2018.11.023>.
- [241] A. Dahash, F. Ochs, M.B. Janetti, W. Streicher, Advances in seasonal thermal energy storage for solar district heating applications: A critical review on large-scale hot-water tank and pit thermal energy storage systems, *Applied Energy* 239 (2019) 296–315. <https://doi.org/10.1016/j.apenergy.2019.01.189>.
- [242] C. Chang, Z. Wu, H. Navarro, C. Li, G. Leng, X. Li, M. Yang, Z. Wang, Y. Ding, Comparative study of the transient natural convection in an underground water pit thermal storage, *Applied Energy* 208 (2017) 1162–1173. <https://doi.org/10.1016/j.apenergy.2017.09.036>.
- [243] Y. Bai, M. Yang, J. Fan, X. Li, L. Chen, G. Yuan, Z. Wang, Influence of geometry on the thermal performance of water pit seasonal heat storages for solar district heating, *Build. Simul.* (2020). <https://doi.org/10.1007/s12273-020-0671-9>.
- [244] T. Schmidt, T. Pauschinger, P.A. Sørensen, A. Snijders, R. Djebbar, R. Boulter, J. Thornton, Design Aspects for Large-scale Pit and Aquifer Thermal Energy Storage for District Heating and Cooling, *Energy Procedia* 149 (2018) 585–594. <https://doi.org/10.1016/j.egypro.2018.08.223>.
- [245] X. Li, Z. Wang, J. Li, M. Yang, G. Yuan, Y. Bai, L. Chen, T. Xu, A. Gilmanova, Comparison of control strategies for a solar heating system with underground pit seasonal storage in the non-heating season, *Journal of Energy Storage* 26 (2019) 100963. <https://doi.org/10.1016/j.est.2019.100963>.
- [246] A. Rosato, A. Ciervo, G. Ciampi, M. Scorpio, S. Sibilio, Impact of seasonal thermal energy storage design on the dynamic performance of a solar heating system serving a small-scale Italian district composed of residential and school buildings, *Journal of Energy Storage* 25 (2019) 100889. <https://doi.org/10.1016/j.est.2019.100889>.
- [247] H. Cheng, J. Wu, Z. Luo, F. Zhou, X. Liu, T. Lu, Optimal Planning of Multi-Energy System Considering Thermal Storage Capacity of Heating Network and Heat Load, *IEEE Access* 7 (2019) 13364–13372. <https://doi.org/10.1109/ACCESS.2019.2893910>.
- [248] J. Yuan, C. Cui, Z. Xiao, C. Zhang, W. Gang, Performance analysis of thermal energy storage in distributed energy system under different load profiles, *Energy Conversion and Management* 208 (2020) 112596. <https://doi.org/10.1016/j.enconman.2020.112596>.
- [249] A. Castell, M. Medrano, C. Solé, L.F. Cabeza, Dimensionless numbers used to characterize stratification in water tanks for discharging at low flow rates, *Renewable Energy* 35 (2010) 2192–2199. <https://doi.org/10.1016/j.renene.2010.03.020>.
- [250] J. Fernández-Seara, F.J. Utrilla, J. Sieres, Experimental analysis of a domestic electric hot water storage tank. Part II: dynamic mode of operation, *Applied Thermal Engineering* 27 (2007) 137–144. <https://doi.org/10.1016/j.applthermaleng.2006.05.004>.
- [251] Egging-Bratseth, R., Kauko, H., Knudsen, B. R. Bakke, S. A., Ettayebi, A., Haufe, I. R., Seasonal storage and demand side management in district heating systems with demand uncertainty, *Applied Energy* 285 (2021) 116392. <https://doi.org/10.1016/j.apenergy.2020.116392>.
- [252] R. McKenna, D. Fehrenbach, E. Merkel, The role of seasonal thermal energy storage in increasing renewable heating shares: A techno-economic analysis for a typical residential district, *Energy and Buildings* 187 (2019) 38–49. <https://doi.org/10.1016/j.enbuild.2019.01.044>.
- [253] K. Narula, F. de Oliveira Filho, J. Chambers, E. Romano, P. Hollmuller, M.K. Patel, Assessment of techno-economic feasibility of centralised seasonal thermal energy storage for decarbonising the Swiss residential heating sector, *Renewable Energy* 161 (2020) 1209–1225. <https://doi.org/10.1016/j.renene.2020.06.099>.
- [254] C. Suárez, J. Pino, F. Rosa, J. Guerra, Analytical approach to ground heat losses for high temperature thermal storage systems, *Int J Energy Res* 43 (2019) 439–454. <https://doi.org/10.1002/er.4278>.

- [255] E. Hahne, Y. Chen, Numerical study of flow and heat transfer characteristics in hot water stores, *Solar Energy* 64 (1998) 9–18. [https://doi.org/10.1016/S0038-092X\(98\)00051-6](https://doi.org/10.1016/S0038-092X(98)00051-6).
- [256] F. Ochs, A. Dahash, A. Tosatto, M. Bianchi Janetti, Techno-economic planning and construction of cost-effective large-scale hot water thermal energy storage for Renewable District heating systems, *Renewable Energy* 150 (2020) 1165–1177. <https://doi.org/10.1016/j.renene.2019.11.017>.
- [257] Tosatto, A., Dahash, A., Ochs, F., Bianchi Janetti, M., Development of a Numerical Model for Large-Scale Seasonal Thermal Energy Storage for District Heating Systems, in: COMSOL Conference 2019, Cambridge, 2019.
- [258] U.-M. Solar Energy Laboratory, TRNSYS: A TRAnSient SYstems Simulation Program. Version 18.0, Solar Energy Laboratory, UW-Madison, Wisconsin-Madison, USA., 2021.
- [259] M. Wetter, W. Zuo, T.S. Nouidui, X. Pang, Modelica Buildings library, *Journal of Building Performance Simulation* 7 (2014) 253–270. <https://doi.org/10.1080/19401493.2013.765506>.
- [260] M. Wetter, M. Bonvini, T.S. Nouidui, W. Zuo, Modelica buildings library 2.0, in: Proc. of The 14th International Conference of the International Building Performance Simulation Association, Hyderabad, India, Hyderabad, India, 2015.
- [261] Introduction to COMSOL multiphysics®, 1998.
- [262] ANSYS Inc., Ansys Fluent: Fluid Simulation Software, 2021. <https://www.ansys.com/de-de/products/fluids/ansys-fluent> (accessed 11 March 2022).
- [263] H.-J.G. Diersch, FEFLOW: Finite Element Modeling of Flow, Mass and Heat Transport in Porous and Fractured Media, Springer Science & Business Media, 2013.
- [264] A. Dahash, F. Ochs, A. Tosatto, W. Streicher, Toward efficient numerical modeling and analysis of large-scale thermal energy storage for renewable district heating, *Applied Energy* 279 (2020) 115840. <https://doi.org/10.1016/j.apenergy.2020.115840>.
- [265] L. Amiri, S.A. Ghoreishi-Madiseh, A.P. Sasmito, F.P. Hassani, A porous medium based heat transfer and fluid flow model for thermal energy storage in packed rock beds, *IOP Conf. Ser.: Earth Environ. Sci.* 268 (2019) 12100. <https://doi.org/10.1088/1755-1315/268/1/012100>.
- [266] J. Fan, J. Huang, A. Chatzidiakos, S. Furbo, Experimental and theoretic investigations of thermal behavior of a seasonal water pit heat storage, in: Solar World Congress 2017.
- [267] D. Sun, J. Xu, P. Ding, Performance Analysis and Application of Three Different Computational Methods for Solar Heating System with Seasonal Water Tank Heat Storage, *Advances in Mechanical Engineering* 5 (2013) 857941. <https://doi.org/10.1155/2013/857941>.
- [268] K.M. Powell, T.F. Edgar, An adaptive-grid model for dynamic simulation of thermocline thermal energy storage systems, *Energy Conversion and Management* 76 (2013) 865–873. <https://doi.org/10.1016/j.enconman.2013.08.043>.
- [269] A. Dahash, F. Ochs, A. Tosatto, Co-Simulation of Dynamic Energy System Simulation and COMSOL Multiphysics, in: COMSOL Conference 2019, Cambridge, 2019.
- [270] H. Bastida, C.E. Ugalde-Loo, M. Abeysekera, M. Qadrdan, J. Wu, N. Jenkins, Dynamic Modelling and Control of Thermal Energy Storage, *Energy Procedia* 158 (2019) 2890–2895. <https://doi.org/10.1016/j.egypro.2019.01.942>.
- [271] F. Ochs, Large-Scale Thermal Energy Stores in District Heating Systems – Simulation Based Optimization, in: Proceedings of the EuroSun 2014 Conference, Freiburg, Germany, International Solar Energy Society, Freiburg, Germany, 2015.
- [272] M.V. Jensen, J.E. Nielsen, Seasonal pit heat storages - Guidelines for materials & construction: IEA SHC FACT SHEET 55.C-D2, 2020.
- [273] G. Gauthier, Benchmarking, and improving models of subsurface heat storage dynamics. Comparison of Danish PTES and BTES installation measurements with their corresponding TRNSYS models. GEOTHERMICA – ERA NET Cofund Geothermal, 2020.
- [274] L. Mazzarella, Multi-flow stratified thermal storage model with full-mixed layers: Type 142, Institut für Thermodynamik und Wärmetechnik Universität Stuttgart-FRG, Stuttgart, 1992.

- [275] M. Homberger, "ICEPIT"—A TRNSYS model for cold storage., in: Proceedings of EUROTHERM Seminar No. 49: Physical Models for Thermal Energy Stores, Eindhoven, The Netherlands, 1996.
- [276] K. Narula, F.D.O. Filho, J. Chambers, M.K. Patel, Simulation and comparative assessment of heating systems with tank thermal energy storage – A Swiss case study, *Journal of Energy Storage* 32 (2020) 101810. <https://doi.org/10.1016/j.est.2020.101810>.
- [277] K. Narula, F. de Oliveira Filho, W. Villasmil, M.K. Patel, Simulation method for assessing hourly energy flows in district heating system with seasonal thermal energy storage, *Renewable Energy* 151 (2020) 1250–1268. <https://doi.org/10.1016/j.renene.2019.11.121>.
- [278] P. Sorknæs, Simulation method for a pit seasonal thermal energy storage system with a heat pump in a district heating system, *Energy* 152 (2018) 533–538. <https://doi.org/10.1016/j.energy.2018.03.152>.
- [279] A. Dahash, F. Ochs, A. Tosatto, Simulation-based design optimization of large-scale seasonal thermal energy storage in renewables-based district heating systems, in: Proceedings of BauSIM 2020 Conference, Graz, 2020.
- [280] M. Reisenbichler, K. O'Donovan, C.R. Tugores, W.V. Helden, F. Wotawa, Towards More Efficient Modeling and Simulation of Large-Scale Thermal Energy Storages in Future Local and District Energy Systems, in: Proceedings of Building Simulation 2021, Bruges, Belgium, KU Leuven, 2021.
- [281] A. Dahash, M.B. Janetti, F. Ochs, Detailed 3-D models of a large-scale underground thermal energy storage with consideration of groundwater conditions, in: International Sustainable Energy Conference 2018, Graz, Austria, 2018, pp. 597–604.
- [282] F. Ochs, Modelling Large-Scale Thermal Energy Stores: submitted to the Faculty of Energy and Process and Bio Technology, University of Stuttgart, as partial fulfilment of the requirements for the degree of Doctor of Engineering. Dissertation, Stuttgart, 2009.
- [283] MathWorks, R2021a at a Glance, 2021. [https://www.mathworks.com/products/new\\_products/latest\\_features.html](https://www.mathworks.com/products/new_products/latest_features.html) (accessed 7 September 2021).
- [284] MathWorks, Simscape - Model and simulate multidomain physical systems (Version 5.0), 2021. <https://www.mathworks.com/help/physmod/simscape/> (accessed 7 September 2021).
- [285] T. Urbaneck, U. Schirmer, Central solar heating plant with gravel water storage in Chemnitz (Germany), in: M. Benner, E. Hahne (Eds.), Terrastock 2000: Terrastock 2000, 8th International 8th Conference on Thermal Energy Storage, first ed., Stuttgart, 2000.
- [286] A. Saggion, R. Faraldo, M. Pierno, Thermodynamics, Springer International Publishing, Cham, 2019.
- [287] T. Urbaneck, Berechnung von Kies-Wasser-Speichern. Dissertation, Chemnitz, 2004.
- [288] V. Gnielinski, Neue Gleichungen für den Wärme- und den Stoffübergang in turbulent durchströmten Rohren und Kanälen, *Forschung im Ingenieurwesen* 41 (1975) 8–16.
- [289] V. Gnielinski, New equations for heat and mass transfer in turbulent pipe and channel flow, *Int. Chem. Eng.* 16 (1976) 359–368.
- [290] Verein Deutscher Ingenieure, VDI-Gesellschaft Verfahrenstechnik und Chemieingenieurwesen (GVC), VDI-Wärmeatlas: Berechnungsblätter für den Wärmeübergang, Neunte, überarbeitete und erweiterte Auflage, Springer Berlin Heidelberg, Berlin, Heidelberg, s.l., 2002.
- [291] C. Wemhöner, B. Hafner, K. Schwarzer, Simulation of solar thermal systems with CARNOT blockset in the environment Matlab/Simulink, in: Eurosun 2000, Copenhagen, 2000.
- [292] Solar-Institut Juelich, CARNOT Toolbox, Ver. 7.0, 07/2019 for Matlab/Simulink R2018b. User Manual: [https://fh-aachen.sciebo.de/index.php/s/0hxub0iJrui3ED?path=%2FCARNOT\\_documentation\\_7.1](https://fh-aachen.sciebo.de/index.php/s/0hxub0iJrui3ED?path=%2FCARNOT_documentation_7.1), FH Aachen, Aachen, 2020.
- [293] R. Ilgaz, R. Yumrutaş, Heating performance of swimming pool incorporated solar assisted heat pump and underground thermal energy storage tank: A case study, *Int J Energy Res* (2021). <https://doi.org/10.1002/er.7221>.

- [294] G. Emmi, A. Natali, S. Cesari, P. Fausti, M. Bottarelli, Use of an Outdoor Swimming Pool as Seasonal Heat Source in Heat Pump Applications, *TI-IJES* 65 (2021) 337–344. <https://doi.org/10.18280/ti-ijes.652-430>.
- [295] Ecoglas, Technische Daten, 2021. <https://www.ecoglas.de/files/Technische-Daten.pdf> (accessed 10 June 2021).
- [296] Deutsches Institut für Normung e.V., Wärmeschutz und Energie-Einsparung in Gebäuden - Teil 4: Wärme- und feuchteschutztechnische Bemessungswerte (Thermal insulation and energy economy in buildings - Part 4: Hygrothermal design values), Beuth, Berlin, 2020. <https://www.beuth.de/de/norm/din-4108-4/327502903> (accessed 10 September 2021).
- [297] BBSR, Ortsgenaue Testreferenzjahre (TRY) von Deutschland für mittlere und extreme Witterungsverhältnisse: Release date: 2021-06-08. Test datasets for environmental conditions, Deutscher Wetterdienst (German Weather Service), Bonn, 2017.
- [298] W.R. van Wijk, *Physics of Plant Environment*, Soil Science 98 (1964) 69.
- [299] A. Dahash, F. Ochs, A. Tosatto, Techno-economic and exergy analysis of tank and pit thermal energy storage for renewables district heating systems, *Renewable Energy* 180 (2021) 1358–1379. <https://doi.org/10.1016/j.renene.2021.08.106>.
- [300] M.A. Rosen, I. Dincer, Exergy methods for assessing and comparing thermal storage systems, *International Journal of Energy Research* 27 (2003) 415–430. <https://doi.org/10.1002/er.885>.
- [301] I. Sifnaios, D.M. Sneum, A.R. Jensen, J. Fan, R. Bramstoft, The impact of large-scale thermal energy storage in the energy system, *Applied Energy* 349 (2023) 121663. <https://doi.org/10.1016/j.apenergy.2023.121663>.
- [302] M. Sun, T. Liu, X. Wang, T. Liu, M. Li, G. Chen, D. Jiang, Roles of thermal energy storage technology for carbon neutrality, *Carb Neutrality* 2 (2023). <https://doi.org/10.1007/s43979-023-00052-w>.
- [303] S. Zhang, P. Ochoń, J.J. Klemeš, P. Michorczyk, K. Pielichowska, K. Pielichowski, Renewable energy systems for building heating, cooling and electricity production with thermal energy storage, *Renewable and Sustainable Energy Reviews* 165 (2022) 112560. <https://doi.org/10.1016/j.rser.2022.112560>.
- [304] International Renewable Energy Agency, IRENA-IEA-ETSAP Technology Brief 4: Thermal Storage.
- [305] R. Jacob, M. Hoffmann, J.M. Weinand, J. Linßen, D. Stolten, M. Müller, The future role of thermal energy storage in 100% renewable electricity systems, *Renewable and Sustainable Energy Transition* 4 (2023) 100059. <https://doi.org/10.1016/j.rset.2023.100059>.
- [306] Chavan, S., Panwar, V., Rathod, R., Review on Thermal Energy Storage Techniques, *International Journal of Engineering Development and Research* 3 (2015) 944–948.
- [307] J. Ríos-Arriola, N. Velázquez-Limón, J.A. Aguilar-Jiménez, S. Islas, J.D. López-Sánchez, F.J. Caballero-Talamantes, J.A. Corona-Sánchez, C.A. La Cásares-De Torre, Comparison between Air-Exposed and Underground Thermal Energy Storage for Solar Cooling Applications, *Processes* 11 (2023) 2406. <https://doi.org/10.3390/pr11082406>.
- [308] G.K. Dolgun, A. Keçebaş, M. Ertürk, A. Daşdemir, Optimal insulation of underground spherical tanks for seasonal thermal energy storage applications, *Journal of Energy Storage* 69 (2023) 107865. <https://doi.org/10.1016/j.est.2023.107865>.
- [309] A. Tosatto, F. Ochs, A. Dahash, C. Muser, F. Kutscha-Lissberg, P. Kremnitzer, Influence of Heat and Mass Transfer on the Performance of Large-Scale Thermal Energy Storage Systems, in: P. Schossig, P. Droege, A. Riemer, M. Speer (Eds.), *Proceedings of the International Renewable Energy Storage Conference (IRES 2022)*, Atlantis Press International BV, Dordrecht, 2023, pp. 470–488.
- [310] I. Sifnaios, A.R. Jensen, S. Furbo, J. Fan, Heat losses in water pit thermal energy storage systems in the presence of groundwater, *Applied Thermal Engineering* 235 (2023) 121382. <https://doi.org/10.1016/j.applthermaleng.2023.121382>.
- [311] C. Zhu, J. Zhang, Y. Wang, Z. Deng, P. Shi, J. Wu, Z. Wu, Study on Thermal Performance of Single-Tank Thermal Energy Storage System with Thermocline in Solar Thermal Utilization, *Applied Sciences* 12 (2022) 3908. <https://doi.org/10.3390/app12083908>.

- [312] D. Olsthoorn, F. Haghghat, P.A. Mirzaei, Integration of storage and renewable energy into district heating systems: A review of modelling and optimization, *Solar Energy* 136 (2016) 49–64. <https://doi.org/10.1016/j.solener.2016.06.054>.
- [313] Y. Zhang, Applicability of thermal energy storage in future district heating system - Design methodologies and performance evaluations. Thesis for the degree of licentiate of engineering, Gothenburg, Sweden, 2021.
- [314] A.G. Olabi, A.A. Abdelghafar, H.M. Maghrabie, E.T. Sayed, H. Rezk, M.A. Radi, K. Obaideen, M.A. Abdelkareem, Application of artificial intelligence for prediction, optimization, and control of thermal energy storage systems, *Thermal Science and Engineering Progress* 39 (2023) 101730. <https://doi.org/10.1016/j.tsep.2023.101730>.
- [315] G. de Goeijen, Developing a Method for the Operational Control of an Ecovat System, 2019.
- [316] A. Tosatto, A. Dahash, F. Ochs, Simulation-based performance evaluation of large-scale thermal energy storage coupled with heat pump in district heating systems, *Journal of Energy Storage* 61 (2023) 106721. <https://doi.org/10.1016/j.est.2023.106721>.
- [317] L. Hermans, R. Haesen, A. Uytterhoeven, W. Peere, W. Boydens, L. Helsen, Pre-design of collective residential solar districts with seasonal thermal energy storage: Importance of level of detail, *Applied Thermal Engineering* 226 (2023) 120203. <https://doi.org/10.1016/j.applthermaleng.2023.120203>.
- [318] C. Bott, I. Dressel, P. Bayer, Closed, In-ground, Water-based Seasonal Storage Systems for Thermal Energy - “ State-of-technology in Europe, in: *Proceedings World Geothermal Congress 2020, Reykjavik, Iceland, The Hague, The Netherlands*, 2020.
- [319] M. Noethen, H. Hemmerle, P. Bayer, Sources, intensities, and implications of subsurface warming in times of climate change, *Critical Reviews in Environmental Science and Technology* 53 (2023) 700–722. <https://doi.org/10.1080/10643389.2022.2083899>.
- [320] G.J. van den Brink, C.J. Hoogendorn, Ground water flow heat losses for seasonal heat storage in the soil, *Solar Energy* 30 (1983) 367–371.
- [321] C. Griebler, H. Brielmann, C.M. Haberer, S. Kaschuba, C. Kellermann, C. Stumpp, F. Hegler, D. Kuntz, S. Walker-Hertkorn, T. Lueders, Potential impacts of geothermal energy use and storage of heat on groundwater quality, biodiversity, and ecosystem processes, *Environmental Earth Sciences* 75 (2016). <https://doi.org/10.1007/s12665-016-6207-z>.
- [322] Alejandro García Gil, Miguel Mejías Moreno, Current Legal Framework on Shallow Geothermal Energy Use in Spain, *J Sustain Res* 2 (2019). <https://doi.org/10.20900/jsr20200005>.
- [323] C. Bott, M. Ehrenwirth, C. Trinkl, P. Bayer, Component-based modeling of ground-coupled seasonal thermal energy storages, *Applied Thermal Engineering* (2022) 118810. <https://doi.org/10.1016/j.applthermaleng.2022.118810>.
- [324] The Mathworks Inc., MATLAB, The Mathworks Inc., Natick, Massachusetts, USA, 2023.
- [325] COMSOL AB, COMSOL Multiphysics, COMSOL AB, Stockholm Sweden, 2023.
- [326] The Modelica Association, Functional Mock-up Interface: The leading standard to exchange dynamic simulation models, The Modelica Association, Linköping, Sweden, 2023.
- [327] COMSOL AB, LiveLink for Simulink: User’s Guide. Version 6.1, Stockholm Sweden, 2021.
- [328] H. Drück, MULTIPOINT Store-Model for TRNSYS: Stratified fluid storage tank with four internal heat exchangers, ten connections for direct charge and discharge and an internal electrical heater. Version 1.99F, Stuttgart, Germany, 2006.
- [329] Solar-Institut Juelich, CARNOT Toolbox: Release 8.0.1 (Matlab 2021b), Solar-Institut Juelich, FH Aachen, Aachen, 2023.
- [330] Verein Deutscher Ingenieure, Thermal use of the underground: Fundamentals, approvals, environmental aspects, Beuth Verlag GmbH, Berlin, 2010.
- [331] I. Dressel, C. Bott, P. Bayer, Converting idle infrastructure to large scale seasonal heat storage systems, in: *45th IAH Congress, Daejeon, Korea*, 2018.

- [332] C. Bott, I. Dressel, P. Bayer, Paraffin wax as self-sealing insulation material of seasonal sensible heat storage systems-A laboratory study, *PLoS One* 15 (2020) e0236056. <https://doi.org/10.1371/journal.pone.0236056>.
- [333] E. Valor, V. Caselles, Mapping Land Surface Emissivity from NDVI: Application to European, African, and South American Areas, *Remote Sensing of Environment* 57 (1996) 167–184.
- [334] S. Krähenmann, *Handbuch: Ortsgenaue Testreferenzjahre von Deutschland für mittlere, extreme und zukünftige Witterungsverhältnisse*, Offenbach, 2017.
- [335] A. Dahash, M. Michele Bianchi Janetti, F. Ochs, Numerical Analysis and Evaluation of Large-Scale Hot Water Tanks and Pits in District Heating Systems, in: *Proceedings of Building Simulation 2019: 16th Conference of IBPSA, Rome, Italy, IBPSA, 2020*, pp. 1692–1699.
- [336] H. Brielmann, C. Griebler, S.I. Schmidt, R. Michel, T. Lueders, Effects of thermal energy discharge on shallow groundwater ecosystems, *FEMS Microbiol. Ecol.* 68 (2009) 273–286. <https://doi.org/10.1111/j.1574-6941.2009.00674.x>.
- [337] A. Retter, C. Karwautz, C. Griebler, Groundwater Microbial Communities in Times of Climate Change, *Curr. Issues Mol. Biol.* 41 (2021) 509–538. <https://doi.org/10.21775/cimb.041.509>.
- [338] C. Beyer, S. Popp, S. Bauer, Simulation of temperature effects on groundwater flow, contaminant dissolution, transport and biodegradation due to shallow geothermal use, *Environ Earth Sci* 75 (2016). <https://doi.org/10.1007/s12665-016-5976-8>.
- [339] M. Bonte, P.J. Stuyfzand, G.A. van den Berg, W.A.M. Hijnen, Effects of aquifer thermal energy storage on groundwater quality and the consequences for drinking water production: a case study from The Netherlands, *Water Sci. Technol.* 63 (2011) 1922–1931. <https://doi.org/10.2166/wst.2011.189>.
- [340] A. García-Gil, E. Garrido Schneider, M. Mejías, D. Barceló, E. Vázquez-Suñé, S. Díaz-Cruz, Occurrence of pharmaceuticals and personal care products in the urban aquifer of Zaragoza (Spain) and its relationship with intensive shallow geothermal energy exploitation, *Journal of Hydrology* 566 (2018) 629–642. <https://doi.org/10.1016/j.jhydrol.2018.09.066>.
- [341] J. Becher, C. Englisch, C. Griebler, P. Bayer, Groundwater fauna downtown - Drivers, impacts and implications for subsurface ecosystems in urban areas, *J. Contam. Hydrol.* 248 (2022) 104021. <https://doi.org/10.1016/j.jconhyd.2022.104021>.
- [342] C.M. Agudelo-Vera, M. Blokker, H. de Kater, R. Lafort, Identifying (subsurface) anthropogenic heat sources that influence temperature in the drinking water distribution system, *Drink. Water Eng. Sci.* 10 (2017) 83–91. <https://doi.org/10.5194/dwes-10-83-2017>.
- [343] L. van den Bos, Quantifying the effects of anthropogenic heat sources on the water temperature in the drinking water distribution system. Master's Thesis, Delft, The Netherlands, 2020.
- [344] P. Blum, K. Menberg, F. Koch, S.A. Benz, C. Tissen, H. Hemmerle, P. Bayer, Is thermal use of groundwater a pollution?, *J. Contam. Hydrol.* 239 (2021) 103791. <https://doi.org/10.1016/j.jconhyd.2021.103791>.
- [345] V. Bürger, S. Braungardt, C. Maaß, M. Sandrock, P. Möhring, *Agendwa Wärmewende 2021: Studie im Auftrag der Stiftung Klimaneutralität und Agora Energiewende*, Freiburg/Hamburg, 2021.
- [346] B. Zhang, K. Gu, B. Shi, C. Liu, P. Bayer, G. Wei, X. Gong, L. Yang, Actively heated fiber optics based thermal response test: A field demonstration, *Renewable and Sustainable Energy Reviews* 134 (2020) 110336. <https://doi.org/10.1016/j.rser.2020.110336>.
- [347] J. Acuña, B. Palm, Distributed thermal response tests on pipe-in-pipe borehole heat exchangers, *Applied Energy* 109 (2013) 312–320. <https://doi.org/10.1016/j.apenergy.2013.01.024>.
- [348] B.F. Des Tombe, M. Bakker, F. Smits, F. Schaars, K.-J. van der Made, Estimation of the Variation in Specific Discharge Over Large Depth Using Distributed Temperature Sensing (DTS) Measurements of the Heat Pulse Response, *Water Resources Research* 55 (2019) 811–826. <https://doi.org/10.1029/2018WR024171>.

- [349] Andreas Herwig, Luise Umbreit, Dr.-Ing. Karin Rühling, Temperaturfeldmessung in Großwärmespeichern von KWK-basierten Fernwärmesystemen als Werkzeug zur Effizienzsteigerung: Final Report of the SPICE (Speichereffizienz) project (project no. 03ET1322A), Dresden, 2019.
- [350] G. Steindl, M. Stagl, L. Kasper, W. Kastner, R. Hofmann, Generic Digital Twin Architecture for Industrial Energy Systems, *Applied Sciences* 10 (2020) 8903. <https://doi.org/10.3390/app10248903>.
- [351] T. Kohne, L. Theisinger, J. Scherff, M. Weigold, Data and optimization model of an industrial heat transfer station to increase energy flexibility, *Energy Inform* 4 (2021). <https://doi.org/10.1186/s42162-021-00179-z>.
- [352] O. San, The digital twin revolution, *Nat Comput Sci* 1 (2021) 307–308. <https://doi.org/10.1038/s43588-021-00077-0>.
- [353] J.A. Douthwaite, B. Lesage, M. Gleirscher, R. Calinescu, J.M. Aitken, R. Alexander, J. Law, A Modular Digital Twinning Framework for Safety Assurance of Collaborative Robotics, *Front. Robot. AI* 8 (2021) 758099. <https://doi.org/10.3389/frobt.2021.758099>.
- [354] W. Jin, T.A. Atkinson, C. Doughty, G. Neupane, N. Spycher, T.L. McLing, P.F. Dobson, R. Smith, R. Podgorney, Machine-learning-assisted high-temperature reservoir thermal energy storage optimization, *Renewable Energy* 197 (2022) 384–397. <https://doi.org/10.1016/j.renene.2022.07.118>.
- [355] G. Henze, J. Schoenmann, Evaluation of Reinforcement Learning Control for Thermal Energy Storage Systems, *HVAC&R Res.* 9 (2003) 259–275. <https://doi.org/10.1080/10789669.2003.10391069>.
- [356] R. Zeh, B. Ohlsen, D. Philipp, D. Bertermann, T. Kotz, N. Jocić, V. Stockinger, Large-Scale Geothermal Collector Systems for 5th Generation District Heating and Cooling Networks, *Sustainability* 13 (2021) 6035. <https://doi.org/10.3390/su13116035>.
- [357] J. Guinée, Handbook on life cycle assessment — operational guide to the ISO standards, *Int J LCA* 6 (2001) 255. <https://doi.org/10.1007/bf02978784>.
- [358] R. Stemmler, P. Blum, S. Schüppler, P. Fleuchaus, M. Limoges, P. Bayer, K. Menberg, Environmental impacts of aquifer thermal energy storage (ATES), *Renewable and Sustainable Energy Reviews* 151 (2021) 111560. <https://doi.org/10.1016/j.rser.2021.111560>.
- [359] A. Mouloupoulos, Life Cycle Assessment of an Aquifer Thermal Energy Storage system: Exploring the environmental performance of shallow subsurface space development. MSc Thesis report, Utrecht, The Netherlands, 2014.
- [360] C. Tomasetta, C.C.D.F. van Ree, J. Griffioen, Life Cycle Analysis of Underground Thermal Energy Storage, in: G. Lollino, A. Manconi, F. Guzzetti, M. Culshaw, P. Bobrowsky, F. Luino (Eds.), *Engineering Geology for Society and Territory - Volume 5*, Springer International Publishing, Cham, 2015, pp. 1213–1217.

# Curriculum vitae

## Personal Information

Name	Christoph Bott
Date of birth	2 July 1992
Place of birth	Solingen, Germany

## Professional Experience

November 2019 – Current: **Research Assistant**, Applied Geology, Institute of Geosciences and Geography, MLU Halle-Wittenberg, Halle (Saale), Germany

June 2018 – May 2021: **Research Assistant**, Geoenergy, Institute of new Energy Systems, University of Applied Sciences, Ingolstadt, Germany

September 2017 – December 2018: **Freelance Geoscientist** for Berufsverband Deutscher Geowissenschaftler (BDG), Bonn, Germany

October 2017 – February 2018: **Student Employee**, Sachtleben Bergbau Verwaltungs-GmbH, Lennestadt-Meggen, Germany

## Education

November 2019 – Current: **PhD Student**, Applied Geology, Institute of Geosciences and Geography, MLU Halle-Wittenberg, Halle (Saale), Germany

April 2018: **Master's Thesis**, Steinmann-Institute for Geology, Mineralogy, and Paleontology, University of Bonn, Germany, title: "Passive water treatment for drainage water of a former sedimentation pond"

September 2015 – March 2018: **M.Sc. Geosciences**, Steinmann-Institute for Geology, Mineralogy, and Paleontology, University of Bonn, Germany

January 2016: **Bachelor's Thesis**: Steinmann-Institute for Geology, Mineralogy, and Paleontology, University of Bonn, Germany, title: "Geogenic and anthropogenic influences of an ore deposit in the Sauerland region"

September 2012 – January 2016: **B.Sc. Geosciences**, Steinmann-Institute for Geology, Mineralogy, and Paleontology, University of Bonn, Germany



**Further publications with the author's contribution, that are not part of the thesis:**

- Menberg, K., Heberle, F., Uhrmann, H., **Bott, C.**, Grünäugl, S., Brüggemann, D., Bayer, P. (2023). Environmental impact of cogeneration in binary geothermal plants. *Renewable Energy*, 119251.
- Bott, C.**, Ehrenwirth, M., Trinkl, C., Schrag, T., Dahash, A., Bayer, P. (2023). Modelling Long-Term Thermal Energy Storage in Water-Gravel-Filled Artificial Basin Systems. Poster presented at the *InterPore2023*, Edinburgh, Scotland.
- Bott, C.**, Ehrenwirth, M., Trinkl, C., Schrag, T., & Bayer, P. (2023). Simulation of Re-Used Basin Structures for Long-Term, Large-Scale Sensible Thermal Energy Storage. Poster presented at the *EGU General Assembly 2023*, Vienna, Austria.
- Bott, C.**, Bayer, P. (2022). Modeling the Thermal Interference Between Closed Large-Scale Heat Storage Facilities and Groundwater. *XXIV International Conference on Computational Methods in Water Resources (CMWR)*, Gdansk, Poland.
- Bott, C.**, Bayer, P. (2022). Modelling environmental interactions of large-scale, closed seasonal thermal energy storage systems, *EGU General Assembly 2022*, Vienna, Austria.
- Bott, C.**, Menberg, K., Heberle, F., Brüggemann, D., & Bayer, P. (2021). Life cycle assessment of geothermal power generation in the Southern German Molasse Basin – The binary plant Kirchstockach, PICO poster presented at the *EGU General Assembly 2021*, online.
- Menberg, K., Heberle, F., **Bott, C.**, Brüggemann, D., Bayer, P. (2021). Environmental performance of a geothermal power plant using a hydrothermal resource in the Southern German Molasse Basin. *Renewable Energy*, 167, 20-31.
- Bott, C.**, Bayer, P., & Dressel, I. (2020). Closed, in-ground, water-based seasonal storage systems for thermal energy – State of technology in Europe. Paper presented at the *World Geothermal Congress*, online.
- Bott, C.**, Bayer, P., & Dressel, I. (2019). Seasonal heat storage systems: Present state of large-scale closed systems in Europe. Paper presented at the *EGU General Assembly 2019*, Vienna, Austria.
- Dressel, I., **Bott, C.**, & Bayer, P. (2018). Converting idle infrastructure to large-scale seasonal heat storage systems. Paper presented at the *45th IAH Conference, Groundwater and Life: Science and Technology into Action*, Daejeon, Korea.
- Weyer, H.-J., & **Bott, C.** (2018). Rohstoffszenarien: Versorgung im Jahr 2050. *Nachrichten aus der Chemie*, 66(6), 609-610.

## **Declaration / Erklärung**

Ich erkläre an Eides statt, dass ich die Arbeit selbstständig und ohne fremde Hilfe verfasst, keine anderen als die von mir angegebenen Quellen und Hilfsmittel benutzt und die den benutzten Werken wörtlich oder inhaltlich entnommenen Stellen als solche kenntlich gemacht habe.

*I declare under penalty of perjury that this thesis is my own work entirely and has been written without any help from other people. I used only the sources mentioned and included all the citations correctly both in word or content.*

---

Ort & Datum / Place & Date

Christoph Bott